Wissenschaftlich-Technische Berichte
FZR-420
2005

Annual Report 2004

Institute of Safety Research

Editors:
Prof. Dr. Frank-Peter Weiss
Prof. Dr. Udo Rindelhardt

Forschungszentrum
Rossendorf

Cover Pictures:
Coupled fluid dynamic/chemical reaction kinetics simulation of the mass transfer of acetic acid from organic to aqueous layer with chemical reaction (neutralization) at the phase interface: temperature distributions at 50 and 100 seconds after onset of convective instability.

Forschungszentrum Rossendorf e.V.
Institut für Sicherheitsforschung

Postfach 51 01 19
D-01314 Dresden
Bundesrepublik Deutschland

Direktor	Prof. Frank-Peter Weiß
Telefon	+ 49 (3 51) 2 60 34 80
Telefax	+ 49 (3 51) 2 60 34 40
E-Mail	f.p.weiss@fz-rossendorf.de
WWW	http://www.fz-rossendorf.de/FWS

CONTENTS

Preface

The Institute of Safety Research (ISR) is one of the six Research Institutes of Forschungszentrum Rossendorf e.V. (FZR e.V.) which is a member institution of the Wissenschaftsgemeinschaft Gottfried Wilhelm Leibniz (Leibniz Association).
Together with the Institute of Radiochemistry, ISR constitutes the research programme „Safety and Environment“ which is one from three scientific programmes of FZR. In the framework of this research programme, the institute is responsible for the two sub-programmes “Plant and Reactor Safety” and “Thermal Fluid Dynamics”, respectively. We also provide minor contributions to the sub-programme “Radio-Ecology”. Moreover, with the development of a pulsed photo-neutron source at the radiation source ELBE (**E**lectron **l**inear accelerator for **b**eams of high brilliance and low **e**mittance), we are involved in a networking project carried out by the FZR Institute of Nuclear and Hadron Physics, the Physics Department of TU Dresden, and ISR.

The research of ISR aims at assessing and enhancing the safety of technical plants and at improving the environmental sustainability of the processes involved. The applications are as well related to nuclear plants of present and future designs as to installations of process industries.
To achieve the goals mentioned, the institute does research in thermal fluid dynamics including magnetohydrodynamics (MHD) and in materials sciences as related to ageing materials and components. The thermal fluid dynamics research work is essentially based on the experiments performed at the **T**ransient Tw**o**-**P**hase **Flow** Test Facility, TOPFLOW. TOPFLOW is one of the large research and user facilities of FZR and represents the reference thermal hydraulic experiment of the so called “German CFD (Computational Fluid Dynamics) Initiative”.

Our work is financed through the basic funding of FZR as well as by external funds from public and private research grants, and from scientific contracts with the industry. 37 % (2.717 k€) of our total budget could be acquired from such external funds, in 2004, with 16 % from research grants of the Federal Government and the Free State of Saxony. 7 % of the funding originated from Deutsche Forschungsgemeinschaft, 7 % from the EU and 7 % from research contracts mainly with the industry (see Fig.1). The deployment of the total budget on the different projects and the user facility TOPFLOW (see Table 1) is illustrated in Fig.2.

Sub-programme	Project/User facility
Plant and reactor safety	Accident analysis of nuclear reactors
	Safety of materials and components
	Particle and radiation transport
	Safety and efficiency of chemical processes
Thermal fluid dynamics	Magnetohydrodynamics
	Thermal fluid dynamics of multi-phase flows
Radio-ecology	Simulation of the migration of radio-nuclides
User facility TOPFLOW	Transient two-phase flow test facility
Networking research activity	Design and construction of a pulsed photo-neutron source at ELBE

Table 1. Research projects and user facility of the Institute of Safety Research, 2004

Together with the Dresden Technical University and with the Zittau University of Applied Sciences, the ISR represents the East German Centre of Competence in Nuclear Technology (Kompetenzzentrum Ost) being a member of the National Nuclear Competence Alliance (Kompetenzverbund Kerntechnik). As such the ISR also takes care to keep and promote the expertise in nuclear engineering. For that end, a strategic partnership was established between Kompetenzzentrum Ost and Vattenfall Europe. Vattenfall represented by its nuclear power branch will sponsor the education of three PhD students in nuclear technology, one in each of the participating institutions.
Beyond this, ISR in general cares for the next generation of young scientists by, e.g., supervising PhD and Diploma students. Two of them, Martina Speck and André Bieberle, received the "Best Diploma Thesis Award" of TU Dresden for their work in the field of computerized tomography. Moreover, a Young Scientists Group on CFD consisting of 6 junior researchers and PhD students was founded in December 2004. This will further push forward our research in CFD.

In 2004, important EURATOM projects of the 5^{th} EU framework programme, as VALCO (Validation of Coupled Neutron Kinetic Thermal Hydraulics Codes) and FLOMIX-R (Fluid Mixing and Flow Distribution in the Reactor Circuit) were successfully accomplished under the leadership of ISR.
We also contributed to the EU project MOST (Molten Salt Reactor Technology). The Molten Salt Reactor (MSR) is one of the candidates for innovative reactor systems being pursued in the Generation IV International Forum. The MSR offers the opportunity to transmute plutonium and minor actinides in a critical reactor. Nevertheless, the MSR technology development requires better understanding of the particular dynamics of this reactor which is significantly influenced by the fact that the flowing molten salt represents both, the fuel and heat carrier at the same time. Therefore, in order to model the kinetics of the MSR, ISR has modified its light water reactor dynamics code DYN3D. The new 3D version DYN3D-MSR takes into account that the flowing salt forwards the delayed neutron precursors out of the core. The new code will be released in 2005.

Further, we succeeded in getting involved into new Integrated Projects and Networks of Excellence of EU FP6 like into PERFECT (Prediction of Irradiation Damage Effects in Reactor Components), SARNET (Severe Accident Research Network), EUROTRANS (European Research Project for the Transmutation of High Level Nuclear Waste in an Accelerator Driven System), and NURESIM (Nuclear Reactor Simulation). This strengthens the position of ISR as one of the major players in European nuclear safety research. In particular it is noteworthy that our reactor dynamics code DYN3D has been decided to become part of the European software platform for reactor simulation, NURESIM.

The ISR contributions to the German CFD initiative and the future input to NURESIM, that both aim at the improvement of thermal hydraulic calculation methods in reactor safety, very much benefit from the progress we reached in the design and use of the thermal hydraulic test facility TOPFLOW. In this context, it is worth mentioning that the measurements done with wire-mesh sensors in vertical test sections of different diameters revealed for the first time worldwide the influence of the pipe scale on the structure of the two-phase flow. It was postulated by others that a pronounced slug flow as it is observed in small pipes will not develop in a 200mm or even larger pipe. We were able to measure with the wire mesh sensors bubble size distributions and could show that there is a direct transition from bubbly to churn turbulent flow in large diameter pipes skipping the region of slug flow. These results were presented in a paper at the NURETH-10 conference in Seoul 2004. The authors, H.-M.

Prasser, et. al., were awarded the “Best Paper Award 2004” of the Thermal Hydraulics Division of the American Nuclear Society.
The new wire mesh sensors, which allow to visualise the transient spatial structure of steam/water two-phase flows with a resolution of 3mm at 2.5kHz imaging frequency up to a pressure of 7MPa and a temperature of 286°C, mean a considerable breakthrough. The sensors can be applied to pipe diameters up to 200mm and constitute the front end in two-phase flow measuring technology.
Significant progress could also be achieved in the CFD simulation of two-phase flows. The multi-phase, multi-bubble size group model, named the inhomogeneous MUSIG model, proposed by ISR has been jointly developed in close cooperation with ANSYS-CFX®, which is the commercial partner in the German CFD initiative. The code CFX was recently extended with the new model by ANSYS-CFX®. It could be demonstrated that the extended code is capable of simulating the effect of bubble break-up and coalescence and of properly describing the radial void fraction distributions. Nevertheless, the validation activities are still going on.
Our CFD work will significantly benefit from the construction of the so called **H**ot **L**eg **T**est **F**acility (HLTF) at TOPFLOW. It is designed to study spatial thermal hydraulic phenomena like counter current flow limitation in the hot leg of a pressurized water reactor during a loss of coolant accident and to make it accessible to CFD modelling. The construction of HLTF very well runs along the schedule and will be finished mid 2005.

ISR`s engagement in thermal fluid dynamics is completed by research in magneto-hydrodynamics (MHD). In general, the target of MHD is to investigate the interactions of magnetic fields with electrically conducting fluids. The particular aim is to influence the flow of liquid metals in metallurgy or, e.g., of liquid semi-conductors in crystal growth by “tailored” external magnetic fields to optimise the processes involved regarding quality and energetic efficiency. Most of our scientific activities in this field are part of the Collaborative Research Centre 609 (Sonderforschungsbereich SFB 609) “Electromagnetic flow control in metallurgy, crystal growth, and electrochemistry” funded by Deutsche Forschungsgemeinschaft. SFB 609 has been running since 2002. It was initiated by ISR and is coordinated by TU Dresden. End of September 2004, the SFB successfully passed the evaluation by DFG (Deutsche Forschungsgemeinschaft) referees. The results of the first 3 years work had to be reported on and the ideas for the period 2005-2008 were to be defended. As result of the very positive evaluation, ISR will coordinate 5 from 17 sub-projects of the SFB and further participates in 4 other sub-projects. Beginning with 2005 , this SFB becomes one of the largest SFBs at all in Germany. This means a total annual funding of about 1.8 M€ for all the 17 projects. This step highlights the continuous development of MHD in the Dresden area over about a decade. Today, Dresden clearly belongs to the worldwide leading places in MHD research. Invitations to joint R&D programmes with Chinese and Japanese teams underline this recognition.

In materials safety research ISR is focussed on irradiation induced ageing phenomena of reactor pressure vessel materials. This topic is of special importance to the Soviet type VVER reactors. Therefore, in cooperation with VTT (Technical Research Centre of Finland), the micro-structural changes of a VVER-440 reactor pressure vessel weld material were investigated after irradiation, thermal annealing, re-irradiation , and repeated annealing. By small angle neutron scattering, it could be shown that the irradiation induced defect clusters provoking material embrittlement dissolve during annealing and that the damage is less after the second irradiation with the same neutron dose. There are also hints that the composition of the defect clusters after the second irradiation differs from that observed after the first

exposition. This might be a consequence of stable Cu segregations generated during the annealing.
Improved insight in irradiation induced ageing is expected from the post-service investigations of specimens that will be obtained from the decommissioned Greifswald reactors in 2005. ISR has contracted taking of through wall specimens from the Greifswald pressure vessels. With our recently licensed hot cell laboratory for the machining of standard specimens from large size materials pieces, we are well prepared for the envisaged testing programme that certainly will attract international attention.

During the reporting period, the ISR again organised important meetings and workshops with international participation. In particular, one should mention the international Workshop on "Multi-Phase Flow: Simulation, Experiment and Application" which was commonly hosted by ISR and ANSYS/CFX® and which continues the series of meetings on that topic in Rossendorf. One should further mention the Workshop on "Flow Control by Tailored Magnetic Fields (FLOCOMAG)" organised by our MHD department in cooperation with TU Dresden (SFB 609) and the "Sino-German Workshop on Electromagnetic Processing of Materials" held in Shanghai. The latter was sponsored by the National Nature Science Foundation of China and Deutsche Forschungsgemeinschaft, respectively.
Meetings like these underline the international scientific reputation of the Institute of Safety Research.

I would like to thank all staff members of the institute for their excellent work and for making the year 2004 one of the most successful since ISR was founded.

F.-P. Weiß Rossendorf, 2 February 2005

Fig. 1: Funding sources 2004

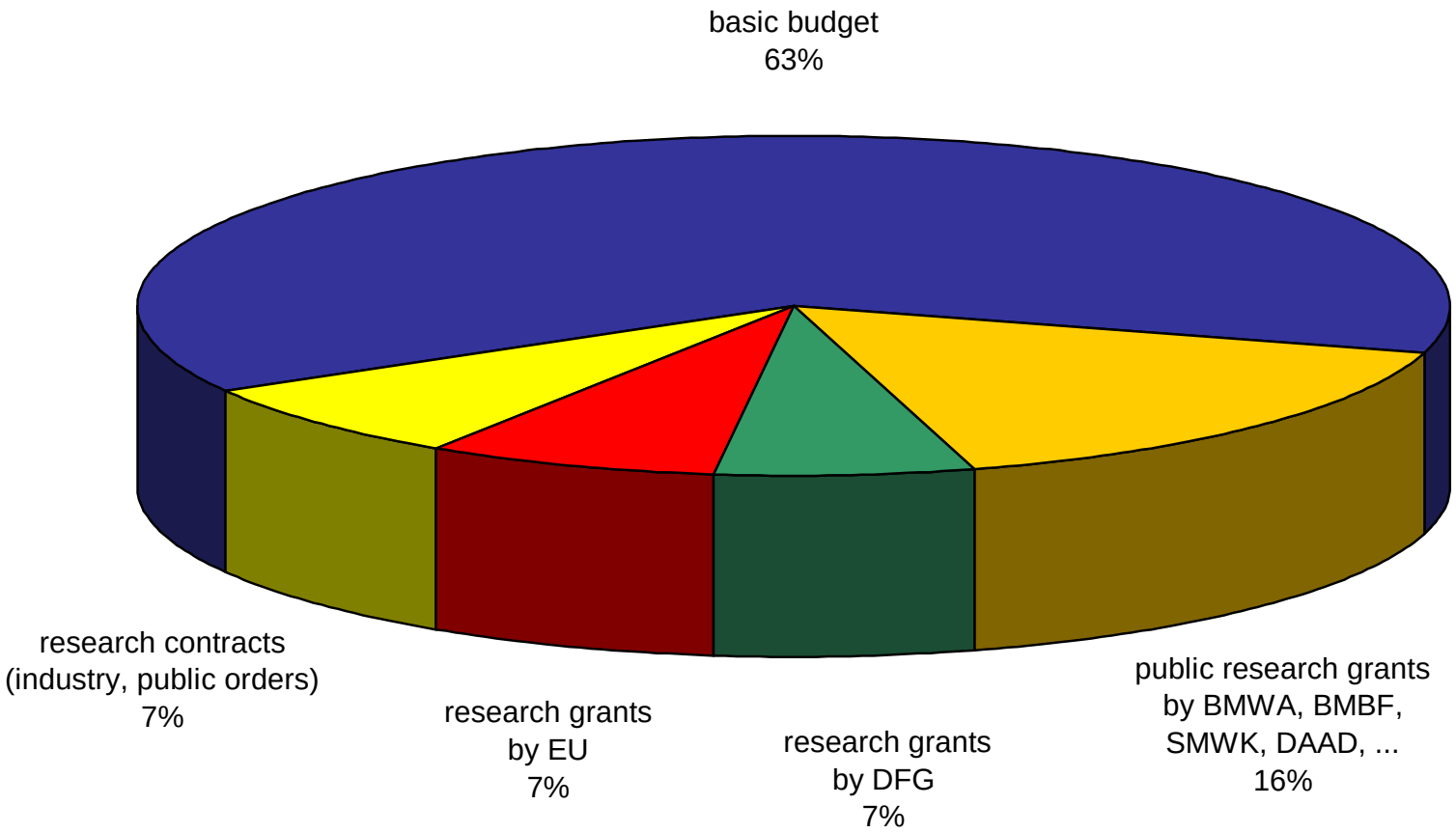

Fig. 2: Deployment of funding on the projects and user facilities 2004

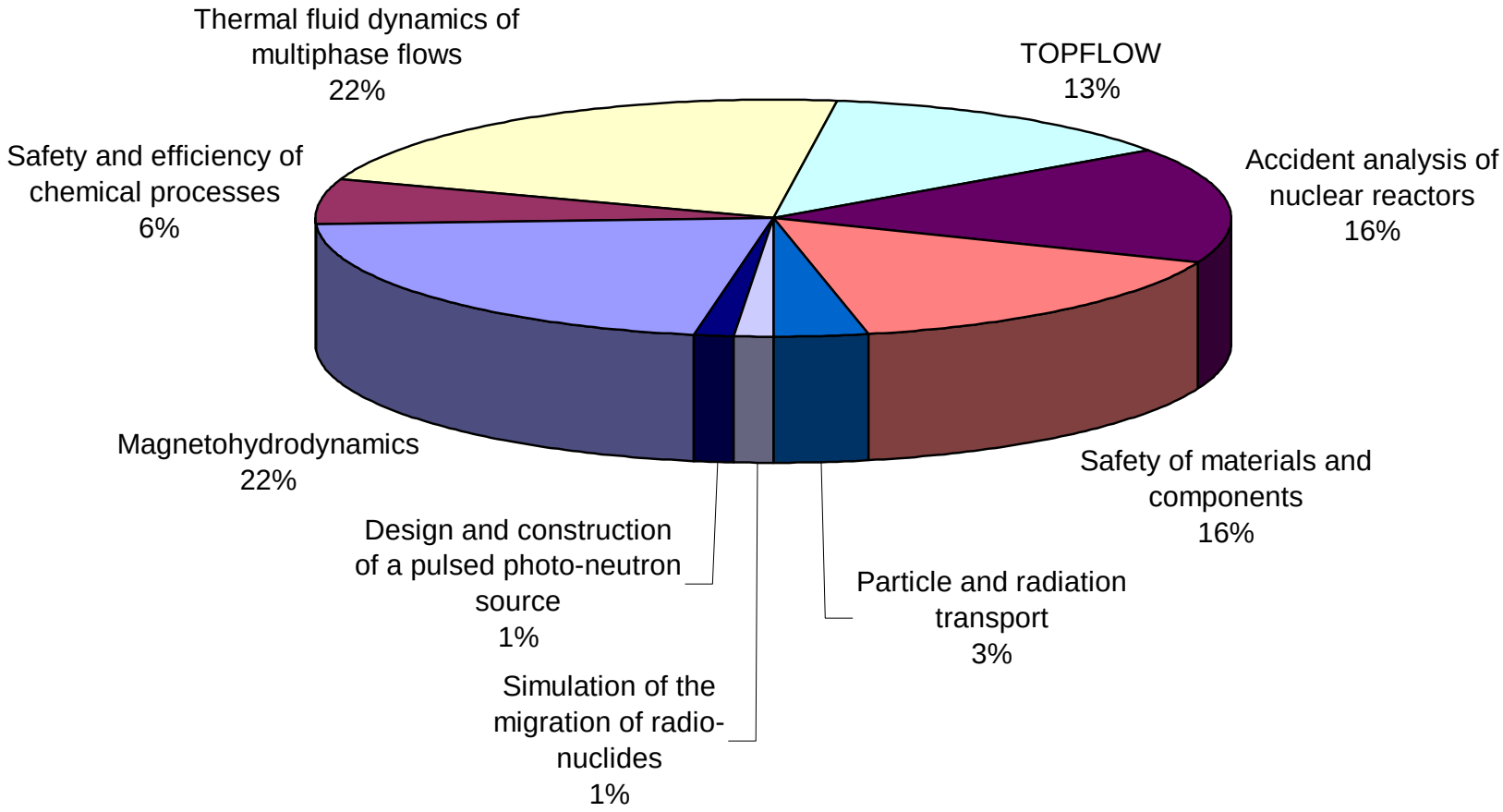

Selected reports

TOPFLOW: DESIGN, RESULTS AND PERSPECTIVES

Horst-Michael Prasser, Matthias Beyer, Helmar Carl, Sabine Gregor, Annalisa Manera, Heiko Pietruske, Peter Schütz, and Frank-Peter Weiss

1. Introduction

TOPFLOW stands for Transient **T**w**O** **P**hase **FLOW**. The new thermal-fluiddynamic test facility of FZR was built for generic and applied studies of transient two phase flow phenomena in power and process industries and has become the reference experiment of the German CFD initiative. Coordinated by GRS, this concerted initiative unites activities of different institutions to develop and validate three-dimensional CFD for application to safety relevant flow simulations in the field of nuclear reactor safety. The reference code chosen for this purpose is CFX. In course of the ongoing research project, FZR has established a close and very fruitful cooperation with the code developer ANSYS-CFX.

The introduction of CFD in the field of reactor safety research is connected with high expectations concerning the quality of the predictions compared to the established one-dimensional thermal hydraulic analyses, since CFD allows to substitute geometry-dependent empirical closure relations by more physically justified closure laws that are formulated on the scale of the structures of the gas-liquid interface. In this way, modelling becomes much more independent from geometrical and thermodynamic boundary conditions and the scale-up to the real reactor becomes more reliable than in case of traditional thermal hydraulic codes.

TOPFLOW is not a dedicated integral test modelling a specific reactor type. It was rather designed as a multi-purpose facility for different single-effect experiments. Object of the experimental studies is a gas-liquid two-phase flow. The latter includes, for instance, investigations of innovative and passive safety systems, like the emergency condenser for boiling water reactors, a model of which is a major component of TOPFLOW. A carefully designed instrumentation including advanced two-phase flow sensors of own development delivers experimental data of high quality, that reflect the addressed phenomena and processes in the necessary detail.

2. History

The new test facility in Rossendorf was constructed using parts of NOKO, a test facility which was successfully operated at the Forschungszentrum Jülich [1] to study passive emergency core cooling systems of novel BWRs. NOKO was dismantled in 2001, the electrical heater and the condenser tank were transferred to the new site in Rossendorf and completed by new components and instrumentation. In the end of 2002 the facility was completed and reached nominal working parameters. The final licence to operate TOPFLOW at high pressure was granted in September 2003. In parallel, the development of instrumentation was continued. The first scientific steam-water experiments at nominal pressure were started in May 2004 with tests in the small test section of DN50. In September 2004 the tests were extended to the DN200 pipe.

The ongoing research project that involves TOPFLOW experiments is entitled "Construction and execution of experiments at the multi-purpose thermal hydraulic test facility TOPFLOW for generic investigations of two-phase flows and the development and validation of CFD codes".

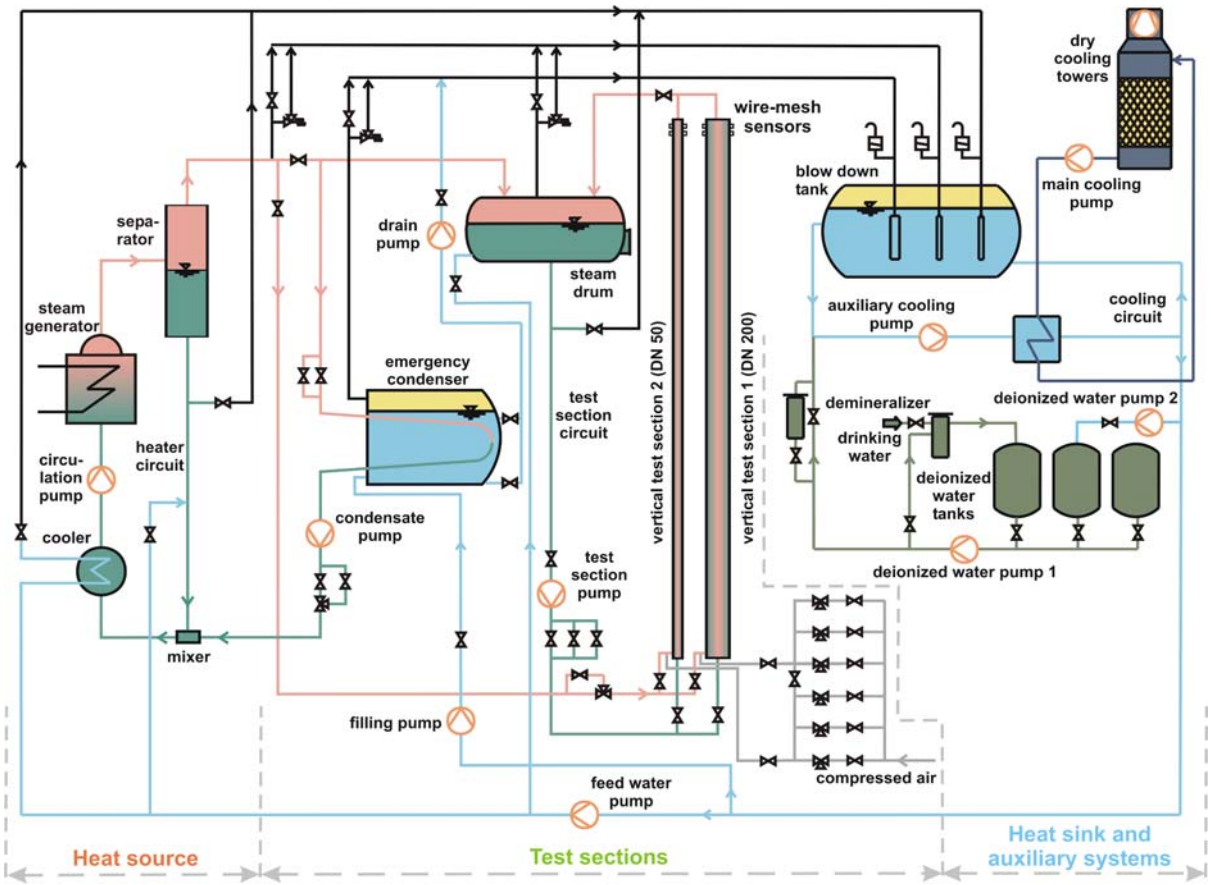

Fig. 1: General scheme of the TOPFLOW facility

It is financed by the German Federal Ministry of Economics and Labour for the period from April 2002 to March 2006. In October 2003 it was decided to significantly extend TOPFLOW for a primary circuit hot-leg test being part of this project. The test will be accommodated in a new wing of the TOPFLOW building which was erected in 2003. The equipment is presently under construction. For the future, it is planned to acquire EU projects, industry contracts and to obtain the status of an international large scale facility.

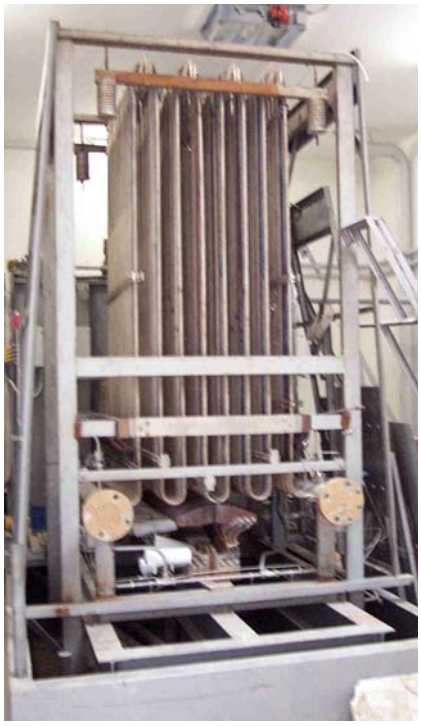

Fig. 2: Heated tubes of the TOPFLOW steam generator

3. Concept of the test facility

An electrical steam generator with a power of 4 MW representing the heat source of the facility and a heat sink consisting of a blow-down tank to quench the exhaust steam, the cooling circuit and the dry cooling tower system are two main infrastructural components of TOPFLOW. Between these two ends the flow passes through various test rigs, which represent the multi-purpose test facility (Fig. 1). The steam is generated in 24 directly electrically heated stainless steel pipes (Fig. 2), supplied from a power transformer. The heater circuit can be operated up to a pressure of 10 MPa and generate about 2 kg/s saturated steam at this pressure. For the time being

TOPFLOW is licensed for an operation at 7 MPa and 286 °C. The main components of TOPFLOW are in the central part of the building shown in Fig. 3, while dry cooling towers can be seen on top of the roof of the mechanical shop in front of the main building. The pressure chamber for the PWR hot-leg test is located in a new wing attached on the right side, which is not visible in Fig. 3.

Fig. 3: TOPFLOW building with dry cooling system on top of the roof of the left wing

The main experimental test rigs are (1) two vertical test sections DN50 and DN200 for basic two-phase flow studies, (2) the emergency condenser test (Fig. 4) and (3) the pressure chamber presently housing the PWR hot-leg experiment being under construction. The vertical test sections are equipped with a test section pump for the water circulation up to 50 kg/s, a steam supply system with mass flow meters and a steam drum for the separation of the two-phase mixture at the outlet of the test sections. The steam drum itself is equipped with flange ports to connect further test sections, like heat exchanger bundles or material samples, to a hot steam-water atmosphere.

Fig. 4: View of TOPFLOW with the BWR emergency condenser test in the foreground

Attention was paid to the accurate steam and water mass flow measurements, which are performed by multi-strand standard nozzle meters designed for an accuracy of 1 % over a mass flow range of 5 decades. Additionally to the high pressure operation it is possible to perform experiments with an air-water flow. For this purpose, TOPFLOW is equipped with an air supply and metering station with a capacity of 850 m^3/h (standard cube meters) taken from the central pressurised air network of the research centre.

4. Vertical test sections

4.1 Air-water tests on flow structure and scaling effects

The first tests carried out on TOPFLOW were aimed at the structure of a gas-liquid two-phase flow in pipes of large diameter. First results were published at the NURETH-10 conference in Seoul [2], the paper won the "Best Paper Award 2004" of the Thermal Hydraulic division of the American Nuclear Society.

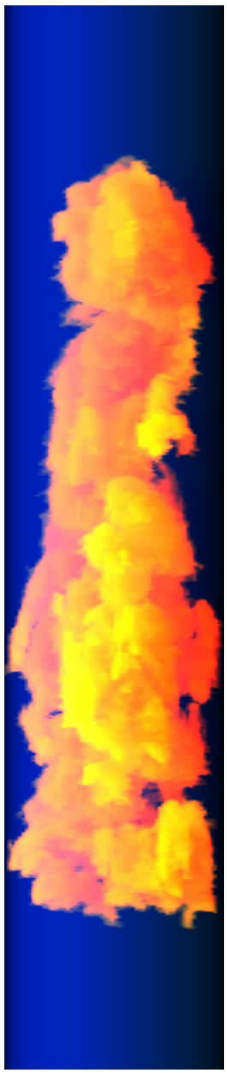

Fig. 5: Isolated large bubble in a churn-turbulent flow in the DN200 test section, J_l = 1 m/s, J_g = 1.3 m/s

The new quality of the measurements at TOPFLOW is based on the availability of wire-mesh sensors [3], which deliver sequences of complete two-dimensional gas fraction distributions from the entire cross section. Even in the large cross-section of the DN200 pipe, a high spatial resolution of 3 mm and a frame rate of 2500 Hz is achieved [4]. This offers excellent conditions for detailed studies on the structure of the gas-liquid flow in large pipes and on scaling effects. A region of well-organised slug flow is no longer observed in pipes of large diameter, which confirms the findings of other authors (e.g. [5]). Rather an immediate transition from bubbly to churn turbulent flow takes place. Irregularly formed large bubbles replace the well-shaped Taylor bubbles found in small pipes. Such bubbles were visualised for the first time (see again [2]). The distortion of the large bubbles is caused by the action of turbulence. Their shape was analysed by separating individual bubbles from the three-dimensional measuring information of the wire-mesh sensors (Fig. 5).

Using the data obtained by a pair of wire-mesh sensors placed shortly behind each other, a novel method for measuring the turbulent dispersion of the gaseous phase was developed. The time delay between signals taken from two identically located measuring points of both sensors obtained by cross-correlation characterises the travelling time of the gaseous phase and can be used to calculate radial velocity profiles. A correlation is also found between measuring points located not exactly above each other, though the maximum cross-correlation coefficient decreases with growing lateral distance. This points at the fact that bubbles are transported not only in the main flow direction, but also perpendicular to it, which is a result of the turbulent motion of the fluid.

The cross-correlation coefficient plotted over the lateral distance is called spatial cross-correlation function (Fig. 6, CCF). The width of the peak carries the desired information about the turbulent diffusion coefficient. To extract this value, it is necessary to correct for a contribution of the finite bubble size to the width of the peak, which is explained by the fact that bubbles usually contact more than one measuring point of the sensors at the same time. This results in a correlation over a lateral distance even within the measuring plane of the first sensor alone (spatial auto-correlation function, Fig. 6, ACF). The evaluation was performed by seeking the transfer function G(r) that transforms the spatial auto-correlation function into the spatial cross-correlation function. It is the idea behind this approach that the spatial cross correlation function CCF is a result of the

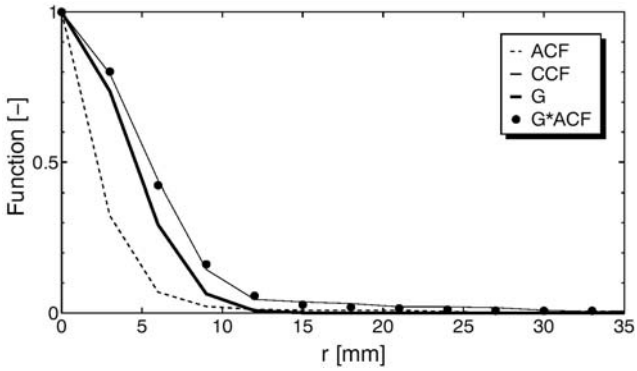

Fig. 6: Cross-correlation coefficients between measuring points of two successive (CCF) or, respectively, one and the same (ACF) mesh sensor as function of their lateral distance and the transfer function G(r) between ACF and CCF

widening of the auto-correlation function ACF by the action of the turbulent diffusion. A Gaussean standard distribution used as a prototype for the transfer function is fitted to the experimental data by numerical deconvolution. The dispersion of the distribution is directly proportional to the turbulent diffusion coefficient. The results are shown in Fig. 7, where the turbulent diffusion coefficient is presented as function of the superficial air and water velocities. For the first time, values of the turbulent diffusion coefficients are experimentally derived at high gas superficial velocities and for slug/churn flow regimes. A paper about these new results was forwarded to the International Journal of Multiphase flows [7].

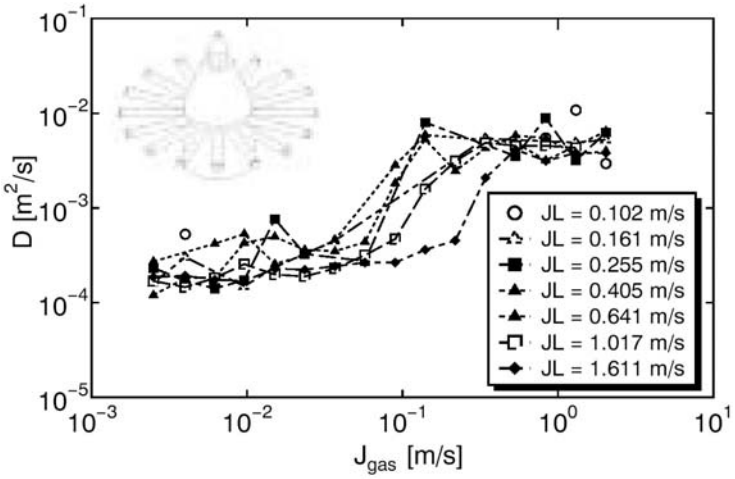

Fig. 7: Turbulent diffusion coefficients extracted from cross-correlation functions as shown in Fig. 6 as a function of the superficial gas and liquid velocities

4.2 Evolution of the gas-liquid interface along the flow direction

One of the important tasks of the experiments at the vertical test sections is the derivation of geometry-independent closure relations for forces acting at bubbles as well as for bubble coalescence and fragmentation rates. Both phenomena are reflected by the evolution of the bubble size distribution along the flow path (see Fig. 13 in section 4.4). In previous projects, the distance between the gas injection and the mesh sensors was varied at identical superficial air and water velocities and bubble size distributions were measured [8]. This was done by a cumbersome disassembling the facility each time when the distance was changed. In case of the large test section of TOPFLOW a more efficient solution was necessary.

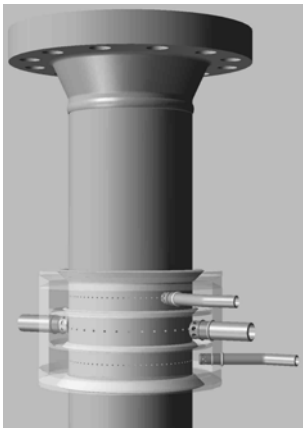

Fig. 8: Three-chamber gas injection unit

To that end the so-called "variable gas injection system" was constructed. The new test section is equipped with gas injection units at six different heights. Each unit has three annular distributing chambers, from which gas or

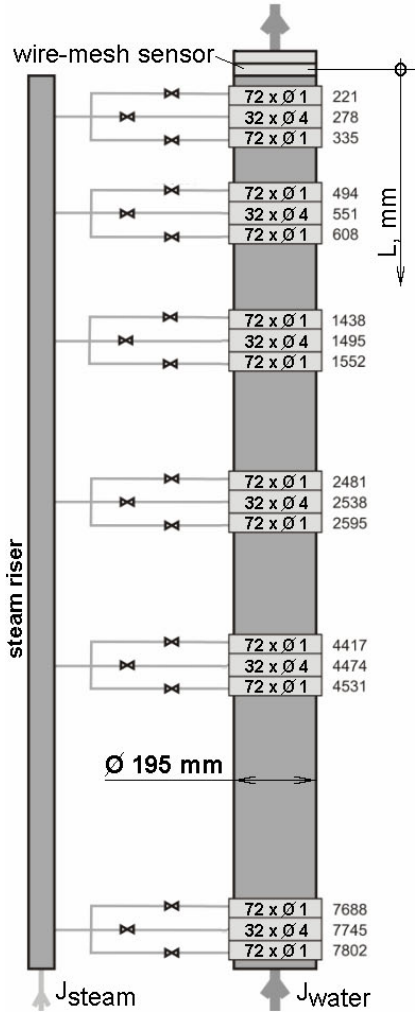

Fig. 9: Vertical test section with variable gas injection system

steam enters the test section via a number of orifices in the pipe wall (Fig. 8). Two different injection diameters allow to change the primary bubble size and to study its influence on the flow structure. In particular, the upper and the lower chambers have 72 orifices of 1 mm diameter, the central chamber has 32 orifices of 4 mm. The achievable combinations of inlet lengths are summarized in Fig. 9.

An extensive test programme was accomplished at the variable test section. Measurements were taken for all feasible inlet lengths (until a certain limit of the gas flow rate all 18 distributing chambers can be operated, at higher gas flow only the chambers with 4 mm orifices) at 21 different combinations of superficial air and water velocities. Again, an assembly of a pair of wire-mesh sensors, each with 64x64 measuring points, was used.

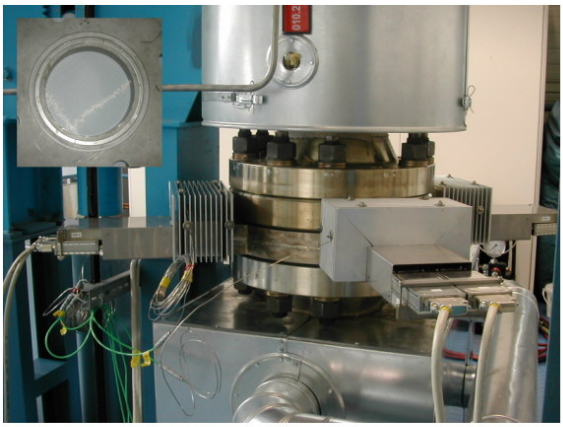

Wire-mesh sensor mounted in the DN200 pipe with cooling bodies

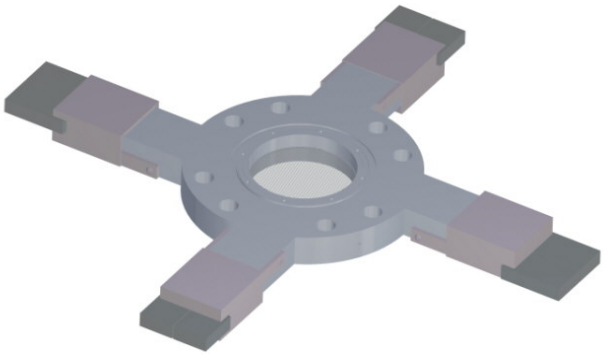

3D CAD model of the high-pressure sensor

Fig. 10: Wire-mesh sensor for the DN200 pipe, working parameters: 7 MPa, 286 °C

4.3 Adiabatic steam-water experiments at high pressure

The variable test section was used for first steam-water experiments at high pressure after the efforts were successful to construct a wire-mesh sensor for 70 bar and 286 °C. Despite of the difficult task to arrange a large number of pressure resistant bushings for the electrode wires, the high spatial resolution of previous air-water sensors could be maintained, i.e. the new sensor has again a measuring matrix of 64x64 cross points, which results in a lateral resolution of 3 mm (Fig. 10).

Tests were carried out at 10, 20, 40 and 65 bar pressure under saturation conditions. The superficial velocities as well as the inlet length were varied. Virtual side projections of the transient void fraction distribution and central side cuts along the pipe axis are shown in Fig. 11 for a test at 65 bar and a relative distance between steam injection and sensor of L/D = 40. A comparison with air-water tests at the same combinations of superficial velocities reveals the influence of the physical properties of the fluid

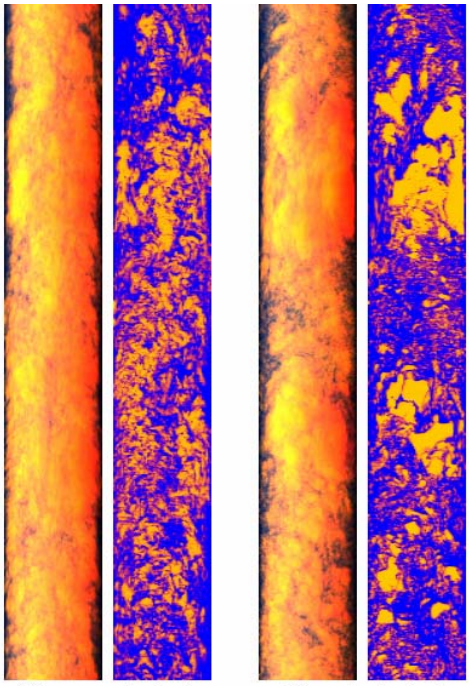

Steam-water test at 6.5 MPa

Air-water test at ambient pressure

Fig. 11: Influence of pressure and temperature on flow structure, J_l =1 m/s, J_g = 0.54 m/s, L/D=40

on the flow pattern. The flow structure appears more fine dispersed in the high-pressure test. This is due to lower surface tension and viscosity at high temperature conditions compared to the air-water test. It is planned to extend the experiments to correlation studies similar to those reported in section 4.1. This requires an installation of a second high-pressure sensor, which will be available in early 2005.

4.4 Steam condensation in contact with sub-cooled water

The implementation of boiling and condensation mass transfer models in CFX is an important task that is envisaged for the second stage of the German CFD initiative starting in 2006. In order to support the definition of the theoretical tasks and to prepare the necessary experiments, preliminary studies were carried out on steam condensation in sub-cooled liquid due to interfacial heat transfer. A limited sub-cooling between 2 and 6 K was induced by throttling the flow at the outlet of the test section a few meters downstream of the wire-mesh sensor position.

The obtained experimental data allow to correlate the intensity of steam condensation in contact with sub-cooled water at elevated pressures with the structure and extension of the interfacial area, which is essential for the model development. Virtual side projections from the mesh sensor signals are shown in Fig. 12, which in the same time illustrate the capabilities of the vertical test section with variable gas injection.

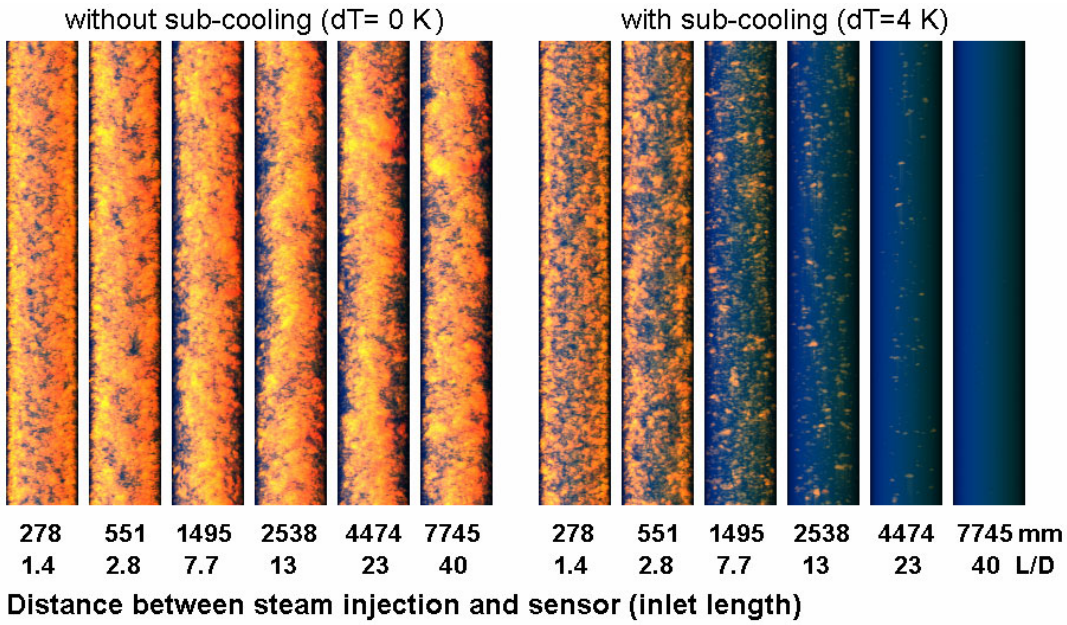

Fig. 12: Virtual side projections of sequences of 2D gas fraction distributions recorded by the wire-mesh data (p = 20 bar, J_{water} = 1 m/s, $J_{0,steam}$ = 0.54 m/s)

Steam bubbles, first found close to the wall, tend to move towards the centre with growing distance from the injection unit. An irregular churn-turbulent flow is formed. In case of sub-cooled water, condensation is superposed to this process. Consequently, size and number of the bubbles decrease. In case of no condensation, bubble size distributions soon converge to an equilibrium (Fig. 13, left side), while the volume sinks caused by condensation do not allow the equilibrium distribution to establish (Fig. 13, right side).

To meet the needs of the code developers, the tests have to be repeated with an extended instrumentation allowing to characterise local sub-cooling close to the measuring planes of the

mesh sensors, to obtain more information on axial void fraction profiles and to increase the range of the sub-cooling by means of a cold water injection system at the bottom of the test section. These extensions are planned for the future.

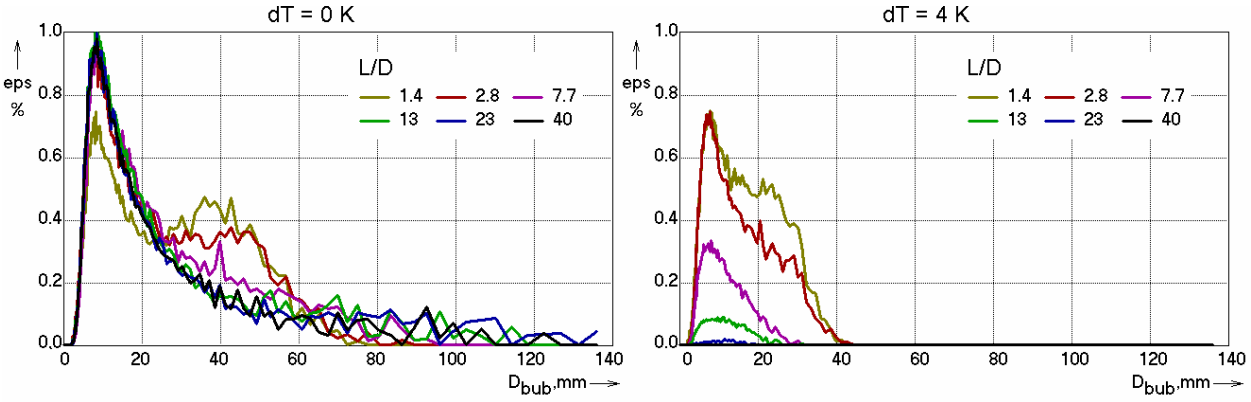

Fig. 13: Bubble size distributions extracted from the mesh sensor signals

4.5 Validation tests in a complex flow geometry

Based on the experiments at the vertical test sections, a novel bubble population model was proposed, which was implemented into CFX. An alpha version of the code release CFX-5.8 containing the new multiphase multi-bubble-class model (inhomogeneous MUSIG) was recently made available to FZR for testing. Beside the verification on experimental data from the vertical test sections it has to be demonstrated that the upgraded CFD code is now capable of correctly responding to more complex boundary conditions. In particular, it has to be shown that the prediction of the flow and gas fraction fields remain correct also when the stream lines have a more pronounced curvature and the flow direction differs significantly from the direction of the action of gravity, which is not the case in the vertical pipes. For generating the necessary validation data, it is favourable to obtain three-dimensional fields in a flow region disturbed by an obstacle. Unfortunately, the wire-mesh sensor can hardly be designed to be movable along the pipe axis for practical reasons, especially in case of high-pressure tests. To solve the problem a special methodology was developed, where the sensor remains stationary and the obstacle - a half-moon diaphragm - is moved up and down in the DN200 test section (Fig. 14). This set-up will allow the registration of the three-dimensional gas fraction field around the obstacle for air-water and steam-water experiments up to the maximum pressure of TOPFLOW. The field can be measured both upstream and downstream of the diaphragm, since the installation shown in Fig. 14 can either be flanged from below or from above after inverting it. The mechanism has recently been built, experiments are planned for early 2005.

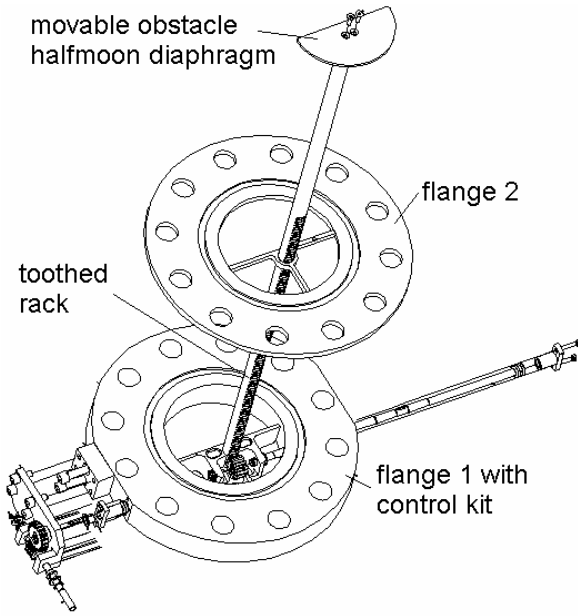

Fig. 14: Movable obstacle for CFD code validation in a situation with complex boundary condition

5. Passive emergency core cooling system tests

The emergency condenser developed for the boiling water reactor SWR-1000 is a heat exchanger with horizontally oriented tubes which are permanently connected with the reactor vessel. In case of a level decrease in the reactor the normal water inventory of these tubes is replaced by steam due to the effect of communicating vessels. In this way, the decay heat removal by condensation starts without active measures. The heat is transferred to the core flooding pool, filled with 3600 m³ of water. The condenser test facility models a segment of 8 heat exchanger tubes of the original (Fig. 15).

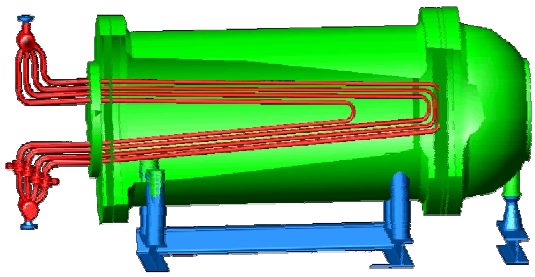

Fig. 15: CAD image of the emergency condenser tank with heat exchanger tubes

Experiments to demonstrate the function of the emergency condenser were already performed in Jülich [9]. The condenser test was incorporated into the TOPFLOW facility in order to allow for an accurate determination of the heat removal capacity with an improved mass flow instrumentation. Experiments were performed at a reactor pressure of up to 7 MPa, where four of the eight heat exchanger pipes were sufficient to remove a power of 3.7 MW.

A major concern is not to exceed the design pressure of the containment during operation of the emergency condenser. A significant pressure increase is expected when the water at the free surface reaches saturation temperature, which was found to depart significantly from the average temperature in the pool due to stratification effects [10]. This means that the pressure history in the wet well is not directly connected with the transferred energy but is result of a complex fluid-dynamic phenomenon - the natural circulation in the core flooding pool, which requires CFD calculations for correct predictions. For these stratification studies, numerous thermocouples were distributed inside the tank. Measurements of the temperature field were taken during the heat-up phase of heat removal capacity measurements. It was shown, that a strong stratification is established that vanishes only when finally saturation is reached in the entire cooling water volume. The data will again be used for CFD code validation.

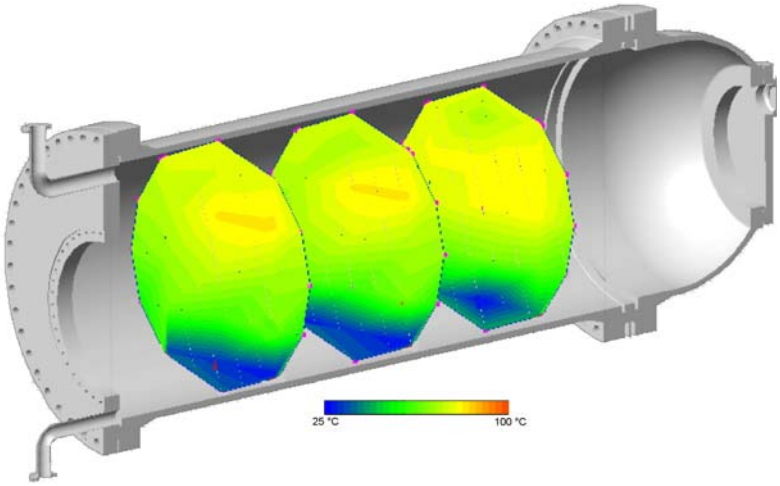

Fig. 16: Temperature stratification on the secondary side of the emergency condenser model after 3/4 of the heat-up time, primary pressure 6.6 MPa, secondary pressure 0.14

6. PWR hot-leg test in a pressurised tank

Within the ongoing TOPFLOW project measurements on the structure of the free surface in the hot leg of a PWR during a reflux-condenser mode are planned. In such a case, the reactor level has decreased below the coolant outlet nozzle due to a loss-of-coolant event. Subsequently steam is flowing in the main coolant lines towards the steam generators. There, it is condensed, which makes up an efficient decay heat removal mechanism, as long as the con-

densate returning to the reactor in a counter-current flow is not obstructed by the steam flow. The phenomenon is called counter-current flow limitation (CCFL) and was extensively studied at the UPTF test facility in Mannheim [11]. CFD codes are still not able to predict CCFL, which would be highly desirable to understand the effect in more detail and to increase the flexibility of predictions.

For the CFD code validation it is more important to ensure a good access for measurements than to create an exact geometric similarity with the original. Therefore, we decided to model the main cooling line by a channel with a rectangular cross section of 250 mm height and 50 mm width instead of a cylindrical pipe (Fig. 17). The channel will be formed by glass side walls to access the flow with optical instrumentation. In the beginning this will be a high-speed digital video camera to register the dynamics of the gas-liquid interface. Later, other techniques like PIV or LDA will be applied.

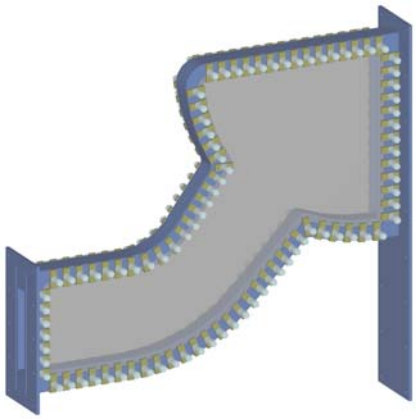

Fig. 17: Glass covered part of the PWR hot-leg test modeling the steam generator entrance

The lack of experimental data of the mentioned kind mainly concerns the region of original pressures and temperatures, because results from air-water tests at ambient conditions are available [12]. An installation of the desired large observation windows would not be feasible at such pressures without special measures. The hot-leg test will therefore be accommodated in a pressure chamber, where it will be operated in pressure equilibrium with the inner atmosphere (Fig. 18). Compressors can increase the air pressure in the chamber to a maximum of 5 MPa, which is also the maximum operation pressure of the hot-leg test.

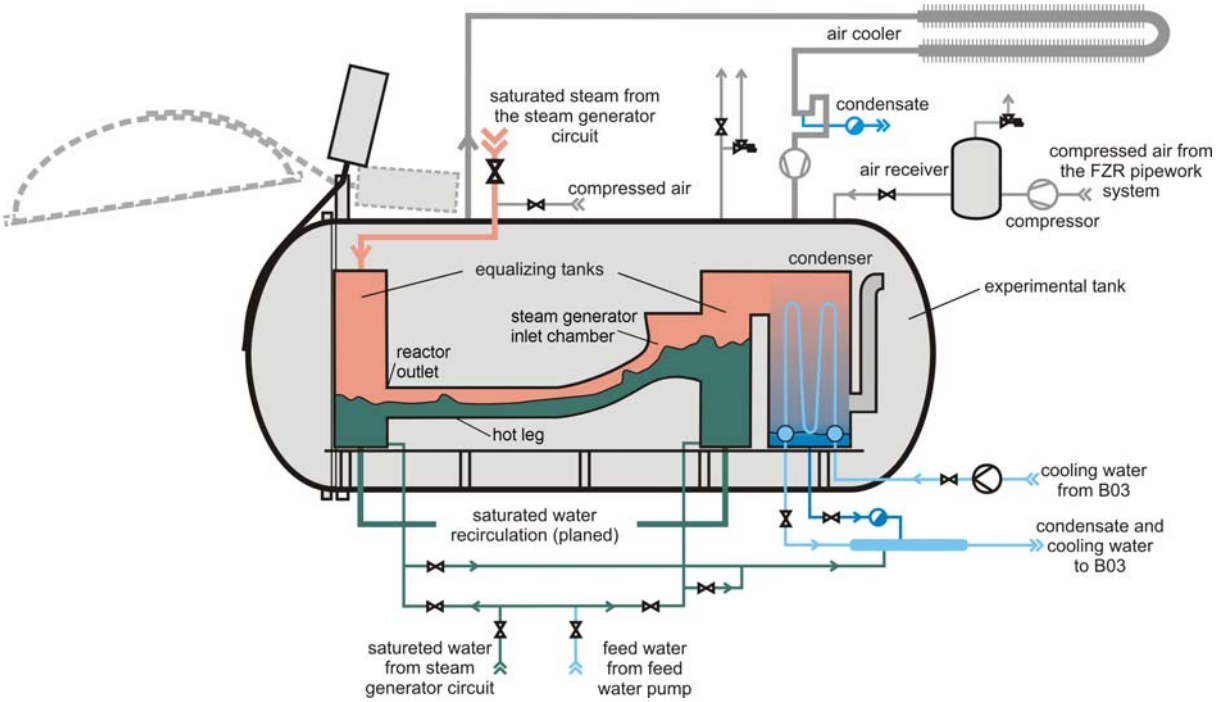

Fig. 18: Pressurised tank for tests carried out under pressure equilibrium ("Diving Chamber Technology")

The exact pressure equilibrium will be guaranteed by a built-in condenser unit, the outlet of which is permanently connected to the inner atmosphere of the tank. Stratification between condensing steam in the upper part of the condenser and the heavier air (the density relation is about 1:3) prevents steam from entering the pressure chamber. The atmosphere in the chamber will be kept below 50 °C by means of an over-roof air cooling system. This allows to put instrumentation like the high-speed camera directly in the pressure chamber.

In order to assure fast and full access to the test set-up inside the pressure chamber, it is equipped with a fast operating full-size port on one side (Fig. 18). The test facility itself can be disconnected from the condenser unit and taken out of the vessel moving it on a rail track. In front of the full-size port there will be a service platform, where parts of the facility can be assembled or dismantled. The entire set-up can also be taken off by the crane and can be replaced by another test section. There are ideas to use the chamber to perform experiments on the so-called pressurised thermal shock phenomenon occurring when cold emergency core-cooling water hits the hot reactor vessel wall.

The strategy to perform pressurised experiments in this way has got the name "Diving Chamber Technology". Main advantages are: (1) the test geometry can have an unrealisable shape for pressurising under normal conditions, (2) the manufacturing of the test section itself will be cheap, since no pressure carrying components are needed, (3) thin walls make it easy to apply instrumentation, for instance optical measurements through glass walls or temperature field measurements by directing an infrared camera to a thin metal wall, (4) no expensive licensing procedures are necessary, because the pressure chamber plays the role of a safety containment. We hope to attract also other research groups to bring their test sections for experiments to TOPFLOW.

7. Summary

The authors of the present paper want to supply a comprehensive overview on the capabilities of the multi-purpose test facility TOPFLOW. The facility is embedded into a running project on CFD code development and validation for gas-liquid flows with emphasis given to nuclear reactor applications. Air-water as well as steam-water experiments at vertical pipes of DN50 and DN200 are being carried out. Emergency condenser heat removal capacity measurements were performed. The construction of a PWR hot leg test using a completely novel experimental approach is close to be completed. It is intended to establish TOPFLOW as an international large scale test facility and to offer the experimental possibilities to external users, both in the frame of EU research projects and industry contracts.

Nomenclature

Sign	Unit	Denomination
D	m	diameter
eps	%	void fraction
G	-	transfer function
J	m/s	superficial velocity
L	m	length
p	MPa	pressure
r	m	radius
T	°C	temperature

Subscripts and abbreviations	
ACF	autocorrelation
bub	bubble
CCF	cross-correlation
DN	nominal diameter
G	gas (air)
L	liquid (water)
MUSIG	multiple size group model
PWR	pressurized water reactor
wms	wire-mesh sensor

Acknowledgements

The authors thank the technical team of TOPFLOW, by name Klaus Lindner, Heiko Rußig, Marko Tamme und Steffen Weichelt. Significant support was given by Forschungszentrum Jülich by granting former NOKO equipment to FZR. The companies involved in construction and commissioning of TOPFLOW are Bick & Letzel, AMS Leipzig, SAAS GmbH Possendorf, ERTECH Energie- u. Rohrtechnik Ing.-Büro GbR, KSC Cottbus, Kress Maschinen- und Anlagen Konstruktions GmbH Großostheim, as well as the Dresden branch of IfE Leipzig and SAXOBRAZE GmbH Chemnitz. The wire-mesh sensor electronics was built by TELETRONIC GmbH. The research work is carried out in the frame of a current project funded by the German Federal Ministry of Economics and Labour, project number 150 1265.

References

[1] E. F. Hicken, A. Schaffrath, M. Fethke, H. Jaegers, Der NOKO-Versuchsstand der Forschungszentrum Jülich (FZR) GmbH - Rückblick auf 7 Jahre experimentelle Untersuchungen zur Erhöhung der Sicherheit von Leichtwasserreaktoren, Atomwirtschaft-Atomtechnik 47 (2002), Nr. 5, S. 343-348.

[2] H.-M. Prasser, M. Beyer, A. Böttger, H. Carl, D. Lucas, A. Schaffrath, P. Schütz, F.-P. Weiss, J. Zschau, Influence of the pipe diameter on the structure of the gas-liquid interface in a vertical two-phase pipe flow, NURETH-10, Seoul, October 5-9, 2003, paper A00308.

[3] H.-M. Prasser, A. Böttger, J. Zschau, 1998, A new electrode-mesh tomograph for gas-liquid flows Flow Measurement and Instrumentation, **9** (1998), 111-119.

[4] H.-M. Prasser, J. Zschau, D. Peters, G. Pietzsch, W. Taubert, M. Trepte, Fast wire-mesh sensors for gas-liquid flows - visualization with up to 10 000 frames per second, ICAPP 2002, Hollywood, Florida, paper #1055.

[5] A. Ohnuki, H. Akimoto, Experimental study on transition of flow pattern and phase distribution in upward air-water two-phase flow along a large vertical pipe, International Journal of Multiphase Flow, **26**(2000)367-386.

[6] Y. Sato, M. Sadatomi, K. Sekoguchi, Momentum and heat transfer in two-phase bubble flow. International Journal of Multiphase Flow, 7, 167-177.

[7] A. Manera, Z. Zaruba, Experimental Investigations on Bubble Turbulent Diffusion in a Vertical Large Diameter Pipe and in a Rectangular Bubble Column, Joint FZR & ANSYS, Multiphase Flow Workshop, Dresden, 28 - 30 June 2004, proceedings on CD-ROM.

[8] H.-M. Prasser, E. Krepper, D. Lucas, Evolution of the two-phase flow in a vertical tube - decomposition of gas fraction profiles according to bubble size classes using wire-mesh sensors, International Journal of Thermal Sciences, **41** (2002) 17-28.

[9] A. Schaffrath, E. F. Hicken, H. Jaegers, H.-M. Prasser, Experimental and Analytical Investigation of the Operation Mode of the Emergency Condenser of the SWR1000, Nuclear Technology 126 (1999), May 1999, p. 123-142.

[10] E. Krepper, E. F. Hicken, H. Jaegers, Investigation of natural convection in large pools on the example of heating up the secondary side of an emergency condenser, International Journal of Heat and Fluid Flow Vol. 23 (2002) pp. 359-365.

[11] UPTF-Fachtagung IV: Versuchsergebnisse, Analysen, Mannheim 25. März 1993, Siemens AG, KWU, KWU R11/93/005, 1993.

[12] G. Petritsch, D. Mewes, Experimentelle Untersuchung der Strömungsform in der heißseitigen Hauptkühlmittelleitung eines Druckwasserreaktors, BMBF Forschungsvorhaben 1501004, Abschlussbericht Teil 1, Universität Hannover, Sept. 1997.

INVESTIGATIONS ON THE STABILITY OF A BUBBLE COLUMN

Dirk Lucas, Horst-Michael Prasser, and Annalisa Manera

1. Introduction

Bubble columns are widely used in industrial applications since they enable an effective mass transfer between the gaseous and liquid phase, e.g. for heterogeneous chemical reactions. The performance of a bubble column strongly depends on the characteristics of the flow. There is a number of possibilities to characterise the flow pattern, e.g. depending on the gas volume flow rate or on horizontal or vertical positions. At least two basic flow patterns occur, mainly in dependence on the gas volume flow rate [1]. For low gas volume flow rates a more or less homogeneous flow (no large vortexes of the liquid, flat profile of the gas volume fraction, bubbles rise uniformly in nearly straight lines and have similar size) was observed. With increasing gas volume flow rates a transition to a heterogeneous regime, which is characterised by a non-regular flow pattern, that means non-regular vortexes of the liquid flow occur, the gas volume fraction is centre peaked, large bubbles are generated by coalescence and bubble rise velocities vary in a wide range (for details see e.g. [2]). If large bubbles are injected (e.g. big orifices) also a 'pure' heterogeneous regime was observed [1]. For this case the heterogeneous regime also exists for low gas volume flow rates.

The dependency of the transition on different parameters as e.g. gas flow rate, gas volume fraction, gas density, liquid viscosity or column dimensions was investigated. There are also a number of investigations on the stability of bubble columns, which aim to predict the transition between the homogeneous and heterogeneous flow regimes (e.g. [3] and [4]). Different mechanisms as the formation of vertical gas fraction waves or the maximum gas flow rate, which enables the backflow of the liquid carried up with the bubbles are considered. As a result these analyses give criteria of stability in dependence on the gas volume fraction or geometric parameters. In [3] also the influence of the deformation of large bubbles on the stability is considered by a modification of the added mass coefficient. There is no general criterion for stability, which really fits the broad spectrum of experimental data. None of the models gives an acceptable explanation for the existence of a 'pure' heterogeneous regime. The transversal lift force was not considered in any of these investigations, but should be important for the stability as shown below.

2. Influence of the lift force on stability

The transversal lift force was studied in detail for flows with strong gradients of the liquid velocity, e.g. for vertical pipe flow, since it is assumed to be proportional to the gradients of the components of the liquid velocity field. It is given by

$$\vec{F}_L = -C_L \rho_l \alpha (\vec{w}_g - \vec{w}_l) \times rot(\vec{w}_l) \,. \tag{1}$$

In bubble columns with stagnant liquid or low liquid volume flow rates this gradient is rather small. Nevertheless recent investigations [5, 6, 7] show, that it has an important influence on the flow pattern. In case of a positive lift coefficient C_L (as originally proposed) the bubbles migrate from the higher to the lower liquid velocity region, e.g. from the centre towards the wall in case of co-current upward vertical pipe flow. This force is the reason for the wall peak in the radial profile of the gas volume fraction, which is observed for small bubbles.

In a bubble column, the role of the lift force is less obvious, since it is absent in a uniform flow field. However, it can appear when a local disturbance of the gas fraction distribution is assumed. Thus, a local increase of the gas volume fraction (=bubble density) causes a local acceleration of the liquid in the upward direction, i.e. a gradient of the vertical component of the liquid velocity is generated. Such gradient is directed in the horizontal plane and according to the lift force the bubbles start to migrate in lateral direction from that region of locally increased gas volume fraction to regions with lower gas volume fraction. This is clearly a stabilising effect and simulations with CFD codes show that the lift force causes an even spreading of the bubbles over the cross section of the bubble column [5, 6]. Even if plumes of small bubbles are generated by the gas injection, they are spread uniformly over the cross section of the column [7].

Theoretical [8] and experimental [9] investigations showed, that for bubbles with large deformations a force occurs, which can be modelled with the same approach as the classical lift force, but with a negative sign of the lift force coefficient. For this reason Tomiyama et al. [9] derived a correlation of the lift force in dependence on the bubble size and material parameter according to their experimental investigations on single bubbles:

$$C_L = \begin{cases} \min[0.288\tanh(0.121\,\mathrm{Re}), f(Eo_d)] & Eo_d < 4 \\ f(Eo_d) & for \quad 4 < Eo_d < 10 \\ 0.27 & Eo_d > 10 \end{cases} \qquad (2)$$

$$with \quad f(Eo_d) = 0.00105Eo_d^3 - 0.0159Eo_d^2 - 0.0204Eo_d + 0.474.$$

Here Eo_d is the modified Eötvös number calculated with the bubble diameter in the horizontal plane d_h:

$$Eo_d = \frac{g(\rho_l - \rho_g)d_h^2}{\sigma} \qquad (3)$$

For air-water flow at ambient conditions the coefficient changes its sign at an equivalent bubble diameter (diameter of a spherical bubble for a given bubble volume) of about 5.8 mm. That means bubbles larger than such a critical diameter migrate into regions with higher liquid velocity, i.e. towards the centre of the pipe in case of co-current upward vertical pipe flow. In previous investigations this correlation of the lift force coefficient was successfully applied to vertical pipe flow (e.g. [10, 11]).

Since with a negative sign of the lift force coefficient the bubbles migrate into regions with higher liquid velocity, the lift force has a destabilising effect when bubbles large enough are present in the bubble column. Again a local increase of the gas volume fraction locally increases the vertical component of the liquid velocity. According to the lift force the large bubbles migrate into the region of increased gas volume fraction, what causes a further increase of the gas volume fraction and with that also a further increase of the liquid velocity. Thus, there is positive feedback for an initial disturbance of the local gas volume fraction on itself. The amplitude of an initial small perturbation grows and the system is thus unstable.

The only mechanism, which can counteract the growing non-uniformity of the gas fraction distribution is turbulent dispersion, which acts to smooth the gas fraction profile. It is modelled by a so called turbulent dispersion force. This force therefore always contributes to stabilise a bubble column.

From these considerations it is clear, that a bubble column with a mono-dispersed bubble flow is stabilised by the lift force – i.e. a homogeneous flow can be observed – if the bubble size is less than the critical one, at which the lift force changes its sign. For larger bubbles it is not clear whether the turbulent dispersion force is able to compensate the destabilising action of the lift force. To answer this question a stability analysis was done. In a first step, a mono-dispersed bubbly flow was assumed. Then the analysis was extended to two bubble classes – one representing bubbles lower than the critical bubble diameter and the other representing bubbles with an equivalent diameter larger than the critical diameter. Finally a simplified criterion for an estimation of the stability in case of N bubble classes or for a given continuous bubble size distribution was proposed. It is valid, if the turbulent dispersion is negligible.

3. Outline of the linear analysis of stability

In this chapter only the main ideas of the stability analysis are given. The complete analysis can be found in [12]. A homogeneous flow pattern of a bubble column without any consideration of the influence of the wall or the gas injection zone is considered (valid at an appropriate distance from the walls and the injection device). The net liquid superficial velocity of the initial state is assumed to be zero, the gas bubbles rise with a constant velocity in vertical direction z, which only depends on the bubble size and material parameter (see Fig. 1). The following approximations and assumptions are made to establish the set of partial differential equations describing the system illustrated in Fig. 1:

- the liquid velocity has only a component in the vertical direction,
- the gradients of the liquid velocity occur only in x-direction,
- pressure gradients are neglected
- the only driving force is assumed to be a local change of the averaged density.

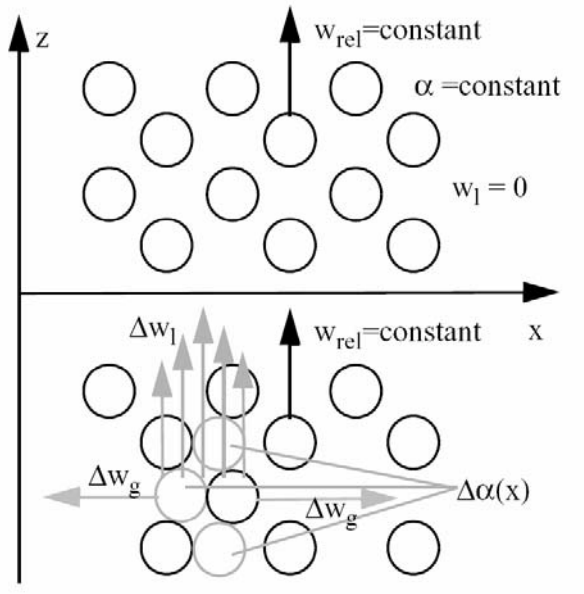

(a) undisturbed system

(b) disturbances

Fig. 1 Simplified model for the stability analysis (from [12]).

The analysis of stability takes into account the consequences of a local disturbance of the gas volume fraction $\delta\alpha(x,t)$ at a horizontal line, i.e. it is one-dimensional. Such a disturbance accelerates the liquid in vertical direction because of the lower local density. As a result

disturbances of the liquid velocity $\delta w_l(x,t)\vec{e}_z$ and of the gradient of the liquid velocity $\delta \frac{dw_l}{dx}(x,t)$ occur. Because the transversal lift force is proportional to this gradient bubbles start to migrate in the x-direction $\delta w_g(x,t)\vec{e}_x$. Depending on the sign of the lift force coefficient this migration can act to decrease (positive coefficient for small bubbles) or to increase the initial disturbance (negative coefficient for large bubbles) of the gas volume fraction. In addition the turbulent dispersion force always acts to flatten the profile of the gas volume fraction, i.e. it stabilizes the system.

Basing on the above mentioned assumptions a simplified Navier-Stokes equation for the liquid, which reflects the time and space dependent change of the vertical liquid velocity caused by a local disturbance of the gas volume fraction, can be obtained. An equation for the lateral bubble velocity is derived from the balance of the forces acting on the bubbles in lateral direction. In this balance the drag force, virtual mass force, lift force and turbulent dispersion force are considered. Finally, the set of equations is completed by the 1D continuity equation for the gas phase.

In the frame of linear stability analysis the feedback of a small initial disturbance on itself is investigated. The transfer functions characterize the effect of a Dirac-shaped disturbance of a given input parameter on the corresponding output parameter. For a compact presentation these transfer functions are derived in the Laplacian space as usual in automatic control theory. Fig. 2 shows the system considered for the analysis in case of a mono-dispersed bubble flow.

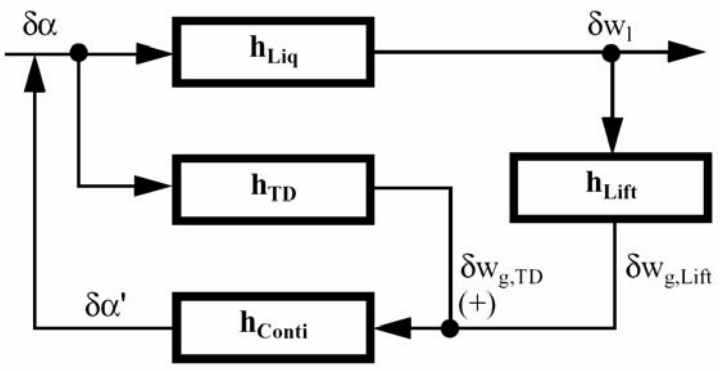

Fig. 2 Propagation and feedback of a disturbance $\delta\alpha$. The transfer functions h characterize the effects of a disturbance of an input parameter on the disturbance of the output parameter (from [12]).

The transfer function h_{Liq} describes the variation of the liquid velocity as a consequence to a perturbation of the local gas volume fraction and can be derived from the Navier-Stokes equation of the liquid, h_{TD} gives the modification of the lateral bubble velocity caused by a local modification of the gas volume fraction by the action of the turbulent dispersion force and can be deduced by the balance of forces acting on the bubbles in lateral direction, the transfer function h_{Lift} represents the modification of the lateral bubble velocity caused by a local modification of the gradient of the liquid velocity by the action of the lateral lift force, and h_{Conti} gives the modification of the local gas volume fraction caused by a modification of the lateral bubble velocity. According to the methods usual in automatic control theory a transfer function for the open system is given by

$$H^{open} = -(h_{Liq}h_{Lift} + h_{TD})h_{Conti} \tag{4}$$

As shown in [12] the feedback of an initial disturbance on itself has the same spatial

dependency as the initial disturbance itself. This result justifies the chosen one-dimensional modelling and the consideration of the amplitudes only for the transfer functions.
The system is stable, if all the poles of the closed-loop transfer function (i.e. the roots of the characteristic polynomial $1+H^{open}$) have negative real parts. To analyse the stability of the system it is not necessary to find all the roots of the characteristic polynom. The Routh-Hurwitz criterion can be applied instead. It states, that the system is stable, if all coefficients of the characteristic equation $1+H^{open} = 0$ and the so called Hurwitz determinants are positive (or have the same sign). This criterion is used for the present analysis.

4. Results of the analysis

In the result of this analysis the following condition for stability was found for mono-dispersed flow:

$$C_L > -4.44 \frac{C_D w_{rel} \nu_l}{g L^2} \tag{5}$$

Here C_D is the drag force coefficient, w_{rel} the relative velocity between gas and liquid, ν_l the kinematic viscosity, g the acceleration due to gravity and L a typical length scale for possible disturbances. For an air-water system at ambient conditions the absolute values for this expression is very small because of the small values of ν_l. The stabilising action of the turbulent dispersion force is very weak. That means that for all mono-dispersed bubble columns with a low liquid viscosity, the change of the sign of lift force can be assumed as the criterion for stability.

The analysis was extended for two bubble classes and by neglecting the turbulent dispersion force also to N bubble classes. For the latter case the following criterion was found:

$$\sum_{i=1}^{N} \alpha_i \frac{C_L^i w_{rel}^i d_b^i}{C_D^i} > 0. \tag{6}$$

This condition is proposed as an approximated, generalized criterion for the stabilizing effect of the lift force. It should be a good approximation for all cases with low liquid turbulence. For a given continuous bubble size distribution, defined on the basis of the differential volume fraction according to:

$$h(d_b) = \frac{d\,\alpha}{d\,d_b} \tag{7}$$

it can be rewritten as:

$$\int_0^\infty \frac{C_L(d_b) w_{rel}(d_b) d_b h(d_b)}{C_D(d_b)} d\,d_b > 0\,. \tag{8}$$

5. Conclusions

The investigations presented have shown, that the influence of the lateral lift force on the stability of the flow is much stronger compared to the bubble dispersion. In case of a positive sign of the lift force coefficient, as observed for small bubbles, it stabilizes the flow. For a negative sign, i.e. in case of large bubbles, it destabilizes the flow. There is a strong connection between bubble size and other parameters, e.g. the gas volume fraction. In case of a transition from the homogeneous to the heterogeneous flow regime large bubbles are generated by coalescence. As the onset of bubble coalescence is strongly connected with the

local gas volume fraction, the generation of vertical gas volume fraction waves has an important influence on the local bubble size distributions. For a general prediction of stability a combination of the different analyses including modelling of bubble coalescence and break-up is necessary.

When the gas fraction distribution has once become non-uniform, there may soon be an onset of strong coalescence in regions of increased gas fraction, which can further destabilize the column. This makes it very difficult to perform detailed measurements of the bubble size distributions in the transition region between the two regimes. For this reason there are up to now no data available, which give an experimental confirmation of the theory. A hint for the correctness of the result of the analysis, is the agreement with the findings in [1], that a 'pure' heterogeneous regime exists for gas injection devices, which produce very large bubbles.

References

[1] M.C. Ruzicka, J. Zahradnik, J. Drahos, N.H. Thomas, Homogeneous-Heterogeneous Regime Transition in Bubble Columuns, Chemical Engineering Science, vol 56, pp. 4609-4626, 2001.

[2] O. Molerus, M. Kurtin, M., Hydrodynamics of Bubble Columns in the Liquid Circulation Regime, Chemical Engineering Science, vol. 41, pp. 2685-2692, 1986.

[3] E. Leon-Becerril, A. Line, A., Stability analysis of a bubble column. Chemical Engineering Science, vol. 56, pp. 6135-6141, 2001.

[4] M.C. Ruzicka, N.H. Thomas, Buoyancy-driven instability of bubbly layers: analogy with thermal convection, International Journal of Multiphase Flow, vol. 29, pp. 249-270, 2003.

[5] E. Krepper, B.N. Reddy Vanga, H.-M. Prasser, M. Lopez de Bertodano, Experimental and Numerical Studies of Void Fraction Distribution in Rectangular Bubble Columns, 3rd International Symposium on Two-Phase Flow Modelling and Experimentation Pisa, September 22-24, 2004.

[6] S. Lain, M. Sommerfeld, LES of Gas-Liquid Flow in a Cylindrical Laboratory Bubble Column, 5th Int. Conf. on Multiphase Flow, ICMF'2004, Yokohama, Japan, May 30 - June 4, 2004, Paper No. 337.

[7] B.N. Reddy Vanga, E. Krepper, A. Zaruba, H.-M. Prasser, M. Lopez de Bertodano, On the Hydrodynamics of Bubble Columns: Comparison of Experimental Measurements with Computational Fluid Dynamics Calculations, 5th Int. Conf. on Multiphase Flow, ICMF-2004, Yokohama, Japan, May 30 - June 4, 2004, Paper No. 264.

[8] E.A. Ervin, G. Tryggvason, The rise of bubbles in a vertical shear flow, Journal of Fluids Engineering, vol. 119, pp. 443-449, 1997.

[9] A. Tomiyama, A., Struggle with computational bubble dynamics, Third International Conference on Multiphase Flow, ICMF'98, Lyon, France, June 8-12, 1998.

[10] D. Lucas, E. Krepper, H.-M. Prasser, Prediction of radial gas profiles in vertical pipe flow on basis of the bubble size distribution, International Journal of Thermal Sciences, vol. 40, pp. 217-225, 2001.

[11] D. Lucas, J.-M. Shi, E. Krepper, H.-M. Prasser, Models for the forces acting on bubbles in comparison with experimental data for vertical pipe flow, 3rd International Symposium on Two-Phase Flow Modelling and Experimentation, Pisa, Italy, September 22-24, 2004.

[12] D. Lucas, H.-M. Prasser, A. Manera, Influence of the lift force on the stability of a bubble column, Chemical Engineering Science, submitted.

DEVELOPMENT OF A MULTIPLE VELOCITY MULTIPLE SIZE GROUP MODEL FOR POLY-DISPERSED MULTIPHASE FLOWS

Jun-Mei Shi, Phil Zwart[1], Thomas Frank[2], Ulrich Rohde, and Horst-Michael Prasser

1. Introduction

Poly-dispersed multiphase flows involving particle allegation and breakage processes are widely encountered in engineering and industrial facilities. Design of these facilities and development of optimal processing techniques require a CFD tool for predicting the local particle number density and the size distribution. These quantities not only have a significant effect on the rate of mixing, reaction and the interfacial heat and mass transfer, but also a direct relevance to the hydrodynamics of the total system, such as the flow pattern and flow regime. The Multiple Size Group (MUSIG) model [1] available in the commercial codes CFX-4 and CFX-5 was developed for this purpose. Mathematically, this model is based on the population balance method and the two-fluid modeling approach. The dispersed phase is divided into N size classes. For each class a continuity equation taking into account of the inter-class mass transfer resulting from particle coalescence and breakup is derived from the population balance equation. By assuming all size groups to share the same velocity field, only one set momentum equations need to be solved for the entire dispersed phase. This assumption significantly reduces the computational cost. As a result, this model allows to use a sufficient number of particle size groups required for the coalescence and breakup calculation and has found a number of successful applications to large-scale industrial multiphase flow problems. Nevertheless, the assumption also restricts its applicability to homogeneous dispersed flows — the slip velocity of particles are approximately independent of particle size; and the particle relaxation time is sufficiently small relative to inertial time scales so that the asymptotic slip velocity may be considered to be attained almost instantaneously —. Hence we refer to the current implementation of the CFX MUSIG model as the homogeneous model.

Failures were reported in flows where this assumption ceases to be valid. One example is the bubbly flow in vertical pipes where the non-drag forces play an essential role on the bubble motion. Especially, the lift force acting on large deformed bubbles is mainly caused by the asymmetrical wake, which is in the opposite direction to the shear induced lift force on a small bubble [2,3]. For this reason, a core peak is measured for the volume fraction of large bubbles and a wall peak for those smaller [4,5]. Nevertheless, the CFX-4 MUSIG model failed to predict this bubble separation as reported in [6].

In general, the motion of particles of different sizes can be dominated by different forces or physical processes and the ratio of the particle response time to the flow convection time scale can cover a wide range. The non-drag forces on a particle are usually size-dependent. For example, we found that the turbulent dispersion of bubbles strongly depends on the particle size [6]. These inhomogeneous features in the dispersed phase are neglected in the homogeneous model. In order to take the inhomogeneous motion of different size classes into account, a full multiphase model, which treats each size group as a different dispersed phase with its own velocity field, has been proposed [8,9]. Nevertheless, this model requires to solve a complete set of transport equations of all dependent variables for each size group.

[1] ANSYS Ltd. Canada, Waterloo On.
[2] ANSYS Germany, Otterfing

Consequently, the required computational effort is as much as $N + 1$ times of a corresponding single phase flow problem. This disadvantage prevents its application to many practical multiphase flows.

In this report we summarize our efforts in developing an efficient inhomogeneous MUSIG model in cooperation with ANSYS CFX. A novel multiple velocity multiple size group model, which incorporates the population balance equation into the multi-fluid modeling framework, was proposed [10]. The original concept was to model bubbles with opposite lift force separately by using two velocity groups and allow each velocity group to have a sub-division of size classes. In this way, the inhomogeneous motion of the dispersed phase is considered efficiently along the line of the MUSIG model. This concept leads to a general framework covering all possible class model variants [11], namely dividing the dispersed phase into N fields (dispersed fluids), each allowing an arbitrary number of sub-size classes (e.g., M_i). We refer to it as the $N \times M$ model. In this sense the full multiphase model becomes the $N \times 1$ special case. The $N \times M$ model is still under evaluation and will be released in CFX5.8. Here we present the model concept and some results from pre-investigation based on the $N \times 1$ variant.

2. The $N \times M$ MUSIG model

Using the multi-fluid modeling approach we might model the dispersed phase by N fields (separated phases) according to the particle sizes to account for the inhomogeneity in the dispersed phase flow. Hence N velocity fields are to be solved for the dispersed phase. For this reason, we refer to these fields as velocity groups. We further divide each velocity group into a sub-division of size cuts (e.g., M_i) and assume that they share the same velocity field corresponding to this velocity group as in the homogeneous MUSIG model. Then only a continuity equation based on the population balance method has to be solved for the mass conservation of a sub-size class coupled with the coalescence and breakup processes. Without loss of the generality, the model equations are presented for an isothermal, laminar multiphase flow of Newtonian fluids and without mass transfer between the continuous and the dispersed phase.

The governing equations describing the mass and momentum conservation for the continuous phase are as follows:

$$\frac{\partial}{\partial t}(r_\ell \rho_\ell) + \nabla \cdot (r_\ell \rho_\ell \mathbf{U}_\ell) = 0 \tag{1}$$

$$\frac{\partial}{\partial t}(r_\ell\, \rho_\ell \mathbf{U}_\ell) + \nabla \cdot (r_\ell\, \rho_\ell \mathbf{U}_\ell \mathbf{U}_\ell) = -r_\ell\, \nabla p - \nabla \cdot (r_\ell\, \underline{\underline{\tau}}_\ell) + r_\ell\, \rho_\ell \mathbf{g} + \mathbf{F}_\ell + \mathbf{I}_\ell \tag{2}$$

where r_ℓ is the volume fraction of the continuous phase, $\mathbf{F}_\ell$ the body force excluding the gravity and $\mathbf{I}_\ell$ the momentum interaction between the continuous and dispersed phase. $\underline{\underline{\tau}}_\ell$ is the stress tensor defined as

$$\underline{\underline{\tau}}_\ell = -\mu_\ell \left(\nabla \mathbf{U}_\ell + \nabla^{\mathbf{T}} \mathbf{U}_\ell) - \frac{1}{3}(\nabla \cdot \mathbf{U}_\ell)\, \underline{\underline{\mathbf{I}}} \right) \tag{3}$$

Defining r_m to be the volume fraction of the velocity group m of the dispersed phase, its continuity equation can be written as

$$\frac{\partial}{\partial t}(\rho_m\, r_m) + \nabla \cdot (\rho_m\, r_m \mathbf{U}_\mathbf{m}) = S_m \tag{4}$$

where S_m is the mass source term, to be specified in eq. (9). The momentum equation can be expressed as

$$\frac{\partial}{\partial t}(\rho_m r_m \mathbf{U_m}) + \nabla \cdot (\rho_m r_m \mathbf{U_m U_m}) = - r_m \nabla p - \nabla \cdot (r_m \underline{\underline{\tau}}_{\mathbf{m}}) + r_m \rho_m \mathbf{g} + \mathbf{F_m} + \mathbf{I}_{\ell,\mathbf{m}} + \mathbf{I}_{\mathbf{d},\mathbf{m}} \quad (5)$$

where $\mathbf{I}_{\ell,\,m}$ represents the interaction with the continuous phase (e.g., the interfacial forces). The quantity $\mathbf{I}_{d,\,m}$ is introduced to denote the secondary momentum transfer, which is related to the mass transfer between the velocity groups resulting from particle coalescence and breakup. Specification of this term is described in detail in [10]. For simplicity the same pressure field as the continuous phase is assumed above.

The population balance equation is applied to each sub-size group. Assume that the size group i is a sub-division of the velocity group m. Defining r_d and r_i to be the volume fraction of the total dispersed phase and of the size group i, respectively, and f_i and $f_{m,i}$ to be respectively the size fraction of the size group i in the total dispersed phase and in the velocity group m, the different flavors of size fractions are related by

$$r_i = r_d f_i = r_m f_{m,i} \quad (6)$$

With these definitions, and recognizing that velocity fields are homogeneous for all size groups within a velocity group m, the population balance equation for the size group i leads to

$$\frac{\partial}{\partial t}(\rho_m r_m f_{m,i}) + \nabla \cdot (\rho_m r_m \mathbf{U}_m f_{m,i}) = S_{m,i} \quad (7)$$

where $S_{m,i}$ is the mass source term.

Then the mass source S_m in eq. (4) can be specified, i.e.

$$S_m = \sum_{i=1}^{N_m} S_{m,i} \quad (8)$$

where N_m is the number of the sub-divisions in the velocity group m, and obviously, we have $\Sigma_m S_m = 0$.

In the case that coalescence and breakup are the only mass transfer mechanism, $S_{m,i}$ can be expressed as follows

$$S_{m,i} = B_{i,B} - D_{i,B} + B_{i,C} - D_{i,C} \quad (9)$$

where $B_{i,B}$ and $D_{i,B}$ are respectively the birth and death rate of the size group i due to breakup and $B_{i,C}$ and $D_{i,C}$ are the coalescence-related counterparts. They are defined as follows

$$B_{i,B} = \rho_d r_d \sum_{j>i} B_{ji} f_j, \tag{10}$$

$$D_{i,B} = \rho_d r_d f_i \sum_{k<i} B_{ik}, \tag{11}$$

$$B_{i,C} = (\rho_d r_d)^2 \frac{1}{2} \sum_{j\le i} \sum_{k\le i} C_{jk} f_j f_k \frac{m_j + m_k}{m_j m_k} X_{jk\to i}, \tag{12}$$

$$D_{i,C} = (\rho_d r_d)^2 \sum_{j} C_{ij} f_i f_j \frac{1}{m_j} \tag{13}$$

where B_{ji} is the specific breakup rate from size group j to i, C_{jk} is the specific coalescence rate between size group j and k, m_i represents the mass of a single particle of the group i. $X_{jk\to i}$ is a factor projecting the corresponding part of the birth particle into the ith size group, defined as follows

$$X_{jk\to i} = \begin{cases} \frac{(m_j+m_k)-m_{i-1}}{m_i-m_{i-1}} & \text{if} \quad m_{i-1} < m_j + m_k \le m_i \\ \frac{m_{i+1}-(m_j+m_k)}{m_{i+1}-m_i} & \text{if} \quad m_i < m_j + m_k < m_{i+1} \\ 1 & \text{if} \quad m_j + m_k \ge m_{max} = m_i \\ 0 & \text{else} \end{cases} \tag{14}$$

with $\Sigma_i X_{jk\to i} = 1$. In addition, the sum of the net mass source over all size groups should vanish, i.e. $\Sigma_i (B_{i,B} - D_{i,B}) = 0$ and $\Sigma_i (B_{i,C} - D_{i,C}) = 0$.

3. Results based on the N × 1 variant

The $N \times M$ MUSIG model is to be released as a CFX5.8 new feature after the validation and evaluation. As a pre-investigation, the $N \times 1$ variant was implemented and applied to gas-liquid flows in a vertical pipe with an inner diameter D=195.3 mm, a test section of the TOPFLOW facility at FZR [12]. Detailed results were presented in [13]. As an example, the numerical results for the radial distribution of the bubble volume fraction α_g of both the total gas phase (r_d) and each velocity group (r_m) at various distances from the injection plane are displayed in Fig. 1 for the test case 074 corresponding to a superficial velocity of 0.0368 m/s for air and 1.017 m/s for water. A number of 4 velocity groups was applied in the simulations and the gas was assumed to be incompressible. The experimental data measured using the wire-mesh sensor technique [12] were also plotted for comparison. The gas was injected from 144 nozzles of 1 mm in diameter in experiments. In simulation the gas injection from each nozzle was approximated by a point mass source. The results confirm that the current model is capable of predicting the separation of bubbles of different size classes and the development of the radial distribution of the gas volume fraction along the pipe. Relatively larger deviations are observed between the simulation and measurements in the cases of smaller distances between the measurement plane and the gas injection. This is mainly due to the approximation introduced for the gas injection condition. In addition, the non-drag force models applied here have only been validated for fully developed flows rather than the developing flows close to the injection plane. Also, different from the simulation, the wire-mesh sensor was fixed in the experiments and measurement data were obtained by varying the gas injection planes. This causes offsets in the hydrostatic pressure between the corresponding

positions in measurements and in simulation. Further investigation is to be carried out to evaluate the effects of these causes. Besides, the investigations also indicate a need in validation of the coalescence and breakup models.

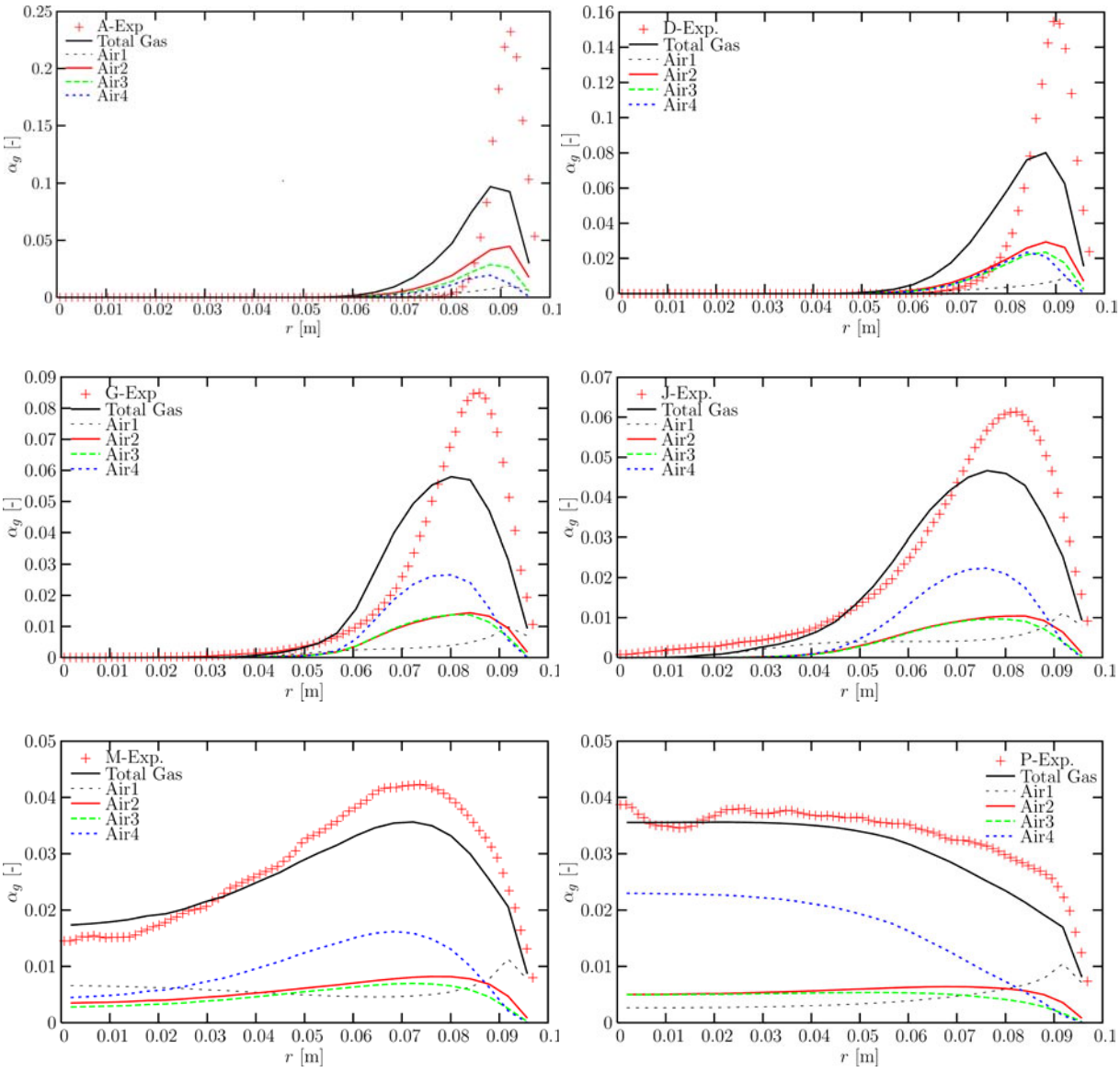

Fig. 1: Experimental and numerical results for the radial distribution of the gas volume fraction in a vertical pipe for the test case 074. The measurement planes denoted by A, D, G, J, M and P correspond to a distance 0.221, 0.494, 1.438, 2.481, 4.417 and 7.688 m, respectively, away from the gas injection.

4. Summary

A generalized multiple velocity multiple size group ($N \times M$ MUSIG) model applicable to inhomogeneous poly-dispersed multiphase flows is developed in cooperation with ANSYS CFX. The preliminary investigations using the $N \times 1$ variant show that this model is able to predict separation of bubbles of different sizes and the development of the radial distribution of the gas volume fraction along the pipe. The results also suggest a need in validation of the non-drag force models for developing flows and the coalscence and breakup model.

References

[1] S. Lo. Application of population balance to cfd modelling of bubbly flow via the MUSIG model. Technical Report AEAT-1096, AEA Technology plc, 1996.

[2] A. Tomiyama. Struggle with computational bubble dynamics. In Third International Conference on Multiphase Flow, ICMF 98, Lyon, France, 1998.

[3] A. Tomiyama, A. Sou, I. Zun, N. Kanami, and T. Sakaguchi. Effect of Eötvös number and dimensionless liquid volumetric flux on lateral montion of a bubble in a liminar duct flow. In A. Serizawa, T. Fukano, and J. Bataille, editors, Advances in Multiphase Flow, pages 3–15. Elsevier Science, 1995.

[4] H.-M. Prasser, E. Krepper, and D. Lucas. Evolution of the two-phase flow in a vertical tube - decomposition of gas fraction profiles according to bubble size classes using wire-mesh sensors. Int. J. of Thermal Sciences, 41:17–28, 2002.

[5] D. Lucas, E. Krepper, and H.-M. Prasser. Evolution of flow patterns, gas fraction profiles and bubble size distributions in gas-liquid flows in vertical tubes. Transactions of the Institute of Fluid-Flow Machinery, 112:37–46, 2003.

[6] E. Krepper and H.-M. Prasser. Measurements and CFX simulations of a bubbly flow in a vertical pipe. In AMIFESF Workshop, Computing methods for two-phase flow, pages 1–8. 2000.

[7] J.-M. Shi. Evaluation of turbulent dispersion of bubbles using a poly-dispersed model. Presentation at the 2004 Meeting of German CFD Association in Nuclear Safety Research, Rossendorf, May 05, 2004.

[8] P.M. Carrica, D. Drew, F. Bonetto, and R.T. Lahey Jr. A polydisperse model for bubbly two-phase flow around a surface ship. Int. J. Multiphase Flow, 25:257–305, 1999.

[9] A. Tomiyama and N. Shimada. A numerical simulation of bubble columns using a 3D multi-fluid model. In Proceedings of 3rd International Conference on Multiphase Flow (CD-ROM), Lyon, France, 1998.

[10] J.-M. Shi, E. Krepper, D. Lucas, and U. Rohde. Some concepts for improving the MUSIG model. Technical report, Institute of Safety Research, Forschungszentrum Rossendorf, March, 2003. submitted to CFX Germany.

[11] P. Zwart, A. Burns, and C. Montavon. Multiple size group models. Technical report, AEA Technology plc, Novermber, 2003. CFX-5.7.

[12] H.-M. Prasser, M. Beyer, A. Böttger, H. Carl, D. Lucas, A. Schaffrath, P. Schütz, F.-P. Weiss, J. Zschau. Influence of the Pipe Diameter on the Structure of the Gas-Liquid Interface in a Vertical Two-Phase Pipe Flow. 10th International Topical Meeting on Nuclear Reactor Thermal Hydraulics (NURETH-10), Seoul, Korea, October 5-9, 2003; Conference Proceedings CD: A00308.

[13] J.-M. Shi, T. Frank, H.-M. Prasser, and U. Rohde. $N \times 1$ MUSIG model — implementation and application to gas-liquid flows in a vertical pipe. In ANSYS CFX & ICEM CFD Conference 2004, Dresden, 10.-12. November, 2004.

Acknowledgments

The model was proposed based on the extensive investigations carried out in Forschungszentrum Rossendorf. The financial support from Ministry of Economy and Labor (BMWA) of Germany to the project “TOPFLOW - Transient two phase flow test facility for generic investigation of two phase flows and further development and validation of CFD codes” is gratefully acknowledged. Thank Alan Burns (CFX Europe, Harwell) for valuable discussions and for providing useful documents.

FLUID MIXING AND FLOW DISTRIBUTION IN THE REACTOR CIRCUIT (FLOMIX-R)

Ulrich Rohde, Thomas Höhne, Sören Kliem, Bengt Hemström[1], John Lillington[2], Martina Scheuerer[3], Timo Toppila[4], Trevor Dury [5], Jan Remis[6], Petr Muhlbauer [7], Ivan Toth [8], Joszef Elter [9], and Yuri Bezrukov[10]

1. Introduction

Coolant mixing inside the nuclear reactor is the most important inherent safety mechanism against boron dilution or overcooling transients and in the case of pressurized thermal shock (PTS) scenarios. In pressurised water reactors (PWR), boron acid is added to the water coolant to compensate the excess reactivity of fresh fuel loadings. Due to different mechanisms or system failures, slugs of low borated water can accumulate in the primary cooling system. This can happen e.g. as a consequence of a small break loss of coolant accident (SB LOCA), when coolant circulation is interrupted and a slug of almost un-borated condensate will accumulate in the cold leg of the primary circuit. During start-up of coolant natural circulation after refilling the primary circuit with the emergency core cooling (ECC) system or by switching on the first main coolant pump (MCP), this slug will be transported into the reactor core causing a significant reactivity insertion by decreasing the concentration of neutron absorber. The mixing of the unborated condensate with borated water in the reactor pressure vessel is in that case the only mitigative mechanism to prevent severe accident consequences. Mixing is relevant not only for nuclear safety, but also for structural integrity. In the case of LOCA, cold ECC water will be injected into the hot primary circuit. When plumes of cold water get in contact with the reactor pressure vessel (RPV) wall, thermal stresses occur, which might endanger RPV integrity. Mixing is even of relevance for normal reactor operation, e.g. to ascertain the coolant temperature distribution at the core inlet in the case of partially switched off MCPs.

In the EC project FLOMIX-R coordinated by Institute of Safety Research, slug mixing and flow distribution in the RPV has been comprehensively investigated experimentally and simulated by using computational fluid dynamics (CFD) tools. Partners from 8 European countries and Russia participated in the project. One objective of the project was to obtain complementary data on slug mixing to understand in sufficient detail, how the slug mixes before it enters the reactor core. Slug mixing experiments have been performed with several 1:5 scaled facilities representing different European reactor types. Additional to slug mixing tests with momentum insertion by starting pumps, experimental results on mixing of fluids driven by density differences were obtained at ROCOM and the FORTUM PTS test facility.

A second objective was to utilise data from steady state mixing experiments and plant commissioning test data to evaluate the primary circuit flow distribution and the effect of thermal mixing phenomena in the context of the improvement of normal operation conditions and structural integrity assessment. Flow distribution data available from commissioning tests (Sizewell-B for PWR, Loviisa and Paks for VVER) were used together with the data from the ROCOM facility as a basis for the flow distribution studies. The test matrix on flow

[1] Vattenfall Utveckling AB, Alvkarleby [2] Serco Assurance, Dorchester, Dorset [3] GRS, Garching [4] Fortum Nuclear Services, Vantaa [5] PSI, Villigen [6] VUJE, Trnava [7] NRI, Rez [8] AEKI, Budapest [9] NPP Paks, Paks
[10] EDO Gidropress, Podolsk

distribution and steady state mixing performed at ROCOM comprises experiments with various combinations of running pumps and various mass flow rates in the working loops.

The experimental data were used to contribute to the validation of CFD codes for the analysis of turbulent mixing problems. CFD calculations were accomplished for selected experiments with two different CFD codes (CFX-5, FLUENT). For quality assurance in the CFD code validation, so-called Best Practice Guidelines (BPG) have been applied. The BPG require a minimization of numerical errors and solution errors by systematic grid and time step refinement and sensitivity tests on the impact of uncertainties in the boundary conditions, before the effect of different physical models can be assessed. The applicability of various turbulence modeling techniques was studied for transient and steady state flow.

2. Test facilities

ROCOM (**Ro**ssendorf **Co**olant **M**ixing Model) is a test facility for the investigation of coolant mixing operated with water at room temperature [1]. The facility models a KONVOI type reactor with all details important for the coolant mixing in a linear scale of 1:5. ROCOM is a four-loop test facility with an RPV mock up made of transparent acryl (Fig. 1). Individually controllable pumps in each loop give the possibility to perform tests in a wide range of flow conditions, from natural circulation to nominal flow rate including flow ramps (pump start up). The transparent material of the pressure vessel allows the measurement of velocity profiles in the downcomer by laser Doppler anemometry. Boron concentration and temperature fields are modelled both by the concentration field of a tracer solution (salted water). The normalised tracer concentration is called the mixing scalar.

For the experimental investigation of the coolant mixing, the tracer solution is injected computer-controlled into the cold leg of one of the loops, while the test facility is operated with de-mineralised water. The test facility is equipped with wire-mesh sensors for electrical conductivity measurement [2], which allow the measurement of the transient tracer concentration with high resolution in space and time. Four such sensors are installed in the reactor pressure vessel model with altogether about 1000 single measurement positions and an imaging frequency of up to 200 Hz.

Fig. 1: View on the test facility ROCOM with the RPV model made from acryl

The Vattenfall mixing test facility is a 1:5 scale model of a Westinghouse PWR [3]. The RPV model is partially made of acryl. Components that can be important for mixing have been modelled, for example thermal shields, inlet pipe diffusers, structures in lower plenum, core support plates and core. The investigation of the relative boron concentration is based on salt water tracering and conductivity measurement, too. Conductivity is measured at 181 positions close to the inlet to the core with a sampling frequency of 60 Hz.

The test facility of EDO "Gidropress" [4] is a steel model of the Russian VVER-1000 reactor in a scale of 1:5. One loop with a loop seal, reactor coolant pump simulator and the reactor core with 151 fuel assembly simulators are modelled. Boron concentration change is simulated by a change in temperature (the deborated water slug is simulated by colder water). About 100 thermocouples are placed in the lower part of the downcomer and at the core inlet to study the mixing of flows.

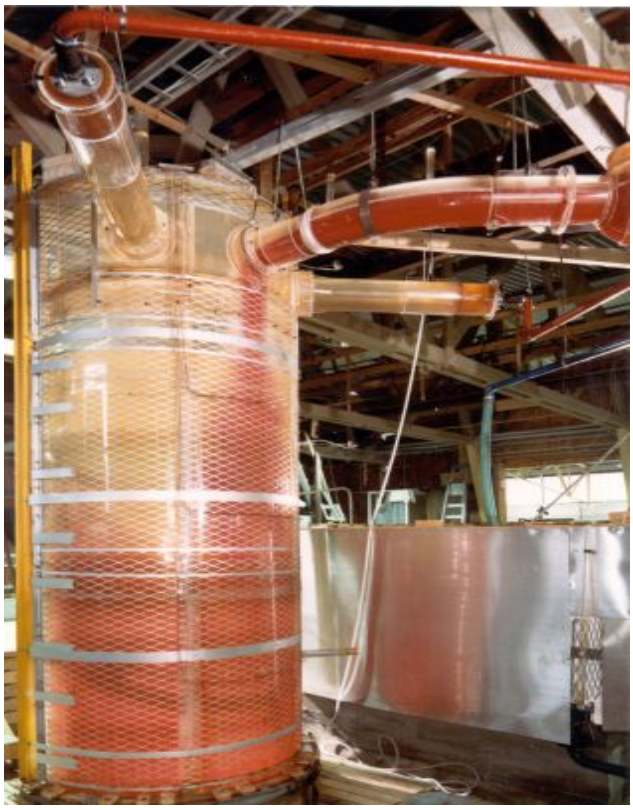

Specific PTS mixing experiments were performed at the Fortum PTS test facility [5]. This facility was a 1:2.56 scaled model of the Loviisa VVER-440 reactor. The facility represented one half of the circumference of the reactor downcomer made of transparent acryl. It included three cold legs, where the middle one was equipped with high pressure injection (HPI) simualtion belonging to the ECCS. Because the choice of the transparent material restricts the tests to a maximum temperature of around 75 °C, an extra buoyancy effect was induced by salt addition to the injected cold HPI water. The relative density difference between HPI and loop flow used in the tests was up to 16 %. The mixing of the HPI water was then observed by measuring temperatures in the downcomer and in the cold leg and visually through the transparent material of the facility.

Fig. 2: View of the Fortum PTS test facility

3. Investigation of momentum controlled and buoyancy driven slug mixing

Fig. 3a shows the time evolution of the mixing scalar at the two sensors in the downcomer in one of the ROCOM slug mixing tests. The mixing scalar distributions are shown over the azimuthally unwrapped downcomer. The position of the loop with the starting up pump is marked by the red arrow. From this visualization it is clearly to be seen, that the de-borated coolant passes around the core barrel instead of flowing directly downstream. Subsequently, at the lower sensor two maximums of the tracer on the “back side” of the downcomer are observed. Therefore, the tracer arrives at the core inlet plane first at positions, which are opposite to the position of the loop with tracer injection.

For the investigation of the influence of density effects, generic experiments have been carried out at the ROCOM test facility. The objective of these experiments was to find the conditions for transition from momentum controlled mixing, as it is typical for pump start-up scenarios, to buoyancy driven mixing, being relevant for PTS scenarios and natural circulation re-start after LOCA. It is expected, that density differences can be neglected, if the flow rates are sufficiently high. Because the ROCOM facility cannot be heated up, the necessary density differences were simulated by adding sugar (glucose) to the water that is

injected into the cold leg. To observe the mixing of the ECC water fed into the cold leg by the HPI system, this water was tracered by small amounts of sodium chloride, as in previous experiments. The maximum density difference created by the addition of glucose was 10%.

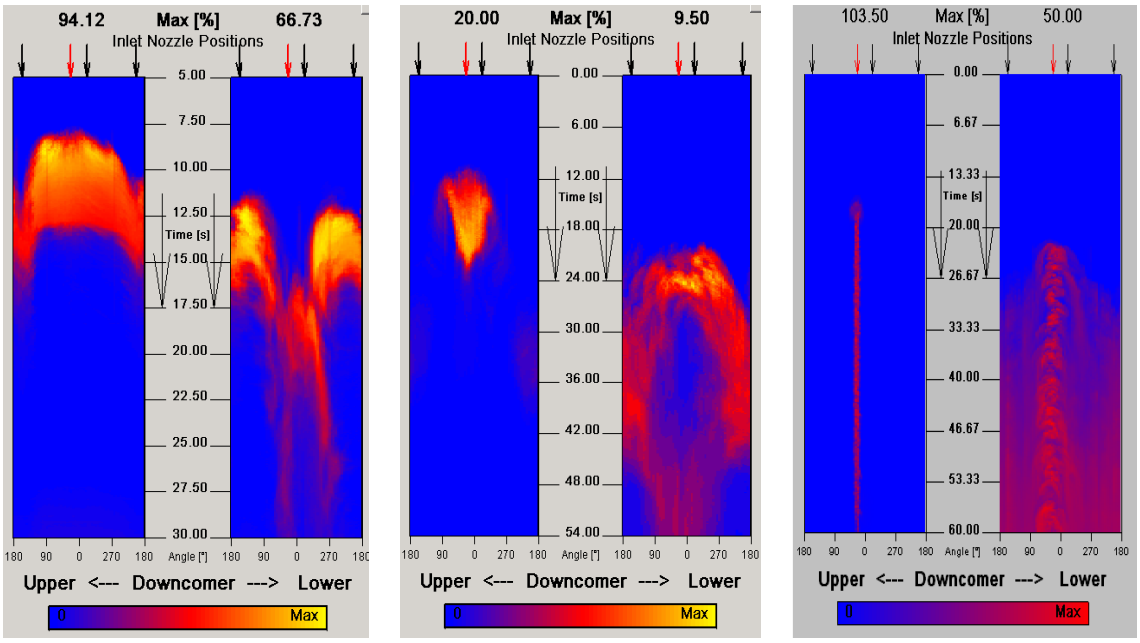

Fig. 3: Time evolution of the mixing scalar unwrapped over the downcomer
a) nominal flow rate, no density diff. *b) 10 % flow rate 10 % density diff.* *c) no flow rate, 10 % density diff.*

An unwrapped view of the time evolution of the tracer concentration measured at the two downcomer sensors in the experiment with 10% density difference and no flow in the injection loop (Fig. 3c) shows, that the sector covered by the ECC water is very small in the upper dowcomer in this case. The ECC water falls down straightly and passes the sensor in the lower part of the downcomer just below the inlet nozzle of the working loop. This mixing pattern is completely different from that one observed in the case of pump-start-up shown in Fig. 3a. Fig. 3b shows the mixing scalar behaviour in an experiment with high density difference, but low flow rate. The spreading of the mixing scalar into two streams is observed only in the lower downcomer. Based on these observations, the experiments with density differences can be divided into three groups: density dominated flow (see Fig. 3c), momentum dominated flow (see Fig. 3a) and the transition region (see Fig. 3b). The conditions at the inlet into the downcomer were used to calculate Froude-numbers of the experiments according to the following formula:

$$Fr_{DC} = \frac{v_{in}}{\sqrt{g \cdot H \cdot \frac{\rho_{in} - \rho_a}{\rho_{in}}}} \qquad (1)$$

where v_{in} is the velocity at the reactor inlet (combined loop and ECC flow), g is the gravitational acceleration, H is the height of the downcomer, ρ_{in} the density of the incoming flow, calculated with the assumption of homogeneous mixing between ECC and loop flow, and ρ_a the density of the ambient water in the downcomer. All experiments, identified as density dominated are characterised by Froude numbers less than 1.0, and all momentum dominated cases are found in the region of $Fr > 1.0$. Therefore, $Fr = 1$ is a critical Froude numbers separating the two flow regimes of momentum dominated and buoyancy driven flow.

The observations on density driven mixing have been confirmed qualitatively in the experiments performed at the Fortum PTS facility. Applying the same Froude scaling as it is given in equ. (1), all Fortum PTS tests are located in the density driven mixing range.

4. CFD code validation

A tremendous work on CFD code validation was performed within the FLOMIX-R project. The commercial CFD codes CFX-4, CFX-5 and FLUENT-6 have been used. Systematic code validation based on so-called Best Practice Guidelines (BPG) was focussed mainly on a number of benchmark cases from the steady-state mixing experiments, slug mixing tests and experiments with density differences. The ERCOFTAC BPG [6], which have been specified for nuclear reactor safety calculations within the ECORA project [7] were used for quality assurance of the validation calculations. The BPG are built on the concept of an error hierarchy. The different types of errors in CFD simulations are divided into the two main categories:

- Numerical errors, caused by the discretisation of the flow geometry and the model equations, and by their numerical solution
- Model errors, which arise from the approximation of physical processes by empirical mathematical models

This concept implies that numerical errors are quantified and reduced to an acceptable level, before comparison with experimental data is made. The BPG contain a set of systematic procedures for quantifying and reducing numerical errors. The knowledge of these numerical errors is a prerequisite for the proper judgement of model errors. Numerical errors are minimised by optimising the computational mesh, numerical schemes, convergence criteria and time step. Another kind of errors are uncertainties arising from insufficient information about the problem definition and set-up, like boundary positions, boundary conditions and internal geometry modelling. These uncertainties can be quantified by sensitivity analyses. Turbulence models are most relevant for physical errors.

Fig. 4 compares the CFD solution and experiment for the time-averaged mixing scalar distribution at the core inlet in a ROCOM steady-state mixing test with running pumps. The best agreement with the experiment was achieved, when even for the steady state a transient calculation was performed to reproduce turbulent fluctuations of the velocity and tracer concentration field observed in the experiment. Note, that the time-averaged distributions are presented on Fig. 4. A tetrahedral mesh with about 7 million elements comprising the detailed resolution of the internal structures, including the sieve drum in the lower plenum with 410 orifices was used. Standard K,ε and Shear Stress Transport (SST) K,ω turbulence models were applied. The different turbulence models provide very similar results.

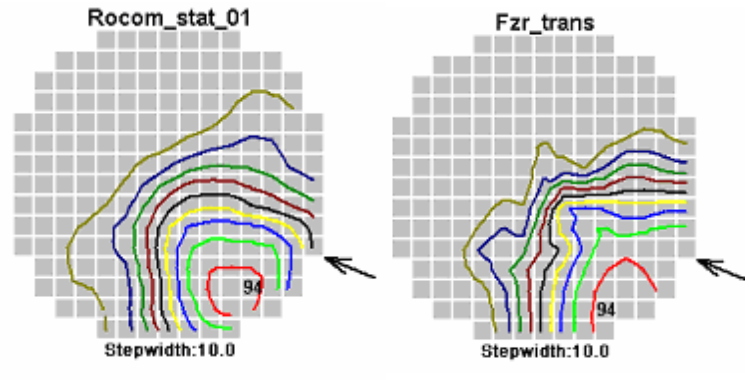

Fig. 4: Comparison between CFD solution (right) and experimental data (left)

The following conclusions were drawn from the CFD validation work:

- For correct description of inlet boundary conditions, at least a part of the cold leg should be modelled.
- Internal geometry should be modelled as detailed as possible due to limitations of the porous body approach. This requires a continuous progress in pre-processors.
- Concerning turbulence models, first order models like K-ε or SST K-ω can be recommended. For buoyancy driven mixing, better results have been obtained with Reynolds stress models. However, no final conclusions can be drawn, because BPG solutions could not be achieved in all cases.

5. Summary

A new quality of research in flow distribution and turbulent mixing inside the RPV of nuclear reactors has been achieved in the FLOMIX-R project. Experimental data on slug mixing with enhanced resolution in space and time have been gained from various test facilities covering different geometrical and flow conditions. The basic understanding of momentum controlled mixing in highly turbulent flow and buoyancy driven mixing in the case of relevant density differences between the mixing fluids has improved significantly. A higher level of quality assurance in CFD code validation has been achieved by consequently applying BPG.

References

[1] Prasser, H.-M., G. Grunwald, T. Höhne, S. Kliem, U. Rohde, F.-P. Weiss: "Coolant mixing in a pressurised water reactor: deboration transients, steam-line breaks, and emergency core cooling injection", Nuclear Technology Vol. 143 (July 2003), pp. 37-56

[2] Prasser, H.-M., Böttger, A., Zschau, J.: "A New Electrode-Mesh Tomograph for Gas Liquid Flows," Flow Measurement and Instrumentation, 9, 111-119 (1998).

[3] Alavyoon, F., Hemström, B., Andersson, N. G., Karlsson; R. I.: "Experimental and Computational Approach to Investigating Rapid Boron Dilution Transients in PWRs," CSNI Specialist Meeting on Boron Dilution Reactivity Transients, State College, PA, USA, October 18-20, (1995).

[4] Logvinov S.A., Ulyanovsky V.N., Bezrukov Yu.A., Kozlov A.N.: "Mixing of coolant with different boron concentration at the VVER-1000 core inlet during RCP start-up", Proc. ANNUAL MEETING ON NUCLEAR TECHNOLOGY 2000, Bonn, 22-24 May 2000.

[5] Tuomisto, H.: "Thermal-hydraulics of the Loviisa reactor pressure vessel vercooling transients", Imatran Voima Oy, Research report IVO-A-01/87, 1987.

[6] ERCOFTAC Best Practice Guidelines, see http://imhefwww.epfl.ch/lmf/ERCOFTAC/

[7] Menter, F. et al.: CFD Best Practice Guidelines for CFD Code Validation for Reactor Safety Applications, Deliverable D01 of the ECORA project, February 2002

Acknowledgement

The project this paper is based on was funded by the European Commission under contract number FIKS-CT-2001-00197.

MEASUREMENTS OF THE VELOCITY FIELD IN LIQUID METALS

Sven Eckert, Gunter Gerbeth, Thomas Gundrum, Frank Stefani, and Willy Witke

1. Introduction

Large effort is permanently directed to optimise methods and facilities for material processing technologies like melting, refining or casting of metals or alloys. The main goals are an improvement of the final product quality, an enhancement of the process efficiency and an economical consumption of resources and energy. In processes involving electrically conducting liquids, the application of an external magnetic field offers efficient opportunities for a contactless flow control and fluid handling. Further developments require a better knowledge about the details of the flow structure, the transport properties of the flow or the melting and solidification process, respectively. A better understanding and optimisation of liquid metal processes requires experimental data of the velocity field. Numerical simulations alone are often of limited value. The choice of commercially available techniques to measure the velocity structure of opaque fluid flows at high temperatures is very poor. Possibilities are known to measure the velocity at a local point by means of different invasive probes such as electromagnetic potential probes [1,2], the Mechano-Optical Probe (MOP) [3], hot-wire anemometers [4] or Karman Vortex probes [5]. New approaches are the application of the Ultrasound Doppler Velocimetry (UDV) [6-8] or the reconstruction of velocity patterns from magnetic field measurements (CIFT) [9]. However, some serious restrictions always exist to apply particular sensors, for instance, the temperature range, the type of liquid metal, the velocity range, the accuracy of the method, or the presence of electromagnetic fields.

During the last years the activities of the MHD department were focussed to develop and to qualify techniques to measure the flow rate and the local velocity of the liquid metal and two-phase flow characteristics such as void fraction, bubble velocity and bubble size, respectively. In liquid metal model experiments local sensors as well as integral methods have been tested and applied. Some promising techniques such as the MOP, the UDV or the Contactless Inductive Flow Tomography (CIFT) will be presented within this paper.

2. Mechano-optical Probe (MOP)

A new system based on a mechano-optical principle has been developed to measure local flow velocities. A sketch of the MOP is shown in Figure 1. The measuring equipment consists of a mechanical sensor, a specialized optical system, a CCD-array and a PC. The sensor is made from a quartz glass tube (∅ 2.5 mm) with a molten tip connected with a very thin rod (∅ < 0.05 mm) concentrically fixed only in the front point of the tip. To allow applications in high temperature melts a cooling system is integrated into the sensor. The interaction with the moving fluid causes a deformation of the sensor tip resulting in a displacement of the upper end of the glass rod, which is observed by the CCD-array sensor being connected via a frame grabber card with the computer. A special software has been implemented allowing the evaluation of the digitized pictures. The drag force acting on the sensor in the fluid was modelled by Eckert et al. [3]. From those estimates the rod displacement shows a parabolic dependence on the flow velocity. Such a qualitative behaviour was confirmed by the results obtained from the calibration of the sensors done at a circular rotating channel.

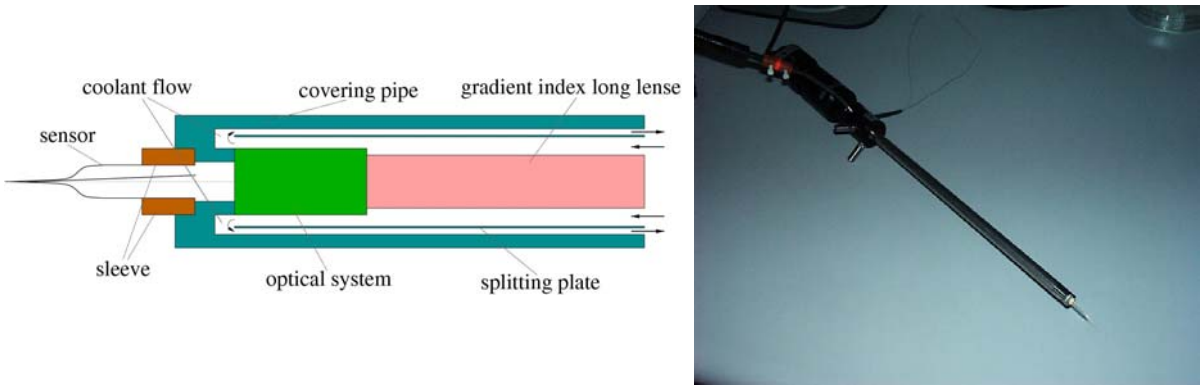

Fig. 1: Scheme and photograph of the Mechano-Optical Probe (MOP)

The suitability of the sensor was demonstrated in water and in GaInSn at room temperature as well as in SnPb and in PbBi at temperatures up to 400 °C. During the experiments the temperature of the optical system inside the sensor was measured by an internal thermocouple. The values observed were always significantly below 100°C. We can therefore expect the sensor to work reliably at higher temperatures of about 800°C. Besides the capability to work at high temperatures the mechano-optical measuring principle excludes perturbations of the signal arising from external electromagnetic fields or electric noise.

3. Ultrasound Doppler Velocimetry (UDV)

UDV is a non-intrusive technique to measure velocities of liquid flows based on the ultrasonic pulsed echo method [6]. The feasibility of velocity profile measurements by UDV has already been demonstrated for low temperature liquid metals as mercury [10, 11] and gallium [12]. Recently, successful measurements have been published for liquid sodium [7]. It is worth to note that the measurements have been performed through the stainless steel wall of the channel. The use of the conventional transducer made of PZT (lead-zirconium-titanate) based materials restricts the range of application of ultrasonic techniques to maximum temperatures of about 150°C (long term load) and 200°C (short term load), respectively. To overcome this problem we followed the approach to apply an acoustic wave-guide for a thermal and chemical decoupling between the active transducer and the fluid. An integrated ultrasonic probe as shown in Figure 2 was designed consisting of the piezoelectric element and the acoustic wave-guide [8]. The wave-guide is fabricated from a stainless steel foil with a thickness of 0.1 mm. The wave-guide is closed at the front end by means of laser beam welding leading to a flat stainless steel surface. This surface being in direct contact with the melt has to be prepared before the measurements to obtain a sufficient wetting with the liquid metal. The wave-guides have a diameter of 7.5 mm and a length between 200 and 1000 mm. The working frequency of the transducer is 4 MHz.

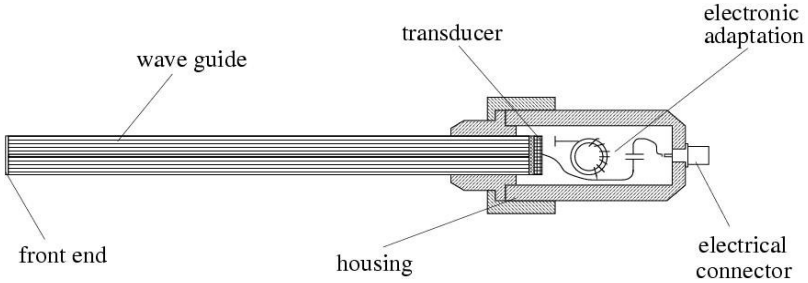

Fig. 2: Schematic view of the integrated ultrasonic transducer

As an example we consider here the motion of single argon bubbles rising in the ternary, eutectic alloy GaInSn ($T_{melt} \approx 10°C$) under the influence of a DC longitudinal magnetic field. As shown in Figure 3 the experiments were performed within an open, cylindrical container made from Perspex with a diameter of R = 100 mm. The cylinder was filled until a height of H = 220 mm. The column is positioned concentrically inside a Helmholtz configuration of two water-cooled copper coils with a vertical distance of 150 mm and an inner diameter of 210 mm. This configuration provides a homogeneous DC longitudinal magnetic field over the fluid volume. The coils were supplied with a D.C. electric current up to 1600 A corresponding to a maximum field strength of 0.3 T. The ultrasonic transducer was installed at the bottom wall outside of the cylinder directly behind the nozzle. The ultrasonic beam was directed vertically along the bubble path allowing measurements of the vertical bubble and liquid velocity component.

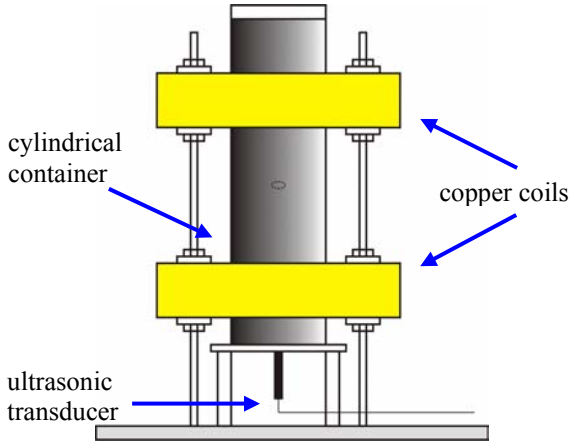

Fig. 3: Schematic scheme of the experimental configuration

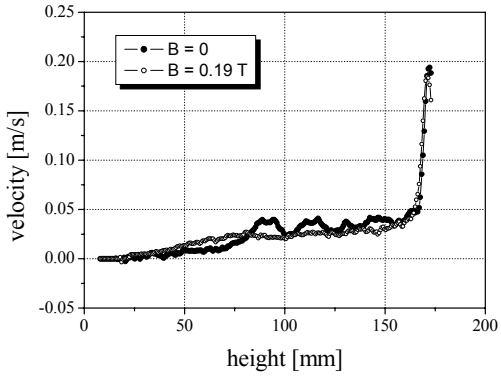

Fig. 4: Snapshots of the vertical velocity in the bubble wake when the bubble has reached a vertical height of 170 mm

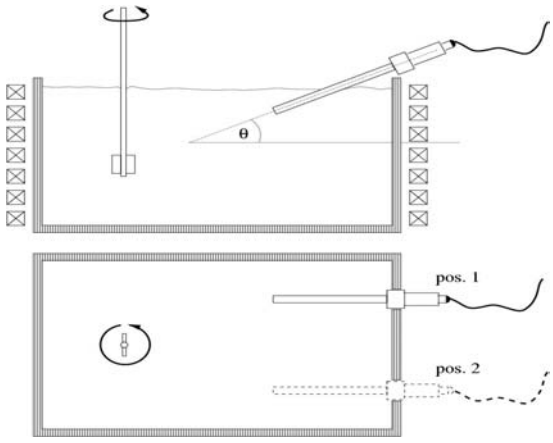

Fig. 5: Schematic view of the arrangement of the CuSn experiment

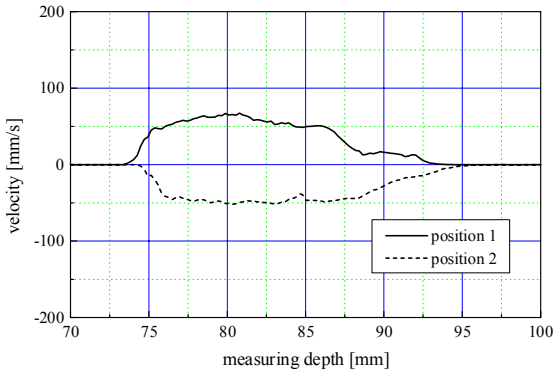

Fig. 6: Velocity profile measured in the CuSn melt at both sensor positions

Vertical velocity measurements along the cylinder axis reveal the magnetic field influence on the bubble wake. Snapshots from these measurements shown in Figure 4 were acquired at those moments when the bubble was detected at a vertical position of 170 mm. In the case without magnetic field the vortex structure of the wake can clearly be recognized in the signal. The vertical liquid velocity behind the bubble generally becomes more uniform if the magnetic field is turned on, in other words the velocity gradient along the field lines is significantly reduced. Besides the damping of the velocity in the wake region, an elongation

of the wake structure in vertical direction due to the anisotropy of the magnetic field influence can be observed. Raising of the magnetic field strength causes an enlargement of the eddies in the wake.

Other demonstrations at high temperatures were done in a CuSn alloy (Cu35Sn65, T_{melt} = 550°C) at a temperature of about 620°C and liquid aluminium at 750°C, respectively. The metal was melted inside a rectangular alumina crucible (130 × 80 mm^2) by means of an inductive heating system. The depth of the melt was about 40 mm. A mechanical stirrer was used to generate a flow. The integrated sensor was dipped into the metallic alloy through the free surface with an angle of 35° with respect to the horizontal line (Figure 5). Results obtained from this experiment are shown in Figure 6. The velocity profiles determined at both measuring positions are similar with respect to the shape and the amplitude and show different signs in accordance with the chosen rotation direction of the mechanical stirrer. Several repetitions of the measurements showed the reproducibility of the results.

4. Contactless Inductive Flow Tomography (CIFT)

The three-dimensional distribution of the velocity field is of crucial interest for a number of metallurgical applications. A contactless determination of the full flow field is highly desirable, even under the restriction that it provided only a rough picture of the velocity structure. Three-dimensional inductive velocity reconstruction was the topic of some recent papers [9, 13-15]. In [13,14] we had addressed the inverse problem of velocity reconstruction in conducting fluids from combined magnetic field and electric potential measurements. Basically, the electromotive force, which is proportional to the cross-product of the desired flow velocity and the externally applied magnetic field, gives rise to an additional induced magnetic field, which is measurable outside the fluid volume, and to an induced electric potential which can be measured at the fluid boundary. A particular result of [14] was that the main velocity structure of the flow can be reconstructed from such a combined magnetic/electric field measurement, apart from an uncertainty in the radial distribution of the flow. Later, in [9,15], we considered the case of using two sets of measured induced magnetic fields instead of a single set together with one set of electric potentials. Such a contactless method is especially interesting for those applications in which the electric potential measurement at the fluid boundary is hard to manage. This seems particularly important for hot and aggressive fluids or for facilities where the fluid boundary is not accessible for technological reasons.

In order to demonstrate the feasibility of the contactless inductive velocity reconstruction method in real applications an experiment has been set up in which the propeller driven flow of a liquid metal has to be reconstructed solely from externally measured magnetic field data (Figure 7). We use 4.4 liters of the eutectic alloy GaInSn. The flow is produced by a motor driven propeller with a diameter of 6 cm inside a polypropylene vessel with 18.0 cm diameter. The height of the liquid metal is 17.2 cm, giving an aspect ratio close to 1. The propeller can rotate in both directions, resulting either in upward or downward pumping. The rotation rate can reach 2000 rpm producing a mean velocity of 1 m/s, which corresponds to a magnetic Reynolds number of $Rm \approx 0.4$. The flow structure for the two directions is not symmetric. The downward pumping produces, in addition to the main poloidal roll, a considerable toroidal motion, too. For the upward pumping, this toroidal motion is, to a large extend, inhibited by guiding blades installed above the propeller. It was one of the tasks of the experiment to discriminate between those different flow structures.

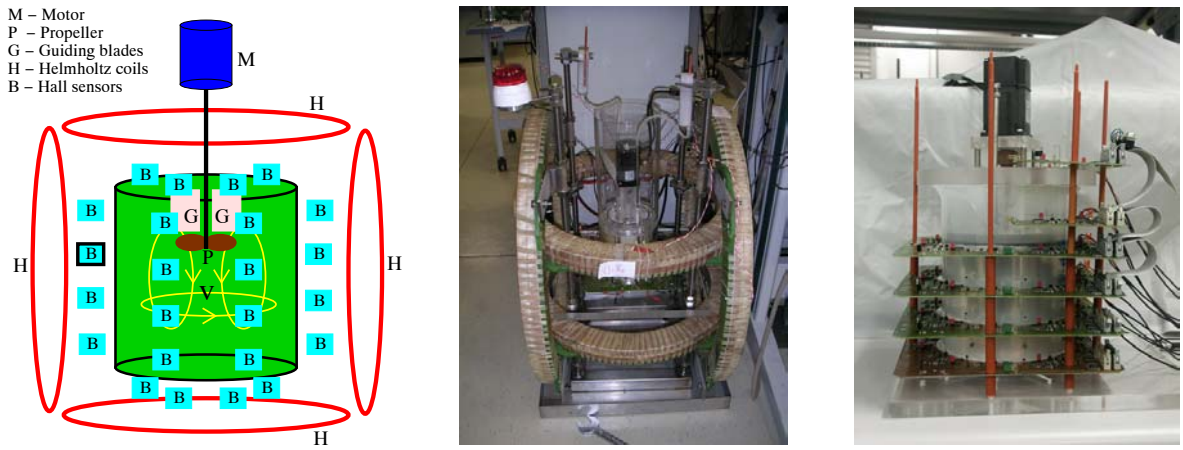

Fig. 7: The CIFT experiment. Schematic view (a), total view (b), and details of the vessel with the circuit boards for the Hall sensors and AD transformer (c).

For upward and downward pumping, Figs. 8 and 9 show the induced magnetic fields measured at the 49 positions, and the inferred velocity field at 52 discretization points. In Fig. 8c we see the upward flow in the center of the cylinder and the downward flow at the rim, but nearly no rotation of the flow. In Fig. 9c we can identify the downward flow in the center and the upward flow at the rim, together with a rotation of the flow. This absence and presence of the swirl is an important feature which can evidently be discriminated by our method. It is worth to note that not only the structure of the flow, but also the range of the velocity scale is correctly reproduced by the inversion.

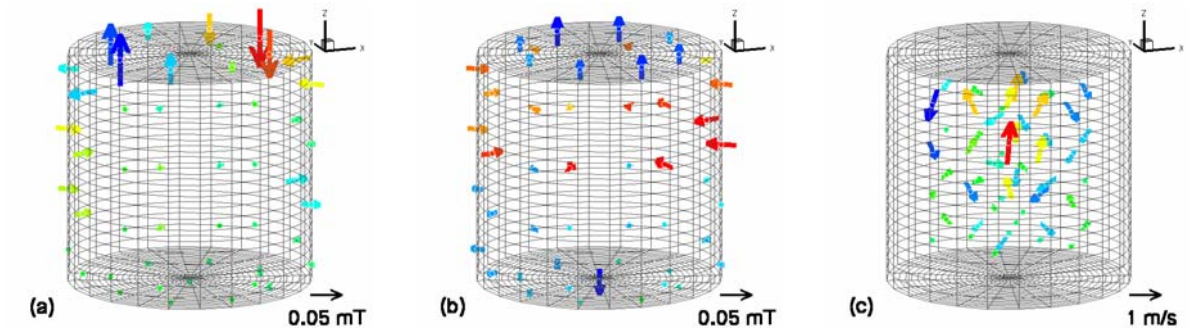

Fig. 8: The measured magnetic fields and the reconstructed velocity field for the case that the propeller pumps upward with 1200 rpm. Measured induced field for transversal applied field (a); measured induced field for applied axial field (b); and reconstructed velocity (c). For (a) and (b) the color coding discriminates between ingoing and outgoing magnetic field lines, for (c) the color coding mirrors the axial component of the velocity.

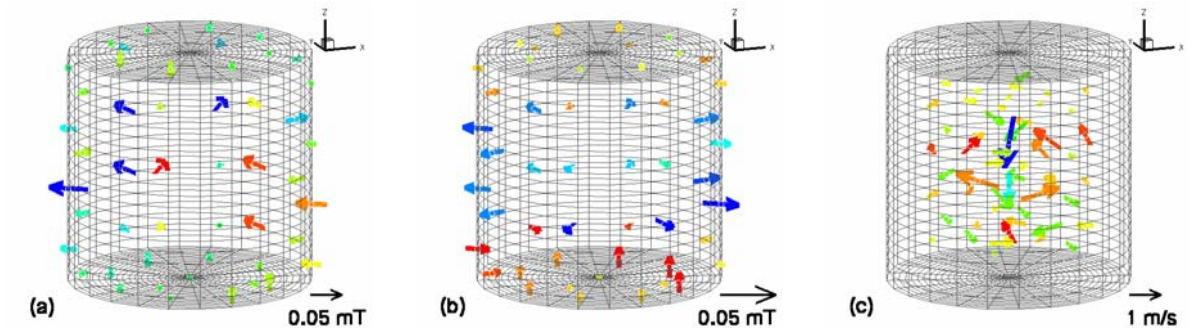

Fig. 9: The same as Figure 8, but for the propeller pumping downward with 1200 rpm.

5. Conclusions

Each measuring technique is marked by a list of advantages and drawbacks, the choice of an optimal method has to be done considering the actual experimental configuration and parameters. Moreover, it is important to identify the kind of information that should be obtained from the experiment (flow rate, local velocities, turbulence intensities,...) as well as the spatial and temporal resolution and accuracy which should be achieved. Nevertheless, we can conclude that for liquid metal model experiments at a range of moderate temperatures (< 300°C) a sufficient number of measuring techniques are available to investigate the flow structure. Moreover, we have presented here some measuring techniques showing the capability to be extended to an application range of high temperatures (700-1000°C) being attractive for industrial applications.

Acknowledgement

The research is supported by the Deutsche Forschungsgemeinschaft (DFG) in form of the SFB 609 “Electromagnetic Flow Control in Metallurgy, Crystal Growth and Electro-chemistry” and under grant GE 682/10-1/2. This support is gratefully acknowledged.

References

[1] R. Ricou, C. Vives, Local velocity and mass transfer measurements in molten metals using an incorporated magnet probe, Int. J. Heat Mass Transfer 25 (1982) 1579-1588
[2] A. Tsinober A., E. Kit , M. Teitel, On the relevance of the potential-difference method for turbulence measurements, J. Fluid Mech. 175 (1987) 447-461
[3] S. Eckert, W. Witke , G. Gerbeth, A new mechano-optical technique to measure local velocities in opaque fluids, Flow Meas. and Instr. 11 (2000) 71-78
[4] M. Sajben, Hot-wire anemometry in liquid mercury, Rev. Sci. Instr. 36 (1965) 945-953
[5] M. Iguchi, H. Kosaka, H. Mizukami, M. Kawamoto, A. Hayashi, Y. Terauchi, M. Kawabata, Development and calibration of a Karman vortex probe for measurement of molten steel velocities, Met. and Mat. Trans. 30B (1999) 53-59
[6] Y. Takeda, Development of an ultrasound velocity profile monitor, Nucl. Eng. Design 126 (1991) 277–284
[7] S. Eckert, G. Gerbeth, Velocity measurements in liquid sodium by means of ultrasound Doppler velocimetry, Exp. Fluids 32 (2002) 542-546
[8] S. Eckert, G. Gerbeth, V.I. Melnikov, Velocity measurements at high temperatures by UDV using an acoustic wave guide, Exp. Fluids 35 (2003) 381-388
[9] F. Stefani, T. Gundrum, G. Gerbeth, Contactless inductive flow tomography, Phys. Rev. E 70 (2004) 056306
[10] Y. Takeda, Measurement of velocity profile of mercury flow by ultrasound Doppler shift method, Nucl. Techn. 79 (1987) 120-124
[11] Y. Takeda, H. Kikura, G. Bauer, Flow measurement in a SINQ mockup target using mercury, ASME FED Summer Meeting, Washington DC, FEDSM98-5074, 1998
[12] D. Brito, H.-C. Nataf, P. Cardin, J. Aubert, J.P. Masson, Ultrasonic Doppler velocimetry in liquid gallium, Exp Fluids 31 (2001) 653–663
[13] F. Stefani, G. Gerbeth, Velocity reconstruction in conducting fluids from magnetic field and electric potential measurements, Inverse Problems, 15 (1999) 771-786
[14] F. Stefani, G. Gerbeth, On the uniqueness of velocity reconstruction in conducting fluids from measurements of induced electromagnetic fields, Inverse Problems, 16 (2000) 1-9
[15] F. Stefani, G. Gerbeth, A contactless method for velocity reconstruction in electrically conducting fluids, Measurement Science and Technology 11 (2000) 758-765

THE RIGA DYNAMO EXPERIMENTS

Frank Stefani, Thomas Gundrum, Gunter Gerbeth, Agris Gailitis[1], Olgerts Lielausis[1], and Ernests Platacis[1]

1. Introduction

Cosmic magnetic fields, including the magnetic fields of the Earth and the Sun, are produced by the hydromagnetic dynamo effect. This effect relies on the mechanism that the interaction of the fluid velocity with a given magnetic field produces an electric current which, in turn, induces exactly the original magnetic field. In mathematical terms, the self-excited magnetic field is an *eigenfield* of the dynamo operator. A necessary condition for the dynamo effect to occur is that the so-called magnetic Reynolds number $Rm = \mu\sigma LU$ (with μ denoting the permeability, σ the electrical conductivity, L a typical length scale and U a typical velocity scale of the fluid flow) exceeds a critical value which is typically in the order of 10-100. It turns out that, even for sodium as the best liquid conductor and for optimized flow helicity, the product LU must be greater than 1 m^2/s. It is this large number which had prevented laboratory dynamo experiments until the year 1999, when the dynamo effect was observed in two liquid sodium facilities in Riga [1] and Karlsruhe [2]. Since that time, a number of additional experiments have been conducted at either place [4]. This interim report is intended to summarize the main results of the Riga experiments. More details can be found in [3-7].

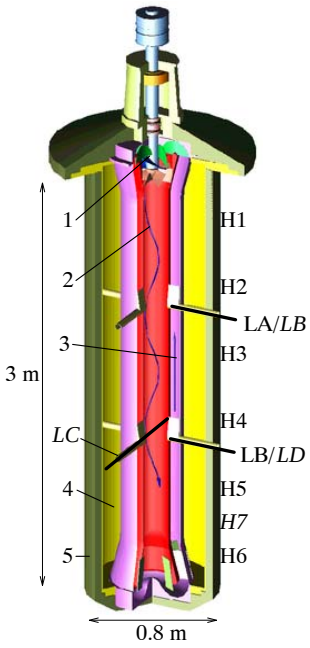

Fig. 1: The central module of the Riga dynamo experiment. 1 - Propeller, 2- Helical flow in central cylinder, 3 - Backflow in second cylinder, 4 - Outer cylinder with sodium at rest, 5 - Thermal insulation. H1-H7 – External Hall sensors. LA-LD – Internal Hall sensor lances.

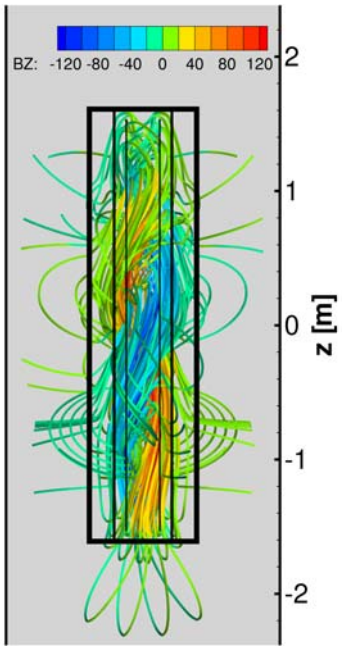

Fig. 2: Illustration of the magnetic eigenfield of the Riga dynamo experiment, as computed by a two-dimensional solver of the induction equation. The color coding reflects the axial component of the magnetic field in mT. The geometry and flow structure in the bending regions is slightly simplified.

[1] Institute of Physics, University of Latvia, Salaspils, Latvia

2. The Riga dynamo and its magnetic eigenfield

The central module of the Riga dynamo facility is sketched in Fig. 1. It comprises three concentric cylinders with different flow structures. The propeller in the upper part of the central cylinder drives a downward helical flow of liquid sodium with the ratio of axial to azimuthal velocity approximately close to one. The flow is bent at the bottom and goes upward in the second cylinder, after the rotation has been taken out by some guiding blades. The sodium in the third cylinder is at rest, at least at the beginning of the experiment. The propeller is driven by two electric motors with a maximum total power of about 200 kW. This enables sodium velocities up to 20 m/s, which is well above the critical point at which the dynamo effect occurs.

An impression of the field structure is given on the right hand side of Fig. 1. This field structure had been computed by means of a two-dimensional solver of the induction equation, which was also used for extensive computations for the optimization of the Riga dynamo experiment. Note the entangled helical structure of the magnetic field lines, which is typical for dynamos.

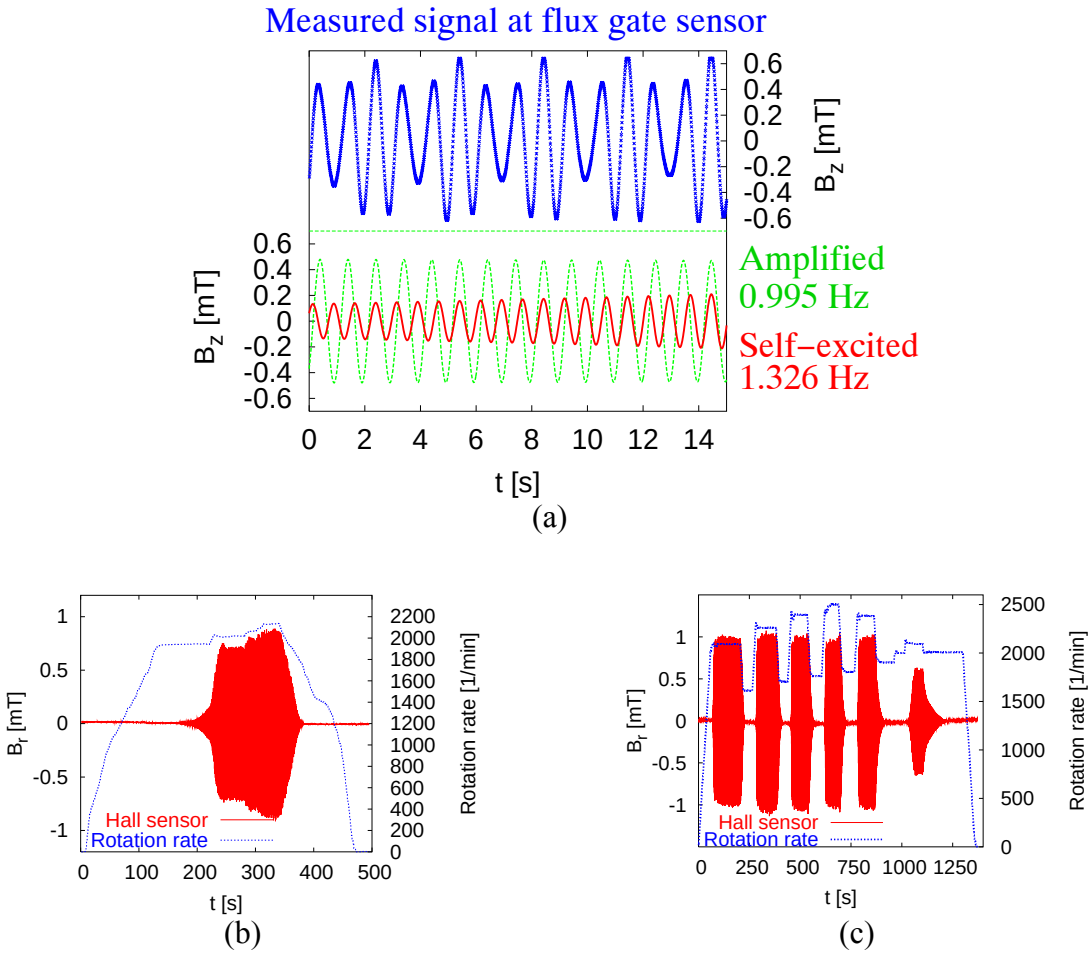

Fig. 3: Magnetic field data and propeller rotation rate during three different campaigns. (a) – First observation of an exponentially growing magnetic eigenfield in November 1999 (on the background of an amplified external signal). (b) - Exponential growth and saturation regime in July 2000. (c) - Switching the dynamo on and off during one run in the May 2004 campaign.

3. The experimental campaigns up to present

From November 1999 until May 2004, a total of six experimental campaigns have been conducted at the Riga dynamo experiment, with increasing complexity of the measurement system for magnetic fields, pressure and velocity.

The main achievement of the November 1999 campaign was the detection of a slowly growing eigenfield with a frequency clearly different from that of an amplified external signal (Fig. 3a). After the repair of a sodium seal, the next campaign took place in July 2000 [3]. It provided a wealth of data on the kinematic as well as on the saturated state of the dynamo. The growth rates and frequencies within the kinematic regime turned out to be in good agreement with the numerical predictions, with deviation of approximately 5 per cent. For the June 2002 campaign the magnetic field measurement had been significantly refined. At two heights, Hall sensor "lances" (LA-LD in Fig. 1) were inserted into the dynamo allowing the measurement of the radial dependence of the fields. The magnetic field measurements were also refined in the February 2003 and July 2003 campaigns, in particular with respect to the time resolution. First successful velocity measurements in the outer cylinder were carried out in the May 2004 campaign. These measurements confirmed the numerical result that the Lorentz force in the outer cylinder leads to a global azimuthal rotation and to two poloidal eddies. Another novelty of the May 2004 campaign was the measurement of the pressure in the inner cylinder by a pressure transducer which is flash mounted at the innermost wall.

4. The main results

In Fig. 4 we compile the growth rate and frequency data as recorded in the campaigns from November 1999 until July 2003. The first point to note is that the results are quite reproducible over the years, despite some slight changes in the facility (e.g. the insertion of tubes with sensor lances inside the innermost channel). The growth rates (Fig. 4a) in the kinematic regime increase with increasing rotation rate, whereas in the saturation regime they are zero by definition. In contrast to this sharp bend of the growth rate behaviour, the frequency (Fig. 4b) continues to increase after the transition from the kinematic to the saturation regime. The numerical predictions for the kinematic case are based on a 2D code for the solution of the induction equation [7]. This code does not include the effect of the lower conductivity of the stainless steel tubes between the different concentric cylinders. This effect of the finite wall thickness was determined by means of a simpler 1D code and is reflected in the corrected curves in Fig. 4a. This wall effect is negligible for the frequencies.

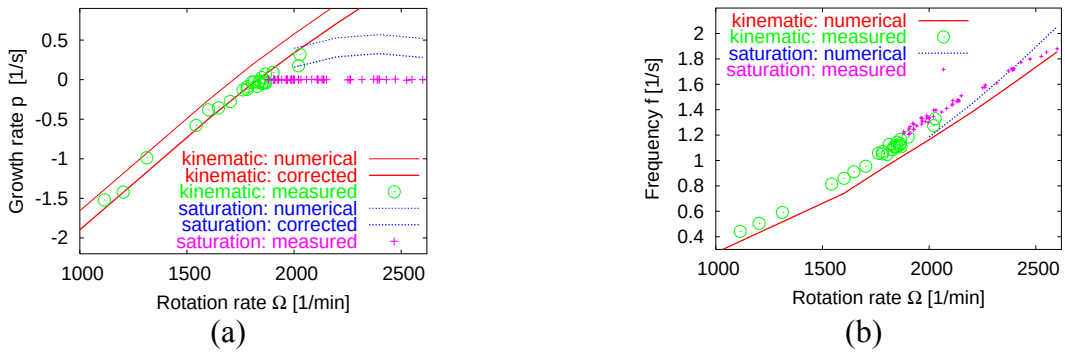

Fig. 4: Computed and measured growth rates (a) and frequencies (b) in the kinematic and the saturation regime.

An interesting observation concerns the ratio of the fields at the upper and the lower lance. In Fig. 5 we observe an upward shift of the magnetic field with increasing propeller rotation rate. Another interesting quantity is the excess power, i.e. the motor power that is needed to feed the magnetic field (Fig. 6). The rather wide scatter of the data is due to the fact that it is not easy to determine the purely hydrodynamic power when the magnetic field is already present. Apart from this, the flatness of the fit curve is remarkable. For a propeller rotation rate that is 40 per cent overcritical, we have only 20 kW excess power, which is approximately 10 per cent of the total power there.

All these observations can be explained within a simple theoretical model [5,7] which gives a quite self-consistent picture of the flat power increase, the growth rate and frequency behaviour, and the axial field deformation. The self-exciting magnetic field produces a Lorentz force with all three components. The axial component acts against the axial flow, hence producing a pressure increase leading to a higher motor power consumption. However, if this were the only effect of the back-reaction, then the flow rate and the propeller rotation rate could not much increase above the critical value. Only the excess power would quadratically increase with the amplitude of the magnetic field. But this is in strict contrast to our observation. At 40 per cent overcritical propeller rotation rate we have only 10 per cent increase of the power consumption. The explanation is given by the action of the azimuthal component of the Lorentz force which leads to a reduction of the azimuthal velocity component. Since the azimuthal velocity is maintained only by inertia, its reduction accumulates downstream. Hence, in the lower part of the cylinder the velocity field looses its excitation capability which results in the change of the magnetic field pattern towards the upper part of the dynamo.

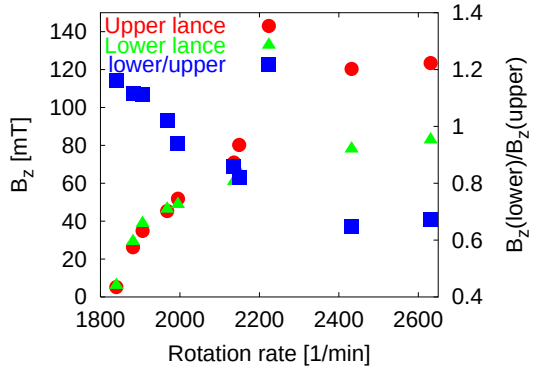

Fig. 5: Dependence of the axial magnetic fields measured close to the innermost wall on the lower and upper lance, and of their ratio, on the propeller rotation rate.

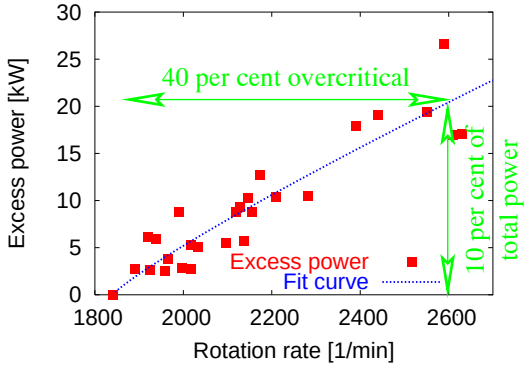

Fig. 6: Dependence of the excess power due to Joule losses on the (temperature corrected) rotation rate. The critical rotation rate is 1840 rpm.

Besides the back-reaction effects on the large scale flow structure, it is interesting to get some knowledge about fluctuations. In Fig. 7 we show two spectra, one from a Hall sensor which is located on the lower measurement level in the central cylinder, about 2 cm from the wall. The other spectrum results from the data of the pressure sensor, which is also mounted on the lower level. The main feature of the magnetic spectra is, of course, the peak at the eigenfrequency f. However, there is also a peak at the triple frequency, and even a small one at the fivefold frequency. Neither of these peaks is seen in the pressure spectrum. Instead we detect here a dominant peak at $2f$ and some smaller peak at $4f$. A common explanation of these peaks is that the magnetic eigenfield with the azimuthal mode number $m=1$ produces a

Lorentz force with a dominant $m=0$ part, but also with a $m=2$ part. The latter part influences the velocity and is also mirrored by the pressure peak at the double frequency. Now, this $m=2$ mode of the velocity induces, together with the dominant magnetic $m=1$ mode, a new contribution with $m=3$ in the magnetic field. The product of $m=1$ and $m=3$ modes of the magnetic field produces the $m=4$ mode in the pressure. All the arguments for m transfer to the multiples of the frequency since the measurement is done at a fixed position. Concerning the inertial range of the spectrum, we have plotted the $f^{-11/3}$ law for the magnetic field in the inertial range and a $f^{-7/3}$ law for the pressure for comparison, without claiming a perfect coincidence. Between the main field frequency f and the propeller frequency f_{prop} there seems to be a region with f^{-1}, which has also been observed experimentally and numerically by other groups.

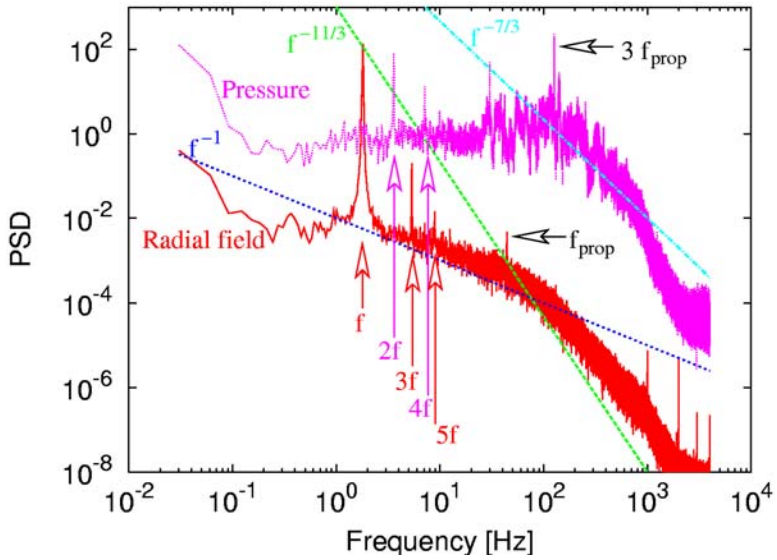

Fig. 7: Spectra of the radial magnetic field and the pressure, both measured on the lower level in the inner cylinder. The pressure sensor was flash mounted to the wall. The data are for a rotation rate of 2530 rpm. The peaks are multiples of the eigenfrequency f of the magnetic field.

4. Conclusions and prospects

With the nearly simultaneous sodium experiments in Riga and Karlsruhe the science of hydromagnetic dynamos has been pushed forward. Kinematic dynamo theory has been proven to be correct and robust with respect to low levels of turbulence and to complicated boundary conditions. The observed saturation effects are nontrivial as they concern not only the expected increase of motor power but also a spatial redistribution of the flow.

While the Karlsruhe facility has been disassembled, the Riga facility is ready for further experiments. The most important goal of the future experiments is to study in more detail the flow deformation under the influence of the self-excited magnetic field. Apart from the ultrasonic measurements in the outermost channel, no direct velocity measurements have been carried out in the sodium facility. Some effort is presently being spent to infer the velocity profile from the measured magnetic field data in the sense of an inverse problem using a new

forward code based on the integral equation approach of dynamo theory and a simplex algorithm for the inversion. However, direct flow measurements seem unavoidable when it comes to confirm the results of the saturation model. Hence, such measurements with micro-magnet probes are envisioned for the next runs.

References

[1] A. Gailitis, O. Lielausis, S. Dement'ev, E. Platacis, A. Civersons, G. Gerbeth, Th. Gundrum, F. Stefani, M. Christen, H. Hänel, G. Will (2000), Detection of a flow induced magnetic field eigenmode in the Riga dynamo facility, Phys. Rev. Lett, 84, 4365

[2] R. Stieglitz, U. Müller (2001), Experimental demonstration of a homogeneous two-scale dynamo, Physics of Fluids, 13, 561

[3] A. Gailitis, O. Lielausis, E. Platacis, S. Dement'ev, A. Civersons, G. Gerbeth, Th. Gundrum, F. Stefani, M. Christen, G. Will (2001), Magnetic field saturation in the Riga dynamo experiment, Phys. Rev. Lett, 86, 3024

[4] A. Gailitis, O. Lielausis, E. Platacis, G. Gerbeth, and F. Stefani (2002), Laboratory experiments on hydromagnetic dynamos, Rev. Mod. Phys., 74, 973

[5] A. Gailitis, O. Lielausis, E. Platacis, G. Gerbeth, and F. Stefani (2002), On back-reaction effects in the Riga dynamo experiment, Magnetohydrodynamics 38, 15

[6] A. Gailitis, O. Lielausis, E. Platacis, G. Gerbeth, and F. Stefani (2003), The Riga dynamo experiment, Surveys in Geophysics, 24, 247

[7] A. Gailitis, O. Lielausis, E. Platacis, G. Gerbeth, and F. Stefani (2004), Riga dynamo experiment and its theoretical background, Phys. Plasmas 11, 2838

CONE-BEAM X-RAY TOMOGRAPHY OF A BATCH REACTOR WITH GASSING STIRRER

Stephan Boden, Uwe Hampel, and Martina Speck

1. Introduction

Stirred chemical reactors have found widespread application in chemical processing. They are used for different chemical production processes, involving multiple fluids or gas-fluid reactions [1]. In this paper we discuss the measurement of gas fraction profiles in a batch reactor with a hollow gassing stirrer. Such devices are used to disperse gas into a liquid by means of mechanical stirring. The aim of gas dispersion is the creation of a large interfacial area where chemical reaction takes place.

In order to control, optimise and model chemical reactions in stirred reactors it is necessary to know the phase distribution and phase velocities under real process conditions. For the problem of gas distribution measurement there exist a few techniques which may be used, namely, liquid level measurement, optical holography [2], videometry [3], laser Doppler techniques [4], hot wire anemometry [5], electrical impedance measurements [6], suction probes [7], electrical impedance tomography (EIT) [8], positron emission tomography [9], gamma densitometry [10], and transmission computed tomography using X-ray or gamma radiation. Among those methods tomography approaches, are most advantageous, because they do not require probe insertion into the reactor vessel, they are well applicable at higher gas fractions, and they are able to measure within the whole reactor volume. An advanced tomographic technique is cone-beam X-ray computed tomography (CBT). With CBT a volume density distribution is reconstructed from a set of two-dimensional radiographs obtained from an object at different projection angles. Radially symmetric material distributions can even be reconstructed from a single radiogram. The technique is especially suitable for time-integrated gas fraction measurements. It provides a spatial resolution of better than one millimetre, but still it requires less effort than PET and gamma radiation techniques concerning radiation protection measures and tracer production. Though CBT is today widely used in medical imaging and material research, it has two inherent problems that must be solved for quantitative gas fraction measurements. These are beam hardening and radiation scattering effects which lead to nonlinearities in the extinction characteristics. The goal of the presented study was therefore the development of a suitable cone-beam CT measurement approach that can be used for visualization and quantitative measurement of the gas fraction field in stirred chemical reactors.

Fig. 1: View of the stirred chemical reactor Ecoclave 150 (Büchi AG).

2. The chemical reactor

Experiments were carried out on a double wall cylindrical reactor Ecoclave 150 (Büchi AG, Switzerland) made of borosilicate glass with an inner diameter of 80 mm (fig. 1). The fluid is stirred by a six blade mechanical stirrer mounted at the lower end of a hollow shaft. The shaft is motor driven with a controllable speed between 50 and 2000 rpm. Between the stirrer blades there are holes which allow gas flow from the upper gas volume into the fluid. With increasing stirrer speed the static pressure in the stirrer region drops accordingly, drawing gas from the upper gas compartment downwards through the hollow shaft. At a critical stirrer speed the fluid-gas interface reaches the holes and is there radially dispersed into the fluid by the mechanical forces of the stirrer. The gas flow rate is thus dependent on the angular stirrer speed.

3. Tomography system

The tomography setup (fig. 2) essentially consists of a medical X-ray source (DI-104H-22/60-150, COMET AG, Switzerland) and a two-dimensional digital X-ray flat panel detector (RID 1640 AL1, Perkin Elmer Optoelectronics GmbH & Co. KG, Germany) arranged opposite to each other. The X-ray source is operated at 125 kV acceleration voltage and at 10 mA beam current. The detector has a resolution of 1024 x 1024 pixels, each of 0.4 mm by 0.4 mm size, and can be read out with a maximum rate of 3 Hz. The chemical reactor is placed between source and detector such that the entire reactor volume is displayed in the X-ray image and the stirrer shaft is vertically oriented in the very centre of the image. The source-detector distance is 1920 mm.

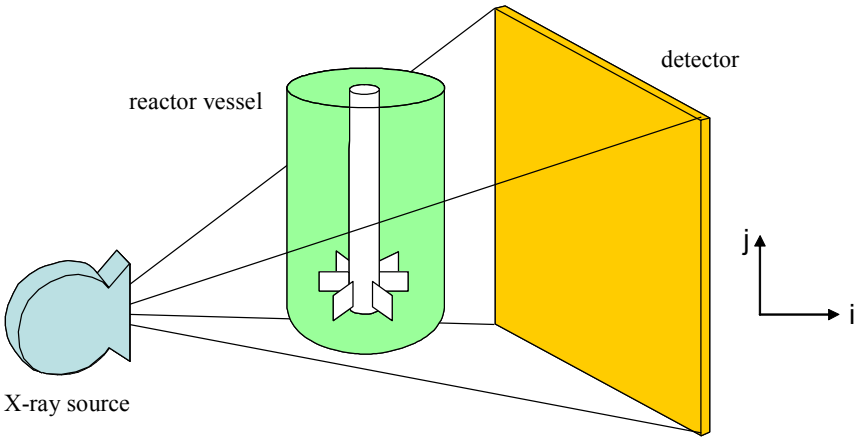

Fig. 2: Schematic representation of the cone-beam setup for measurement of radially symmetric gas distributions.

4. Cone-beam tomography

The forward problem of cone-beam tomography is given as follows. From the measurement we obtain a set of two-dimensional radiograms $I_\alpha(i,j)$ where I is the measured X-ray intensity at detector pixel (i,j) and projection angle α. Let further $I_\alpha^{(0)}(i,j)$ denote a reference measurement taken at a reference object, which may be sole air (zero attenuation), a purely gas-filled, or a fluid-filled reactor. From both measurements we first compute the extinction radiograms

$$E_\alpha(i,j) = -\log \frac{I_\alpha(i,j)}{I_\alpha^{(0)}(i,j)} \tag{1}$$

which represent the integral ray attenuation due to the material difference between reference and object. The extinction value itself represents the integral

$$E_\alpha(i,j) = \int_V L(i,j,\alpha,x,y,z)\ \mu(x,y,z)\,dx\,dy\,dz \tag{2}$$

of the X-ray attenuation coefficient distribution $\mu(x,y,z)$ along the ray L whose volume is defined purely geometrical by the source spot and the pixel extensions. Eq. (2) is the so called forward projection. The inverse problem consists of finding the unknown distribution $\mu(x,y,z)$ given the measured extinction radiograms. In fact this inverse problem is of a challenging three-dimensional nature. There are a few proposals to solve this problem [11, 12, 13, 14] whereby the approximate solution suggested by Feldkamp et al. is the most practical approach. The Feldkamp algorithm is basically a modified backprojection algorithm similar to two-dimensional filtered backprojection. It consists of the following steps:

1. two-dimensional weighting of each extinction value with weight w_L corresponding to the associated ray length according to

$$\hat{E}_\alpha(i,j) = w_L(i,j)\,E_\alpha(i,j) \tag{3}$$

2. one-dimensional filtering of all horizontal lines in all radiograms with the ramp filter H according to

$$G_\alpha(i,j) = \sum_{p=0}^{N_i-1} H((i-p) \bmod N_i), j)\ \hat{E}_\alpha(p,j) \tag{4}$$

3. the 3D backprojection

$$\hat{\mu}(x,y,z) = \sum_{q=0}^{N_\alpha} w_{sd}(x,y,z,\alpha_q)\,G_{\alpha_q}(i,j)\,\Delta\alpha \tag{5}$$

   into the volume, whereby the weight w_{sd} is given by the normalised intersection volume of the ray and the voxel at (x,y,z).

The solution is only approximative. Feldcamp et al. showed, that his algorithm produces negligible errors for small cone angles.

5. Beam hardening correction

Polyenergetic X-ray radiation will be hardened when penetrating thick materials since the effective attenuation coefficient becomes smaller with increasing penetration depth. If uncorrected this leads to systematic errors in quantitative X-ray measurements. Our method to perform beam hardening correction is illustrated in fig. 3. We take two images, one of the reactor completely filled with the fluid and another for the same arrangement plus an

additional acrylic plate of thickness *d* between reactor vessel and detector. From both images we compute the extinction radiogram

$$E_c(i,j) = -\log \frac{I_{\text{filled reactor+plate}}(i,j)}{I_{\text{filled reactor}}(i,j)} . \tag{6}$$

After that the plate is removed. Now any image I taken from the reactor with another fluid-gas distribution inside is processed to the extinction radiogram

$$E(i,j) = -\log \frac{I(i,j)}{I_{\text{filled reactor}}(i,j)} . \tag{7}$$

Taking the ratio of both radiograms gives

$$\frac{E(i,j)}{E_c(i,j)} = \frac{-\mu_{\text{fluid}}(i,j)\int_{L(i,j)} \varepsilon(s)\,ds}{\mu_{\text{plate}}(i,j)\; d / \cos\beta_{i,j}} \approx -\frac{\mu_{\text{fluid}}}{\mu_{\text{plate}}} \frac{\cos\beta_{i,j}}{d} \int_{L(i,j)} \varepsilon(s)\,ds . \tag{8}$$

Thereby $\varepsilon(s)$ denotes the local void fraction, $\int_{L(i,j)}$ the line integral along the ray (i,j), and $\beta_{i,j}$ is the angle between the ray and the detector normal. Note, that in the second term the attenuation coefficients are ray dependent due to the beam hardening whereas in the right term the ratio $\mu_{\text{fluid}}/\mu_{\text{plate}}$ is being considered as energy and thus ray independent. This is reasonably accurate for materials with similar radiological properties such as PMMA and organic fluids or water.

Furthermore, the ratio $\mu_{\text{fluid}}/\mu_{\text{plate}}$ can be determined by measurement. As shown in the right part of fig. 3 it is the better choice to perform the calibration at the filled reactor, since the beam hardening is also to some degree dependent on the overall amount of water in the ray path. Since we are interested to quantify gas fractions of less than 20% in the fluid phase the calibration at full liquid level is more accurate.

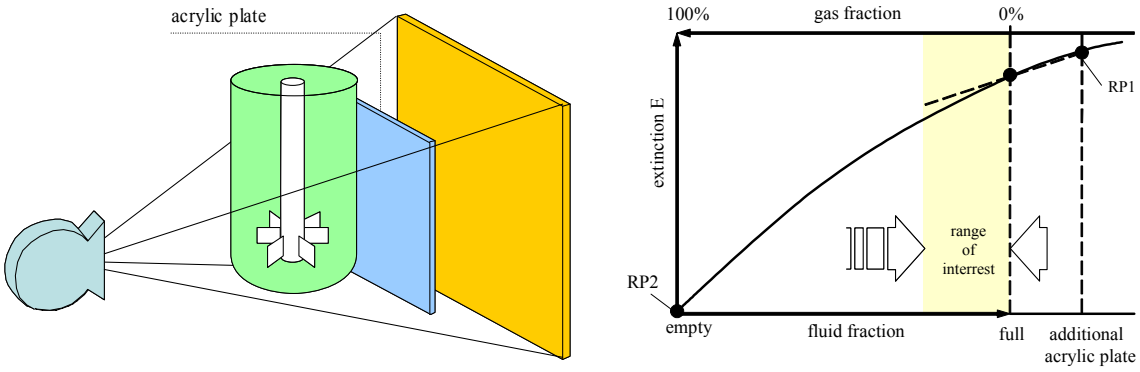

Fig. 3: Principle of beam hardening correction (for explanation see text).

6. Scattering radiation correction

Scattered radiation produces an intensity offset in the radiograms that is dependent on the object structure and leads to errors in quantitative measurements. Filtering by energy discrimination, such as in gamma tomography, SPECT, or PET is not possible due to the polyenergetic radiation of the X-ray source. Furthermore, in cone-beam tomography there is almost no possibility of spatial filtering by collimators. Different suggestions have been made to cope with scattered radiation. Neitzel [15] proposed, that increasing the air gap between object and detector would rise the signal-to-noise ratio in radiographic images. Seibert et al. [16] and Ohnesorge et al. [17] introduced deconvolution and convolution techniques respectively to determine the scatter intensity fraction and to correct radiographic image or projection data by that amount. In our experiments we used a moving slit approach to correct for scattering. This is illustrated in fig. 4. Again we perform an additional calibration measurement on a filled reactor. This time, however, we place a horizontal slit collimator in the ray cone just in front of the X-ray tube. The 1 mm wide slit limits the illumination of object and detector array to a thin radiation fan. In this way less than one percent of the reactor is exposed to radiation which in turn reduces the scattering offset for about more than 99%. The slit collimator is revolved in small steps of 0.5 mm by means of a stepping motor drive and for each step a radiogram is taken. In this way we scan the whole reactor at full liquid level and moderate stirrer rotation and can thus synthesise a scattering free image of the reactor. This synthetic image is then compared to an image obtained without the slit collimator. The difference of both images gives the scattering offset which is hereafter subtracted from all real measurements. This approach is reasonable, since with an increase of stirrer speed the overall mass of the object is conserved and there are only slight changes in the material distribution which does not significantly change the scattering offset.

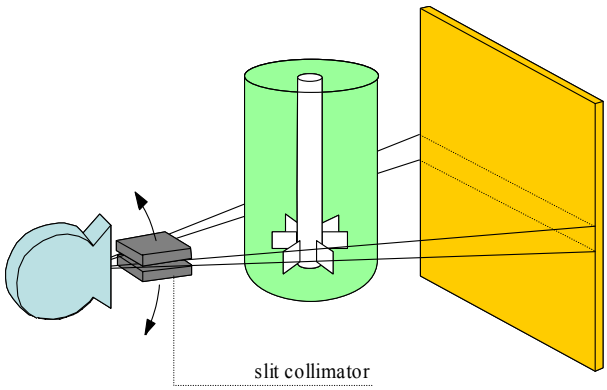

Fig. 4: Schematic representation of the moving slit collimator technique for scattering correction.

7. Results

The cone-beam tomography as described above has been first extensively tested on a special acrylic phantom with drillings simulating a gas fraction. All experiments have been carried out at 125 kV acceleration voltage, 10 mA beam current and with an overall integration time of 250 ms. Fig. 5 shows predicted and measured radial gas fraction distribution modelled by a set of drillings at six distinct radii of the acrylic phantom. With beam hardening but no scatter correction, measurement values are seriously affected by a non-constant offset, which

dramatically rises in the regions close to the shaft. Values inside the shaft are also not plausible at this stage. Repeating the measurements but using the moving slit scatter correction method gives results closest to the predicted ones. The signal-to-noise ratio was estimated to better than one regarding to measurements demanding an accuracy of 1% gas fraction in regions outside the shaft and the blades. Overall accuracy is approximately 3% in gas fraction, whereby the remaining error is suspected in the scattered radiation within the radiation fan.

Fig. 6 shows results obtained from the chemical reactor at different angular rotation speeds of the stirrer. This particular experiment has been carried out with isopropanol as a model fluid. In the region of the shaft and the stirrer blades quantification errors are large, so here this region is shaded with its radiographic representation. The sequence of reconstructed gas profiles shows, that at a critical angular speed of 1050 rpm the gas starts dispersing into the liquid. Another valuable information that can be directly obtained from the images is the evolution of the shape of the gas-fluid boundary, especially its depth and inclination, which is a measure of the angular momentum carried by the fluid and which is an important parameter for the evaluation of numerical flow simulations.

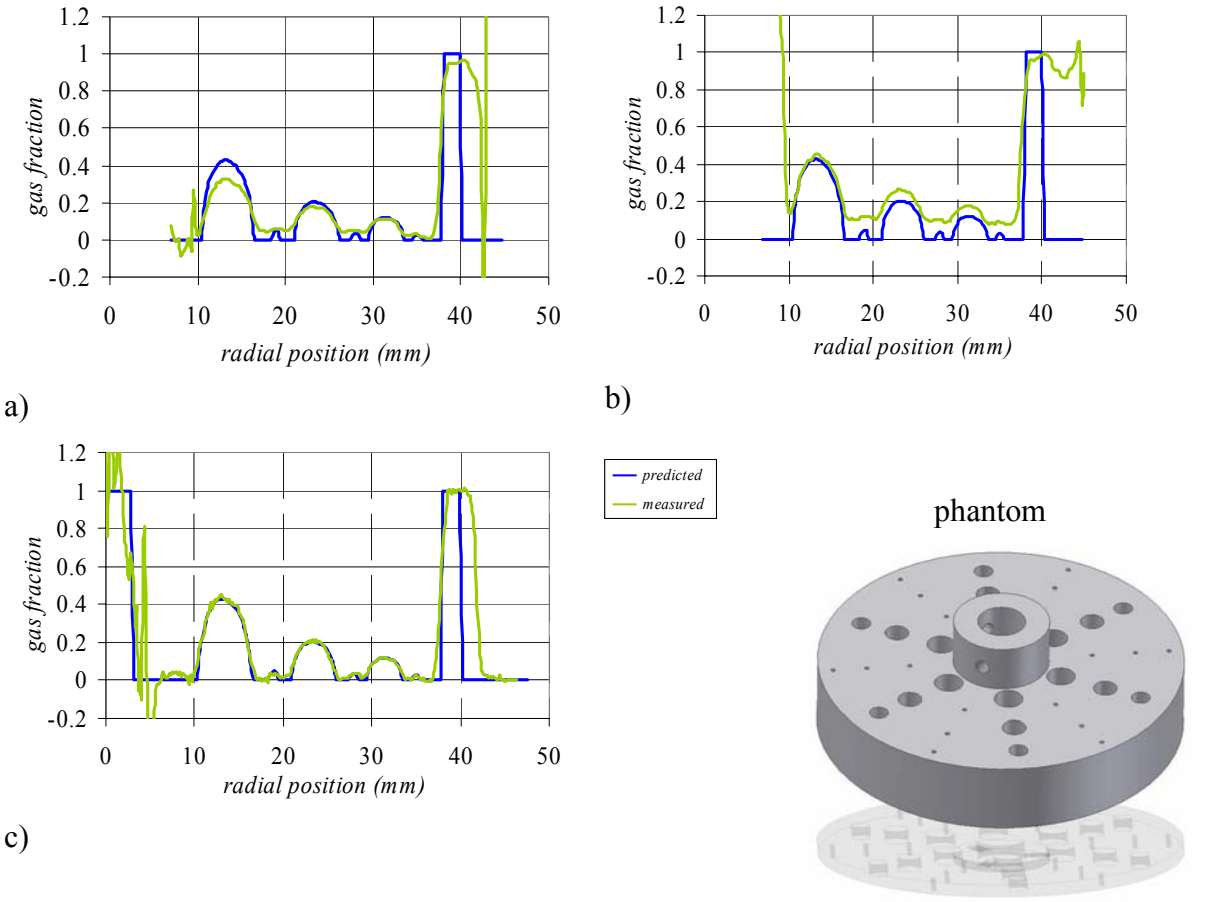

Fig. 5: Predicted and measured radial gas fractions for an acrylic two-phase phantom. a) uncorrected measurement, b) after applying beam-hardening correction, and c) after applying beam-hardening and scattering correction.

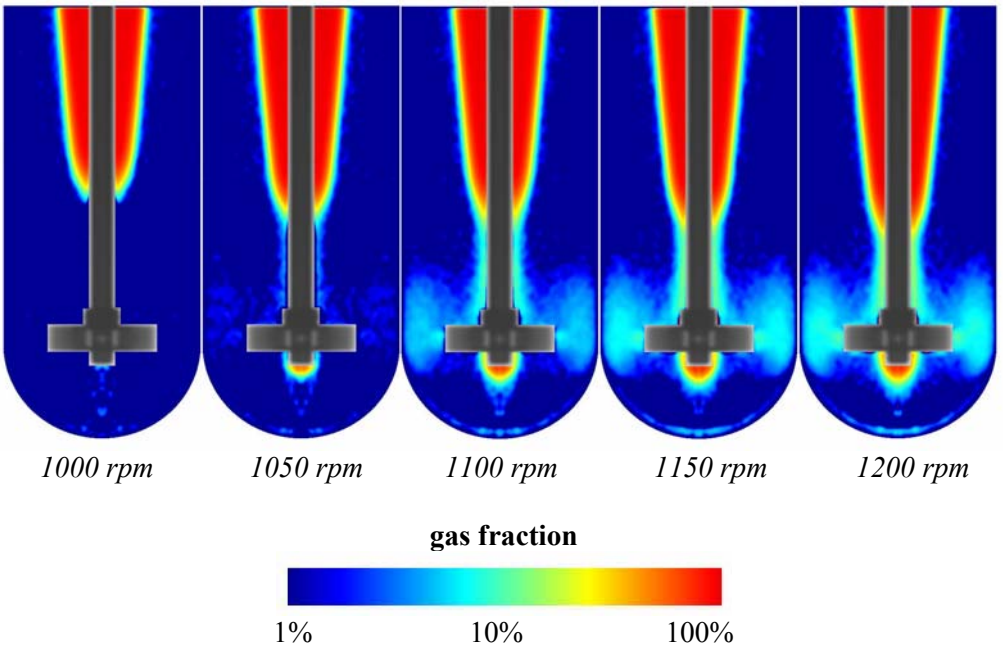

Fig. 6: Reconstructed gas fraction distributions in the reactor at different stirrer speeds.

8. Discussion and Conclusions

For the quantitative measurement of gas distributions in a stirred chemical batch reactor we adapted an X-ray cone-beam computed tomography technique. With this technique we are able to reconstruct radially symmetric two-phase distributions in a volume of a cylindric reactor from a single radiogram obtained with a few seconds integration time. Special care has been devoted to the development and experimental verification of correction methods for beam hardening and radiation scattering, which is necessary to account for the nonlinearities in the extinction characteristics of the probing X-rays. For the beam hardening correction we introduced a calibration method using an additional external plate absorber to obtain two closely spaced calibration points in a linear portion of the extinction function for each pixel of the radiogram. Scattering correction has been performed by means of an adjustable slit collimator that is used to measure the unscattered radiation portion for a representative fluid distribution in the reactor. The accuracy of the gas fraction measurement has been determined from phantom measurements and is approximately 3% in absolute gas fraction for 1 mm x 1 mm radial segments of the volume. In the near future the CBT system will be further developed and applied to experiments with real liquid-gas and liquid-liquid type reactions and mixture problems. One objective will be the validation and optimisation of CFD simulation codes for reactive multi-phase systems.

References

[1] M. Kraume (2003) : Mischen und Rühren. Grundlagen und moderne Verfahren. Weinheim: WILEY-VCH. – ISBN 3-527-30709-5

[2] V. Ilchenko, R. Maurus, T. Sattelmayer (2002), Processing and analysis of holographic images for the bubble characterisation in an aerated stirred tank. in Proceedings of Eurotherm 71 on Visualization, Imaging and Data Analysis In Convective Heat and Mass Transfer

[3] M. Kamiwano, M. Kaminoyama, K. Nishi, D. Shirota (2003), The measurement of bubble diameter distributions and liquid side mass transfer coefficients in a gas-liquid agitated vessel using a real-time, high-speed image processing system, Chem Eng Comm, 190, 1096
[4] K. E. Morud, B. H. Hjertager (1996), LDA measurements and CFD modelling of gas-liquid flow in a stirred vessel. Chem Eng Sci, 51(2), 233
[5] W.-M. Lu, S.-J. Ju (1987), Local Gas Holdup, Mean Liquid Velocity and Turbulence in an Aerated Stirred Tank Using Hot-film Anemomentry, Chem Eng J, 35, 9
[6] A. Paglianti, S. Pintus (2001) An impedance probe for the measurements of liquid hold-up and mixing time in two/three-phase stirred tank reactors. Experiments in Fluids, 31, 417
[7] M. Barigou, M. Greaves (1991), A capillary suction probe for bubble-size measurement, Meas Sci Technol, 2 (4), 318
[8] T. York (2001), Status of electrical tomography in industrial applications, Journ El Img, 10(3), 608
[9] S. L. McKee, R. A. Williams, A. Boxman (1995), Development of solid-liquid mixing models using tomographic techniques, Chem Eng Journ, 56, 101
[10] U. P. Veera, A. W. Patwardhan, J. B. Joshi (2001) Measurement of gas hold-up profiles in stirred tank reactors by gamma ray attenuation technique, Trans IChemE A, 79, 684
[11] B. D. Smith (1985), Image reconstruction from Cone-Beam Projections: Necessary and Sufficient Conditions and Reconstruction Methods, IEEE Trans Med Img, M1-4(1), 14
[12] H. K. Tuy (1983), An inversion formula for cone-beam reconstruction, SIAM J Appl Math, 43(3), 546
[13] P. Grangeat (1991), Mathematical framework of cone beam 3D reconstruction via the first derivative of the radon transform, Lecture notes in mathematics, 1497, 66
[14] L A. Feldkamp, L. C. Davis, J. W. Kress (1984), Practical cone-beam algorithm, J Opt Soc Am A, 1(6), 612
[15] U. Neitzel (1992), Grids or air gaps for scatter reduction in digital radiography: A model calculation, Med Phys, 19(2), 475
[16] J. A. Seibert, J. M. Boone (1998), X-ray scatter removal by deconvolution, Med Phys, 15(4), 567
[17] B. Ohnesorge, T. Flohr, K. Klingenbeck-Regn (1999), Efficient object scatter correction algorithm for third and fourth generation CT scanners, Eur Radiol, 9, 563.

AUTO-CATALYTIC EFFECT OF ACETIC ACID ON THE KINETICS OF THE METHANOL / ACETIC ANHYDRIDE ESTERIFICATION

Stefan Bohm, Günther Hessel, Holger Kryk, Horst-Michael Prasser, and Wilfried Schmitt

1. Introduction

The exothermic esterification reaction of acetic anhydride with methanol is a widely used test process for safety-oriented investigations in the field of chemical engineering. For the modelling and simulation of dynamic processes during fault scenarios caused by runaway reactions, a reaction kinetic model is needed to describe the thermal reaction course over a wide temperature range. At the Institute of Safety Research the esterification reaction is used as a test process to model and simulate pressure relief processes and safety-relevant fault scenarios caused by local exothermicities (i.e. hot spots due to stirrer faults) in stirred tank reactors as well as to simulate reacting flows using CFD codes in general. These research tasks make great demands on the kinetic models to reproduce the thermal and chemical reaction courses over a wide range of the temperature and the concentration. This includes the consideration of special reaction mechanisms like autocatalytic effects. To develop a kinetic model that fulfils these requirements, extensive calorimetric investigations using on-line FTIR analyses were carried out and special evaluation methods have been developed. From these investigations, a two-step kinetic model results in fulfilling the requirements mentioned above.

2. Applicability of existing reaction kinetic models

The exothermic esterification reaction of acetic anhydride with methanol proceeds according to the following reaction equation:

$(CH_3CO)_2O$	+	CH_3OH	→	CH_3COOCH_3	+	CH_3COOH	ΔH_R = -66 kJ/mol
acetic anhydride		*methanol*		*methyl acetate*		*acetic acid*	
AAH		*ME*		*MA*		*AA*	

A basic kinetic model requirement for the use in safety-oriented investigations is the validity of the model in respect of the reproduction of the thermal reaction course over a wide temperature range. For this purpose, in the past the kinetic models were usually developed by means of experiments using adiabatic calorimetry. From the literature, there are some kinetic models available obtained by experiments in adiabatic calorimeters using a fixed initial molar ratio of the educts [1,2]. These so called overall kinetics approaches, describing the reaction rate r as a function of the reaction temperature T and the concentrations of the educts [AAH] and [ME], have the following model structure:

$$r = k_0 \cdot e^{\left(\frac{-E_A}{R \cdot T}\right)} \cdot [AAH]^m \cdot [ME]^n \qquad (1)$$

In equation (1), E_A is the activation energy and k_0 is the frequency factor. The exponents m and n are the reaction orders with respect to the reactants acetic anhydride and methanol. The overall reaction order is given by the sum of the exponents m and n.

To model and simulate different safety-relevant fault scenarios from the start of the reaction

via the fault event to subsequent chemical processes, the kinetic models have to reproduce the thermal reaction course and the concentration courses over wide ranges of the temperature and the concentration. Furthermore, the models should also reproduce the reaction courses in the adiabatic, isothermal and isoperibolic process control. To check the applicability of the existing kinetic models, isothermal and adiabatic esterification reactions at several initial molar ratios of educts were carried out using the RC1 calorimeter (isothermal experiments) and the calorimeter PhiTecII (adiabatic operation). Figure 1 shows the thermal reaction course of an isothermal esterification in comparison to simulation results using kinetic models taken from the literature [1,2]. Both the kinetics are based on adiabatic experiments using an initial molar ratio of [ME] : [AAH] = 2 : 1. The course of the reaction temperature of an adiabatic experiment compared to simulations using the same kinetic models is shown in Fig. 2.

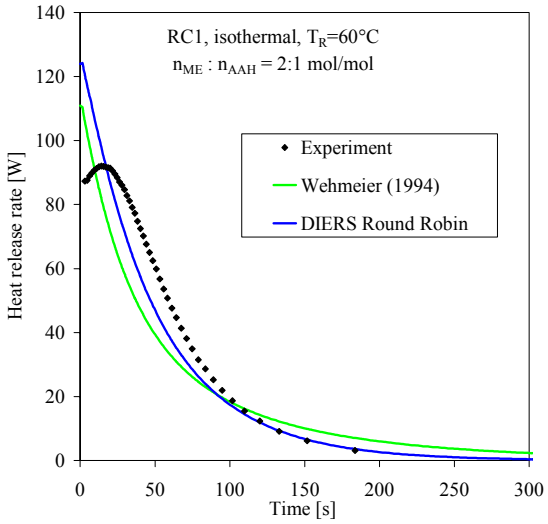

Fig.1: Thermal reaction course of the isothermal esterification

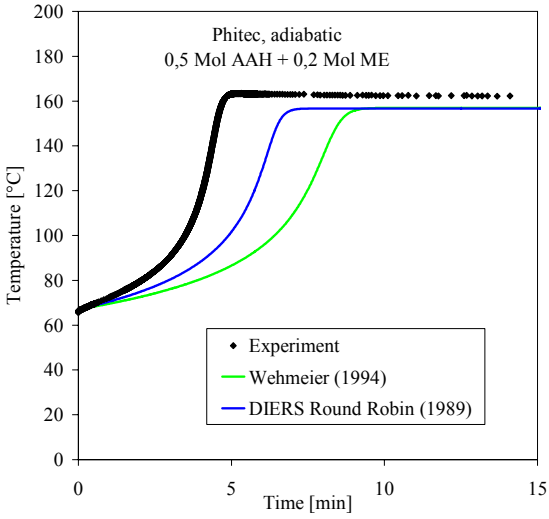

Fig.2: Course of the reactor temperature during the adiabatic esterification

Especially, the thermal process behaviour at the start phase of the isothermal reaction is not describable by the structure of the models. Furthermore, the thermal reaction course in the adiabatic operation is not reproduced if the educt concentrations differ from the initial molar ratio of [ME] : [AAH] = 2 : 1. Thus, the following conclusions were drawn in terms of the model validity in case of this particular reaction:

- The validity of the existing 2nd and pseudo 1st order overall kinetics is confined to the adiabatic operation.
- The validity of the existing kinetics is confined to the educt concentrations used in the experiments to develop the models.

Therefore, the development of advanced reaction kinetic models was necessary to fulfil the model demands mentioned above.

3. Setting up a new model structure

It is assumed that the increasing reaction rate at the beginning of the isothermal esterification (Fig.1) is caused by the autocatalytic effect of the acetic acid formed during the reaction. The autocatalytic behaviour was proven by isothermal esterification using the RC1 calorimeter. For this purpose, different amounts of acetic acid were added to the reaction mixtures before

the reactions were started. Figure 3 shows the thermal reaction courses of the related experiments.

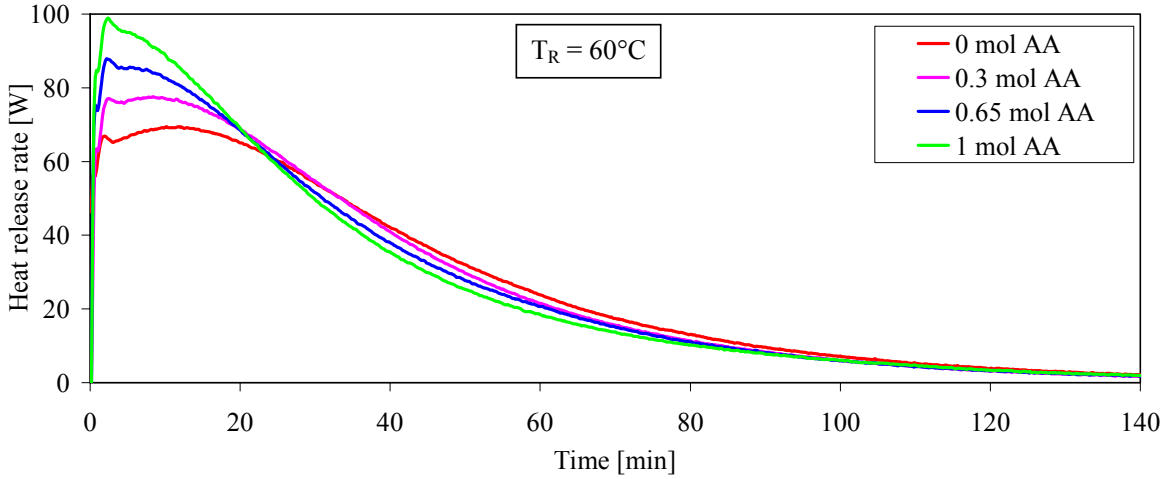

Fig. 3: Thermal reaction courses of isothermal esterification with addition of acetic acid

As can be seen from Fig. 3, the reaction rate at the beginning of the esterification increases with the increasing amount of the added acetic acid. Therefore, the time-dependent acetic acid concentration has to be inserted into the kinetic model as a new model parameter. To maintain the usual structure of the overall kinetic models, the autocatalytic reaction was modelled as two simultaneous reaction steps – the uncatalysed esterification of acetic anhydride according to equation (2) and the esterification catalysed by acetic acid according to equation (3).

$$r_1 = k_{0_1} \cdot e^{\left(\frac{-E_{A_1}}{R \cdot T}\right)} \cdot [AAH]^{m_1} \cdot [ME]^{n_1} \tag{2}$$

$$r_2 = k_{0_2} \cdot e^{\left(\frac{-E_{A_2}}{R \cdot T}\right)} \cdot [AAH]^{m_2} \cdot [ME]^{n_2} \cdot [AA]^{p_2} \tag{3}$$

With $$r = r_1 + r_2 \tag{4}$$

By using the standard overall kinetics structure, most of the commercially available simulation tools can be used to model and simulate the autocatalytic esterification process.

4. Estimation of the model parameters

Since the autocatalytic effect on the reaction course plainest appears under isothermal conditions, the activation energies and the frequency factors have to be estimated by means of isothermal experiments. For the fitting of the isothermal reaction rate constants, the simulation programs ProSim Batch and BatchCAD were used. However, the Arrhenius Plots as a result of the isothermal experiments at different temperatures and educt concentrations to calculate the model parameter $E_{A,i}$ and $k_{0,i}$ based on the isothermal rate constants show different activation energies and frequency factors depending on the initial batch concentration. These dependencies could not be avoided by changing the reaction orders. Therefore, it was decided to set the reaction orders with respect to each substance in the equations (2) and (3) to 1 and to introduce the initial batch concentration, defined as the start molar fraction of acetic anhydride x_0 according to equation (5), as a new parameter into the kinetic model.

$$x_0 = \frac{n_{0,AAH}}{n_{0,AAH} + n_{0,ME}} \quad (5)$$

In equation (5), $n_{0,AAH}$ and $n_{0,ME}$ are the initial amounts of substances of the acetic anhydride and of the methanol, respectively.

The activation energies and the frequency factors depending on the start molar fractions are shown in Fig. 4 and Fig. 5, respectively.

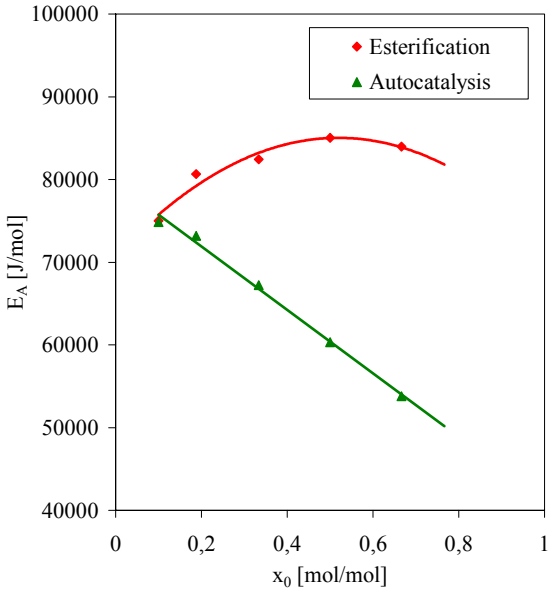

Fig. 4: Activation energies depending on the start molar fraction

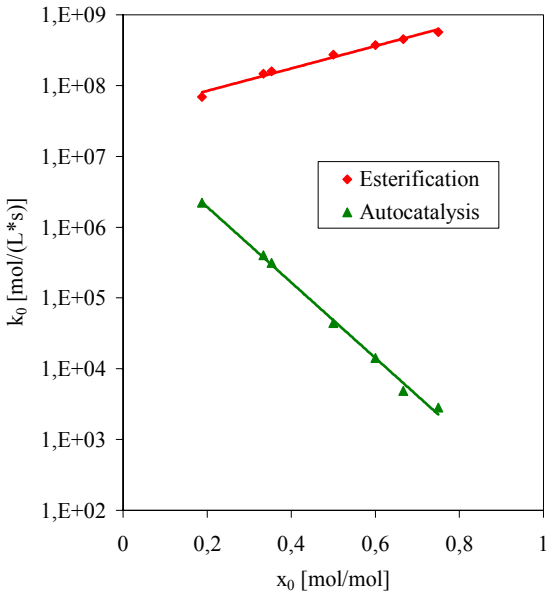

Fig. 5: Frequency factors depending on the start molar fraction

The equations to calculate the model parameters depending on the start molar fraction were obtained by fitting the parameters based on the isothermal experiments and subsequent adjustment by means of adiabatic esterification. As a result, the following reaction kinetic model was obtained [4]:

$$r_1 = k_{0_1} \cdot e^{\left(\frac{-E_{A_1}}{R \cdot T}\right)} \cdot [AAH] \cdot [ME] \quad (6)$$

$$r_2 = k_{0_2} \cdot e^{\left(\frac{-E_{A_2}}{R \cdot T}\right)} \cdot [AAH] \cdot [ME] \cdot [AA] \quad (7)$$

$$E_{A_1} = 15924\,(x_0)^2 + 20568\,x_0 + 77337 \quad (8)$$

$$E_{A_2} = -40472\,x_0 + 80750 \quad (9)$$

$$k_{0_1} = -1.36 \cdot 10^8 + 1.36 \cdot 10^8 \cdot e^{(2.2\,x_0)} \quad (10)$$

$$k_{0_2} = 2 \cdot 10^7 \cdot e^{(-12.28\,x_0)} \quad (11)$$

5. Verification of the reaction kinetics

The verification of the kinetics was carried out by isothermal and isoperibolic experiments using the RC1 calorimeter in conjunction with an on-line FTIR spectrometer as well as by adiabatic esterification using the PhiTecII calorimeter. Figures 6 and 7 show the thermal reaction courses of isothermal experiments in comparison to simulation results for different temperatures and molar fractions of the educts, respectively.

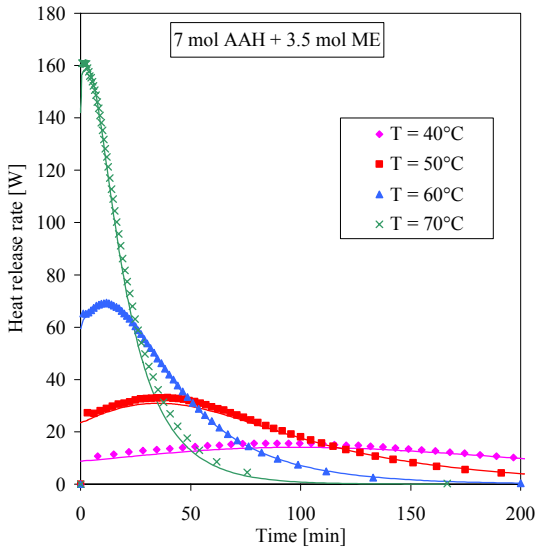

Fig. 6: Thermal reaction courses of isothermal esterification at different temperatures

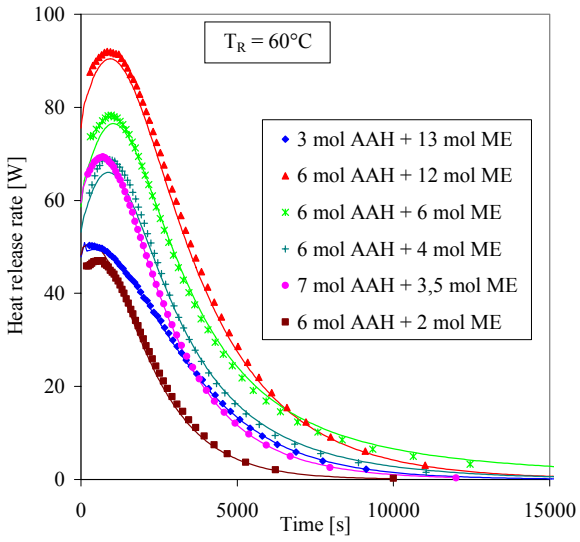

Fig. 7: Thermal reaction courses of isothermal esterification at different start molar fractions

The results of the simulations are in good accordance with the experimental data. Furthermore, the autocatalytic startup behaviour of the reaction is reproduced correctly. To estimate the model accuracy in case of the isoperibolic and the adiabatic process control, results of RC1 and PhiTecII experiments were compared to the related simulations.

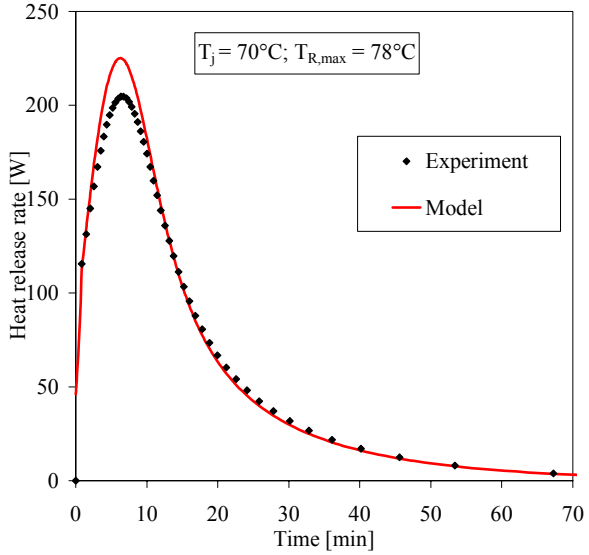

Fig. 8: Thermal reaction course of the isoperibolic esterification

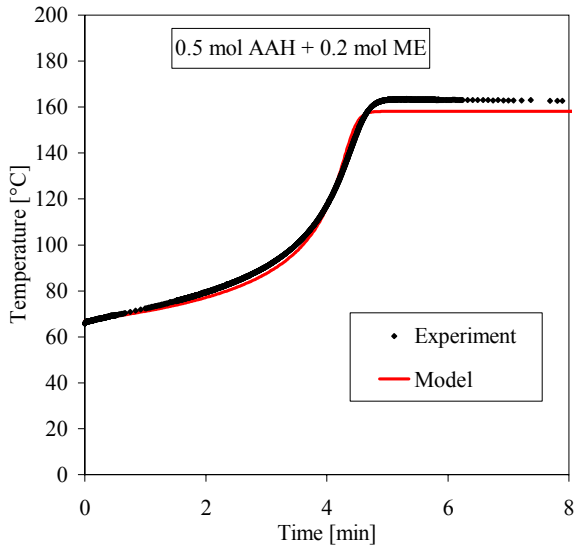

Fig. 9: Course of the reaction temperature during the adiabatic esterification

The thermal reaction courses of selected esterification at isoperibolic and adiabatic conditions are diagrammed in Fig. 8 and 9, respectively. The runs of the curves are reproduced correctly in case of both the isoperibolic and the adiabatic process mode. Solely, in using the kinetics to simulate the isoperibolic process, the maximum heat release rate oversteps the experimental value slightly. However, the relative model inaccuracy never exceeds a value of 10% during the whole process course. As a result of the model verification, it was found that the new re-

action kinetic model is able to reproduce the process behaviour correctly within an educt molar fraction in the range of $x_0 = 0.1875 \ldots 0.75$.

6. Summary and outlook

A new two-step reaction kinetic model was developed for the esterification reaction of acetic anhydride with methanol by using calorimetric investigations and analytical methods. The main advantage of the new model over previously existing overall kinetics is the adaptability on wide educt concentration ranges. By taking into account the autocatalytic effects of the acetic acid, the model now can be used to simulate the process in the isothermal, isoperibolic and adiabatic operation. This wide field of applications is achieved by modelling the process as two simultaneous reaction steps and fitting the activation energies as well as the frequency factors depending on the initial molar fraction of acetic anhydride. For final conclusions on the model performance in terms of the applicability for simulations of safety-relevant fault scenarios like pressure relief processes, the new kinetic model has to be tested using appropriate simulation software (i.e. BRICK [3]).

A problem for the application of the new reaction kinetics to simulate reacting flows results from using empirical functions to estimate the model coefficients depending on the initial molar fraction. Thus, the actual process state described by the model depends on the initial process state. Therefore, it is difficult to simulate processes where the variations of the concentrations are not caused by the chemical reactions exclusively (i.e. semibatch processes, effects of mass transfer). Consequently, an alternative reaction kinetic model having the following structure is developed presently:

$$r = k_0([AA]) \cdot e^{\left(\frac{-E_A([AA])}{R \cdot T}\right)} \cdot [AAH]^m \cdot [ME]^n \qquad (12)$$

In this model, both the activation energy and the frequency factor are inserted as functions of the actual acetic acid concentration [AA] to consider the autocatalytic effects. Thus, the alternative model structure has a stronger theoretical background and comprises model parameters, which depend on the actual process state exclusively. To estimate the functional dependencies $k_0([AA]$ and $E_A([AA])$, a new differential evaluation method was developed. The evaluation of the experiments according to the new method is still in progress but first results show the practicability of the model structure in general.

References

[1] G. Wehmeier (1994), Theoretische und experimentelle Untersuchung der Vorgänge bei der Druckentlastung von Chemiereaktoren, Fortschr.-Ber. VDI Reihe 3, 373, VDI-Verlag Düsseldorf

[2] J. C. Leung, M. J. Creed and H. G. Fisher (1989), Round-robin "Vent sizing package" results, Int. Symp. Runaway React., 264-280

[3] D. Lucas (2000), BRICK - a one-dimensional simulation tool for multiphase flow in vessels, Chemical Engineering and Technology, 23, 845-849

[4] S. Bohm (2004), Erarbeitung eines reaktionskinetischen Modells der Veresterung von Essigsäureanhydrid mit Methanol zur Einbindung in Druckentlastungs-Simulationsprogramme und CFD-Codes, Diploma thesis, TFH Berlin

ASSESSMENT OF DIFFUSION COEFFICIENTS IN COMPACTED KAOLINITE BY THROUGH-DIFFUSION EXPERIMENTS

Jens Mibus, Roland Küchler, and Mouad Lambarki[1]

1. Introduction

Clays are widespread in the geologic environment and usual components of many soils, sediments, and pelitic rocks. Clay rock is a potential host rock for a deep repository for nuclear waste. Again, plastic clays, in particular swellable smectites, are used as clay liners in landfills or as integral part of the geo-engineered barrier system in the immediate vicinity of the spent-fuel containers, the so-called near field of underground repositories. Diffusion is the main transport mechanism due the low permeability of clayey media. Therefore, risk assessment requires an adequate description of the diffusion process. The diffusion coefficient and the porosity or the rock capacity factor are fundamental parameters for modeling the migration of radionuclides in clay. Reactive tracers such as actinides are strongly retarded due to adsorption on the clay surface. In contrast, anionic tracers as for example iodide or selenate are excluded from a portion of the pore volume due to electrostatic repulsion by negatively charged clay surfaces. In order to quantify these processes it is necessary to know the effective pore volume of the porous medium. Tritium in form of tritiated water (HTO) is the ideal tracer for that purpose. Because HTO behaves as a conservative tracer, i.e., there is no interaction between tracer and matrix. Thus, for example sorption can be neglected. However, the measurement of porosity by the most common method of through-diffusion with constant gradient is interference-prone in the first transient stage of the experiment [1]. Better results are obtained from measuring the out-diffusion of the tracer from the clay sample. Alternatively, the trough-diffusion with variable gradient can be used. Modeling the latter two problems are related to non-linear solutions. In this study the assessment of effective diffusion parameters in compacted kaolinite and derivation of adequate modeling equations are presented. Kaolinite is a common and well-characterized clay mineral, which is often used in geo-engineering.

The investigations to the diffusion behavior of radio nuclides in clays are carried out together with the institute of radiochemistry within the frame of a common research project.

2. Materials and Methods

Kaolinite from Hirschau (Amberger Kaolinwerke, Hirschau, Germany) was compacted to a dry bulk density of $\rho = (1.1 \pm 0.03)$ g cm^{-3} in a Proctor mould. Subsequently it was placed in a diffusion cell of a cross-sectional area of $A = (78.6 \pm 0.5)$ cm^2 and a layer thickness of $L = (2.1 \pm 0.05)$ cm and fixed between two filter plates as shown in Fig. 1. The diffusion cell comprises a sample holder containing the clay plug, two filter plates, and two chambers for rinsing the filter plates. It is connected with tubes to two storage vessels. A peristaltic pump continuously circulates the solutions. All components are made of polyethylene except for the sample holder which is made of acrylic glass. Two reservoirs of (180 ± 1) ml Milli-Q water (Milli-Q-System, Millipore, Molsheim, France), respectively, were used. One reservoir was labeled with HTO (Amersham Biosciences, Buckinghamshire, UK) yielding a starting activity of (2.2 ± 0.002) Bq ml^{-1} in the high-concentration reservoir.

[1] RWTH-Aachen University, Department of Engineering Geology and Hydrogeology, Aachen

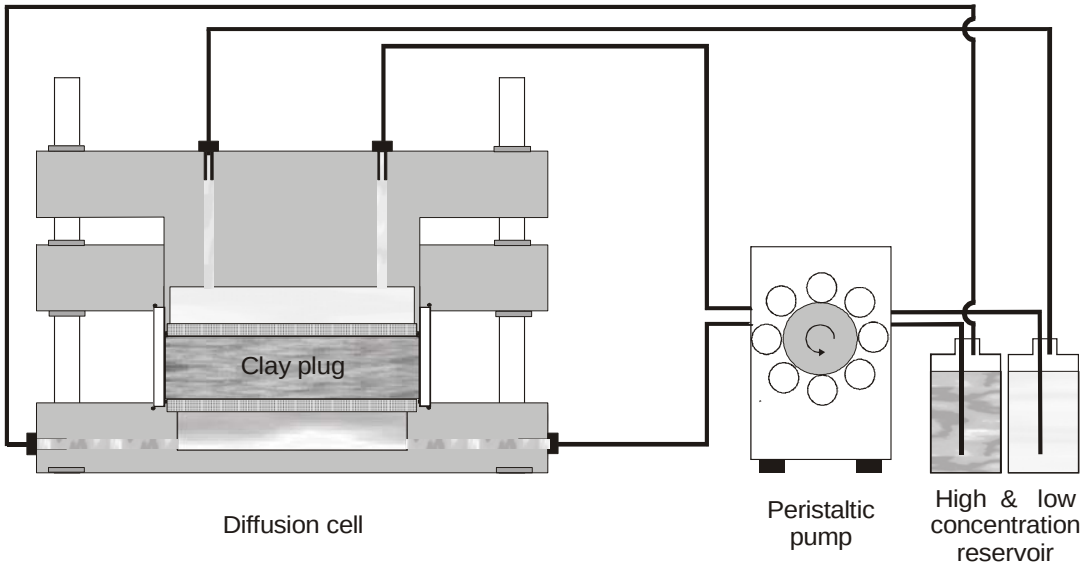

Fig. 1: Schematic set-up of the diffusion experiment

Both solutions, the labeled and the unlabeled, were circulated behind the filter plates. Each reservoir has been re-circulated twelve times per day. The tracer concentration (or activity) was allowed to balance between both reservoirs by diffusion through the clay plug. The activities in both reservoirs were measured periodically by liquid scintillation counting (LSC; Wallac, Perkin Elmer). A quantity of 100 µl sample solution was placed in a scintillation vial and 5 ml scintillation cocktail Ultima Gold (Canberra-Packard, Zurich, Switzerland) were added. The counting time was 10 minutes, background measurements were performed with Milli-Q-water. A consideration of tritium decay was not necessary since its half life of 12.4 years is long enough compared to the duration of the experiment of 60 days.

3. Modeling of Through-Diffusion with Concentration Variation in Limited Reservoirs

The traditional though-diffusion model assumes a constant concentration at the inlet and a zero concentration at the outlet as a function of time. With this assumption, one derives an expression for the percolated quantity at the outlet. The constant boundary conditions must be enforced in the experiment by a complex control system. Free boundary conditions can easily be established in the experiment. The modeling however leads to ordinary differential equations at the boundary surfaces. The solution of this problem is derived in the following.

For a one-dimensional diffusion process through a sheet the flux is given by Fick's first law:

$$j = -D_e \frac{\partial C}{\partial x}.$$

The diffusion equation for a tracer in the sheet can be expressed as follows:

$$\frac{\partial C(x,t)}{\partial t} = D \frac{\partial^2 C(x,t)}{\partial x^2} - \lambda \cdot C(x,t). \qquad (1)$$

where *C(x,t)* is the tracer concentration in the pore water of the medium [Bq/ml], λ is the radioactive decay constant, t is diffusion time [h]; x is distance from the porous medium sample surface. *D* [cm^2/h] is the apparent diffusion coefficient: The relationship between the diffusion coefficients *D*, D_e, D_w, and the geometric parameters is given by:

$$D = \frac{D_e}{\varepsilon} = \frac{D_w}{\tau^2} \tag{2}$$

where D_w is the diffusion coefficient in water, τ is the tortuosity, and ε the diffusion accessible porosity.

In the experimental set-up the porous medium sheet is in contact with perfectly mixed reservoirs, that means the concentration in the reservoirs depends only on time. The sheet occupies the space $0 \le x \le L$. If this condition is fulfilled, the following ordinary differential equations can be formulated for the concentration in the reservoirs: At the high-concentration side (tracer enter the sheet)

$$\frac{dC_{in}}{dt} = -\lambda C_{in} + q - \varepsilon \cdot D \frac{A}{V_{in}} \left. \frac{\partial C(x,t)}{\partial x} \right|_{x=L}, \quad C_{in}(0) = C_0, \quad C_{in}(t) = C(L,t), \tag{3}$$

holds and for the low- concentration side (tracer leave the sheet)

$$\frac{dC_{out}}{dt} = -\lambda C_{out} + \varepsilon \cdot D \frac{A}{V_{out}} \left. \frac{\partial C(x,t)}{\partial x} \right|_{x=0}, \quad C_{out}(0) = 0, \quad C_{out}(t) = C(0,t), \tag{4}$$

is valid. *A* [cm^2] is the cross-sectional area of the sheet accessible for diffusion, V_{in}, V_{out} are the volumes of reservoirs, and *q* is a constant source term. The initial condition is: $C(x,t=0)=0$, meaning that the porous medium is initially free of tracer. One comfortably gets the solution of this above system of differential equations by the method of the Laplace transformation [2]. In the following only the key equations are summarised. The tracer concentration in the porous medium is given by:

$$C(x,t) = e^{-\lambda \cdot t} \left[\frac{(C_0 - q/\lambda) \cdot V_{in}}{V_{in} + V_{out} + \varepsilon \cdot V_{dif}} + \sum_{i=1}^{n} (C_0 - \frac{q}{\lambda + \delta \cdot k_i^2}) \cdot a_i \cdot \varphi_i(x) \cdot e^{-\delta \cdot k_i^2 \cdot t} \right] + \phi(x), \tag{5}$$

with $\delta = \frac{D}{L^2}$, $V_{dif} = L \cdot A$, $sv = \frac{V_{in} + V_{out}}{\varepsilon \cdot V_{dif}}$, $pv = \frac{V_{in} \cdot V_{out}}{(\varepsilon \cdot V_{dif})^2}$, $\beta = \sqrt{\frac{\lambda}{\delta}}$, the individual terms in

equ. (5) have the following form:

$$\varphi_i(x) = k_i \cdot \sin\left(k_i \frac{x}{L}\right) - \varepsilon \frac{V_{dif}}{V_{out}} \cos\left(k_i \frac{x}{L}\right)$$

$$a_i = \frac{2 \cdot sv \cdot pv \cdot k_i}{\left[(sv+1) + \left[sv^2 + pv \cdot (sv - 2 + pv \cdot k_i^2)\right] \cdot k_i^2\right] \cdot \sin(k_i)}$$

$$\phi(x) = \frac{q \cdot pv \cdot \left[\beta \cdot \sinh\left(\beta \frac{x}{L}\right) + \varepsilon \frac{V_{dif}}{V_{out}} \cosh\left(\beta \frac{x}{L}\right) \right]}{\beta \cdot D \cdot \left[(pv \cdot \beta^2 + 1) \cdot \sinh(\beta) + \beta \cdot sv \cdot \cosh(\beta) \right]}.$$

The k_i are the roots of the transcendental equation:

$$(pv \cdot k^2 - 1) \cdot \sin(k) - k \cdot sv \cdot \cos(k) = 0. \tag{6}$$

The function $\phi(x)$ describes the tracer concentration in the steady-state.

4. Parameter Estimation and Results

The measured temporal developments of the activities in both reservoirs are depicted in Fig.°2. As expected, on the high concentration side the tracer activity immediately decreases. In contrast, on the low concentration side the activity starts rising significantly after a time period of two days. The equilibration concentration on both sides is reached after about 60 days. The best-fit of the solution (5) to the measurements determines D. For the experimental set-up q in equ. (5) is equal to zero and the decay constant of tritium is so small that it can be set zero too. To estimate the diffusion coefficient *D* the chi-square function

$$\chi^2 = \frac{1}{2} \sum_{i=1}^{m} \left(\frac{C(L,t_i) - C_{in}(t_i)}{\sigma_i^{in}} \right)^2 + \left(\frac{C(0,t_i) - C_{out}(t_i)}{\sigma_i^{out}} \right)^2 \tag{7}$$

was minimized by means of a fitting procedure.

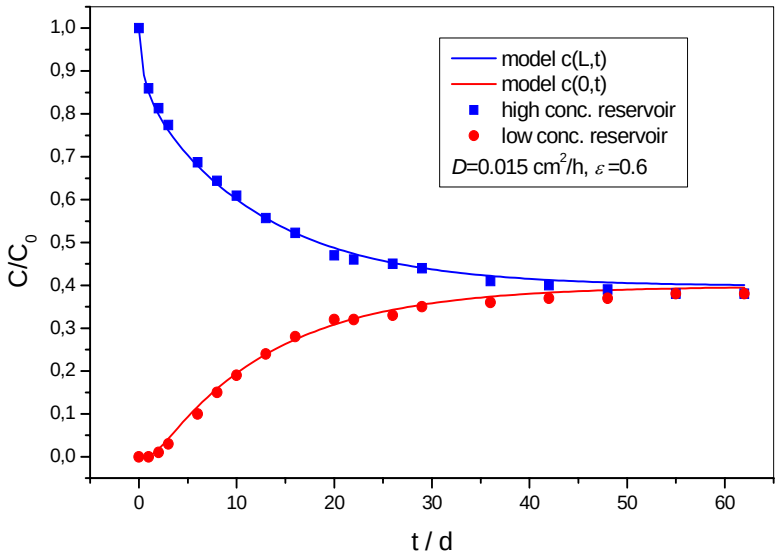

Fig. 2: Measured and calculated tracer concentration in both reservoirs versus time

C_{in}, C_{out} are the concentrations in the inlet- and outlet reservoir measured at m time points, and σ_i is the measurement error (standard deviation) of the *i*th data point For the measuring error of the complete analysis procedure how described above was estimated $\sigma_i \approx C_0 \cdot 0.044$.

The solid lines in Fig. 2 are the results of the fits. Both series of measurements are quite well reproduced by the fits. The apparent diffusion coefficient determined in this manner is in the range $D = (4.1 \pm 0.2) \cdot 10^{-10}$ m^2/s. The corresponding accessible porosity is: $\varepsilon = 0.60 \pm 0.02$

5. Conclusions

The parameters D and ε determined from the concentration curves are in the range of natural clayey sediments [3]. Our experimental result yield a tortuosity factor $\tau = 2.3$. The diffusion coefficient in free water has the value [4]: $D_w = 2.2 * 10^{-9}$ m ^{2}/s. In consolidated pelitic rocks τ ranges between 1.1 and 1.7 [5] whereas in marine sediments a value of 1.7 was found [3]. This minor difference may result from compositional and granulometrical properties. Furthermore, a technologically compacted material is likely to offer a texture different from diagenetically matured sediments [6].

A comparison with long-lasting stationary diffusion experiments using reactive tracers and natural sealing material (loess loam) is of practical relevance. Here D_e was found to be 2.47, 3.04, and $4.14 \cdot 10^{-10}$ m^2/s for Cu, Pb, and Zn, respectively. These results indicate that the diffusion parameters of the natural and the engineered barrier material are in the same order of magnitude.

Acknowledgement

The authors wish to thank D. Tondera (Freiberg University of Mining and Technology) for technological support and S. Brockmann for taking the measurements.

References

[1] L.R. Van Loon, J.M. Soler (2004), Diffusion of HTO, $^{36}Cl^-$, $^{125}I^-$, and $^{22}Na^+$ in Opalinus Clay: Effect of confining pressure, sample orientation, sample depth and temperature, PSI-Bericht Nr. 04-03, Paul-Scherrer-Institute, Villigen, Switzerland.

[2] A. Kneschke (1962), Differentialgleichungen und Randwertprobleme, Band III, Leipzig, B.G. Teubner Verlagsgesellschaft

[3] N. Iversen, B.B. Jørgensen (1993), Diffusion coefficients of sulphate and methane in marine sediments, Geochim. Cosmochim. Acta. 57, 571-578

[4] Y.H. Li, S. Gregory (1974); Diffusion of ions in seawater and deep-sea sediments, Geochim. Cosmochim. Acta. 38, 703-714

[5] L.R. Van Loon, J.M. Soler, A. Jakob and M.H. Bradbury (2003),. Effect of confining pressure on the diffusion of HTO, $^{36}Cl^-$ and $^{125}I^-$ in a layered argillaceous rock (Opalinus Clay): diffusion perpendicular to the fabric, Appl. Geochem. 18, 1653-1662

[6] P.M.H. Kau, P.J. Binning, P.W. Hitchcock and D.W. Smith (1999), Experimental analysis of fluoride diffusion and sorption in clays, J. Contam. Hydrol. 36, 131-151 Dresden, Germany

COUPLED FINITE ELEMENT ANALYSIS OF PRESSURE VESSEL CREEP FAILURE EXPERIMENTS

Hans-Georg Willschuetz and Eberhard Altstadt

1. Introduction

The hypothetical scenario of a severe accident with core meltdown and formation of a melt pool in the lower plenum of a Light Water Reactor (LWR) Pressure Vessel (RPV) can result in the failure of the RPV and the discharging of the melt to the containment. One accident management strategy could be to stabilize the in-vessel debris or melt pool configuration in the RPV as a major barrier against uncontrolled release of heat and radionuclides into the containment.

To obtain an improved understanding of the melt pool convection, the vessel creep, possible failure processes and modes occurring during the late phase of a core melt down accident the FOREVER-experiments (Failure Of REactor VEssel Retention) have been performed at the Division of Nuclear Power Safety of the Royal Institute of Technology, Stockholm [1]. These experiments were simulating the behavior of the lower head of the RPV under the thermal loads of a convecting melt pool with decay heating, and under the pressure loads that the vessel experiences in a depressurized vessel scenario (cf. Fig. 1). The geometrical scale of the experiments was 1:10 compared to a prototypic LWR.

An axisymmetric Finite Element (FE) model was developed based on the multi-purpose code ANSYS/Multiphysics®. Using the Computational Fluid Dynamics (CFD) module FLOTRAN the melt pool convection was simulated and the temperature field within the melt pool and within the vessel wall was calculated [2]. But due to the lack of a turbulence model for very high internal Rayleigh numbers of up to 10^{17} in the prototypic case and due to the very time consuming CFD-solution, the Effective Conductivity Convectivity Model (ECCM) as proposed by Bui [3] has been implemented. Based on the calculated temperature field in the vessel wall, the transient structural mechanical calculations are then performed applying a creep model which takes into account the large temperature, stress and strain variations. A main task for the numerical creep model approach is the development and validation of the creep data base (CDB). The source for the CDB are uniaxial creep tests, like the REVISA-experiments [4]. The CDB includes the primary, secondary and tertiary creep stages. In the calculation the creep strain rate is then evaluated in dependence on the current total strain, temperature and equivalent stress.
In the prior work only a one-way coupling between the thermal and the mechanical model

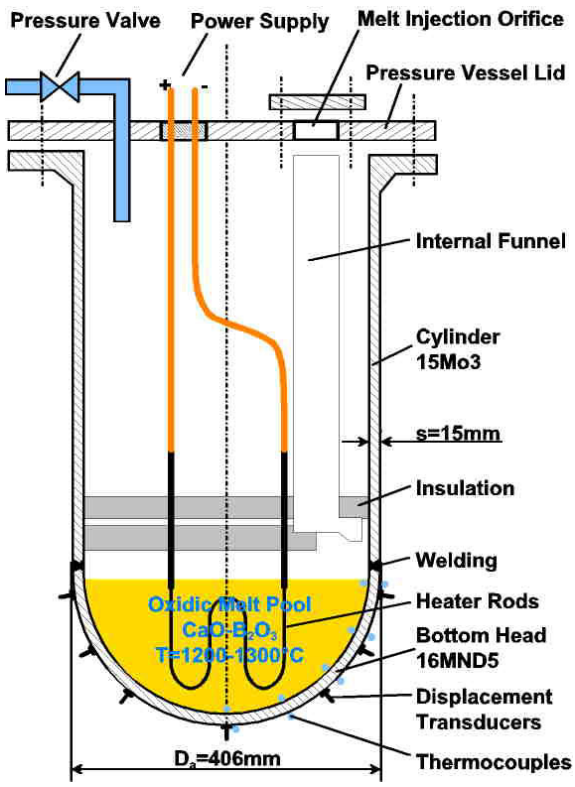

Figure 1: Principal experimental setup of FOREVER - not to scale.

was applied: first the transient temperature field was calculated and then the transient mechanical calculation was performed applying the appropriate temperature field at each time step. To take into account the melt level drop by thermal expansion the initial level was lowered "by hand". The feedback from the viscoplastic deformation to the temperature field is not correctly considered in the one-way coupling. But the investigations in [2] showed that slight temperature shifts of only 10 K at an overall temperature level clearly above 1000 K had significant effects concerning the failure time of the vessel.

To overcome these disadvantages of the one-way coupling model a new recursively coupled model is developed. In this model the following effects are additionally considered in the thermal model:

- Change of melt pool geometry and melt level decrease due to the viscoplastic vessel wall deformation
- Decrease of wall thickness (and thereby of heat resistance) due to viscoplastic deformation
- Increase of the surface of the vessel wall and thereby the increase of the heat releasing surface

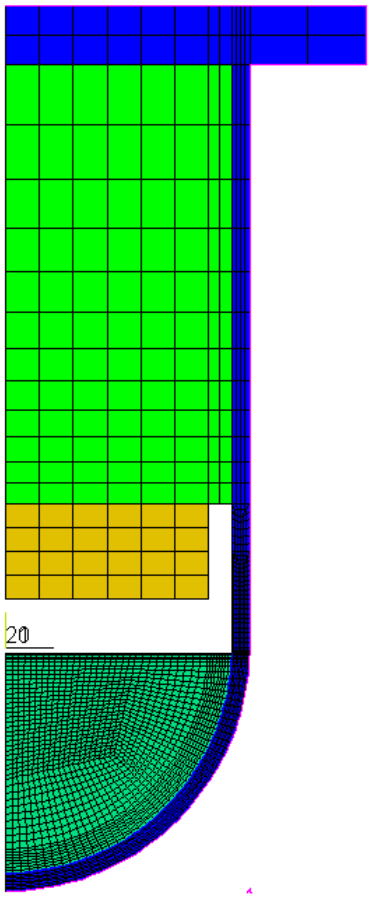

Figure 2: Element plot of the general physics model

2. Finite-element model with recursive coupling of thermal and mechanical calculations

According to the ANSYS Manual [5] description first a General Physics Environment (GPE) is modeled. The GPE describes those features of the model which remain the same in each of the different sub-models (thermal and mechanical). This relates mainly to the geometry and the attributes of the different regions. Figure 2 shows the entire axisymmetric FE-Model for the FOREVER scenario with different colors for the different materials. Blue refers to the steel of the vessel. Light green corresponds to a fictitious region with internals for the fixation of the funnel, the heater (cf. Fig. 1), and the isolation (orange), which are not modeled in detail, but smeared to a fictitious material. All empty space inside the vessel is filled by Argon during the test. This applies to the green and white regions within the vessel. Since the convective heat transfer by the Argon is neglected and it is not participating in radiative heat transfer, the white region is modeled like vacuum for the radiative heat transfer. The dark green region in the lower head represents the melt, which is internally heated by the heater. It is assumed that the heat is released homogeneously within the range of the heater rods. Outside of the vessel air at atmospheric conditions has to be modeled.

For an adequate model of the thermal processes different features have to be captured. In the following the physical requirements and the applied solution and element type usage are described:

- A melt region with internal heat sources has to be simulated. This is done with quadrilateral-elements (PLANE55) and different materials with anisotropic thermal conductivity.

- Due to the creep process of the vessel wall a moving interface between the melt region and the vessel wall has to be modeled. This contact simulation is done with target- (TARGE169) and contact-elements (CONTA171).
- Radiative heat transfer within the internal vessel enclosure is modeled via a radiation matrix (AUX12-Method) using bar-elements (LINK32) to generate the superelement (MATRIX50).
- Convective heat transfer is modeled on the external surfaces of the PLANE55-elements of the vessel wall. Since only one boundary condition can be applied to PLANE55-surfaces, the radiative heat transfer on the vessel outside has to be modeled with additional surface-effect-elements (SURF151).

For the viscoplastic mechanical simulation of the vessel, only the cylindrical part and the lower hemisphere are modeled with PLANE182-elements. The body load of the temperature field is applied from the preceding thermal solution. Additionally the load of the melt dead-weight and the internal pressure are considered on the vessel inside. To describe the visco-plastic deformation a numerical creep data base (CDB) was developed [6]. In this way the use of a single creep law, which employs constants derived from the data for a limited stress and temperature range, is avoided. For an evaluation of the failure times a damage model according to an approach of Lemaitre is applied [2, 7].

To simulate the dropping melt pool a melt deformation model is built up using HYPER56-elements for the melt region and TARGE169 and CONTA171-elements for the moving boundary of the vessel wall inside. Figure 3 shows a element plot at a late stage of the simulation before and after movement. Within the transient solution loop the thermal and mechanical models are solved with variable time step durations. The melt deformation solution is independent of these time steps, since it is only used to move the melt with the creeping vessel wall. The damage of the vessel wall during the mechanical solution is the exit criterion from the solution loop. If the first element is "killed" due to its damage value, the calculation is stopped.

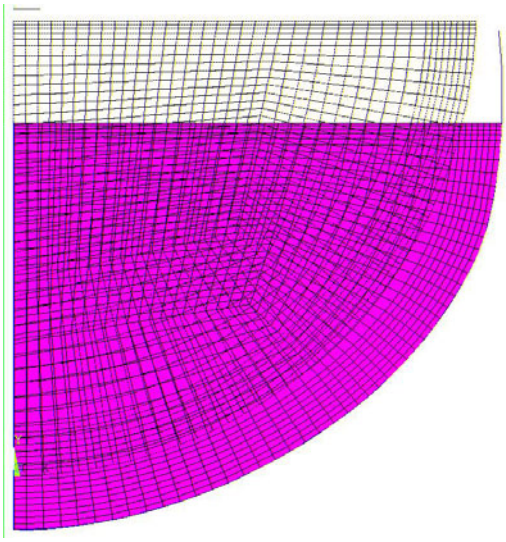

Figure 3: Element plot of the melt deformation model before and after displacement.

3. Discussion of the results

The comparison of the results with the experimental measurements can be done for the thermal results and for mechanical results. But especially for the mechanical data it must be kept in mind, that the mechanical response of the vessel is strongly influenced by the temperature field. Figure 4 shows the external temperatures of three different FOREVER-tests at the time of the highest measured temperature. Additionally the calculated temperatures of the FLOTRAN-CFD-model are given. The result of the new ECCM-approach within the fully coupled model is represented by the "PESCOTA h-10"-curve. Qualitatively the agreement of the temperature distribution is good. The temperature difference between the calculations and the experiments can be explained by the thermocouple fixation on the vessel wall, i.e. the measurement should give a lower temperature than the real vessel wall temperature. The two numerical solutions (CFD and ECCM) most significantly differ in the high temperature re-

gion, the so called hot-focus. The ECCM-approach gives a peak-shaped temperature distribution while the CFD-results show a more flat high temperature plateau.

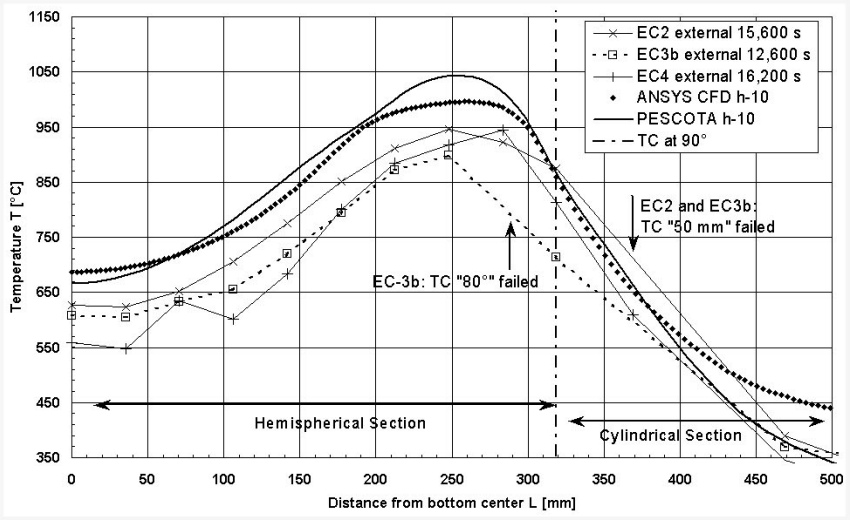

Figure 4: Comparison of the outer wall temperatures of experimental measurement, CFD-calculation and PESCOTA/ECCM-calculation

Figure 5 shows a contour plot of the temperature fields at the beginning (left) of the recursively coupled solution loop and at failure time (right). To demonstrate the effect of the moving vessel and melt a fictitious plot is given where the vessel is moved back to its original shape with the temperatures of each node at failure time. Figure 6 shows the transient heat generation load (Power) of the experiment EC2 and the comparison of the calculated and measured external vessel wall temperatures over time for two positions. One main feature observed in the experiments was the falling temperature level while the heating power was kept constant. This could not be reproduced by the prior single coupled calculations, where the changing geometry had no influence on the temperature field. The time dependent temperatures in Figure 6 represent the vessel external surface temperatures at an angle of 70° (experiment: "TeR4 70°"; calculation: "PES_56 70°"), and at 90°(experiment: "TeR5 90°"; calculation: "PES_56 90°"), which is at the welding line between the hemisphere and the cylinder. During the course of the experiment EC2 unscheduled transients occurred. Instead of the scheduled power of 38 kW and a constant pressure of 25 bar, the power was much lower during the first 3 hours and partially heating failed completely. Additionally the pressure was also fluctuating. It can be seen that the model is not able to represent the temperature response to strong power changes. In case of a cool down the calculated temperatures are falling

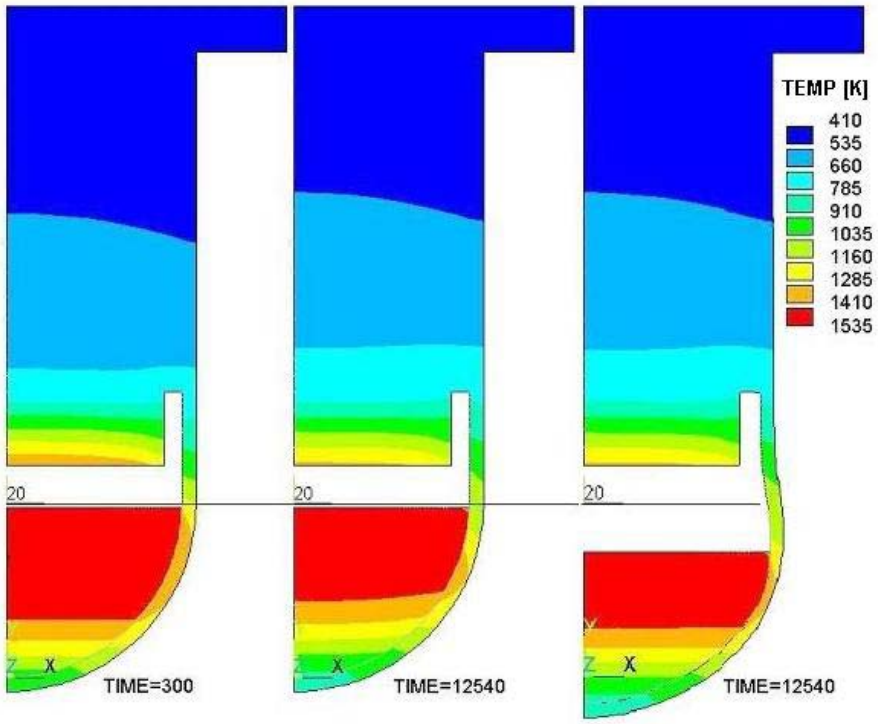

Figure 5: Temperature distribution within vessel and melt at the beginning of a coupled calculation (left) and at failure time (right). Middle: failure time temperature field for the initial shape

too fast and in case of a heat up the calculated temperatures are rising too slowly. The error in the simulation results from the crust formation and ablation model, which is dependent on the time step size and on the element size and is not designed for very fast transients in the heating power. Another reason could be the emissivity of the radiation surfaces. In the model a constant emissivity is assumed, but in fact the emissivity could be time and temperature dependent as a consequence of the surface oxidation. But nevertheless the important effect of the lowering temperatures during the "constant phase" is qualitatively reproduced by the simulation, which is especially visible at the 90°-position. It can be stated here, that all main thermal aspects of the experiment can be reproduced qualitatively by the new coupled model. Some further improvements concerning the crust modeling and the emissivity could be useful, but looking forward to prototypic nuclear power scenarios there is no need to model abrupt power changes, since the radioactive decay heat generation is decreasing slowly.

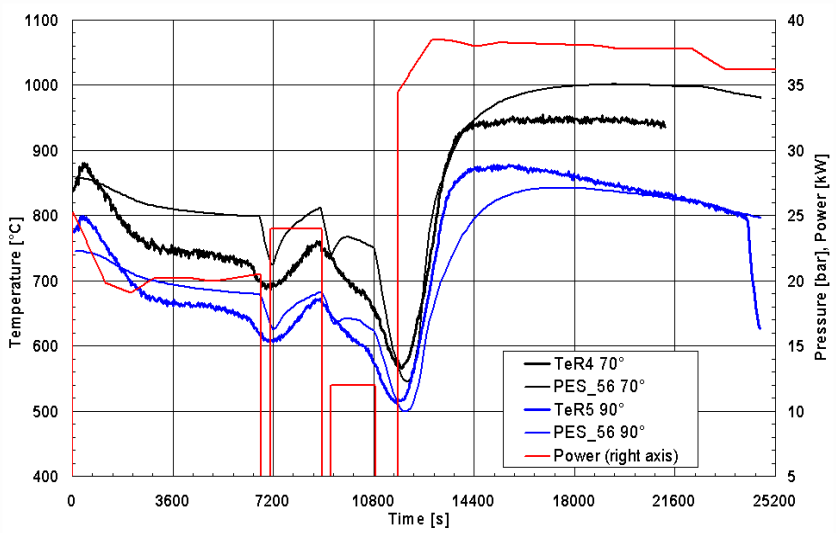

Figure 6: Transient loading conditions of the experiment EC2 and comparison of the calculated and measured external vessel wall temperatures over time.

Figure 7 shows the displacement velocity of the vessel bottom center over time for the measurement (EC2 dU/dt) and for a non-conservative calculation (PESCOTA_56). The calculation was made non-conservative by a relatively high emissivity of 0.75 in the thermal model to get slightly lower temperatures and therefore a late failure time. It can be seen that the displacement velocity is rather sensitive to slight pressure changes especially close to the failure time. It was observed in different analyses that the failure time depends strongly on the overall temperature level. This behavior was also observed in the simple one-way coupled model [2].

To investigate the effect of the fully coupled model against the simple one-way coupled model a reference calculation was performed, where ideal experimental conditions were assumed: A steady state temperature field from a 38 kW power input at the beginning and afterwards a constant power

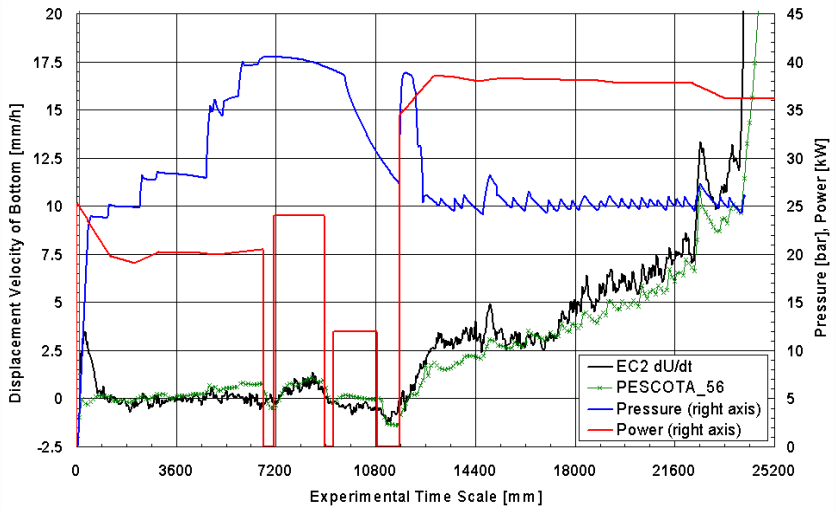

Figure 7: Transient loading conditions of the experiment EC2 and comparison of the calculated and measured velocity of the bottom center over time.

of 38 kW and a constant pressure of 25 bar. Table 1 summarizes the results. In the one-way coupled model, the temperature field was evaluated for the beginning and not changed during the creep of the vessel until failure. The highest temperature observed within the wall was 1,378 K. The failure time was calculated to 6,090 s. The fully coupled calculation had a time step size of 300 s for the solution loop at the beginning. After the most damaged element reached a damage of 70 %, the time step size was reduced to 30 s. Due to the geometrical effects listed in the introduction, a temperature drop during the calculation is observed. For the failure time at 13,740 s the maximum temperature results to 1,323 K. Due to the falling temperatures the failure time is more than doubled. This strong effect has not been expected, although it was known, that a temperature difference of 50 K can result in a doubled failure time.

Table 1: Comparison of the coupling effect

	One-Way Coupled	Fully Coupled
Max. Wall Temperature at Beginning	1,378 K	1,378 K
Max. Wall Temperature at Failure	1,378 K	1,323 K
Failure Time	6,090 s	13,740 s

4. Conclusions

So far the results show that a recursively coupled thermal and mechanical solution is closer to reality than a single coupled model where the mechanical deformations have no impact on the thermal model. The effect of wall thinning, external surface enlargement and melt level drop due to the vessel wall deformation calculated in the mechanical model causes lower temperatures and therefore longer failure times. Due to the scaling effect it is expected, that the fully coupled model is necessary to be able to perform reliable best estimate calculations for prototypic light water reactor scenarios.

References

[1] B.R. Sehgal, A. Theerthan, A. Giri, A. Karbojian, H.G. Willschütz, O. Kymäläinen, S. Vandroux, J.M. Bonnet, J.M. Seiler, K. Ikkonen, R. Sairanen, S. Bhandari, M. Bürger, M. Buckg, W. Widmann, J. Dienstbier, Z. Techy, P. Kostka, R. Taubner, T. Theofanous, T.N. Dinh: Assessment of reactor vessel integrity (ARVI). NUCLEAR ENGINEERING AND DESGIN, vol 221, pp 23-53, 2003

[2] H.-G. Willschuetz, E. Altstadt, B. R. Sehgal, and F.-P. Weiss: Simulation of Creep Tests with French or German RPV-steel and investigation of a RPV-support against failure. ANNALS OF NUCLEAR ENERGY, vol 30, 10, pp 1033-1063, 2003.

[3] V.A. Bui: Phenomenological and mechanistic modelling of melt-structure-water interactions in a light water reactor (LWR) severe accident. Dissertation Kungl Tekniska Högskolan, Stockholm, 1998.

[4] C. Sainte Catherine: Tensile and creep tests material characterization of pressure vessel steel (16MND5) at high temperatures (20 up to 1300°C). Rapport SEMT/LISN/RT/98-009/A, CEA, France, (experimental data files), 1998.

[5] ANSYS Manuals, ANSYS Inc., 2001-2004.

[6] E. Altstadt, Th. Moessner: Extension of the ANSYS® creep and damage simulation capabilities. Report FZR-296, Forschungszentrum Rossendorf, Dresden, 2000.

[7] J. Lemaitre: A Course on Damage Mechanics. ISBN 3-540-60980-6, 2nd edition Springer-Verlag Berlin, Heidelberg, New York , 1996.

PRESSURE VESSEL INVESTIGATIONS OF THE GREIFSWALD WWER-440 UNITS: AN INTEGRATED APPROACH

Joerg Konheiser, Udo Rindelhardt, and Hans-Werner Viehrig

1. Introduction

Reactor pressure vessel (RPV) integrity assessment after long-term service irradiation is commonly based on surveillance program results. Radiation loading, metallurgical and environmental histories, however, can differ between surveillance and RPV materials. Therefore, the investigation of RPV material from decommissioned NPPs offers the unique opportunity to evaluate the real toughness response. A chance is given now through the investigation of material from the decommissioned Greifswald NPP (VVER-440/230) to evaluate the material states of a standard RPV design and to assess the quality of prediction rules and assessment tools. The well documented different irradiation/annealing states of the four Greifswald RPVs are very useful for an integrated approach to study the embrittlement phenomena. This approach will include:

- neutron and gamma fluence calculations,
- Nb-based experimental dosimetry and
- a comprehensive material investigation program.

First calculations of the neutron fluence of the RPVs were reported earlier [1]. Here the results of new, more accurate calculations of the neutron fluence will be given. Further, the change of the RPV dismantling strategy requires a new approach for the trepanning procedure. The new procedure will be shortly described as well as some aspects of the material investigation program.

2. Neutron fluence calculations

Previous calculations of the neutron fluence distribution of RPV were based on the Green's function technique. The functions were calculated by the Monte Carlo code TRAMO [1,2]. In these calculations the neutron data were taken from the 26-group ABBN-78 library, the horizontal fission source distributions were assumed to be constant over each fuel assembly and the results were obtained only at the inner and outer RPV walls for a rather coarse space grid (30° azimuthally ; 25 cm vertically).

The new transport calculations were carried out using TRAMO with the following improvements:

- The fluences were directly determined at the designated trepan positions
- A 60° sector was calculated over the relevant height segment
- Very detailed geometrical models were considered
- Up-to-date nuclear data libraries and finer energy group structure were used
- Additional calculation of thermal neutron fluences and of gamma fluences
- Exact consideration of pin wise distribution of the neutron and gamma sources in the three external fuel assembly rows
- Improvement of the statistical accuracy (1-σ error for relevant quantities less than 1%)
- Determination of the fluence gradient over the thickness of the RPV.

Especially the inclusion of gamma effects and the fine spatial resolution should be mentioned. The calculation models covers the region from 200 cm below the core to 130 cm above the reactor core. A 60° sector was modelled in horizontal plane in every case.

2.1 The code system TRAMO and input data

TRAMO [2] is a flexible multigroup transport code system based on the Monte Carlo method for coupled neutron and gamma flux calculations. The system includes programs for data preparation, data analysis and the code for the calculation of space and energy dependent importance functions.

TRAMO is capable of using the latest nuclear data. The microscopic group cross sections are generated by NJOY [3]. The ENDF/B-VI (release 8) nuclear data library was used for neutron cross sections and gamma production, and the library PHOTX [4,5] for the gamma cross sections. The cross sections were generated in the BUGLE-96 (47 neutron groups and 20 gamma groups) energy group structure. The inelastic scattering cross sections were represented by Legendre polynomials. Equiprobable angular intervals were generated for a number of energy points in case of the elastic scattering and the scattering in the thermal region. Alpha/beta factors were employed for the thermal scattering on hydrogen, and the other nuclides were computed relying on the free gas model.

The compositions of the different materials were taken from [6]. Uranic dioxide (enrichment 3.6%) was generally used as fuel without considering the burnup. The different water densities in the reactor core were taken into account. Resonance self-shielding was considered applying the F-factors formalism. The complete data file for the MC-calculations contains 31 different compositions based on 48 different nuclides.

The neutron source distributions were also taken from [6]. The gamma sources were assumed to be proportional to those of the neutrons. The proportionality factor was determined on the basis of U-235 fission. The particles were started pin by pin in the outer assemblies. The number and the position of the used source zones were optimized corresponding to its influence on the corresponding result. In addition, a source biasing was applied depending on the source position.

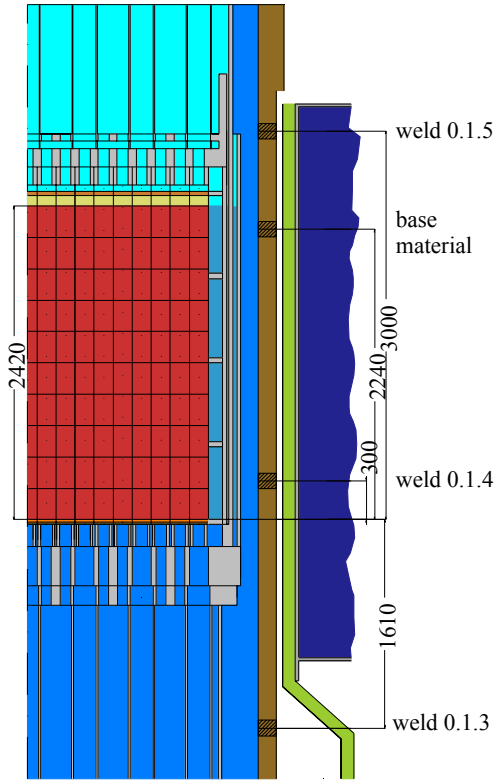

Fig. 1: Calculation Model and trepan positions (hatched areas)

The energy distribution of neutron and gamma sources corresponds to the fission spectra of U-235, taking into account 415 neutron and 19 gamma energy groups, respectively a quota sampling was used for the source.

The coupled neutron and gamma calculations were started only with neutrons. The fission reaction was treated as capture reaction without gamma production. The photons were

produced only by neutron reactions from inelastic scattering and capture reactions. Separate calculations were carried out for the photons from fission.

2.1 Results

Here, the results will be exemplarily described for unit 1 of the Greifswald NPP. At this unit trepans shall be taken from five different positions (see Fig.1). The most interesting trepans are those from the weld 0.1.4 in the lower core region and in the base material in the upper core region outside of the annealing zone. Two trepans will be additionally taken from reference (i.e. low irradiated) positions. These positions are far below and above the reactor core with negligible neutron loads (welds 0.1.3 and 0.1.5).

For each trepan position a separate geometrical model was defined. In addition, other geometrical models had to be created for the last 4 cycles because the use of dummy assemblies at the core periphery during these cycles. The weld 0.1.4, well known as the critical weld, was annealed in unit 1 after the 13th cycle.

The maximum calculated neutron fluence (E > 0.5 MeV) is in the range of $4.64*10^{19}$ n/cm^2 at the inner surface of the RPV (weld 0.1.4) for all cycles and for cycles 14 and 15 in the range of $3.41*10^{18}$ n/cm^2. The maximum fluence was found near an azimuthal angle of 30° for all 15 cycles. In the cycles 14 and 15 the maximum of the fluence was found near 0° which reflects the influence of the dummy steel assemblies. Figure 2 shows typical gradients of different integral fluences through weld 0.1.4.

The calculated maximum of gamma fluences (E > 1.0 MeV) was found to be $3.05*10^{20}$ photons/cm^2, which is one order of magnitude higher than the neutron fluences.

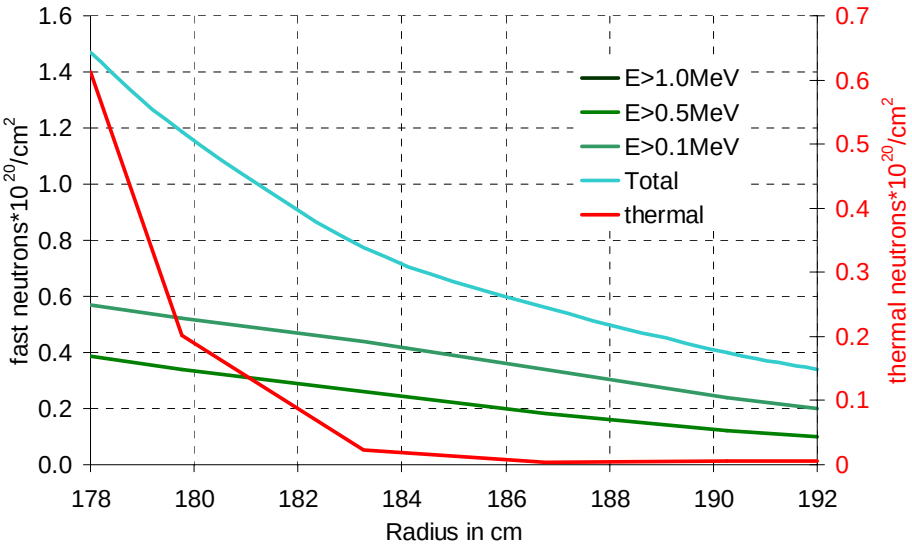

Fig. 2: Gradients of integral fluence values via all 15 cycles through the weld 0.1.4 of the RPV.

The maximum fluence at the positions of the reference trepans is about $1.0*10^{16}$ n/cm2 for the weld 0.1.3 and $1.5*10^{17}$ n/cm^2 for the weld 0.1.5 (for E > 0.5MeV). The values are 2 to 3 orders of magnitude smaller than in the core middle level (maximal fluence position). Therefore, from a material point of view, the reference positions can be regarded as unirradiated.

It is remarkable that the integral neutron fluence (E>0,5MeV) at the reference position 0.1.3 was found to be greater at the outer RPV surface than at the inner RPV surface (up to a factor 10). The reason for that is, that on the one hand neutrons are scattered on components outside

of the RPV, and one the other hand the neutrons inside of the RPV are absorbed by the massive bottom plate below the core. Because of the small cross sections a similar behaviour was not found in case of gamma fluences.

The calculations in base material position results in a maximum neutron fluence of $2.9*10^{19}$ n/cm^2. The maximum gamma fluence is $2.25*10^{20}$ photons/cm^2.

Table 1 shows a comparison between the here presented results and the older TACIS results [1]. The TACIS results had to be interpolated for the comparison. The differences are in average 10 %. The main reason can be attributed to the inadequate consideration of the pin source distribution in the older calculations. The sources at the periphery of the core were overestimated in the older calculations.

Table 1: Comparison of integral fluence values at the weld 0.1.4 of the RPV with earlier results [1]

Integral fluence values (15 cycles, angle 30°)						
	Outer surface			Inner surface		
	new	From [1]	ratio	New	From [1]	ratio
E>1.0 MeV	4.4 E+18	4.9 E+18	1.11	2.94 E+19	3.30 E+19	1.12
E>0.5 MeV	1.12 E+19	1.18 E+19	1.01	4.64 E+19	5.16 E+19	1.11

Greater differences (near 30%) were found in the results of cycles 14 and 15. It is assumed that the influence of the dummy assemblies was underestimated in applying the Green functions in the TACIS calculations.

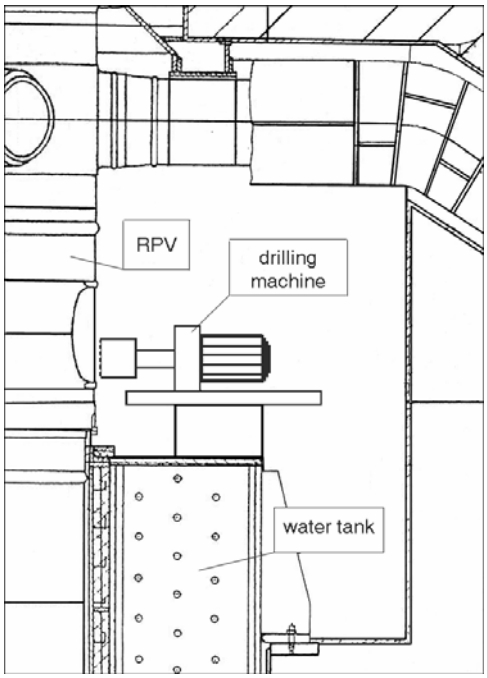

Fig. 3: Arrangement of the drilling machine

During the 12th cycle neutron-activation detectors were irradiated in an ex-vessel cavity at unit 1 [7]. The analyzed dosimetry reactions were ^{58}Ni(n,p), ^{54}Fe(n,p), ^{46}Ti(n,p), ^{63}Cu(n,α) and ^{93}Nb(n,n'). The detector activities for the end of the irradiation were calculated on the base of the power history using the dosimetry cross section libraries IRDF-90, rev.2, JENDL-D99 and RRDF-98.

The measured results were compared with activities calculated by TRAMO. Measured and calculated activities of detectors agree within the range of ± 15%. Greater differences, which could not be clarified, were found for all Nb values.

3. The trepanning procedure

Because of a change in the dismantling strategy for the RPVs a new approach for the trepanning procedure had to be developed. Unlike the originally planned cutting of the RPV in pieces of about 1m x 0,5m, now the RPVs will be transferred to the interim storage without being cut into pieces.

It is now intended to gain the trepans by a special drilling machine, which will be developed and tested within the next months. This remotely controlled machine will be mounted outside the RPV in the height of the coolant loops (see Fig. 3). To get the trepans from the predefined positions, the whole RPV will be lifted and rotated by the crane. A number of technological problems have to be solved during the construction and the testing of the drilling machine. The trepanning of unit 1 is expected to start in Summer 2005.

4. The material investigation program

The current RPV integrity assessments of Russian WWER-440 units are based on the Russian regulatory document PNAE G-7-002-86 "Strength Calculation Standards for Components and Pipelines of Nuclear Power Installations". This regulatory document defines neutron dosimetry requirements, forecast of critical material property degradation depending on neutron irradiation, and the assessment criteria for brittle failure of the RPV. In general, he current practice in the Russian regulatory document to ascertain the fracture toughness of the material follows the international approach and is an indirect and correlative method using universal and experimentally verified lower bound reference fracture toughness, K_{IC}, curves with a shape according to Eq. (1):

$$K_{IC} = A + B \cdot \exp\left(C \cdot \left(T - T_K\right)\right) \qquad (1)$$

where A, B and C are material constants and T_K is a reference ductile-to-brittle transition temperature, DBTT. With the use of a reference temperature the behaviour of a specific material is considered. These methods allow the determination of a lower bound linear elastic fracture toughness that has consistently been shown to be conservative relative to the measurement of the actual fracture toughness. In the Russian code a so-called critical temperature of brittleness, T_k, is used as reference temperature. The T_k concept is formulated in detail in Appendix 2 of the Russian Safety Guide RB-007-99 "Expert evaluation of residual lifetime of VVER pressure vessel". The critical temperature of brittleness is determined for both the unirradiated, T_{K0}, and irradiated, T_K, condition by Charpy V-notch transition temperatures.

Recently, industry and regulatory attention has been focussed on the direct use of measured fracture toughness properties and the application of the Master Curve (MC) approach in the RPV integrity assessment. The ASTM E 1921 "Standard Test Method for Determination of Reference Temperature, T_0, for Ferritic Steels in the Transition Range" adopts the MC approach and lays the basis for a consistent fracture mechanics based integrity assessment of components and constructions. This direct measurement approach is preferred over the correlative and indirect methods used in the past to assess irradiated RPV integrity.

In the United States the direct approach has been implemented in the ASME Code Case N629 "Use of Fracture Toughness Test Data to Establish Reference Temperature for Pressure Retaining Materials for Section XI". This new parameter is termed RT_{T0} and given by

$$RT_{T_0} = T_0 + 35F\ (19.4K) \qquad (2)$$

The available K_{IC} lower bound curve is indexed on the temperature axis with the directly measured T_0. The benefit of this methodology is that both the reference temperature for the unirradiated, irradiated and irradiated and annealed material state are related to a fracture mechanics parameter which can be directly measured on specimens. This approach was

originally stipulated to index the existing ASME Code reference toughness curve. However, the ASME RT_{T0} has also been adopted in the codes of countries outside the USA.

The main emphasis of the research project using the material of the decommissioned Greifswald units is put on direct measurement of the MC based reference temperature T_0. The MC based fracture toughness values will be compared with the fracture toughness determined according to the current Russian regulatory document. Hence both Charpy-V and fracture toughness data have to be evaluated.

The through-wall basic characterisation of base and weld metal got from the different units should include the following:

- cleavage fracture toughness values and Master Curve based reference temperatures (T_0),
- J-Δa curves and ductile initiation fracture toughness values,
- full Charpy-V transition curves,
- tensile properties,
- hardness HV10 properties,
- chemistry profiles, in more detail for weld than for base metal
- metallographic characterisation
- neutron dosimetry of the specific block positions

The material investigations are expected to start in 2005.

References

[1] B. Boehmer, J. Boehmert, U. Rindelhardt: RPV Integrity Assessment by Operational Feedback: Post Service Investigations of VVER-type, Transactions of ANS, Vol. 88(2003), p. 547

[2] H.-U. Barz, J. Konheiser, Monte-Carlo Programm TRAMO - Möglichkeiten und Anleitung zur Nutzung , FZR Bericht-245,Rossendorf ,Dezember 1998

[3] R. E. MacFarlane, D. W. Muir (1994), The NJOY Nuclear Data Processing System (Version 91), Los Alamos, LA-12740-M

[4] V. McLane, ENDF-102 data formats and procedures for the evaluated nuclear data file ENDF-6, Revised April 2001, BNL-NCS-44945-01/04-Rev.

[5] R.W. Roussin, J.R. Knight, J.H. Hubbell, R.J.Howerton, Description of the DLC-99/HUGO Package of Photon Interaction Data in ENDF/B-V Format, ORNL/RSIC-46 (ENDF-335) (Dezember 1983)

[6] G. Suschowk, Daten zur Berechnung von Neutronenflussdichten in den Reaktordruckgefäßen der Blöcke 1 bis 4 der EWN GmbH, Technische Unterlage 6252/BK/H0031266

[7] H.-C.Mehner, B.Böhmer, I.Stephan,“ Neutronendosimetrie an der Druckgefäßaußen-wand des Blocks 1 im KKW Greifswald bei Einsatz von Abschirmkassetten“ Arbeitsbericht ZfK – RPM 6/88

MODELLING OF VACANCY CLUSTER EVOLUTION IN NEUTRON IRRADIATED IRON

Aleksandr Gokhman[1], Frank Bergner, and Andreas Ulbricht

1. Introduction

There is experimental evidence for the formation of stable nm-sized vacancy clusters (VC) in low-copper iron alloys irradiated with fast neutrons under in-service conditions of reactor pressure vessels (RPVs) [1,2]. Modelling of the evolution of VCs in pure iron under neutron irradiation is both of fundamental interest and of practical importance, because vacancies and VCs (even if not present after long-term irradiation) may play an intermediary role in the formation of Cu-rich clusters in RPV steels resulting in an irradiation-induced degradation of mechanical properties. In the present investigation we apply rate theory (RT) to simulate the evolution of VCs in pure bcc iron. Similar work was reported by Odette [3] and Hardouin Duparc et al. [4]. Odette directly solved the master equation with clustering of self-interstitial atoms (SIAs) neglected. Hardouin Duparc et al. considered both planar SIA clusters and planar VCs and transformed the master equation into a Fokker-Planck equation, which may be a problem at small cluster sizes. The objective of the present investigation is to introduce the effect of lattice relaxation into the framework of Odette's approach.

2. Method

The cluster dynamics approach is based on the following assumptions:

- Generation rates of vacancy clusters (VCs) are adopted from molecular dynamics calculations quoted in [5].
- VCs are assumed to be spherical.
- Both agglomeration and direct generation of clusters of self-interstitial atoms (SIAs) are neglected as in [3].

The rate of change of the number density of VCs is specified by the following master equation:

$$\frac{dC_n}{dt} = \beta_{n-1,v}C_{n-1} + \left(\beta_{n+1,i} + \alpha_{n+1,v}\right)C_{n+1} - \left(\beta_{n,i} + \beta_{n,v} + \alpha_{n,v}\right)C_n + G_{n,v} \tag{1}$$

C_n … concentration of VCs consisting of n vacancies ($n > 1$)
$\alpha_{n,v}$ … rate of emission of vacancies by VCs containing n vacancies
$\beta_{n,k}$ … rate of absorption of vacancies ($k = v$) or SIAs ($k = i$) by VCs containing n vacancies
$G_{n,v}$ … rate of direct generation of VCs containing n vacancies

In the diffusion-limited regime the rate, at which vacancies (SIAs) are absorbed for spherical VCs, is given by:

$$\beta_{n,k} = \frac{4\pi R_n D_k C_k}{\Omega_a} \tag{2}$$

[1] South Ukrainian Pedagogical University, Odessa, Ukraine

where R_n is the radius of a spherical VC containing n vacancies, D_k is the diffusivity of vacancies ($k = v$) or SIAs ($k = i$), Ω_a is the atomic volume of iron, and C_k is the number density of free vacancies ($k = v$) or SIAs ($k = i$). The evolution of C_k with time is given by integration of the RT equations according to [3]:

$$\frac{dC_k}{dt} = G_k - \frac{4\pi r(D_v + D_i)C_v C_i}{\Omega_a} - D_k C_k S_k \tag{3}$$

Here r is the recombination or trap radius, G_k is the production rate of free vacancies ($k = v$) or SIAs ($k = i$), and S_k is the sink strength for vacancies ($k = v$) or SIAs ($k = i$). Eq. (3) is the special form of Eq. (1) for $n = 1$. In Eq. (3) it is assumed that the rate of emission of vacancies from VCs is much less than the production rate. S_k is taken to be proportional to the dislocation density, ρ [3] with a factor of proportionality of 1 (1.2) for vacancies ($k = v$) or SIAs ($k = i$) [5]. G_k is taken to be proportional to the neutron dose rate expressed in units of dpa/s (dpa = displacements per atom) with a factor of proportionality of 0.183 for both vacancies and SIAs. Taking into account that the recombination term in Eq. (3) for SIAs is much less than the sink term, Eq. (3) can be solved analytically [6]. Odette [3] used the stationary values of C_v and C_i obtained from the condition, $dC_{v(i)}/dt = 0$, instead of the time-dependent solution of Eq. (3).

The vacancy emission rates, $\alpha_{n,v}$, are related to the absorption rates, $\beta_{n,v}$, and the change of Gibbs free energy, ΔG, in accordance with the detailed balance principle:

$$\alpha_{n,v} = \beta_{n-1,v} \exp\left[\frac{\Delta G(n) - \Delta G(n-1)}{k_B T}\right] \tag{4}$$

Here k_B is Boltzmann's constant; T is the temperature in K and $\Delta G(n)$ is the change of Gibbs free energy, when a VC of n vacancies is formed. Ignoring any interaction between VCs and matrix except surface energy, $\Delta G(n)$ is given by:

$$\Delta G(n) = -n\Delta\mu + 4\pi R_n^2 \gamma \tag{5}$$

where $\Delta\mu$ is the change of chemical potential and γ is the specific surface energy. In the case of an ideal solution [7]:

$$\Delta\mu = k_B T \ln\left(\frac{C_v}{C_{Rn}}\right) \tag{6a}$$

where the Thomson-Freundlich term, C_{Rn}, is given by:

$$C_{Rn} = \exp\left(3 - \frac{E_f}{k_B T} + \frac{2\gamma\Omega_a}{k_B T R_n}\right) \tag{6b}$$

and E_f is the energy of formation of a single vacancy.

The maximum considered number of vacancies in a cluster corresponds to the number of equations in the system, Eq. (1). We have chosen $n_{max} = 9000$ in agreement with the

maximum VC radius of about 3 nm observed in SANS experiments on low-copper model alloy A [8]. The values of the material parameters used in the calculations are listed in Table 1. These values have been adopted from [3]. The direct generation rates of VCs listed in Table 2 have been adopted from molecular dynamics calculations quoted in [5].

For computational purposes the system of equations, Eqs. (1) to (6), was transformed into a dimensionless representation. The program D02EJF (NAG Fortran Library Manual) applied to solve the master equation integrates a stiff system of first order ordinary differential equations using a variable order, variable step method implementing the backward differential formulae.

We have observed that the mean radius of the calculated VC distribution strongly depends on the dislocation density, ρ. Furthermore, the total volume fraction of VCs turned out to depend strongly on the surface energy, γ. Therefore, these quantities have been taken as fitting parameters in order to reproduce the mean radii and volume fractions observed by means of SANS experiments for the irradiation conditions of the low-copper alloy A (Table 3).

Table 1: Material parameters

Parameter	Data taken from [3]
Vacancy migration energy	1.3 eV
Vacancy pre-exponential	0.5 x 10^{-4} m^2/s
Interstitial migration energy	0.4 eV
Interstitial pre-exponential	5 x 10^{-6} m^2/s
Vacancy formation energy, E_f	1.64 eV
Recombination radius, r	0.574 nm
Surface energy, γ	1-2 J/m^2
Dislocation density, ρ	5 x 10^{14} $1/m^2$
Lattice parameter, a_0	0.2866 nm

Table 2: Direct generation rate of cascade VC containing n vacancies

n	$G_{n,v}$ in 10^{-9} dpa/s		
	Data taken from Fig. 8 of Ref. [5]	Values calculated for condition A1 (Tab. 3)	Values calculated for condition A2 (Tab. 3)
1	17.5	0.0732	0.549
2	0.26	0.0011	0.0082
3	0.25	0.0010	0.0078
4	0.25	0.0010	0.0075
5	0.23	0.0010	0.0072
6	0	0	0
7	2.5	0.0105	0.0784
8	1.75	0.0073	0.0549
≥9	0	0	0

Relaxation of the lattice is considered by introducing an additional term, *W(n)*, into Eq. (5).

$$\Delta G(n) = -n\Delta\mu + 4\pi R_n^2\gamma + W(n) \tag{7}$$

The binding energy of a vacancy in a cluster containing a number of *n* vacancies,

$$E_b^V(n) = E_f + \Delta G(n-1) - \Delta G(n), \tag{8}$$

assumes the general form

$$E_b^V(n) = E_f - x\left[n^{2/3} - (n-1)^{2/3}\right] + y \tag{9a}$$

$$x = 2.5\left(\frac{8\pi}{3}\right)^{1/3} a_0^2\gamma \tag{9b}$$

$$y = \left[\ln(C_v) - 3\right]k_B T - \left[W(n) - W(n-1)\right] \tag{9c}$$

Table 3: Irradiation conditions and SANS results for the low-Cu model alloy A [8]

Irradiation condition	A1	A2
Neutron dose rate, 10^{-9} dpa/s	0.4	3
Mean radius of VCs, nm	1.0 ± 0.1	1.0 ± 0.1
Volume fraction of VCs, %	0.02 ± 0.005	0.10 ± 0.01

Fitting results of molecular dynamics calculations reported in [9] with Eq. (10), we obtained $x = 2.79$ eV and $y = 0.11$ eV. This fit is as least as good as the one-parameter fit (Eq. (9a) with y set to 0) performed in [9], which gave $x = 2.59$ eV. The term *W(n)-W(n-1)* to be introduced into Eq. (4) was calculated from Eq. (9c) using the value obtained for *y*. The remaining procedure corresponds to the one described above.

3. Results

In a sensitivity study the effect of several material parameters on the size distribution function (SDF) of VCs has been investigated for the case of lattice relaxation neglected. Depending on the value of the dimensionless quantity *c*, $c = C_i D_i / C_v D_v$, the shape of the SDF varies essentially. If $c > 1$, the calculated SDF has only one peak at a radius of about 0.3 nm. This peak corresponds to the direct generation of VCs as a result of the cascade stage (Table 2). If $c < 1$, a second peak appears at a radius greater than 0.3 nm. The radius of the second peak is an increasing function of irradiation time. The SDF calculated for the same set of material parameters and several irradiation times is shown in Fig. 1. After one year of irradiation, the volume fraction that corresponds to the second peak is much larger than the volume fraction covered by the first peak. We have also observed that, after a certain irradiation interval, the mean radius of VCs is mainly determined by the dislocation density, whereas the volume fraction of VCs is most sensitive to the surface energy.

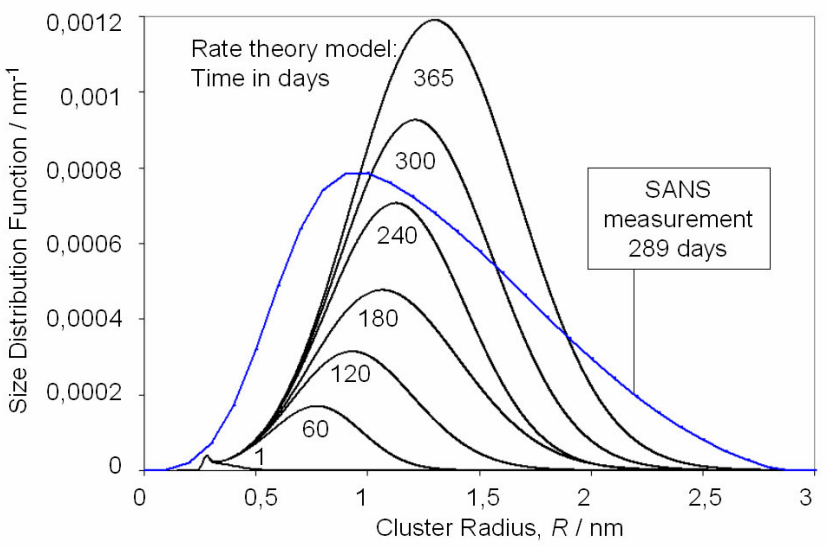

Fig. 1: Calculated (relaxation of the adjacent lattice neglected) evolution of volume related cluster size distribution for a dose rate of 3 x 10^{-9} dpa/s after irradiation intervals as indicated. SANS-based experimental results for irradiation condition A2 of model alloy A (Tab. 3) are shown for comparison.

The experimental values of the mean radius (Table 3) are reproduced best, if a dislocation density, $\rho = 1.84 \times 10^{14}$ m^{-2}, is assumed. For irradiation conditions A1 and A2 (Table 3), best fit with respect to the volume fraction is obtained for values of the surface energy, $\gamma = 0.67$ J/m^2 and $\gamma = 0.82$ J/m^2, respectively.

The behaviour of the model with lattice relaxation taken into account is similar as described above. In this case, however, best fit with respect to the volume fraction is obtained for values of the surface energy, $\gamma = 1.94$ J/m^2 (condition A1) and $\gamma = 2.02$ J/m^2 (condition A2).

4. Discussion

The first peak of the calculated SDF of VCs (at about 0.3 nm) cannot be resolved by means of small-angle neutron scattering (SANS), because measuring errors strongly increase for radii below 0.5 nm. Experimental evidence is, however, available from positron annihilation measurements reported in [2] for the same alloy. The second peak of the calculated SDF corresponds to the experimental results obtained from SANS measurements. As variation of the irradiation interval in model calculations shows, the mean radius of VCs increases according to a $t^{1/5}$-law, which is slower than $\sim t^{1/3}$ predicted by the Lifshitz-Slyozov theory.

The values of the dislocation density and the surface energy obtained by adjustment of the model with experimental data are reasonable estimates (compare Table 1). The closer agreement of the surface energies obtained in the second set of calculations indicates both that consideration of cluster-matrix interaction is important and that the method is appropriate. Therefore, the corresponding estimation of the surface energy, $\gamma \approx 2.0$ J/m^2, is more reliable than a value at or below 1 J/m^2 obtained without consideration of cluster-matrix interaction.

The shape of the size distribution function has not been considered so far. The experimentally obtained distribution is observed to be wider than the calculated ones (Fig. 1). However, prior to comparison a more detailed analysis has to be performed with respect to both estimation of

experimental errors including error propagation due to Fourier transformation and identification of model parameters influencing shape.

5. Conclusion

The present model of vacancy cluster evolution in bcc iron under neutron irradiation, which is based on rate theory according to [3], can be adjusted in such a way that both volume fraction and mean size of irradiation-induced vacancy clusters measured by means of SANS are reproduced. The values of the specific surface energy of clusters and the dislocation density needed to adjust the model are reasonable estimates for the alloy under investigation. The expectation that the surface energies for the two dose rates considered should agree is fulfilled more closely, if in addition to surface energy the relaxation of the lattice is taken into account by introducing an additional term, *W(n)*, into cluster-matrix interaction.

References

[1] J. Böhmert, A. Ulbricht, A. Kryukov, Y. Nikolaev, and D. Erak (2001), Composition effects on the radiation embrittlement of iron alloys, in: Effects of Radiation on Materials: 20th International Symposium, ASTM STP 1405, (S.T. Rosinski, M. L. Grossbeck, T. R. Allen, and A.S. Kumar, Eds.), American Society of Testing and Materials, West Conshohocken, PA, 383-398.

[2] S. E. Cumblidge, A. T. Motta, G. L. Catchen, G. Brauer, and J. Böhmert (2003), Evidence for neutron irradiation-induced metallic precipitates in model alloys and pressure vessel weld steel, Journal of Nuclear Materials, 320, 245-257.

[3] G. R. Odette (1998), Modelling irradiation embrittlement in reactor pressure vessel steels, in: Neutron Irradiation Effect in Reactor Pressure Vessel Steels and Weldments, IAEA-IWG-LMNPP-98/3 (M. Davies, ed.), International Atomic Energy Agency, Vienna, 438-504.

[4] A. Hardouin Duparc, C. Moingeon, N. Smetniansky-de-Grande, and A. Barbu (2002), Microstructure modelling of ferritic alloys under high flux 1 MeV electron irradiations, Journal of Nuclear Materials, 302, 143-155.

[5] F. Christien and A. Barbu (2004), Modelling of copper precipitation in iron during thermal aging and irradiation, Journal of Nuclear Materials, 324, 90-96.

[6] A. Gokhman and J. Böhmert (2003), Kinetics study of vacancy cluster evolution under VVER-type reactor conditions, Rad. Eff. & Def. in Solids, 158, 499-511.

[7] J. Schmelzer, G. Röpke, and R. Mahnke (1999), Aggregation Phenomena in Complex Systems. Wiley-VCH, Weinheim, p. 459.

[8] A. Ulbricht and F. Bergner (2004), Detecting Irradiation Induced Damage in RPV Steels by SANS, Proceedings of the 30th MPA-Seminar in conjunction with 9th German-Japanese Seminar 'Safety and Reliability in Energy Technology', MPA Stuttgart, Vol. 1, pp. 10.1-10.13.

[9] N. Soneda and T. Diaz de la Rubia (1998), Defect production, annealing kinetics and damage evolution in α-Fe: an atomic-scale computer simulation, Phil. Magazine A, 78, 995-1019.

Acknowledgement

This work was supported by the European Commission within the Integrated Project PERFECT of the 6th Research Framework Programme.

REACTOR CELL CALCULATIONS WITH THE CODES HELIOS, MCNP, AND TRANSRAY AND COMPARISON OF THE RESULTS

Carsten Beckert and Reinhard Koch

1. Introduction

The successive solution of the transport equation with the neutron flux density as searched function of the independent variables of space, moving direction, energy and time is the basic method for calculation of the neutron field in a whole reactor core. The classic neutron transport calculation for the whole reactor core can be divided in three sequential steps: In the first step, microscopic multi-group or pointwise data are generated from measured data of the neutron-nucleus interactions. In the second step, few-group data are calculated on the basis of the generated by step one multi-group or pointwise data using transport calculations over fuel cells or sub-assemblies. These calculations are carried out using so-called cell codes and as a result the cross sections are now homogenised and condensed to few energy groups. In the third step, the neutron field calculation, mostly in diffusion approximation, is carried out for the whole reactor core by means of the few-group data provided by step 2. In such a way, the neutron flux distribution over a relative coarse space mesh and for few energy groups can be calculated. The necessity of the additional subdivision into step 2 and 3 is imposed by the computational power required for the 3d-transport calculation for the whole reactor core with many energy groups and a fine space mesh, which currently is still considerably exceeding the capacity of the available computers. With the development of the computational technique it might be attempted to handle the reactor core more and more precisely with the transport codes and/or to integrate step 2 and 3 into one.

The DYN3D [1] code allowing to calculate the whole reactor core (step 3) of light water reactors and its transient behaviour has been developed at the Forschungszentrum Rossendorf. It treats the 3d-neutron kinetics with a two-group diffusion approximation using the nodal method for assemblies with quadratic and hexagonal geometry. The reactor core is divided into a coarse space mesh. As input data DYN3D needs two-group cross sections for the neutrons, which are averaged over each space element. These cross sections are generated using the 2d-code system HELIOS [2]. The transport and burn-up code HELIOS uses the integral transport method of first collision probabilities, which are calculated by the ray-tracing method [3]. The 2d-calculation is carried out for one horizontal plane of the reactor. When a significant 3d-dependence on the geometric configuration or on the material composition for an assembly is observed an interpolation between the values computed two-dimensionally for vertical neighbouring planes is performed. The necessity to calculate these two-group cross sections three-dimensionally needs to be evaluated. For that purpose the 2d- and 3d-cell code TransRay was specially developed using the same solution method employed by HELIOS. Reactor cells, at which three-dimensional effects at the data generation can be expected, were investigated with TransRay: A partially inserted control rod and void (or moderator with a lower density respectively) around a fuel rod as a model for a steam bubble in the moderator region. Therefore, in TransRay the possibility was built in to treat also regions with void using the ray-tracing method. The obtained TransRay-results were compared with the results generated by HELIOS and the Monte-Carlo code MCNP [4].

2. Theory

The eigenvalue form of the transport equation is considered in the TransRay code in order to determine the dominant eigenvalue k and the corresponding stationary neutron flux density Ψ (the eigenfunction). For each energy group g, the eigenvalue form of the transport equation for the group flux $\Psi_g(\vec{r},\vec{\Omega}) = \int_{\Delta E_g} \Psi(\vec{r},\vec{\Omega},E)\,dE$ is given by:

$$\begin{aligned} [\vec{\Omega}\cdot\vec{\nabla} + \sigma_g(\vec{r})]\,\Psi_g(\vec{r},\vec{\Omega}) &= q_g(\vec{r},\vec{\Omega}) \qquad \text{with} \\ q_g(\vec{r},\vec{\Omega}) = \sum_{g'}\int d\Omega'\sigma_{gg'}(\vec{r},\vec{\Omega}'\to\vec{\Omega})\,\Psi_{g'}(\vec{r},\vec{\Omega}') &+ \frac{1}{k}\cdot\frac{1}{4\pi}\chi_g(\vec{r})\sum_{g'}\nu\sigma_{fg'}(\vec{r})\,\Phi_{g'}(\vec{r}), \end{aligned} \tag{1}$$

where $\sigma_{gg'}$ are the scattering cross sections from the group g′ into the group g. The second term in the group source q_g represents the source density of the fission neutrons times 1/k. When an isotropic scattering is assumed q_g is also isotropic, $q_g(\vec{r},\vec{\Omega}) \equiv \frac{1}{4\pi}Q_g(\vec{r})$. Integrating equation (1) back along the path of neutron travel from the point $\vec{r}$ to the boundary point $\vec{r} - R\vec{\Omega}$ yields the integral equation

$$\Psi(\vec{r},\vec{\Omega}) = \frac{1}{4\pi}\int_0^R Q(\vec{r}-\lambda\vec{\Omega})\cdot e^{-\int_0^\lambda \sigma(\vec{r}-R'\vec{\Omega})dR'}\,d\lambda + \Psi(\vec{r}-R\vec{\Omega},\vec{\Omega})\cdot e^{-\int_0^R \sigma(\vec{r}-R'\vec{\Omega})dR'}, \tag{2}$$

where the group index g is suppressed. Additionally as further approximation in TransRay it is assumed that the incoming flux at the boundary is isotropic. Integrating equation (2) over all moving directions yields an equation for the scalar flux. The definition equation describing the neutron current escaping from the boundary is chosen as a second equation. In order to get the discretised forms of these two equations the whole volume is divided into partial volumes having the same material and the boundary into boundary segments. By taking into account the spatially averaged scalar neutron fluxes Φ_i und neutron sources Q_i for each partial volume V_i and the spatially averaged incoming and outgoing neutron currents J_{-j} and J_{+j} for each boundary segment S_j, the collision probability equations for each energy group can be written as:

$$\begin{aligned} \sigma_i V_i \Phi_i &= \sum_{i'} P\left[V_i \leftarrow V_{i'}\right] V_{i'} Q_{i'} + \sum_{j'} P\left[V_i \leftarrow S_{j'}\right] S_{j'} J_{-j'}, \\ S_j J_{+j} &= \sum_{i'} P\left[S_j \leftarrow V_{i'}\right] V_{i'} Q_{i'} + \sum_{j'} P\left[S_j \leftarrow S_{j'}\right] S_{j'} J_{-j'}. \end{aligned} \tag{3}$$

Here $P[V_i \leftarrow V_{i'}]$ and $P[V_i \leftarrow S_{j'}]$ are the first collision and $P[S_j \leftarrow V_{i'}]$ and $P[S_j \leftarrow S_{j'}]$ the escape probabilities. In the TransRay code these probabilities are expressed as twofold integrals in two dimensions and as fourfold integrals in three dimensions and are numerically calculated with the ray-tracing method. After this the equation system (3) is iteratively solved by the Jacobi or the Gauß-Seidel method. σ_i is the macroscopic total group cross section in V_i. In the first equation in (3) Φ_i was multiplied with $\sigma_i V_i$ getting the collision rate in V_i on the left hand side. The iteration matrix [5] belonging to (3) is irreducible and diagonal dominant assuring convergence of the solution based on the Jacobi or the Gauß-Seidel method [5]. If the partial volume V_i is empty (void test case) then $\sigma_i = 0$ and the first equation in (3) is only multiplied with V_i. In such a case, the diagonal dominance of the iteration matrix is not guar-

anteed. Nevertheless, for the investigated void test case it turned out that the used methods in TransRay converge producing reasonable results. Finally, the dominant eigenvalue k and the stationary flux are calculated using the iteration method known as the inverse power method [5]. At each iteration step the equation system (3) is solved for each energy group. The iteration matrix, which is not explicitly available in TransRay, is generally nonnegative and irreducible. These properties of the matrix guarantee the existence of a greatest positive eigenvalue and a corresponding eigenvector with positive elements according to the theorem of Perron and Frobenius [5]. That is, a positive fundamental mode of the flux exists, which is also required from a physical point of view.

In the computational model the neutron field is discretised in space and energy. In order to describe the real neutron field as good as possible with this model, the averaged cross sections for the Volume V (divided into partial volumes V_i) and for the energy group G (divided into fine groups g) must be computed using a suitable method:

$$\sigma_{V,G} = \frac{\int_V dV \int_G dE\, \sigma(\vec{r},E) \int d\Omega\, \Psi(\vec{r},E,\vec{\Omega})}{\int_V dV \int_G dE \int d\Omega\, \Psi(\vec{r},E,\vec{\Omega})} = \frac{\sum_{V_i \in V} \sum_{g \in G} \sigma_{i,g} \Phi_{i,g} V_i}{\sum_{V_i \in V} \sum_{g \in G} \Phi_{i,g} V_i} . \qquad (4)$$

The right hand side in the above equation represents the averaged cross sections with the calculated matrix $\Phi_{i,g}$ of the spatially averaged group fluxes. This formula states the condition that the reaction rates are well approximated within the volume V and the energy group G at all computational steps of the neutron field.

A common procedure of cross sections $\sigma_{V,G}$ generation required as input data for DYN3D is outlined considering an example when the control rods are inserted into a volume V. 2d-calculations are carried out with HELIOS for the two cases of the completely inserted and drawn control rods respectively. Using equation (4) the cross sections with control rods $\sigma^R_{V,G}$ and without control rods $\sigma^0_{V,G}$ are obtained. In the first approximation a linear interpolation between $\sigma^R_{V,G}$ and $\sigma^0_{V,G}$ can be applied to estimate the cross sections $\sigma_{V,G}$. In a slightly more detailed model two neighbouring volumes V^R and V^0 are considered. The cross sections $\sigma^R_{V,G}$ are considered in V^R and the cross sections $\sigma^0_{V,G}$ in V^0. Hence, the control rods are completely inserted into V^R and reach precisely to the boundary with V^0. A 3d-calculation provides the fluxes $\Phi_{V^R,G}$ and $\Phi_{V^0,G}$ which are spatially averaged over the volumes. With these fluxes the cross sections $\sigma^R_{V,G}$ and $\sigma^0_{V,G}$ are additionally weighted by the interpolation:

$$\sigma_{V,G}(h) = \frac{\sigma^R_{V,G} \cdot h \cdot \Phi_{V^R,G} + \sigma^0_{V,G} \cdot (H-h) \cdot \Phi_{V^0,G}}{h \cdot \Phi_{V^R,G} + (H-h) \cdot \Phi_{V^0,G}} , \qquad (5)$$

where H is the height of the volume V and h is the insertion depth of the control rods. The interpolation (5) was modelled with TransRay. The averaged cross sections with control rod $\sigma^R_{V,G}$ and without control rod $\sigma^0_{V,G}$ were calculated two-dimensionally using (4). A three-dimensionally investigated reactor cell was divided into two volumes V^R and V^0 at a height of H/2. A 3d-transport calculation with TransRay was carried out with the cross sections $\sigma^R_{V,G}$ in

V^R and $\sigma^0_{V,G}$ in V^0. The fluxes $\Phi_{V^R,G}$ and $\Phi_{V^0,G}$ spatially averaged over V^R and V^0 were calculated and the interpolation correlation (5) was applied.

Using the SIMULATE [6] code an additional 1d-calculation is performed in the axial direction z in order to determine a flux function $\Phi(z)$. In the volume V $\sigma_{V,G}$ is received when the group cross section $\overline{\sigma}_G(z)$ is weighted by $\Phi(z)$.

3. Results

Cell calculations were carried out for the core configuration of a reference pressurised-water reactor. The geometry of the assemblies was quadratic. An U-235 enrichment in the fuel (UO_2) of 1.9 % and a boric concentration in the moderator of 960 ppm was chosen for the numerical simulations. The following 3d-problems of reactor cells were investigated: As a first model an inserted control rod surrounded by eight fuel rods was considered with different insertion depths. As a second model a fuel rod was investigated around which the moderator material was replaced with void step-by-step increasing the height of the void. For the void model two cases were considered: A single fuel cell with void and a fuel cell with void surrounded by eight fuel cells without void. For the single fuel cell the additional variant was investigated when the moderator was replaced with moderator with a lower density (10 %, 1 % and 0.1 % of the real density) in identical to the void case way. In each test case the eigenvalue and the averaged two-group cross sections (total, absorption, scattering and production cross sections) were calculated (group boundary between the fast and the thermal energy range = 3.9279 eV). In MCNP and TransRay the cell height was 24 cm, which is approximately the height of a node in DYN3D. More cell different heights (0.1, 1, 10, 24, 50, 75 and 100 cm) were considered with MCNP. At the outer boundaries of each reactor cell reflexion boundary conditions were assumed. The data of the macroscopic group cross sections necessary as an input for the TransRay code were prepared two-dimensionally using HELIOS. In general an own 3d-data preparation would be necessary for the 3d-calculations with TransRay.

In the case of the inserted control rod the relative deviations between the TransRay results and the HELIOS and MCNP ones were usually less than 5 % considering a cell height of 24 cm and for the eigenvalue less than 3 %. The values for the absorption and the production cross section of the thermal group are exemplarily shown in fig. 1, which also depicts that TransRay always overestimated the influence of the absorber on the averaged absorption cross section compared to MCNP. The MCNP calculations with different cell heights revealed that the eigenvalue as well as the averaged two-group cross sections depend on the cell height. The interpolation model determined by equation (5), which was applied in TransRay, showed satisfactory prediction behaviour compared to the full 3d-simulations also performed with TransRay, considering a cell height of 24 cm (fig. 1). At other cell heights this interpolation was inadequate compared to MCNP predictions.

For the test case of the fuel cell with void surrounded by eight fuel cells without void the relative deviations between the TransRay results and the HELIOS and MCNP ones were less than 2 % for the averaged two-group cross sections and less than 0.31 % for the eigenvalue considering a cell height of 24 cm. The dependence of the eigenvalue and the averaged two-group cross sections on the void portion in the central fuel cell was essentially linear. This held also for those two-group cross sections, which were averaged only over the central fuel cell with the void. The MCNP calculations with different cell heights showed merely partially a small deviation from the linearity with increasing cell height. That is, in order to get the averaged

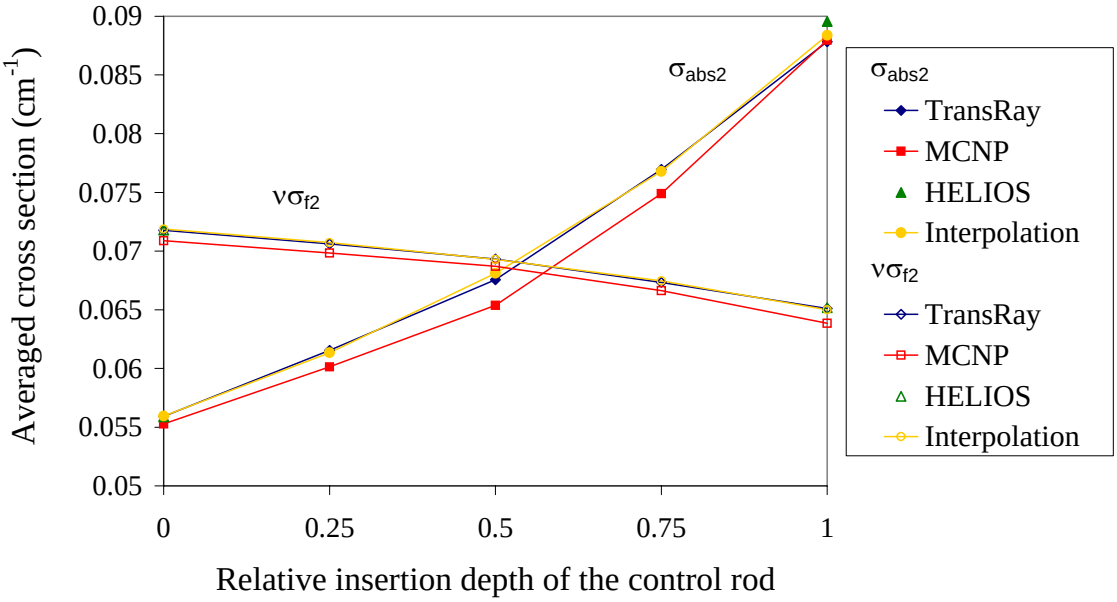

Fig. 1: The averaged absorption and production cross section σ_{abs2} and $\nu\sigma_{f2}$ of the thermal group depending on the insertion depth of the control rod calculated with MCNP, HELIOS (2d-values for the fully drawn and fully inserted control rod) and TransRay; for comparison the TransRay values are given calculated with the interpolation model according to equation (5); cell height = 24 cm.

cross sections in the case of a void portion in the moderator region of the central fuel cell it is possible to interpolate linearly between the values computed two-dimensionally. These values belong to the both 2d-cases only with moderator and only with void.

For the single fuel cell the relative deviations between the TransRay results and the HELIOS and MCNP ones were usually less than 5 % for the averaged two-group cross sections and for the eigenvalue considering a cell height of 24 cm. The dependence was investigated of the eigenvalue and the averaged two-group cross sections on the relative height of the void or of the moderator with a lower density respectively. For each of the treated cell heights this dependence was qualitatively equal, regardless whether void or moderator with a lower density was used. Additionally, this dependence was obviously non-linear for the eigenvalue and the averaged two-group cross sections, especially for the thermal group. That is, linear interpolation between the values computed two-dimensionally to get the averaged cross sections is not applicable. The linear interpolation almost always provides lower values than the three-dimensionally computed cross sections for both cases, partial void and partial moderator with a lower density. For the partial void case the absorption cross sections of the thermal group are shown in fig. 2 considering a cell height of 24 cm. The MCNP value is absent when the relative height of the void equals 1, because the thermal neutron flux computed with MCNP was zero. Additionally to the 3d-calculations with MCNP and TransRay respectively, 2d-calculations have been performed with HELIOS with homogeneous dilution of the moderator density by 25, 50 and 75 %. The results are shown in fig. 2. The differences between the 2d-calculations with homogeneously diluted moderator and the 3d-calculations are caused by spatial effects. Therefore, 3d-effects can be relevant in the case of a strong axial heterogeneity like a water level over large regions of the core. The interpolation model for inserted control rods determined by equation (5) was also applied in TransRay for the case of void around a single fuel rod. Fig. 2 illustrates that this interpolation provides unsatisfactory prediction compared to the full 3d-simulations also performed with TransRay. This result demonstrates that this interpolation is not applicable for the case of void around a single fuel rod.

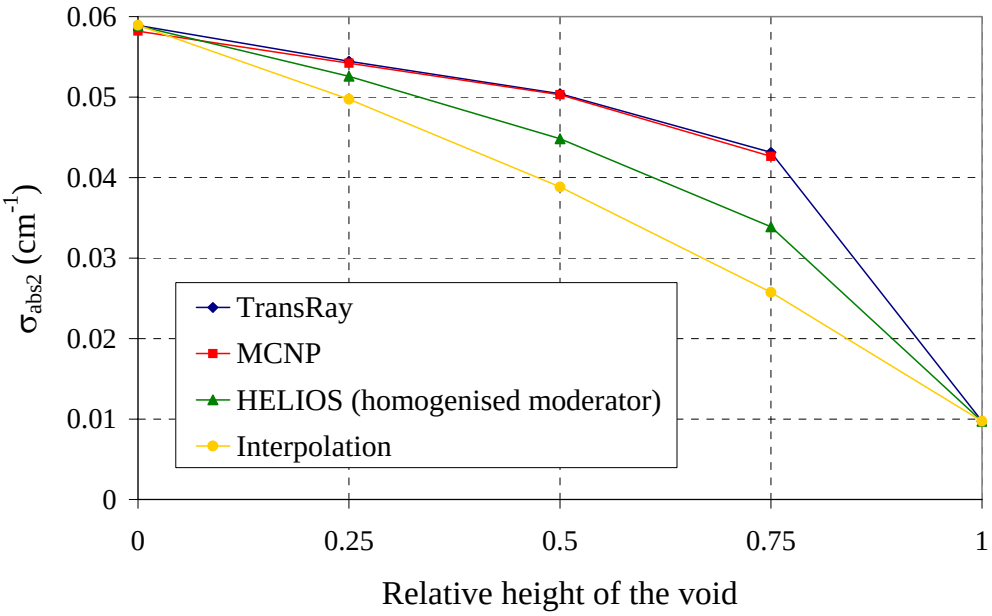

Fig. 2: The averaged absorption cross section σ_{abs2} of the thermal group depending on the relative height of the void in the moderator region of the single fuel cell calculated with MCNP, HELIOS (2d-values for homogenised moderator) and TransRay; for comparison the TransRay values are given calculated with the interpolation model according to equation (5); cell height = 24 cm.

4. Conclusion

Though the reflexion boundary conditions in axial direction are non-realistic in all considered cases, the decisive question is related to the differences in the nodal cross sections due to the 3d- or 2d-data preparation. At least, reflexion boundary conditions are simple to handle and using them the decisive tendencies can be recognised. The case of a single fuel rod fully surrounded by void can be considered the limiting case of a fully voided reactor. However, for the investigated cases of a partially inserted control rod and a single fuel rod partially surrounded by void or by moderator with lower density respectively, it can be concluded that a three-dimensional data generation of averaged two-group cross sections is rather necessary for reactor cells with steam than for reactor cells with absorbers.

References

[1] U. Grundmann, U. Rohde, DYN3D – Three dimensional core model for steady-state and transient analysis of thermal reactors, Proceedings of the 2000 ANS International Topical Meeting on Advances in Reactor Physics and Mathematics and Computation into the Next Millennium (PHYSOR 2000), Pittsburgh (USA), May, 7 – 11, 2000

[2] Studsvik® Scandpower, HELIOS methods, Version 1.8, November 2003

[3] E. E. Lewis, W. F. Miller Jr., Computational methods of neutron transport, A Wiley-Interscience Publication, John Wiley and Sons, Inc., 1984

[4] J. F. Briesmeister, Editor, MCNP a general Monte-Carlo n-particle transport code, Version 4A, LA 12625 M, November 1993

[5] R. S. Varga, Matrix iterative analysis, Prentice-Hall, Englewood Cliffs, New Jersey, 1962

[6] T. Bahadir, S.-O. Lindahl, S. Palmtag, K. Smith, SIMULATE-4: New nodal code development activities, Studsvik Scandpower, CMS/FMS User's Group, April 2004

DYN3D – OVERVIEW ON MODEL EXTENSIONS

Ulrich Grundmann, Sören Kliem, Jirí Křepel, Siegfried Mittag, and Ulrich Rohde

1. Introduction

The computer code DYN3D developed in the Institute of Safety Research is used by research institutions, universities and regulatory bodies in Germany and other European countries for the safety assessment of nuclear reactors. According to the increasing requirements on the safety analysis, the code is undergoing a permanent development with respect to improved physical models and numerical methods. A new version of the code has been released containing an improved nodal expansion method for enhancement of the accuracy of the neutron flux calculation and so-called assembly-wise discontinuity factors for reducing the homogenisation errors. These improvements are of special importance in the case of larger and more heterogeneous fuel assemblies as well as the non-multiplying assemblies describing the radial reflector. The correct calculation of the different components of the external and feedback reactivity according to perturbation theory allows a deeper physical analysis of the feedback mechanisms being important inherent safety features. A special numerical algorithm with significantly reduced numerical diffusion based on the 'particle-in-cell' method was implemented for the description of boron transport. An interface has been developed to use the results of computational fluid dynamics (CFD) simulations and the semi-analytical coolant mixing model SAPR [1] for getting realistic boundary conditions for the analysis of boron dilution and overcooling transients. Several libraries of group constants different reactor types with enhanced accuracy were linked to DYN3D. Internal, external and parallel coupling of DYN3D with the system code ATHLET was performed to investigate a wide range of transients with feedback from the coolant system. The version DYN3D-MSR is under development which allows to model molten salt reactors (MSR).

2. DYN3D Model

The computer code DYN3D simulates the reactor core behaviour under steady-state and transient conditions [2]. It was developed for safety analyses of nuclear reactors after reactivity perturbations of the system, but it can be used also for fuel management calculations. The three-dimensional flux and power distributions in the reactor core, subdivided into calculational nodes, are calculated by nodal expansion methods for the solution of the neutron diffusion equation for quadratic or hexagonal fuel assembly geometry. Based on the fission power distribution, the fuel temperature distribution and heat released to the coolant are calculated from the solution of the radial heat conduction equation in fuel and cladding. The one- or two-phase coolant flow is calculated from the balance equations of momentum, mass and energy of the coolant, using the heat released to the coolant as source term. The distribution of the boron absorber in the coolant is ascertained by the solution of the convective boron transport equation. The two group constants homogenized for the core nodes are obtained from the linked neutronic data library for the given burn-up of the fuel and for the calculated state variables as fuel temperature, coolant density, coolant temperature and boron concentration. Burn-up calculations can be performed for the determination of the reactor conditions prior to the considered transient. Besides transients initiated by reactivity perturbations with characteristic times of seconds or minutes, the xenon dynamics can be investigated.

3. Nodal approximations for hexagonal fuel assemblies

The accuracy of the solution of the neutron diffusion equation can be checked by so-called mathematical benchmarks. A mathematical benchmark consists of a reference solution for a defined reactor configuration with given sets of homogenized group constants of nodes. A code solving the neutron diffusion with finite differences is mostly used for the generation of the reference solution. The reference solution is obtained by calculations with mesh sizes h in the order of the diffusion length and smaller. Generally, the reference solution is the result of a calculation with sufficiently small h or by extrapolation for h approaching 0.

Considering the VVER-1000 reactor with the larger fuel assembly pitch of 23.6 cm, the maximum deviation of the original DYN3D neutron kinetics against the reference solution of a mathematical benchmark was in the order of 5% for the nodal powers. The deviations of the DYN3D results were caused by the nodal approximation which was based on the flux separation in radial and axial direction, nodal expansion with Bessel functions, and the coupling of nodes with the help of side averaged partial currents. Two new methods HEXNEM1 and HEXNEM2 were developed for hexagonal-z geometry to improve the accuracy. In the nodes, the transverse integration of the three-dimensional diffusion equation is used to obtain a one-dimensional equation in axial direction and a two-dimensional equation in the hexagonal plane. The two equations are coupled by the transverse leakage. Inside of the nodes, the fluxes are approximated by polynomials up to second order and exponential functions being the solutions of the homogeneous equations. The nodes are coupled by the side averaged partial currents in HEXNEM1. In HEXNEM2, in addition to the side averaged currents the nodes are coupled in the hexagonal plane by the partial currents at the corners. The comparison of the assembly powers of HEXNEM2 with the published reference solution of the AER VVER-1000 benchmark problem [3] can be seen in Fig. 1. Tab. 1 gives the deviation of k_{eff}, the maximum and average deviations of nodal and assembly powers for the previous DYN3D-method, HEXNEM1 and HEXNEM2. The improvement by using the HEXNEM2-method is obvious.

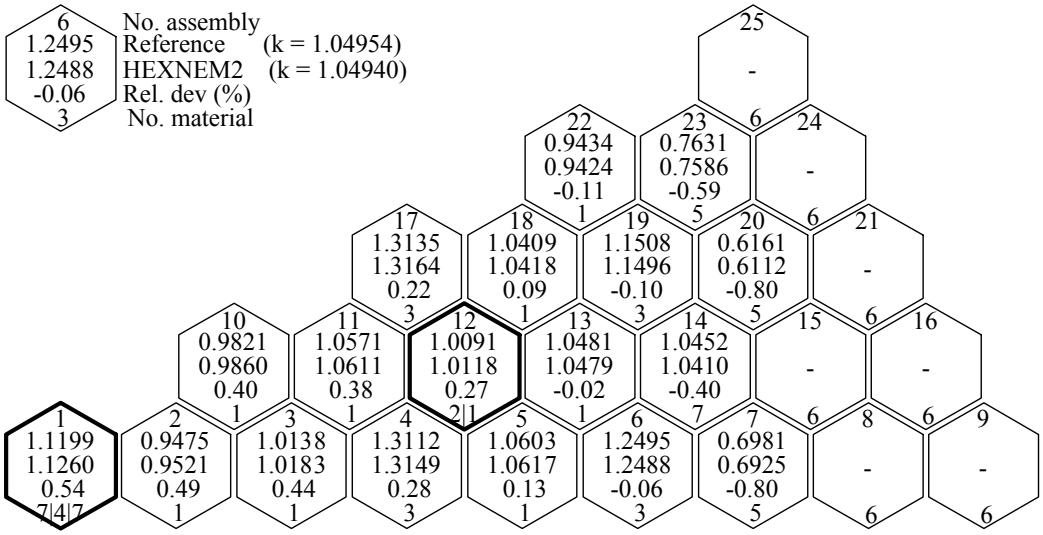

Fig. 1: Comparison of the assembly powers of HEXNEM2 with the reference solution of the AER VVER-1000 benchmark.

Table 1: Deviations of k_{eff}, the nodal powers P_i and the assembly powers P_i^{ass} of the DYN3D models from the reference results of the AER VVER-1000 benchmark.

Method	Δk_{eff} (pcm)	$\max_i \frac{\lvert\Delta P_i\rvert}{P_i}$ (%)	$\frac{1}{N}\sum_{i=1}^{N}\frac{\lvert\Delta P_i\rvert}{P_i}$ (%)	$\max_i \frac{\lvert\Delta P_i^{ass}\rvert}{P_i}$ (%)	$\frac{1}{N_{ass}}\sum_{i=1}^{N_{ass}}\frac{\lvert\Delta P_i^{ass}\rvert}{P_i}$ (%)
DYN3D	62	5.51	1.83	3.00	1.53
HEXNEM1	40	3.97	1.30	2.16	1.30
HEXNEM2	14	2.18	0.60	0.80	0.33

4. Assembly discontinuity factors (ADF)

Starting from the equivalence theory between the neutron diffusion equation of the original heterogeneous node and the homogeneous node the agreement between the node averaged fluxes can be improved by introduction of so-called assembly discontinuity factors (ADF) [4]. The ADF describe the ratio of the averaged fluxes at the node side *i* of the heterogeneous and homogeneous calculations for each energy group *g*.

$$f_g^i = \frac{\overline{\Phi}_{g,het}^{i}}{\overline{\Phi}_{g,\hom}^{i}} \qquad (1)$$

$f_g^i = 1$ in the case of a homogeneous assembly. The more heterogeneous the assembly is, the more f_g^i deviates from 1. The heterogeneities of an assembly are be caused by inserted absorber rods, different fuel pins in the assembly etc. Large heterogeneities exist in boiling water reactor nodes with inserted control rod (CR) crosses which are located in the water gaps between the fuel assemblies. Half of the water gap or the half of CR plates forming the crosses belong to the nodes. Their neutron group constants are smeared over the whole node in the homogenisation procedure. In the case of inserted CR the heterogeneous flux at the node boundary is lower than the flux of the homogenized node and $f_g^i < 1$ is obtained. By definition, the equations of the full heterogeneous problem have to be solved for the calculation of the ADF. Due to the fact that this is not possible, approximations are applied. For the fuel assemblies, approximate ADF are obtained from cell calculations with symmetrical boundary conditions. The effect of the ADF on the local power distribution in a boiling water reactor (BWR) is shown in Figures 2 and 3 [5]. The axial behaviour of the

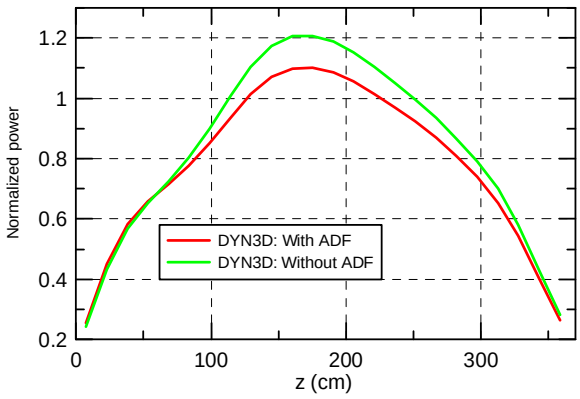

Fig. 2: Axial power distributions in a rodded BWR assembly

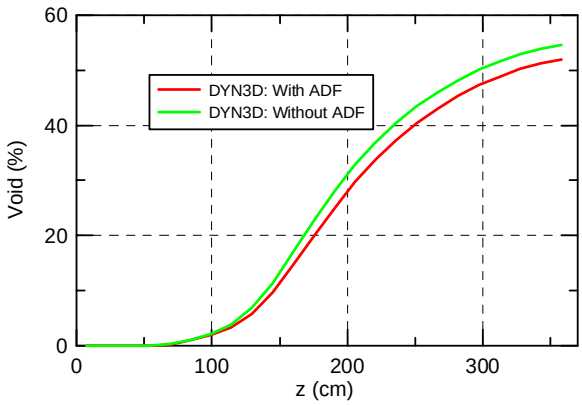

Fig. 3: Axial void distributions in the rodded BWR assembly of Fig. 2

3-dim. normalized power and void distributions of a BWR assembly with inserted CR can be seen for DYN3D calculations with and without consideration of ADF. The ADF concept can be also used in the homogenisation procedure of reflector and absorbing assemblies without fuel (VVER-440 control rods). Rather than of simulating one assembly in the cell calculation with reflecting boundary conditions, the consideration of larger regions of core improves the results for the ADF [6].

5. Calculation of Dynamic Reactivities

Applying the point kinetic equations for the description of the transient behaviour of the neutrons in the reactor core the reactivity is a key core averaged parameter to understand the response of the reactor power on perturbations of the neutron multiplication. Unfortunately the point model is a too simple model for a large power reactor. A more detailed space-dependent simulation of the reactor core by solving the three-dimensional neutron diffusion equation became possible by the development of powerful computers. The changes of reactor power distributions are the response of the reactor to changes of the cross sections. First of all the eigenvalue of the steady state is calculated which is connected with the static reactivity. A dynamic reactivitiy during the transient can be introduced by the separation of the flux distribution $\Phi_g(\boldsymbol{r},t)$ of the neutron energy group g in an amplitude function $N(t)$ and a shape function $\Psi_g(\boldsymbol{r},t)$ [7]:

$$\Phi_g(\boldsymbol{r},t) = N(t)\cdot\Psi_g(\boldsymbol{r},t) \tag{2}$$

The dynamic reactivity $\rho(t)$ which occurs in the generalized point kinetic equations for the amplitude function can be obtained from the flux distribution and the steady-state adjoint flux $\Phi^*_g(\boldsymbol{r},t)$ by the perturbation theory expression:

$$\rho(t) = \frac{\sum_n \int_{V_n} dV \left\{ \sum_{g=1}^{2} \Phi^{*n}_g(\boldsymbol{r}) \sum_{g'=1}^{2} \left\{ \frac{\chi_g \delta\nu\Sigma^n_{f,g'}(t)}{k_{eff}} + \delta\Sigma^n_{g,g'}(t) \right\} \Phi^n_{g'}(\boldsymbol{r},t) - \sum_{g=1}^{2} \left(\nabla\Phi^{*n}_g(\boldsymbol{r})\right) \delta D^n_g(t) \left(\nabla\Phi^n_g(\boldsymbol{r},t)\right) \right\}}{\sum_n \int_{V_n} dV \sum_{g=1}^{2} \Phi^{*n}_g(\boldsymbol{r}) \frac{\chi_g}{k_{eff}} \sum_{g'=1}^{2} \nu\Sigma^n_{f,g'}(t) \Phi^n_{g'}(\boldsymbol{r},t)} \tag{3}$$

The changes of the diffusion coefficients D^n_g and the macroscopic cross sections $\nu\Sigma^n_{f,g'}$, $\Sigma^n_{g,g'}(t)$ against their initial values occur in the numerator. $\Sigma^n_{g,g'}(t)$ describes the negative removal cross section for $g'=g$ and the scattering cross section for $g'\neq g$. V_n are the volumes of the nodes n. Considering small changes of fuel temperature, moderator density, moderator temperature, boron concentration and control rod (CR) positions the changes of the neutron group constants can be separated by their different origins, i.e. the total change of the group constants is the sum of the changes caused by the single perturbations. The interaction of the effects cannot be neglected for larger perturbations. Fig. 4 shows the dynamic reactivities and the reactor power for the withdrawal of a control rod bank in a VVER-1000.

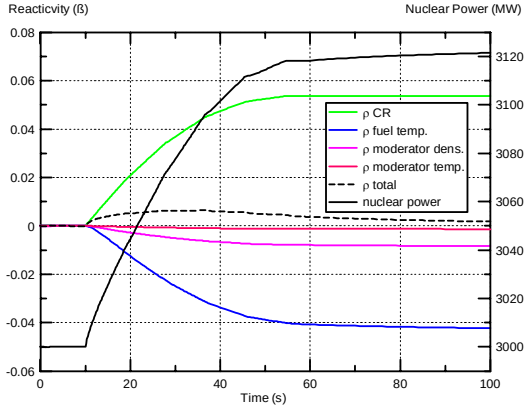

Fig. 4: Behaviour of nuclear power and the dynamic reactivities ρ for an assumed withdrawal of a control rod bank in a VVER-1000 reactor.

6. Boron transport

Due to different mechanisms or system failures, slugs of low borated water can accumulate in the primary cooling system of pressurized water reactors. This can happen e.g. as a consequence of a small-break-loss-of-coolant accident, when coolant circulation is interrupted and a slug of almost un-borated condensate will accumulate in the cold leg of the primary circuit. During start-up of coolant natural circulation after refilling the primary circuit with the emergency core cooling system or by switching on the first main coolant pump, this slug will be transported into the reactor core causing a significant reactivity insertion by decreasing the concentration of neutron absorber. The mixing of the unborated condensate with borated water in the reactor pressure vessel is in that case the only mitigative mechanism to prevent severe accident consequences. Realistic boundary conditions at the core inlet, that means, time-dependent boron concentration and temperature fields, will be provided by the mixing models, e.g. SAPR. Besides of mixing in the reactor pressure vessel, the description of boron transport in the core is important for the analysis of the consequences of hypothetical boron dilution events. The calculated distribution of the boron concentration in the reactor core during the transport of the slug through the core can be influenced by the numerical diffusion. Using the standard transport model of DYN3D numerical diffusion occurs, if the Courant criterion

$$\frac{\Delta z}{\Delta t} = v \tag{4}$$

is not fulfilled (Δz - the thickness of axial layers, Δt - the time step, v - velocity of the coolant). Depending on the fast processes in the core a small time step has to be chosen, but the coolant velocity is too small to satisfy the Courant criterion. By this reason the so-called particle-in-cell (PIC) method is used in DYN3D for a more correct description of boron transport in the core. Each axial node is divided into a large number of layers. The number of boron particles in each layer is connected to the boron concentration in the node. The individual transport of the particles is calculated. Based on the number of particles in the layers the boron concentration of each axial node is calculated. Considering a 36 m^3 boron free slug in one loop of a PWR and assuming pump start-up, the boron concentration at inlet and outlet of an arbitrarily fuel element 3 can be seen in Fig. 5. The inlet conditions are based on measurements at the ROCOM test facility. The time behaviour of the boron concentration

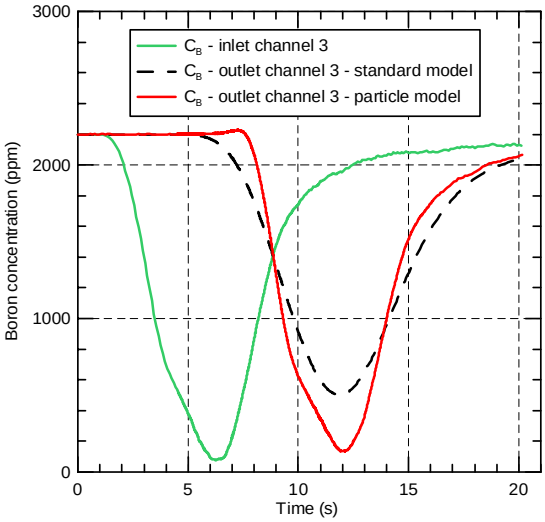

Fig. 5: Boron concentration at inlet and outlet of channel 3 – effect of PIC-model.

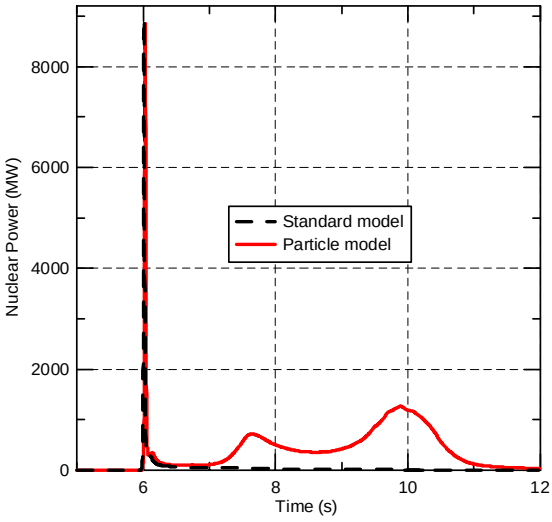

Fig. 6: Nuclear power – effect of PIC-model.

at the core outlet obtained from the PIC model is nearly the same as at the core inlet shifted by the transport time through the core. The standard model leads to unrealistic attenuation of the under-boration. This results in different reactivity insertions which are greater than $ß_{eff}$ in any case. Fig. 6 shows the nuclear power for the two calculations. The first power peak which is limited by the Doppler feedback is nearly the same. Two additional power maximums are observed in the calculation with the PIC model, but not in the standard model. The standard model is not conservative for this type of transient. Safety limits were not exceeded even when applying the PIC model.

7. Coupling DYN3D with ATHLET

DYN3D is coupled with various thermo-hydraulic system codes (ATHLET, RELAP5) using different mathematical approaches (internal, external and parallel coupling). Attention will be focused on the coupling of DYN3D with the system code ATHLET of the Gesellschaft für Anlagen- und Reaktorsicherheit which has been developed at ISR. Besides of coupling with ATHLET, DYN3D has been coupled to the widely used code RELAP5 within scientific-technical co-operation projects with IPPE Obninsk and VUJE Trnava in an internal and a parallel manner. A wide range of transients and accidents for pressurized and boiling water reactors can be simulated by the different types of coupling. The schemes of the coupling types concerning ATHLET are shown in Fig. 7.

Depending on the considered transient a special type of coupling is preferred. If reverse flow occurs in the core e.g. during a LOCA, the internal coupling should be applied, because it cannot described by the thermal hydraulic model of DYN3D. If a large number of fuel assemblies has to be simulated in a boiling water reactor, the parallel coupling should be used by reasons of stability of calculation. Considering a larger number of fuel assemblies of a pressurized water reactor computer runs with external coupling need lower CPU-time, caused

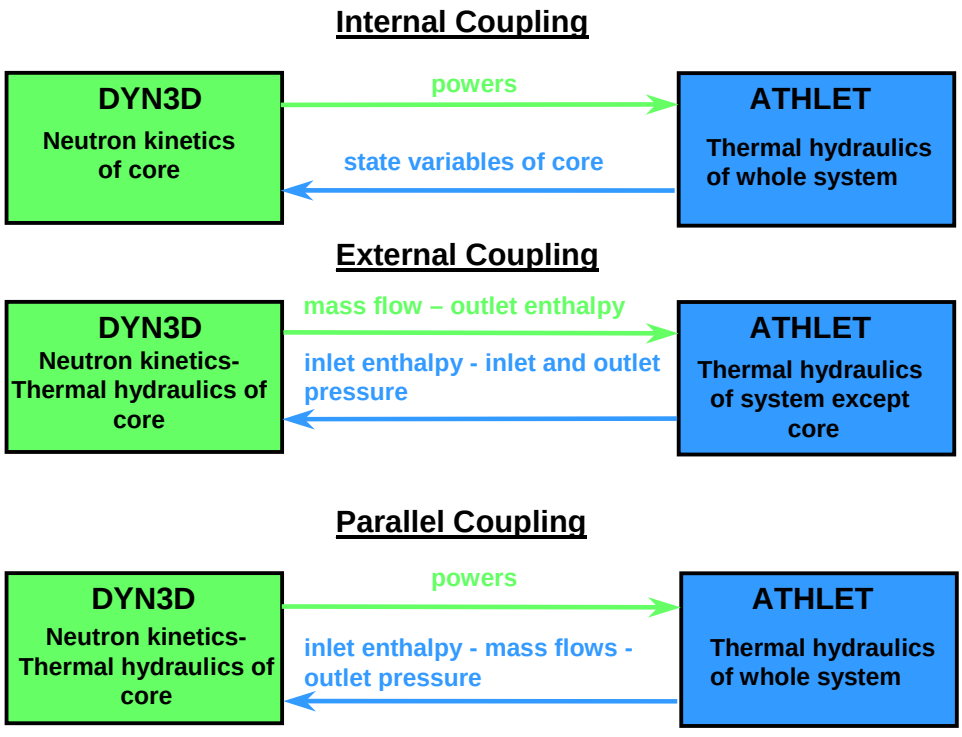

Fig. 7: Coupling schemes of DYN3D/ATHLET.

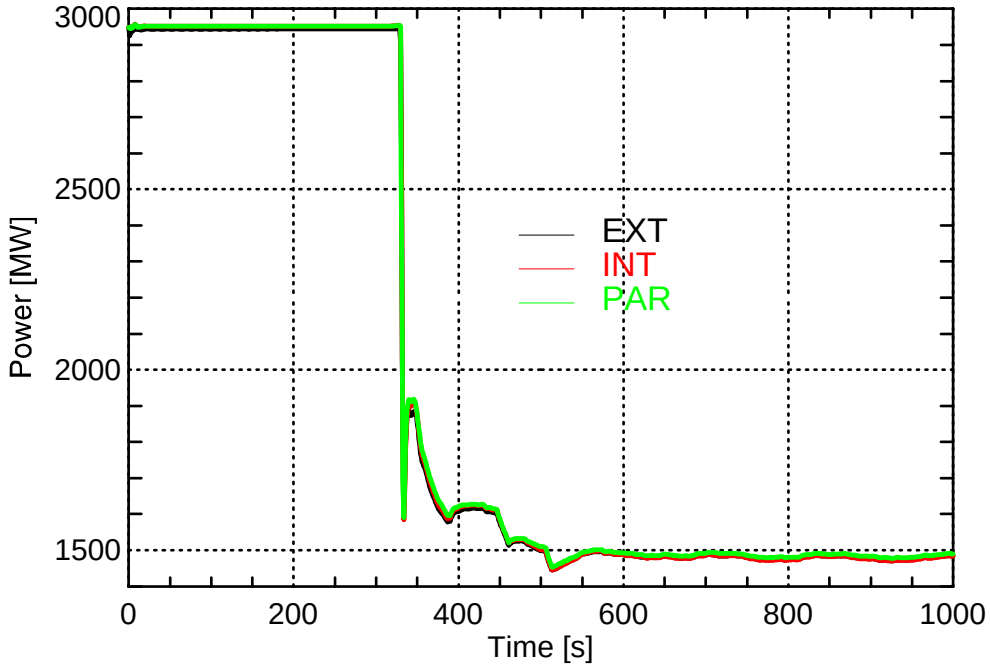

Fig. 8: VVER-1000 Transient: Nuclear power versus time calculated by external, internal and parallel coupling of DYN3D/ATHLET.

by the faster convergence of the thermal hydraulic model of DYN3D. There are also transients with no preference of any type of coupling. The results of all three types should be nearly the same. As an example the VVER-1000 Balakovo-4 operational transient "Switching-off of one from two working steam generator feed water pumps" was analysed by the different DYN3D/ATHLET couplings. Fig. 8 compares the nuclear power when using the three types of coupling. The thermal hydraulic models and the fuel rod models of ATHLET and DYN3D are different. In spite of this, the agreement was obtained by equal values for heat conductivity, heat capacity and gas gap conductance for fuel and cladding and the equal steady-state mass flow rates without any further tuning of models.

8. DYN3D-MSR for molten salt reactors

The nodal expansion method and the thermal-hydraulic (TH) model of the DYN3D code[2] was used as the base of a numerical code for dynamics studies of Molten Salt Reactors (MSR) which is one of the 'Generation IV' concepts. The graphite-moderated channel type MSR was selected for the numerical simulation as a representative of the reactors with liquid fuel. The DYN3D-MSR version [8] of code represents a stand-alone code and includes new routines for modelling of the liquid fuel reactor of MSR type. Two main modifications are made in the code. The model of delayed neutrons (DN) precursors includes the solution of the precursors equation with convective term. The distribution of DN is determined in the whole primary circuit. Furthermore, the heat release in the MSR is contrariwise to the classical PWRs. The energy from fission is predominantly released directly to the liquid fuel and the surrounding solid graphite is heated only with the gamma and neutrons radiation. However, the presence of heat sources in the graphite, even though they are small, causes the temperature to be higher as in the fuel which is practically cooling the graphite.

The data measured in the sixties during the Molten Salt Reactor Experiment (MSRE) in the Oak Ridge National Laboratory [9] were used to validate the MSR kinetics in 1D approach, especially the delayed neutrons model. MSRE was a 10 MW_{th} thermal reactor with liquid

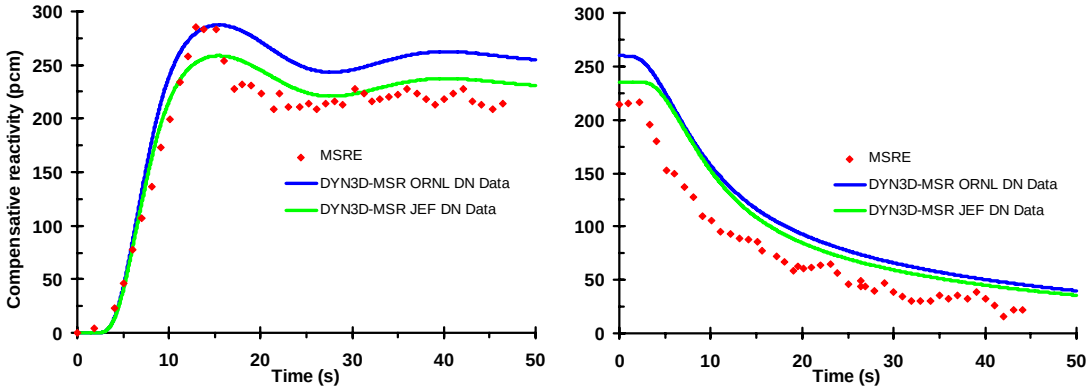

Fig. 9: Compensative reactivity inserted by control rods during the fuel pump start-up (left) and coast-down (right) transients.

molten salt fuel, moderated by graphite. It was constructed for the verification of MSR technology. The results for the zero power fuel pump start-up and the coast-down transients used to validate the code are shown in Fig. 9. In the two cases, the reactivity is changed to maintain a constant power level. Original ORNL DN data and calculated JEF DN data were used. The difference between the results is given by the different steady state loss of DN for each data set. The development of DYN3D-MSR is presently almost completed, however further extensions of the code are practicable. Because the decay of DN precursors in the fuel outside the reactor is important for the kinetics, the code should be completed by a fuel circuit model.

9. Conclusions and Outlook

Based on the improvements of the DYN3D models and on the coupling with the system codes ATHLET and RELAP5 a wide range of transients and accidents in PWR, BWR and VVER reactors can be simulated. The code version DYN3D-MSR can be used for the analysis of transients in molten salt reactors as a perspective reactor concept. Due to the extended capabilities of the code, the available developments, the validation status, and the support provided by the DYN3D development team, the code is used by research institutions and technical expert organizations in Germany and abroad, like:

- Energoproject – Nuclear Research Institute, Řež (Czech Republic)
- Scientific-Technological Centre of the NRC of Ukraine, Kiev (Ukraine)
- Institute of Physics and Power Engineering, Obninsk (Russia)
- VUJE Trnava (Slovak Republic)
- Technical University Budapest (Hungary)
- Institute of Nuclear Research and Nuclear Energy, Sofia (Bulgaria)
- ENPRO Sofia (Bulgaria)
- RWTH Aachen University (Germany)
- FRAMATOME-ANP, Erlangen (Germany)
- TÜV-Süd, München (Germany)

Several developments, validations and applications were performed in close cooperation with some of these institutions. The wide-spread use of DYN3D for VVER reactor safety analysis lead to the decision to integrate the code into the European code platform being elaborated within the European Integrated Project NURESIM coordinated by the French CEA.

References

[1] S. Kliem, H.-M. Prasser, T. Höhne, U. Rohde, „Development and Application of a Fast Running Model for the Description of Coolant Mixing Inside the Pressure vessel of Pressurized Water Reactors", Proceedings of PHYSOR 2002, Seoul, Korea, October 7-10, 2002.

[2] U. Grundmann, U. Rohde, and Siegfried Mittag "DYN3D – Three Dimensional Core Model for Steady-State and Transient Analysis of Thermal Reactors", Proceedings of the 2000 ANS International Topical Meeting on Advances in Reactor Physics and Mathematics and Computation into the Next Millennium (PHYSOR 2000), Pittsburgh (USA), May, 7 – 11, 2000.

[3] N. P. Kolev, R. Lenain, C. Fedon-Magnaud,"Solutions of the AER 3D Benchmark for VVER-1000 by CRONOS", 7th Symposium of AER, Hörnitz near Zittau (Germany), Proceedings, 650 – 665 (1997).

[4] Smith, K. S., "Assembly Homogenization Techniques for Light Water Reactor Analysis", Progress in Nuclear Energy, **17**, No. 3, pp 303-335 (1986).

[5] Grundmann, U.; Kliem, S.; Rohde, U. ; "Analysis of the Boiling Water Reactor Turbine Trip Benchmark with the Codes DYN3D and ATHLET/DYN3D", Nucl. Sci Engng, 148, 226-234 (2004).

[6] Mittag, S.; Petkov, P.; Grundmann, U. ; "Discontinuity factors for non-multiplying material in two-dimensional hexagonal reactor geometry", Annals of Nuclear Energy 30/13, 1347-1364 (2003).

[7] Radkowski, A., "Naval Reactor Physics Handbook, Vol. 1", United States Atomic Energy Commission (1964).

[8] J.Krepel, U. Grundmann, U. Rohde: "Development and Verification of Dynamics Code for Molten Salt Reactors", Proc. of the ICONE 12th - International Conference on Nuclear Engineering, Arlington, Virginia, 25-29 April, 2004.

[9] P. N. Haubenreich: "Molten-Salt Reactor Experiments", ORNL-4396.

UNCERTAINTY AND SENSITIVITY ANALYSIS OF A VVER-1000 START-UP EXPERIMENT USING THE COUPLED CODE DYN3D/ATHLET AND THE STATISTICAL CODE PACKAGE SUSA

Sören Kliem, Siegfried Mittag, Frank-Peter Weiss, and Siegfried Langenbuch[1]

1. Introduction

The transition from the application of conservative models to the use of best-estimate models raises the question about the uncertainty of the obtained results. This question becomes especially important, if the best-estimate models should be used for safety analyses in the field of nuclear engineering. Different methodologies were developed to assess the uncertainties of the calculation results of computer codes. One of them is the statistical methodology developed by Gesellschaft fuer Anlagen- und Reaktorsicherheit (GRS) which is implemented in the statistical code package SUSA. The method was already applied in different fields, a great number of applications was addressed to thermal hydraulics problems of nuclear reactors [1].

In the frame work of the recently finished EU FP5 funded research project VALCO, that methodology was extended and successfully applied to different coupled code systems, including the uncertainty analysis for neutronics [2]. These code systems consist of a thermal hydraulic system code and a 3D neutron kinetic core model. One of the code systems applied was ATHLET coupled with the Rossendorf kinetics code DYN3D. Two transients measured at NPPs with VVER-type reactors, which had been documented within a former EU Phare project (SRR1/95), were selected for analyses.

2. Methodology for uncertainty and sensitivity analysis

The GRS methodology for the assessment of uncertainty and sensitivity is a statistical technique. It considers the effect of the uncertainty of input parameters, initial and boundary conditions, computer models and solution algorithms. The uncertainty of the input and model parameters is quantified by their ranges of technically and physically realistic values and their subjective probability distributions. Based on this knowledge random samples of input parameter vectors are generated by Monte-Carlo-methods.

The final result of the application of this method are statistical tolerance intervals for the output parameters with a certain probability content and a certain statistical confidence level. Further, the importance of the identified uncertainties to the output parameters is assessed.

Details about the statistical tools can be found in [1, 3] and in the references listed there.

The GRS methodology consists of the following principal steps:

1. Definition of important parameters
2. Identification of potentially relevant uncertainties
3. Definition of uncertainty range
4. Judgement about the subjective probability distribution of uncertain parameters

[1] Gesellschaft für Anlagen- und Reaktorsicherheit mbH Garching

5. Determination of number of necessary (coupled) code runs
6. Calculation of random parameter vectors, which quantify the input uncertainty
7. Implementation of the vectors into the input decks of the coupled code
8. Application (carry out the computational runs)
9. Extraction of results (time dependencies of variables under investigation)
10. Evaluation of results (Determination of tolerance intervals and ranking coefficients)
11. Conclusions on the obtained results

In the following sections, the application of the method to the calculation of a start-up experiment at the NPP Balakovo-4 (VVER-1000) is described.

3. Application of the method to the calculation of the start-up experiment at Balakovo-4

3.1 Description of the experiment

A detailed description of the plant transient and results from analyses by coupled codes can be found in [4, 5]. During a test in the Balakovo-4 VVER-1000 (Russia), one of two working main steam generator feed water pumps was switched off at nominal power. Two seconds after the pump switch-off, the power control system responded by inserting the control rod group K1 from top to bottom within four seconds. As a result, the core power decreased down to about 63 % of nominal power within 10 s. Also the control rod group K10 started moving in at a rate of 2 cm/s. The initial axial position was at 275 cm. The slow insertion of control rod group K10 down to an axial position of 140 cm resulted in a further power decrease to about 45 % of nominal power. The reactor was stabilized at this level by the automatic power control. As all four main coolant pumps continued operating, the differences between the temperatures of the hot legs and the corresponding cold legs of the four primary loops decreased proportionally to the thermal power reduction, the temperatures in the loops stabilized at a new level. Initially, the primary pressure decreased, later on the primary pressure increased again, determined by the heat balance. The transient led to a strong decrease of the water level in the pressurizer in the early phase, then the level increased again to nominal values.

At the secondary side, the feed water flow rate through the second feed water pump, which was still in operation, increased by about 50 % within 16 s after the initiating event and partly compensated the deficient feed water flow. In the following, the flow rate of this second feed water pump was reduced again to match the reduced thermal power of the primary circuit. During the whole transient, the water levels in the steam generators were always kept well above the heater tubes.

3.2 Uncertain input parameters

In the first step, the possible uncertain parameters have to be identified. This step requests a basic understanding of the physical processes being relevant for the specific analysis. All relevant model parameters and assumptions should be included. On the basis of the discussion among the VALCO participants, the list of 11 parameters shown in Table 1 was agreed [1]. In the next step, the state of knowledge of the identified parameters should be expressed by subjective probability distributions. For this purpose, it is necessary to specify the possible range of each parameter and the distribution of the parameter inside this range. Both steps require expert knowledge about the parameters and their behaviour throughout the process under investigation. They are subjective, which can have some influence on the results of the analysis.

Table 1: List of the identified uncertain parameters with ranges and probability distributions

N°	Parameter	Range	Distribution
1	Magnitude of secondary pressure: correction factor *	0.9; 1.1	uniform
2	Total reactivity worth of control rod group K1	0.7;1.0;1.1	triangular
3	Total reactivity worth of control rod group K10	0.7;1.0;1.1	triangular
4	Shape of axial burn-up distribution**: correction factor	0.8;1.0	uniform
5	Fuel temperature feedback: correction of the global core response	-0.2; 0; 0.2 (each 1/3)	discrete
6	Moderator density feedback: correction of the global core response	-0.2; 0; 0.2 (each 1/3)	discrete
7	Heaters in PRZ: heat-up time-constant [s]	2.0; 20.0	uniform
8	Heaters in PRZ: protection influence factor***	1;2 (each 1/2)	discrete
9	Fuel rod gap heat transfer coefficient [W/m²K]	3000.0; 5000.0	uniform
10	Mass flow of the feed water	0.9; 1.1	uniform
11	Enthalpy of the feed water	0.9; 1.1	uniform

*The ATHLET input deck contains a simplified description of the secondary side with a time-dependent pressure boundary condition in the main steam header obtained from the experimental data. This function is multiplied by the correction factor.

**The axial burn-up distribution is rotated with the correction factor, center of rotation is the middle of the core. In this way, the difference in burn-up between lower and upper half of the core is decreased (<1) or increased (>1). The total burn-up of the core and the relative differences between single fuel elements remain constant.

***A protection is implemented in the logic of pressurizer heater activation: the heaters are switched-off, when the temperature change in the primary circuit is higher than a given value. No information was recorded about the activation of this protection during the experiment. Therefore it was included into the list of uncertain parameters with two options: 1-available; 2-not available.

The information contained in Table 1 is sufficient to generate the parameter vectors for the sequence of computer calculations. Only the number of necessary computer runs should be determined.

The uncertainty of the results is assessed by means of statistical tolerance intervals. These tolerance intervals are associated with a probability content β and a statistical confidence level γ in the following way: At least β (e.g. 90%) of the uncertainty of the output variable is covered by the corresponding interval bounds. This holds with a statistical confidence of at least γ (e.g. 95%). It is the main advantage of the GRS methodology that the minimum number of code calculations N is independent from the number of uncertain parameters to be investigated. It is only connected with the desired probability content and confidence level through the following formulae [1]:

$$1-\beta^N - N\cdot(1-\beta)\cdot\beta^{N-1} \geq \gamma \qquad (1)$$

On the one hand, from (eq. 1) follows, that the probability content and the statistical confidence increases with increasing number of variations calculations. On the other hand, the calculation of a real transient by a coupled code system requires long computation times. In the case of the Balakovo VVER-1000 transient under investigation the CPU-time for one run using DYN3D/ATHLET is about 4 h.

Thus the number of 100 variation calculations is appropriate. With 100 variation runs a probability content of 90 % with a statistical confidence of 95 % can be reached.

Using the “simple random sampling” algorithm being part of the SUSA package, 100 vectors of input parameters were created. The corresponding values were chosen from the respective distributions independently for each vector.

4. Results of DYN3D/ATHLET calculations

For the evaluation of the results, output parameters were selected, for which experimental data are available. Fig. 1 shows the time histories of the relative core powers in the 100 single calculations. The transient was initiated after a zero-transient calculation at t = 330 s. Two seconds later, the first control rod group started moving down, which was accompanied by a fast power reduction. The spreading of the results within these first seconds is clearly due to the varied Doppler feedback and the variation of the weight of the control rod group K1. After stabilisation of the core power, in the second phase of the transient in 31 of the 100 calculations, a remarkable power decrease is observed, while in the remaining calculations the power remains more or less stable until the end of the considered period of 1000 s.

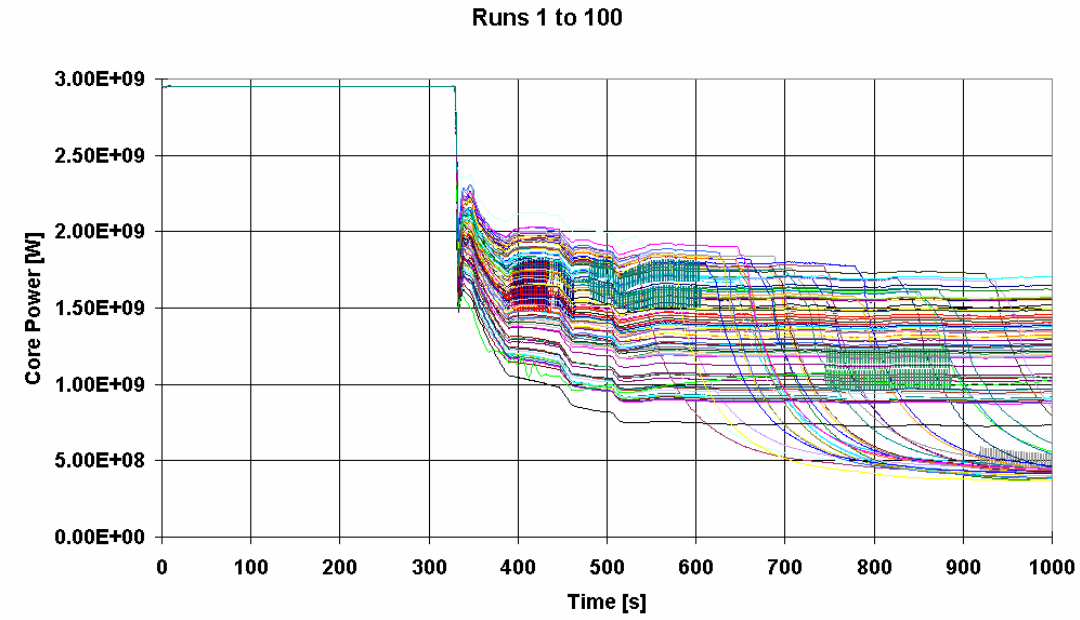

Fig. 1: Core power in the 100 variation calculations

The record of the coolant temperature in the hot leg shows an increase in the same 31 runs (Fig. 2). Fig. 3 depicts the behaviour of the calculated mixture level at the secondary side of the steam generator. By analysing these three figures, the reason for the different behaviour could be found. The following chain of events was revealed: The deviating behaviour (in the reference calculation the power remains constant, see later and [1]) occurs only in calculations, where the power level after the drop of the first control rod group stabilizes at a higher value. This is a consequence of the reduced weight of the control group K1 and the reduced Doppler feedback. Independently from this influence, the feed water mass flow rate to the steam generator secondary side was varied, too. In the identified cases, the combination of higher core power and reduced feed water mass flow rate leads to a permanent decrease of the steam generator water level. At different times, the level reaches a value of 0.5 m below the nominal one. This triggers the switch-off of the main coolant pump in the corresponding loop. The observed decrease of the power level is connected with the decrease of the core mass flow rate due to the partial pump coast down.

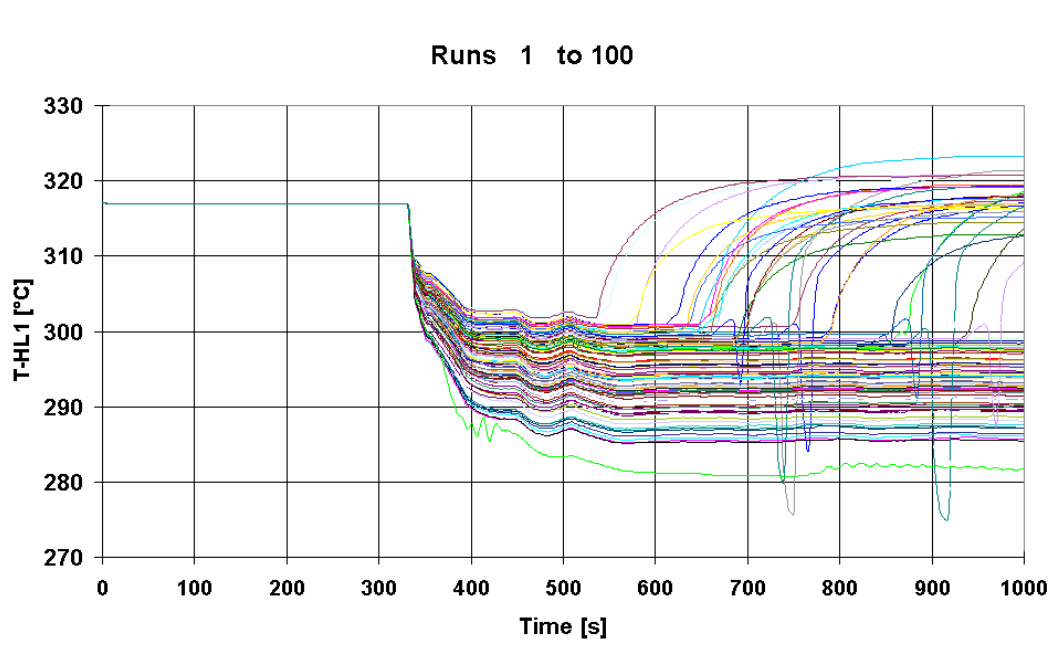

Fig. 2: Hot leg temperature in the 100 variation calculations

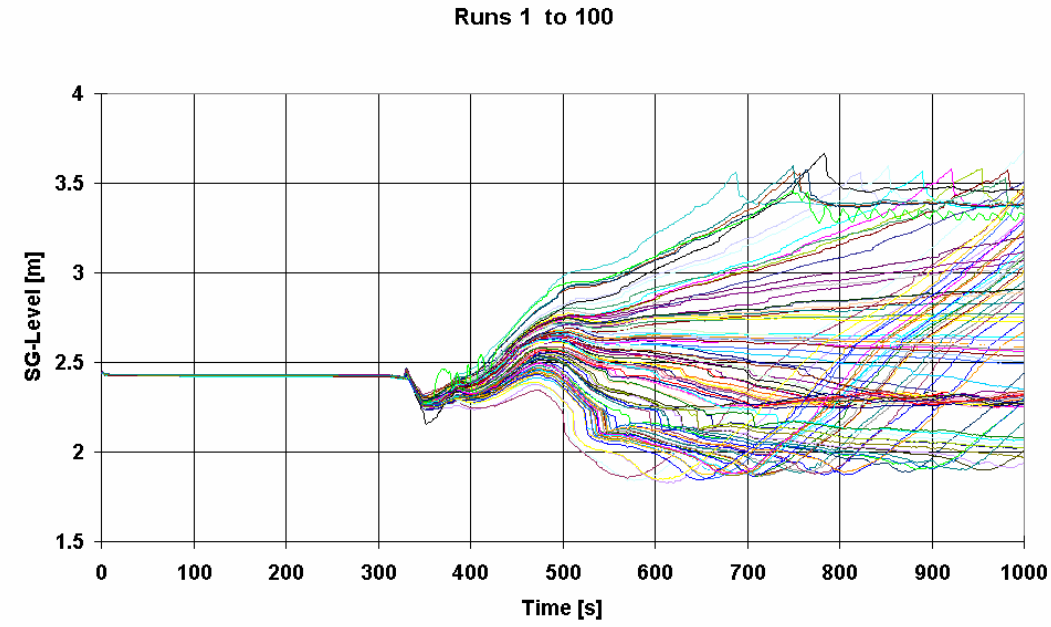

Fig. 3: Steam generator mixture level in the 100 variation calculations

Table 2: Ranking of the influence of input parameters on different output parameters

Output parameter	First phase			Second phase		
	1	2	3	1	2	3
Core power	6	5	2	10	-	-
Hot leg temperature	6	5	2	6	5	4
Cold leg temperature	6	1	5	1	10	6
Upper plenum pressure	6	5	8	6	5	9
Steam generator level	10	11	6	6	5	-

For five different output parameters, the three most significant input parameters are compiled in Table 2 (the numbers of the parameters correspond to the numbers in Table 1). This

compilation is divided into two parts due to the different physical processes, controlling the transient in the two phases. From Table 2 it follows, that the primary circuit parameters in the first phase of the transient are mainly determined by the variation of the moderator density and the Doppler feedback. The variation of core power, hot leg temperature and upper plenum pressure are controlled mainly by the same input parameters. Only the pressure reflects the influence of the pressurizer heater operation. Beside the mentioned feedback effects, the variation of the cold leg temperature is controlled by the secondary pressure behaviour. In the second phase of the transient, the core power is mainly influenced by the feed water mass flow rate to the steam generator. The reason for this unexpected dependence is the feed water mass flow rate being responsible for switching-off the main coolant pumps in a part of the calculations, which causes the power decrease, as explained above. In the first phase, the steam generator level is controlled by the variation of the mass flow rate and the enthalpy of the feed water. In the later phase of the transient, the determining parameters are the feedback coefficients for the core power, which influence the power transferred to the secondary side and therefore the steam flow.

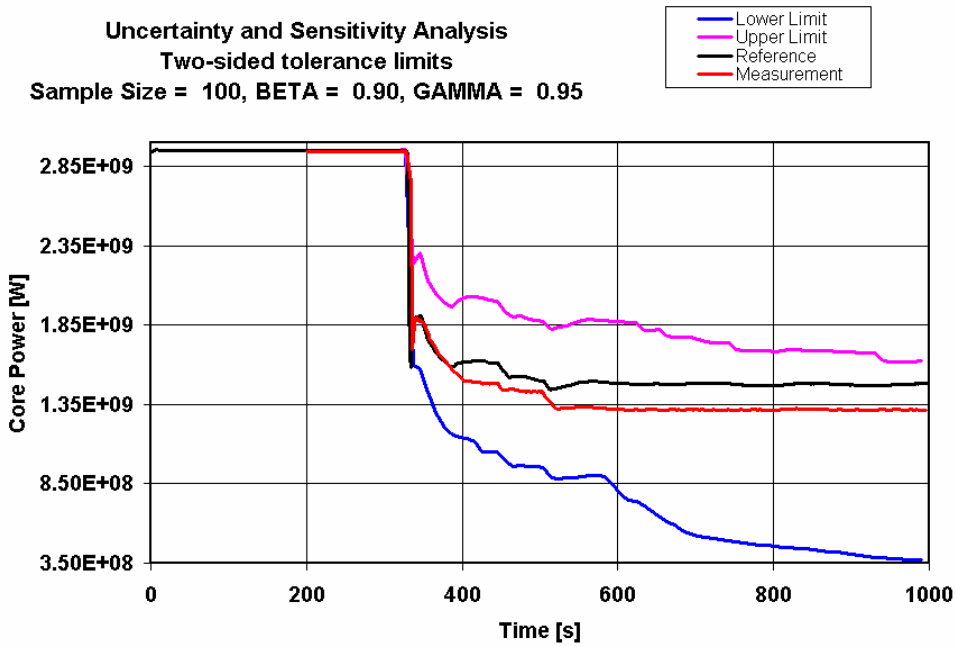

Fig. 4: Core power (reference solution, measured data and tolerance intervals)

On the basis of the 100 variation calculations, the time dependent tolerance limits for the output values were calculated. Fig. 4 to 6 show the time behaviour of the reference solution, the tolerance limits for a coverage of 90 % and a statistical confidence of 95 %, and the measured value for three different output parameters. Measured and calculated (reference solution) core powers are inside the tolerance interval during the whole transient. A similar coverage has been observed for the pressurizer level. The experimental upper plenum pressure is outside the tolerance limits in the very late phase of the transient over a time period of about 100 s. Over-estimation of the pressure in the first part of the reference calculation is fully covered by the tolerance limits. It can be seen, that the variation of the input parameters leads to a non-symmetric spreading of the tolerance limits in comparison to the reference solution. This phenomenon can be explained by the switch-off of the main coolant pumps in a part of the calculations, leading to a shift of the tolerance limits to lower values (core power, pressure, pressurizer level and cold leg temperature) or higher values (hot leg temperature and steam generator mixture level).

The measured temperatures in the hot and the cold leg are low pass filtered values due to the characteristics of the thermocouples. Such a filtering was not taken into account for the calculated values. Therefore, during fast changes the measured values are outside the tolerance interval in the first part of the transient.

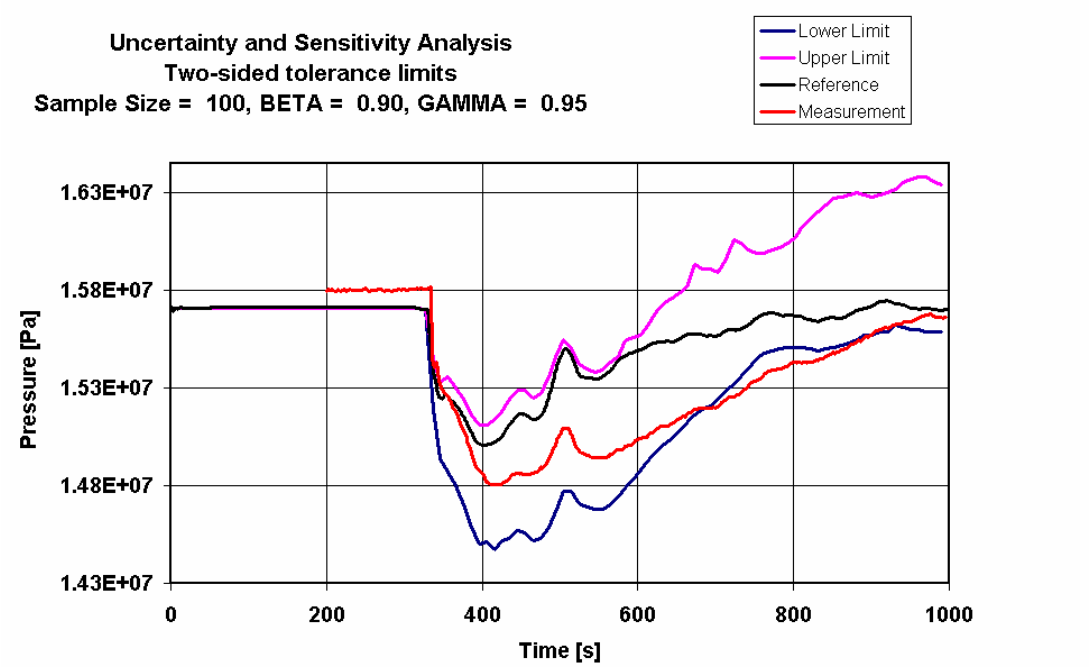

Fig. 5: Upper plenum pressure (reference solution, measured data and tolerance intervals)

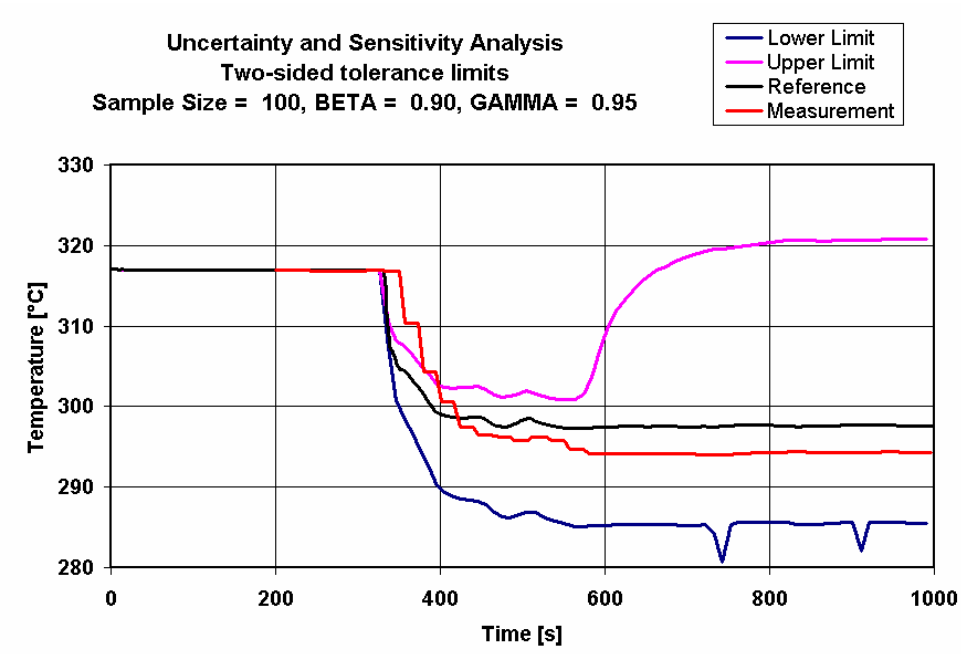

Fig. 6: Hot leg temperature (reference solution, measured data and tolerance intervals)

5. Conclusions

The GRS methodology for uncertainty and sensitivity analysis was applied first time to calculations using coupled neutron kinetics core models/thermal hydraulic system codes.

Nearly all available measurement data are covered by the tolerance limits assessed on the basis of the uncertainty of the input parameters. This underlines the good agreement between the measurement data and the obtained reference solution. A significant part of the calculations led to different hardware actions, which did not occur in the real plant transient and in the reference solution. So, the uncertainty and sensitivity analysis shows the spectrum of possible evolutions based on the same initiating event.

It was found, that the fuel temperature- and the moderator density feedback are the most sensitive input parameters in the calculation of this special transient. They provided the main contribution to the width of the tolerance limits. This clearly shows the direction, where an improved description of the input parameters would have the greatest impact. In this context, it is worth mentioning that the spreading of the solutions of the 5th Dynamic AER Benchmark (calculation of a hypothetical main steam line break in a VVER-440 using coupled code systems) was mainly due to the different cross section libraries used by the participants [6].

The experience gained during the application of the uncertainty and sensitivity analysis to a real plant transient forms a good basis for the use of the method in safety analyses for NPPs using coupled code systems.

Acknowledgement

The work was funded by the EU within the 5th Frame Work Programme (FIKS-CT-2001-00166).

References

[1] S. Langenbuch, B. Krzykacz-Hausmann, K.-D. Schmidt et al. (2004): Uncertainty and Sensitivity Analysis of two VVER Plant Transients in Loviisa-1 (VVER-440) and Balakovo-4 (VVER-1000), EU FP5 report VALCO/WP2/D10, Brussels, Belgium

[2] S. Mittag, U. Grundmann, S. Kliem et al.: “Validation of coupled neutronic/thermal hydraulic codes for VVER reactors”, EU FP5 report VALCO/WP4/D14, Brussels, Belgium (2004)

[3] S. Langenbuch (2002): Status report on uncertainty and sensitivity methods, EU FP5 report VALCO/WP2/D02, Brussels, Belgium

[4] S. Mittag, S. Kliem, F.-P. Weiß et al.: Validation of Coupled Neutron-Kinetic/Thermal-Hydraulic Codes for VVERs by Analysis of Plant Transients, Proc. OECD / CSNI workshop on Advanced Thermal–Hydraulic and Neutronic Codes Application, Barcelona (2000); NEA/CSNI/R(2001)2/ v.I, pp. 309-324

[5] S. Mittag, S. Kliem, F.-P. Weiß et al. (2001): Validation of coupled neutron kinetic / thermal-hydraulic codes Part 1: Analysis of a VVER-1000 transient (Balakovo-4), Annals of Nuclear Energy, 28/9, pp.857-873

[6] S. Kliem, S. Danilin, R. Kyrki-Rajamäki et al. (1999): A Benchmark for Coupled 3D Neutron Kinetics/Thermohydraulics System Codes - Main Steam Header Break in a NPP with VVER-440 Reactor, Proc. International Conference on Mathematics and Computation, Reactor Physics and Environmental Analysis in Nuclear Applications (MC ‘99), vol. 1, pp. 359-368, Senda Editorial, S.A. Madrid (Spain)

Summaries of research activities

Accident analysis of nuclear reactors

The research is aimed at the enhancement of the predictive capability of computer simulations of accident scenarios in light water reactors (LWR). This will be achieved by improvements of the neutron kinetics methods and e.g. by coupling of the reactor dynamics core model DYN3D to computational fluid dynamics (CFD) simulations. In particular, it is the objective to promote the basic understanding of coolant mixing phenomena relevant for boron dilution and pre-stressed thermal shock scenarios and to better ascertain the capabilities of measures for in vessel retention of corium melt during severe LWR accidents.

U. Grundmann, S. Kliem, S. Mittag, U. Rohde, F. Schäfer

Improvement and application of DYN3D and coupled thermo-hydraulic system codes

The Rossendorf reactor dynamics code DYN3D is undergoing a continuous development with respect to the improvement of physical models and numerical methods. A new version of the code has been released containing an improved nodal expansion method and so-called assembly-wise discontinuity factors assuring higher accuracy of the neutron flux calculation. A research project has been launched to develop and to implement into the code a simplified neutron transport approach (SP_3 method) which is expected to overcome shortcomings of the diffusion theory, especially in the case of significant heterogeneities in the reactor core.

The code complex DYN3D coupled with the thermo-hydraulic system codes ATHLET and RELAP5 was validated by calculating numerous real nuclear plant transients in the frame of the EC project VALCO and within the scientific-technical co-operation (STC) with the Ukraine and Russia. In the Russian STC project, the Institute of Safety Research (ISR) is participating in the OECD/NEA Benchmark V1000CT on VVER-1000 reactor plant transients. Moreover, the Russian partners used DYN3D for comprehensive studies on the burning of weapon grade plutonium in VVER-1000 reactors.

partly supported by BMWA

T. Höhne, S. Kliem, H.-M. Prasser, U. Rohde, T. Sühnel

Analysis of deboration transients

The European project FLOMIX-R under the leadership of the Institute of Safety Research (ISR) has been completed. Within this project, a comprehensive data base from coolant mixing experiments performed at the different European test facilities, among them the Rossendorf ROCOM facility, was established and provided for CFD code validation. Slug mixing in boron dilution scenarios has been investigated as well as buoyancy driven mixing under the impact of density differences, being important for thermal stress problems. The investigations contributed to a better understanding of the transition from momentum controlled to buoyancy driven mixing. For quality assurance in the CFD code validation, so-called Best Practice Guidelines (BPG) have been applied. The BPG require a minimization of numerical errors and solution errors by systematic grid and time step refinement and sensitivity tests with respect to the boundary conditions, before the effect of physical models is assessed. The applicability of various turbulence modeling techniques was studied for transient and steady state flow.

The semi-analytical mixing model SAPR has been implemented into the coupled code system DYN3D-ATHLET to provide realistic boundary conditions for the analysis of boron dilution and overcooling transients.

SAPR has been validated on slug mixing experiments at the ROCOM facility. A special numerical algorithm with significantly reduced numerical diffusion was implemented in DYN3D for the description of boron transport in the core.

funded by EU, TÜV and industries

U. Grundman, J. Krepel, U. Rohde

Development of a DYN3D version for Molten Salt Reactors

The development of a version of the code DYN3D for dynamics studies of Molten Salt Reactors (MSR), which is one of the 'Generation IV' concepts, has been almost completed. Modifications were made in the code to take into account the specifics of molten salt fuel. The model of delayed neutrons now includes the convection of the precursor nuclei with the molten salt fuel. Furthermore, the heat conduction model and thermodynamic properties functions had to be changed because contrariwise to an LWR, in the MSR the energy from fission is predominantly released directly to the liquid fuel, while the surrounding solid graphite is heated only with the gamma and neutrons radiation.

Data measured in the sixties during the Molten Salt Reactor Experiment in the Oak Ridge National Laboratory were used to validate the MSR kinetics in 1D approach, especially the delayed neutrons model. Zero power fuel pump start-up and coast-down transients were calculated within the EC project MOST.

supported by the EU

E. Krepper, A. Grahn

Simulation of sedimentation and re-suspension of insulating material in the reactor sump

Insulating material (mineral wool) may be released from pipes and components during loss-of-coolant accidents in NPP and will be transported with the coolant towards the reactor sump. There, it might lead to blockage of the sieves separating the suction chambers of the safety injection pumps from the sump and would impede late phase safety injection.

The related project funded by BMWA aims at the simulation of sedimentation and re-suspension of the mineral wool particles in the sump pool flow. The work is done in co-operation with the University Zittau/Görlitz (FH), where the experiments are performed, while FZ Rossendorf is responsible for the CFD modelling. Based on sedimentation tests using original isolation materials, the sinking and transport behaviour of the mineral wool fibres in the water flow was simulated using the Euler/Euler continuum approach with an adjusted model of the interfacial drag. The sedimentation and the re-suspension of the fibres in the sump was modelled assuming dependence of the viscosity on the volume fraction of insulation material. A porous body approach was developed for the simulation of the blockage of the sump sieve.

supported by BMWA

H.-G .Willschütz, E. Altstadt

In-vessel corium melt retention in LWRs

An improved thermo-mechanic finite element model has been developed for the evaluation of a possible reactor vessel failure during a core melt down accident scenario. The thermal hydraulic and the mechanical calculations are sequentially and recursively coupled. In the prior work only a one-way coupling between the thermal and the mechanical model was applied: first the transient temperature field was calculated and then

the transient mechanical calculation was performed applying the appropriate temperature field at each time step. The recursively coupled model also simulates the feedback from viscoplastic deformation of the vessel wall in the thermal calculations. In this way the following effects are considered: 1) change of melt pool geometry and melt level decrease due to the viscoplastic vessel wall deformation; 2) decrease of wall thickness (and thereby of heat resistance) due to viscoplastic deformation; 3) increase of the surface of the vessel wall and thereby the increase of the heat releasing surface. The model was applied to the FOREVER experiments performed at the KTH Stockholm. Additionally the mechanical consequences of an external flooding were analysed. First calculations have been carried out for the LWR geometry.

supported by BMWA and EU

Materials and components safety

The change in the toughness behaviour of reactor pressure vessel materials as a result of neutron and gamma irradiation is investigated. The consequences are evaluated related to the safety of light water reactors (LWRs). For this purpose, material and fracture mechanical parameters of irradiated specimens have to be measured under hot cell conditions. The interpretation of the experiments is supported by finite element calculations. The micro-structural reasons and mechanisms of the neutron embrittlement are studied by small angle neutron scattering experiments and by nano-scaled modeling.

U. Rindelhardt, H.-W. Viehrig, E. Altstadt

Investigation of reactor pressure vessel material of the dismantled Greifswald NPP

The second part of the radio nuclide laboratory has been approved by the Saxonian authority after successful inactive pilot run. In February 2004 we received the license to handle radioactive material. In this way the preconditions for the investigation of pressure vessel material of the dismantled Greifswald NPP are fulfilled.

In co-operation with industry partners the technical project has started for cutting out material from the reactor pressure vessel of unit 1 of the Greifswald NPP. According to this project, the material will be available for testing by fall 2005.

H.-W. Viehrig, M. Abendroth, M. Werner, E. Altstadt, C. Zurbuchen

Application of the Master Curve Concept for irradiated material

In the FP6 of the EU the FZR is involved in the Integrated Project PERFECT (Prediction of Irradiation Damage Effects in Reactor Components). FZR is leading a work package within the sub-project Mechanics Modelling. In this context, the VVER-440 RPV steel of the Greifswald NPP (unit 8) is analysed. The unirradiated material exhibits a large scattering of the fracture toughness and inter-granular cleavage fracture. It is therefore a suitable material for testing the applicability of the Master Curve Concept to inter-granular cleavage fracture and to inhomogeneous microstructure. An irradiation experiment in the LYRA facility of the JRC Petten was prepared. More than 100 specimens (Charpy, tensile, CT) were manufactured from the Greifswald material. This experiment will start in January 2005.

In the frame of an industry co-operation with E.ON Kernkraft fracture mechanic tests were performed for an RPV nozzle outage of the Isar-2 NPP (KKI-2). After machining of the specimens, tensile tests and Charpy impact tests were done. The reference temperature was determined according to the Master Curve Concept (ASTM E1921-02) using 1T-C(T) specimens. All the tests were supervised by the TÜV Süddeutschland.

The research project “Application of the Master Curve Concept for the toughness characterization of neutron irradiated reactor pressure vessel steels” was started within the framework of the BMWA funded German nuclear reactor safety research programme. It is the aim of the project to apply of the Master Curve Concept to highly irradiated RPV steels.

The interpretation of fracture mechanic tests was supported by finite element calculations. An improved algorithm of the plasticity model of Gurson, Tvergaard and Needleman was implemented into the FE code

ANSYS. This enables the effective simulation of crack growth. For the brittle fracture, the BEREMIN model has been implemented into the ANSYS code. Additionally, an ANSYS macro for the calculation of the 3d J-integral was developed and verified.

supported by EU, industry and BMWA

F. Bergner, A. Ulbricht, A. Gokhman, G. Müller,

Analysis of the irradiation induced micro-structural changes

Micro-structural changes of different RPV steels were investigated after irradiation and thermal annealing, as well as after repeated irradiation and subsequent thermal annealing. By small-angle neutron scattering (SANS) analyses it could be shown that the irradiation-induced clusters dissolve after annealing and the damage being less after the second irradiation compared to the first irradiation. This could be a hint that the sensitivity to embrittlement decreases after a thermal treatment.

The influence of hydrogen (H) on the toughness reduction of irradiated RPV steels was studied. At operating temperatures the deformation behaviour is not significantly changed by H deposition even at high neutron doses. In accordance with that result, also the SANS measurements gave no indication for an interaction between micro-structural irradiation defects and H atoms. However, a significant additional embrittlement by hydrogen is observed at low irradiation temperatures.

supported by BMWA

F. Bergner, A. Gokhman

Modelling of the irradiation induced embrittlement

Within the physics subproject of PERFECT a model for the simulation of irradiation-induced defects in RPV steels has been developed. It describes the evolution of vacancy clusters in pure bcc iron. The model is based on the rate theory considering the effect of lattice relaxation. The size distribution functions and the volume content were calculated and compared to those obtained by SANS measurements. By adjusting two model parameters – the surface energy and the dislocation density – a good agreement could be achieved.

supported by EU

Particle and radiation transport

The research project aims at the development, verification and application of computational methods for particle and radiation transport. At present, the focus is on neutron/gamma/electron transport with applications in reactor physics, shielding and radiation physical experiments. The transport of radio-nuclides in water-unsaturated geological zones is a further topic of high relevance in the context of final disposal of radioactive waste and in the context of the left backs of uranium mining.

J. Konheiser, B. Böhmer

Reactor dosimetry research projects

In the framework of the EU research project REDOS neutron/gamma calculation results obtained with the TRAMO code for VVER-1000 and VVER-440 mock-ups were compared with results of other project participants and with experiments. In REDOS for the first time, such comparisons were done for neutron and gamma spectra and in a broad range of radial reactor positions. As the participants used different codes and nuclear data sets, the scatter of calculation results and the deviations from experimental data characterize the accuracy of present-day neutron/gamma fluence calculations. The project revealed deficiencies especially in gamma- and low-energy neutron measurements and calculations. The TRAMO results agreed reasonably with the experimental data and were well situated in the scatter band of calculation results of all the other participants.

To prepare material investigations of reactor pressure vessel (RPV) steel samples, which will be taken from the decommissioned VVER-440 reactors of the former Greifswald NPP, neutron and gamma fluence spectra were calculated by means of the TRAMO code inside the volumes of samples from several RPV positions of unit 1. The calculated neutron/gamma fluences together with the measured material parameters of these samples will be the base for the derivation of a correlation between accumulated irradiation and RPV material damage. Further calculations are planned for the other three units. This project is running in the framework of the STC agreement between Germany and Russia in the field of safety research for nuclear reactors.

supported by EU and BMW,

K. Noack, A. Rogov

Verification of MCNP for reactor dosimetric neutron/gamma fluence calculations

Neutron/gamma transmission measurements were carried out in the framework of an integrated DFG research project at the research and training reactors of Technical University Dresden and of the University of Applied Sciences Zittau/Görlitz (FH). Most of transmission modules investigated were composed of steel-water layers with a structure typical for the PWR construction from the core edge up to the pressure vessel. The experiments were modelled in detail by means of the Monte Carlo code MCNP-4C2 and calculated using the library of evaluated nuclear data ENDF/B-VI of recent release 8. The great number of calculations is finished. The assessment of calculation and measurement results is still going on.

supported by DFG

C. Beckert

Analysis of the effects of two-dimensional approximations for the generation of nuclear data

The DYN3D code allowing to calculate the whole reactor core of light water reactors and its transient behaviour has been developed at Forschungszentrum Rossendorf (FZR). It treats the three-dimensional (3d) neutron kinetics with a two-group diffusion approximation using the nodal method for assemblies with quadratic and hexagonal geometry. As input data, DYN3D needs two-group cross sections for the neutrons, which are averaged over each node. These cross sections are generated using the 2d-code-system HELIOS. The necessity to calculate these two-group cross sections three-dimensionally was evaluated with the Monte-Carlo code MCNP and the 2d- and 3d-cell-code TransRay respectively, which has been developed for that purpose at FZR. TransRay uses the same solution method as employed by HELIOS. The following reactor cells were investigated: A partially inserted control rod and void (or moderator with a lower density respectively) around a fuel rod as a model for a steam bubble in the moderator region. In general it could be concluded, that a three-dimensional data generation of averaged two-group cross sections is rather necessary for reactor cells with steam bubbles than for reactor cells with absorbers.

A. Myasnikov,
R. Koch

Code system for the calculation of transmutation in a Molten Salt Reactor

The renewed interest on Molten Salt Reactors (MSR) has stimulated the development of computational tools for this reactor type. A new code system is being developed at Forschungszentrum Rossendorf for the analysis of the burn-up behaviour and transient simulation. The computation method is based on the coupling between the well-known Monte Carlo transport code MCNP-4C2 and the burn-up code ORIGEN 2.1. The developed system allows to take into account the special feature of a liquid fuel system, namely, the reprocessing during reactor operation. For that purpose the interface between both codes offers several options for the simulation of feeding and extracting the molten salt fuel during the burn-up calculation. It aims at full integration of the constraints and flexibility of a MSR into the calculation scheme. In particular, two scenarios can be simulated that are under international discussion: the AMSTER scenarios of a self-breeder and of an actinide transmuter, and the SPHINX scenario of an actinide transmuter respectively. The calculations provide the precise time evolutions of reactor-physical parameters, nuclide inventories and of waste production from start-up to equilibrium.

R. Küchler,
K. Noack,
W. Hirsch,
V. Brendler,
J. Mibus

Weathering of minerals in the water unsaturated zone

Batch and column experiments are carried out to study the weathering process of pyrite mineral in unsaturated soil matrices of different porosity and saturation. The aim of these experiments is to ascertain the influence of both parameters on the reactive surface of pyrite grains. Under the conditions of an unsaturated water flow the reactive surface of mineral grains can be reduced considerably compared to saturated water

The project is commonly worked on by the Institutes of Safety Research and of Radiochemistry of Research Centre Rossendorf.

conditions. Without considering this effect the results of calculations of long-term radio-nuclide transports involving mineral weathering become wrong. First experimental results confirm the assumption of another research group that the reactive surface of pyrite grains is approximately reduced by the factor porosity times saturation.

Pulsed Photo-Neutron Source at the radiation source ELBE

The Rossendorf LINAC ELBE provides electrons of 20-40MeV. The pulsed electron beam can be injected into several beam lines to generate other types of radiation like parametric X-rays, infrared light, and neutrons. The neutrons are generated by (γ,n) reactions when the high energy electrons hit a high Z-target (liquid Pb) producing Bremsstrahlung. With the envisaged design, neutron source intensities in the range between 10^{12}-$10^{13}s^{-1}$ will be achieved. The ELBE parameters allow to convert the picosecond electron pulses into nanosecond neutron pulses which will be used to measure energy resolved neutron cross sections in a time of flight (TOF) facility. Due to the very short neutron pulses, an energy resolution of better than1% can be reached after a TOF distance of only 3.6m. The usable energies range from 660keV to approx. 10MeV with an electron beam repetition rate of 3.25 MHz. This is an interesting energy interval to measure neutron cross sections needed e.g. in the context of minor actinide transmutation. Lower neutron energies from 30-100 keV are accessible with a reduced intensity for nuclear astrophysics experiments.
The work is performed in close cooperation with the physics department of TU Dresden and the Rossendorf Institute of Nuclear and Hadron Physics.

E. Grosse,
A. Junghans,
H. Freiesleben,
C. Beckert,
K. Noack,
V. Galindo,
A. Rogov,
F.-P. Weiss

Design optimisation and construction of the photo-neutron source

The photo-neutron target essentially consists of a liquid Pb target confined by a Mo channel which is accommodated in a vacuum chamber, the beam dump absorbing the unused radiation in forward direction (electrons, photons, neutrons), the collimator decoupling the neutrons from the production target under an angle of 90°with respect to the electron beam, and the TOF detectors. The liquid lead target (through a heat exchanger) and the beam dump need to be cooled by a water circuit. The construction of the single components has started as well as the assembling of the main mechanical parts. The design of the instrumentation and control system including the interfaces with the ELBE LINAC has been finished. Thermal hydraulic and structural mechanic calculations were necessary to improve the design of the Pb/water heat exchanger in order to allow for a faster response to changing heat deposition in the Pb target and to exclude freezing or overheating of the Pb in the circuit. A hot Pb test experiment (400-500°C) is run in a dedicated loop to gather long term experience on the behaviour of those components and materials that are in permanent contact with the liquid Pb. The key issues are related to the materials compatibility of Mo and stainless steel on the one side and the hot Pb on the other side.

Monte Carlo calculations were performed with MCNP to optimise the collimator. The optimisation aimed at lowering the background of inelastically scattered neutrons and of photons at the measuring place. It was found that collimator insertions made from borated polyethylene together with Pb represent the best solution to absorb the photon flash coming from the radiator. These insertions lower the background and do not disturb the time of flight to energy correlation of the neutrons.

A BaF_2 scintillation detector array of up to 60 crystals is being developed for (n,γ) measurements. The time resolution reached with fast UV sensitive photo tubes is approx. 0,65 ns (FWHM). For neutron detection, Li-glass scintillators and a plastic scintillator wall is being built.

Supported by DFG

Safety and efficiency of chemical processes

The project aims at increasing the safety, efficiency and environmental sustainability of processes and plants in chemical engineering. Therefore, clarification of chemical processes is carried out using smart sensors and advanced online measuring techniques. The results provide the basis for the numerical process simulation at normal operating conditions as well as during safety relevant fault scenarios, e.g. during depressurisation caused by exothermic runaway. For such numerical simulation, CFD codes are required with integrated models for reaction kinetics.

G. Hessel, H. Kryk, H.-M. Prasser, W. Schmitt, S. Bohm

Depressurisation of multi-component systems

The kinetics of the esterification of methanol with acetic acid anhydride, which is an exothermal model reaction for safety studies in chemical engineering, was modelled on basis of an analysis of experimental data obtained at the automatic laboratory scale reactor (ALR). The auto-catalytic effect of the acetic acid was quantified and a new integral kinetic equation was proposed. The main advantage of the new model over previously existing overall kinetics ones is the adaptability to a wide range of educt concentrations. Thus, significant progress was made to derive a system of kinetic equations applicable with CFD codes.

An experimental key step was completed in the development of special relief channels, which allow directly accessing the critical cross-section of the vent line by an optical sensor measuring the void content.

S. Boden, M. Speck, U. Hampel

Strongly exothermic chemical reactions

X-ray micro-tomography was used to characterize the size, shape and porosity of polymer particles grown in the monomer flow during the production of polypropylene. The feasibility of in-situ polymer particle imaging for micro-reactors has been demonstrated by the development of a special experimental micro-tomography facility and by applying cone-beam tomography algorithms. This experimental work was performed in co-operation with the University of Twente, Netherlands, and aims at the development of new diagnostic tools for the optimisation and control of production processes for functional polymers.

G. Hessel, H. V. Hristov, H. Kryk, H.-M. Prasser, W. Schmitt, S. Boden, U. Hampel

Processes in stirred tank reactors

The automatic laboratory scale stirred reactor (ALR) was modelled using the CFX-5 fluid-dynamics code. A gas-liquid system was simulated dynamically where the liquid consists of two components of different density in order to study the transient mixing behaviour of an initially stratified state. The gas phase was involved to investigate the effect of the free surface deformation on the mixing process. Better understanding of such mixing is essential for making accurate predictions of the local physico-chemical properties as well as for performing a correct scale-up. Further work will include the implementation of chemical reaction models into CFX-5. The accuracy of the numerical simulations is evaluated using visual experimental technique where the mixing of the lighter (alcoholic) coloured component with the heavier (water) transparent was captured by a video camcorder and subsequently a digital image processing was applied.

An X-ray cone-beam computed tomography technique was adapted to quantitative measurements of gas distributions in stirred chemical batch reactors. Radially symmetric two-phase distributions in a stirred vessel were obtained using reconstruction techniques for single radiograms. The experiments provided information on the gas phase distribution as a function of the angular stirrer speed and allowed to visualize the gas-liquid surface around the stirrer shaft.

H.-M.Prasser,
A. Zaruba,
A. Böttger,
W. Zimmermann

Desulphurisation of acid mining effluents

A mock-up of an electrolytic cell for electrochemical treatment of acid mine effluent was studied under process-like conditions. It was demonstrated, that an appropriate flow regime can be established in the cathode chamber in order to ensure a high efficiency of the water treatment. The hydrogen generated as a side product can be extracted together with the catholyte flow without causing a flow blockage.

Liquid metal magnetohydrodynamics

Magneto-hydrodynamics investigates the interaction of electrically conducting liquids (liquid metals and semiconductors, electrolytes) with magnetic fields. In various applications, the use of magnetic fields provides a comfortable contact-less possibility to control the transport processes in such liquids. Moreover, problems as MHD turbulence or the homogeneous dynamo are the subject of intensive basic research.

A. Cramer,
I. Grants,
S. Eckert,
R. Lantzsch,
A. Pedchenko,
K. Varshney,
Ch. Zhang,
G.. Gerbeth

Basics of MHD flows and MULTIMAG

The experimental set-up MULTIMAG is now completed. It provides any arbitrary combination of rotating, travelling, pulsating and steady magnetic fields over an experimental volume of about 40 litres. The experimental program at MULTIMAG started with extensive studies on the linear and non-linear flow stability in combined rotating, travelling and steady magnetic fields. A theoretical tool has been developed in order to analyse the occurrence of sub-critical non-normal instabilities in fluid flows, and these predictions were fully verified in the experiments: whereas a transition to turbulence occurs in the rotating field case at a control parameter about 400% below the linear stability threshold, the transition in case of the travelling field follows the classical line of a linear instability. These results have direct consequences on magnetic field applications in crystal growth for such cases where the flow should be kept laminar.

In the turbulent case experimental studies have been performed on an optimised mixing of the melt. It turned out that a combination of different alternating fields provides a much better melt mixing compared to the rather fixed motions induced by the alternating magnetic fields separately. The flow in a pulsating magnetic field showed pronounced low-frequency spatio-temporal variations of the mean velocity profile for which no adequate theoretical description exists up to now.

The motion of single argon bubbles rising in the eutectic alloy GaInSn under the influence of steady longitudinal as well as transverse magnetic fields was examined using the ultrasonic Doppler velocimetry. The measurements revealed a distinct electromagnetic damping of the bubble induced liquid velocity leading to more rectilinear bubble trajectories. Raising of the magnetic field strength causes an enlargement of the eddies in the wake.

supported by DFG

F. Stefani,
Th. Gundrum,
U. Günther,
M. Xu,
G. Gerbeth

Dynamo effect

Further campaigns at the Riga dynamo allowed to measure the magnetic field fluctuations with higher resolution, thus allowing the analysis of the frequency spectra. For the first time, a pressure transducer was installed flash mounted to the inner wall of the dynamo module. The pressure fluctuations showed clear peaks in its frequency spectrum corresponding to the back-reaction of the induced magnetic field on the flow field.

The developed integral equation approach for dynamos has been applied to the French VKS dynamo experiment. It turned out that serious modifications of the flow field are needed if a dynamo action should be observed in that experiment.

A suitable extension of the simple model of an oscillating mean-field dynamo allowed to reproduce the basic features of Earth magnetic field reversals. They are shown to be generic consequences of the dynamo action in the vicinity of those points where the dynamo switches between a steady and an oscillatory behaviour.

supported by EU, DFG

Th. Gundrum, F. Stefani, G. Gerbeth

Velocity reconstruction by magnetic tomography

For the first time a fully contact-less velocity reconstruction has been demonstrated in a demo-experiment. An externally applied steady magnetic field is disturbed by the flow, and this field disturbance can be measured outside of the fluid volume by an array of magnetic field sensors. The mean flow field is then reconstructed by means of an inverse solver using a regularization technique. In the demo-experiment the velocity field has in parallel been measured by ultrasonic Doppler velocimetry. The magnetic reconstruction provides the correct three-dimensional mean flow field even in a good quantitative approximation. The method turned out to be rather robust and stable. With a time resolution of about 3 seconds, even the transient development of the flow field could be followed.

supported by DFG

S. Eckert, A. Cramer, M. Kamnev, K. Varshney, Ch. Zhang, G. Gerbeth

Ultrasonic measuring techniques for liquid metals

The ultrasonic Doppler velocimetry (UDV) has been successfully applied to velocity measurements in high-temperature liquid melts like PbSn, PbBi or aluminium. For a longer operation of the ultrasonic wave-guide in a tin melt, systematic corrosion studies have been performed with various wave-guide materials. A wave-guide of 1 m length for liquid tin has been developed and successfully applied at a glass-producing industrial partner.

supported by DFG, Industry

J. Priede, G. Gerbeth

Crystal growth

The standard theory for the description of solute distribution in crystal growth breaks down if the mean flow in the melt is directed away from the solidification front. The latter, however, often occurs if rotating or travelling magnetic fields are applied to crystal growth processes. An analytical approach has been developed for the solute distribution under such flow conditions. Surprisingly, a more intensive stirring of the melt does not necessarily lead to a more homogeneous solute distribution. Instead, a concentration peak may occur on the symmetry axis.

supported by DFG

S. Eckert, B. Willers

Solidification studies

In order to influence the microstructure of solidified metals, basic studies on the role of convection during the solidification process have been performed. Various compositions of a Pb-Sn-alloy have been solidified under the influence of a rotating magnetic field. The microstructure changed, from a columnar dendritic one without magnetic field to an equiaxed one in case of an additional stirring of the liquid phase due to the magnetic field action. For the first time, an in-situ measurement of the velocity field during the solidification process could be done by ultrasonic Doppler velocimetry.

supported by DFG

T. Weier,
Ch. Cierpka,
G. Mutschke,
V. Shatrov,
G. Gerbeth

Boundary layer control in electrolytes

Systematic investigations have been performed on the influence of the oscillating force wave-form on the resulting electromagnetic flow control for the separating flow of an electrolyte around different hydrofoils. The lift increase at the most effective excitation frequency is mainly determined by the peak momentum input. This offers an optimisation potential for the energetic effort by applying only short electromagnetic pulses for the purpose of the electromagnetic flow control.

In a theoretical analysis, it has been shown that an energetically attractive flow control can only be obtained if the induced electric currents are in the same order as the applied ones.

Thermal fluid dynamics of multiphase systems

The work of the Institute in the field of thermal fluid-dynamics aims at the development of models for Computational Fluid Dynamics (CFD) codes that describe the transient evolution of gas-liquid two-phase flows along the flow path in pipes and complex geometries. The models have to describe as well bubble size dependent void fraction distributions as bubble coalescence and fragmentation. The theoretical work is based on sound experiments at the TOPFLOW test facility using advanced two-phase measuring instrumentation.

D. Lucas,
J. Shi,
T. Höhne,
E. Krepper

Qualification of CFD models

The models for interfacial momentum transfer implemented into the code CFX-5, i.e. lift force, wall force and turbulent dispersion force were validated using experimental data on void fraction and bubble size distributions obtained at the TOPFLOW facility with an own 1D model as well as with CFX-5.7. Scaling effects were investigated analysing the measurement data from bubbly flow in vertical tubes of 50 mm and 200 mm diameter, respectively. Lift and wall force models according to Tomiyama combined with the "Favre averaged drag model" for the turbulent dispersion force were found to reflect best the measured radial gas volume fraction profiles at the upper end of the pipe (approximately fully developed flow). Similar results were obtained using a newer correlation for the wall force by Tomiyama, if it is combined with a deformation force. A first version of a multi-bubble-class model was implemented in CFX-5 in co-operation with ANSYS-CFX (developer of CFX). In this model every bubble class is represented by a separate phase. First calculations using this model and including models for bubble coalescence and break-up were done. Further research on bubble coalescence and break-up is necessary.

H.-M. Prasser,
A. Böttger,
J. Zschau,
H. Pietruske,
E. Schleicher,
T. Sühnel

Wire-mesh sensors

Wire-mesh sensors making use of the different electrical conductivity of gas/steam and water are used to measure void fraction and bubble size distributions in the experimental test sections of TOPFLOW. Now, the first wire-mesh sensor with 64x64 measuring points for an application at saturation pressures up to 7 MPa was constructed and successfully applied at the vertical test section DN200 of TOPFLOW. The goal was reached to maintain, also for experiments at high pressure and temperature, the lateral resolution of 3 mm as it was typical for the previous air-water tests.

H.M. Prasser,
U. Hampel,
M. Speck,
St. Boden

High-speed X-ray tomography with deflected electron beam

Ultra-fast X-ray tomography with deflected electron beam was developed as a non-intrusive alternative to wire-mesh sensors while maintaining the high spatial and temporal resolution achieved by the sensor. An extended detector arc was designed and manufacturing was started. A first vacuum-proof two-phase flow experiment is under preparation, which can be tested in the vacuum chamber of the electron beam test assembly built in co-operation with IKE Stuttgart.

H.M. Prasser,
U. Hampel,
D. Hoppe,
C. Zippe,
E. Schleicher,
A. Bieberle,
T. Sühnel

Resolution improvement of gamma tomography

A tomography system was developed and constructed for the measurement of the time-averaged void distribution in an electrically heated fuel rod bundle test of FANP. The experiments aim at the optimisation of boiling water reactor fuel elements concerning their CHF (Critical Heat Flux) behaviour. The tomography system is equipped with a high-resolution detector arc of 320 single scintillation crystals coupled to avalanche photo-diodes. The application of the tomography set-up is planned for 2005. The detector arc can later be used for rotation-angle synchronised gamma-tomography, as well. The spatial resolution will be improved from about 7 mm achieved by the previous system of 64 detectors to about 2 mm.

H.-M. Prasser,
U. Hampel

Optical measuring methods

Optical methods based on the processing of bubble images extend the experimental possibilities to bubble sizes below the resolution of the wire-mesh sensor, if the gas fractions are not too high. Furthermore, the evaluation of image sequences allows to measure velocities of individual bubbles in a non-intrusive way. High-speed camera imaging in a transparent bubble column was used to validate correlations for the turbulent dispersion force of the gaseous phase. Further, an optical micro-bubble sensor earlier developed for industrial application was adapted to the application in the pressure relief line of a chemical batch reactor model. The new sensor allows directly to visualise the multi-phase flow in the critical discharge orifice. In order to obtain sharp images at the given high velocities, the exposure time was reduced from 1 µs down to 50 ns by improving the developed pulse illumination technique.

TOPFLOW thermohydraulic test facility

The acronym TOPFLOW stands for Transient Two Phase Flow Test Facility. This multi-purpose thermal hydraulic facility is used for the investigation of generic and applied steady state and transient two phase flow phenomena in either steam-water or air-water-mixtures. It provides data for the development and validation of models of Computational Fluid Dynamics (CFD) codes. TOPFLOW has a maximum heating power of 4MW and allows operation at pressures up to 7MPa in pipes and vessel geometries of industrial relevance. In the past, experiments were focused on saturated flow conditions but will be extended to flow regimes influenced by heat and mass transfer.

H.-M. Prasser, H. Carl, M. Beyer, K. Lindner, P. Schütz, C. Zippe

supported by BMWA

Evolution of the flow structure in vertical pipes

After finishing air-water tests in the vertical test sections, experiments with a steam-water mixture at pressure levels of 1, 2, 4 and 6.5 MPa and temperatures up to 285 C° were carried out in vertical pipes of DN50 and DN200. The structure of the interfacial area was recorded using a novel wire-mesh sensor, which was developed for an operation at high pressures and temperatures. For the experiments on the evolution of the two-phase flow structure along the flow path, a special test section DN200 was used with variable gas injection. The data were assessed with respect to the influence of the physical properties of the fluid upon the flow structure. The data evaluation is performed in the frame of the R&D project "thermal fluid dynamics of multi-phase systems".

H.-M. Prasser, M. Beyer, P. Schütz, H. Carl, H.Rußig

supported by BMWA

Two-phase flow in complex geometries

After upgrading the CFD code by implementing model equations verified by experiments in the vertical test sections it has to be validated against more complicated flow fields such as those found in bends or T-junctions. In order to supply the necessary experimental data a special experimental methodology was developed: a movable obstacle creating a non-symmetric disturbance in the vertical pipe flow was constructed. The applied half-moon shaped disc can be placed either upstream or downstream of a wire-mesh sensor. By changing the distance between sensor and disc using a toothed bar mechanism, the full three-dimensional void field around the obstacle can be recorded. In the flow field created in this way stream lines and gravity enclose significant angles, which is a sensitive test case for the CFD code.

H.-M. Prasser, M. Beyer, P. Schütz, H. Carl, M. Tamme, Ch. Vallee

supported by BMWA

Flow structure in the hot leg of a PWR during a loss of coolant accident

The construction of the new hot leg test section of TOPFLOW is on schedule. The pressure vessel to accommodate the test section as well as all major components were delivered by end of the 2004. The commissioning is planned in March 2005. The experiment is mostly financed by project funds of BMWA.

H.-M. Prasser, M. Beyer, P. Schütz,

Thermal hydraulic performance of an emergency condenser

A series of measurements of the thermal hydraulic characteristics of the heat exchanger bundle of the SWR-1000 emergency condenser model

H. Carl,
H. Pietruske,
St. Weichelt

supported by
BMWA

was carried out. The condensation power was measured as function of the pressure difference across the bundle. The heat-up phases of these measurements were used to record three-dimensional temperature distributions in the large water volume of the secondary side of the emergency condenser, which show a pronounced stratification effect. The data will be used for CFD code validation.

Publications

Publications in journals

Abendroth, M.; Kuna, M.
Determination of ductile material properties by means of the small punch test and neural networks
Advanced Engineering Materials, Vol.6 - No.7, July 2004, 536-540

Alsmeyer, H.; Albrecht, G.; Meyer, L.; Häfner, W.; Journeau, C.; Fischer, M.; Hellmann, S.; Eddi, M.; Allelein, H.-J.; Bürger, M.; Sehgal, B. R.; Koch, M. K.; Alkan, Z.; Petrov, J.; Gaune-Escard, M.; Altstadt, E.; Bandini, G.
Ex-vessel core melt stabilization research (ECOSTAR)
Nuclear Engineering and Design, in press

Altstadt, E.; Fischer, E.; Kumpf, H.; Nagel, G.; Sgarz, G.; Weiss, F.-P.
Thermal and mechanical analysis of a PWR core baffle considering creep
International Journal for Nuclear Power - atw 49. Jg. (2004) Heft 5, S. 333-336

Altstadt, E.; Kumpf, H.; Weiß, F.-P.; Fischer, E.; Nagel, G.; Sgarz, G.
Analysis of a PWR core baffle considering irradiation induced creep
Annals of Nuclear Energy, Vol 31/7 (2004) p. 723-736

Bergner, F.
Scaling of self-similar long fatigue crack growth in aluminium alloys
Materials Science and Engineering, accepted

Bergner, F.; Müller, G.; Ulbricht, A.; Ouytsel, K. van; Blank, C.; Bras, W.; Dewhurst, C.
Deformation-induced small-angle scattering contrast in aluminium alloys
Nuclear Instruments and Methods in Physics Research B (Beam Interactions with Materials and Atoms), accepted

Böhmert, J.; Viehrig, H.-W.; Ulbricht, A.
Correlation between irradiation-induced changes of microstructural parameters and mechanical properties for RPV steels
Journal of Nuclear Materials 334 (2004) 71-78

Cramer, A.; Eckert, S.; Galindo, V.; Gerbeth, G.; Willers, B.; Witke, W.
Liquid metal model experiments on casting and solidification processes
Journal of Materials Science 39 (2004) 7285-7294

Cramer, A.; Gerbeth, G.; Terhoeven, P.; Krätzschmar, A.
Fluid velocity measurements in electro-vortical flows
Materials and Manufacturing Processes 19 (2004) 665-678

Cramer, A.; Zhang, C.; Eckert, S.
Local flow structures in liquid metals measured by ultrasonic Doppler velocimetry
Flow Measurement and Instrumentation 15 (2004) 145-153

Dzugan, J.; Viehrig, H.-W.
Application of the normalization method for the determination of J-R curves
Materials Science and Engineering A, (2004) 387-389, p. 307-311

Eckert, S.; Willers, B.; Gerbeth, G.
Measurements of the bulk velocity during solidification of metallic alloys
Metallurgical and Materials Transactions, in press

Fillip, O.; Hermann, R.; Gerbeth, G.; Priede, J.; Shatrov, A.; Güth, A.; Schultz, L.
Influence of melt convection on the microstructure of levitated and undercooled Nd-Fe-B alloys
Journal of Magnetism and Magnetic Materials, 272-276(2004) Suppl. 1, p. 1857-1858

Gailitis, A.; Lielausis, O.; Platacis, E.; Gerbeth, G.; Stefani, F.
Riga dynamo experiment and its theoretical background
Physics of Plasmas 11 (2004) 2828-2843

Gokhman, A.; Böhmert, J.; Ulbricht, A.
Multi-component clustering in VVER-type pressure vessel steels - thermodynamic aspects and impact on SANS
Journal of Nuclear Materials 334 (2004) 195-199

Grants, I.; Gerbeth, G.
Rayleigh-Benard instability in a cylinder under influence of rotating and steady magnetic fields
Physics of Fluids, Vol. 16 (2004) 2088-2096

Grants, I.; Gerbeth, G.
Stability of melt flow due to traveling magnetic field in a closed ampoule
Journal of Crystal Growth 269 (2004) 630-638

Grundmann, U.; Kliem, S.; Rohde, U.
Analysis of the boiling water reactor turbine trip benchmark with the codes DYN3D and ATHLET/DYN3D
Nuclear Science and Engineering 148 (2004) 226-234

Günther, U.
Intertwiners of pseudo-Hermitian 2×2-block-operator matrices and a no-go theorem for isospectral MHD dynamo operators
Proceedings of the Institute of Mathematics of the National Academy of Sciences of Ukraine, V. 50, (2004), 780-787, ISBN: 966-02-3224-1

Günther, U.; Starobinsky, A.; Zhuk, A.
Multidimensional cosmological models: cosmological and astrophysical implications and constraints
Physical Review D 69 (2004) 044003

Günther, U.; Stefani, F.; Gerbeth, G.
The MHD α^2-dynamo, Z2-graded pseudo-Hermiticity, level crossings, and exceptional points of branching type
Czechoslovak Journal of Physics 54 (2004) 1075-1089

Hammer, R.; Bergner, F.; Flade, T.; Jurisch, M.; Kleinwechter, A.; Schaper, M.
Material related fundamentals of cutting techniques for GaAs wafer manufacturing
Zeitschrift für Metallkunde, accepted

Hampel, U.;Schleicher, E.; E.G. Wüstenberg, E.G.; Hüttenbrink, K.-B.
Optical measurement of nasal swellings
IEEE Trans. Biom. Eng. 2004, 51(9), 1673-1679.

Hampel, U.; Hoppe, D.; Diele, K.-H.; Fietz, J.; Höller, H.; Kernchen, R.; Prasser, H.-M.; Zippe, C.
Application of gamma tomography to the measurement of fluid distributions in a hydrodynamic coupling
Flow Measurement and Instrumentation, accepted

Hermann, R.; Filip, O.; Gerbeth, G.; Priede, J.; Schultz, L.
Microstructure evolution of Nd-Fe-B alloys in consideration of magnetohydrodynamics
Journal of Magnetism and Magnetic Materials, 272-276 (2004) Suppl. 1, p. 1855-1856

Hermann, R.; Behr, G.; Gerbeth, G.; Priede, J.; Uhlemann, H.-J.; Fischer, F.; Schultz, L.
Magnetic field controlled FZ-single crystal growth of intermetallic compounds
J. Cryst. Growth, in press

Hoppe, D.
Virtuelle tomografische Rekonstruktionsbilder infolge ungeeigneter Abtastraten
Technisches Messen 12/2004, 640-642

Hoppe, D.; Hampel, U.; Zippe, C.; Prasser, H.-M.; Kernchen, R.
Tomografische Rekonstruktion zweier asynchron rotierender Objekte am Beispiel einer hydrodynamischen Kupplung
Technisches Messen 12/2004, 634-639

Kliem, S.; Rohde, U.; Weiss, F.-P.
Core response of a PWR to a slug of under-borated water
Nuclear Engineering and Design, 230 (2004) 121-132

Kryk, H.; Schmitt, W.; Hessel, G.; Tefera, N.
Prozesskinetische Untersuchungen zur Modellierung reaktionsgetriebener Druckentlastungen
Chemie Ingenieur Technik 76, No. 9 (2004) 1312

Krepper, E.; Lucas, D.; Prasser, H.-M.
On the modelling of bubble flow in vertical pipes
Nuclear Engineering and Design, accepted

Kuechler, R.; Noack, K.; Zorn, T.
Investigation of gypsum dissolution under saturated and unsaturated water conditions
Ecological Modelling 176 (2004) 1-14

Langenbuch, S.; Krzykacz-Hausmann, B.; Schmidt, K.-D.; Hegyi, G.; Kereszturi, A.; Kliem, S.; Hadek, J.; Danilin, S.; Nikonov, S.; Kuchin, A.
Comprehensive uncertainty and sensitivity analysis for coupled code calculations of VVER plant transients
Nuclear Engineering and Design, accepted

Manera, A.; Rohde, U.; Prasser, H.-M.; van der Hagen, T. H. J. J.
Modeling of flashing-induced instabilities in the start-up phase of natural-circulation BWRs using the code FLOCAL
Nuclear Engineering and Design, accepted

Manera, A.; Prasser, H.-M.; van der Hagen, Tim H. J. J.
Suitability of drift-flux models, void-fraction evolution and 3D flow pattern visualization during stationary and transient flashing flow in a vertical pipe
Nuclear Technology, accepted

Maximov, V. V.; Anikeev, A. V.; Bagryansky, P. A.; Ivanov, A. A.; Lizunov, A. A.; Murakhtin, S. V.; Noack, K.; Prikhodko, V. V.
Spatial profiles of fusion product flux in the gas dynamic trap with deuterium neutral beam injection
Nuclear Fusion 44 (2004) 542-547

Mibus, J.; Lambarki, M.; Küchler, R.
Determination of effective diffusion parameters in compacted kaolinite
Geochim. Cosmochim. Acta 68 (2004) A165.

Mittag, S.; Grundmann, U.; Weiß, F.-P.; Petkov, P.T.; Kaloinen, E.; Keresztúri, A.; Panka, I.; Kuchin, A.; Ionov, V.; Powney, D.
Neutron-kinetic code validation against measurements in the Moscow V-1000 zero-power facility
Nuclear Engineering and Design, accepted

Plevachuk, Yu.; Sklyarchuk, V.; Yakymovich, A.; Willers, B.; Eckert, S.
Electronic properties and viscosity of liquid Pb-Sn alloys
Journal of Alloys and Compounds, in press

Prasser, H.-M.; Baranyai, G.; Böttger, A.; Ezsöl, G.; Guba, A.; Perneczky, L.; Toth, I.; Zschau, J.
Nitrogen transport in the primary circuit of a VVER during a LOCA occurring under plant cool-down Conditions
Kerntechnik 69 (2004) 4

Rohde, U.; Kliem, S.; Höhne, T.; Karlsson, R. et al.
Fluid mixing and flow distribution in the reactor circuit: Measurement data base
Nucl. Eng. Design, accepted in 2004 (invited paper)

Scheuerer, M.; Heitsch, M.; Menter, F.; Egorov, Y.; Toth, I.; Bestion, D.; Pigny, S.; Paillere, H.; Martin, A.; Boucker, M.; Krepper, E.; Willemsen, S.; Muhlbauer, P.; Andreani, M.; Smith, B.; Karlsson, R.; Henriksson, M.; Hemstrom, B.; Karppinen, I.; Kimber, G.
Evaluation of computational fluid dynamic methods for reactor safety analysis (ECORA)
Nuclear Engineering and Design, accepted

Shi, J.-M.; Breuer, M.; Durst, F.
A combined analytical-numerical method for treating corner singularities in viscous flow predictions
International Journal for Numerical Methods in Fluids, 45(2004) 659-688

Shi, J.-M.; Gerlach, D.; Breuer, M.; Biswas, G.; Durst, F.
Heating effect on steady and unsteady horizontal laminar flow of air past a circular cylinder
Physics of Fluids, 16 (2004) 4331

Stefani, F.; Gerbeth, G.
A contactless inductive velocity reconstruction method for metallic and semiconducting melts
Materials and Manufacturing Processes 19 (2004) 651 - 663

Stefani, F.; Gerbeth, G.; Gailitis, A.; Lielausis, O.; Platacis, E.
Dynamo experiments: where we stand and where we go
Geophysical Research Abstracts, Vol. 6 (2004), 02933

Stefani, F.; Gundrum, T.; Gerbeth, G.
Contactless inductive flow tomography
Physical Review E 70 (2004) 056306

Ulbricht, A.; Boehmert, J.
Small angle neutron scattering analysis of the radiation susceptibility of reactor pressure vessel steels
Physica B 350 (2004) E483-E486

Ulbricht, ; Boehmert, J.; Viehrig; H.-W.
Microstructural and mechanical characterization of the radiation effects in model reactor pressure vessel steels
Journal of ASTM International, accepted

Ulbricht, A.; Boehmert, J.; Uhlemann, M.; Müller, G.
Small-angle neutron scattering study on the effect of hydrogen in irradiated reactor pressure vessel steels
Journal of nuclear materials, accepted

Vanttola, T.; Hämäläinen, A.; Kliem, S.; Kozmenkov, Y.; Weiß, F.-P.; Kereszturi, A.; Hadek, J.; Strmensky, C.; Stefanova, S.; Kuchin, A.
Validation of coupled codes using VVER plant measurements
Nuclear Engineering and Design, accepted

Wangjiraniran, W.; Aritomi, M.; Kikura, H.; Motegi, Y.; Prasser, H.-M.
A study of non-symmetric air water flow using wire-mesh sensor
Experimental Thermal and Fluid Science, accepted

Weier, T.; Hueller, J.; Gerbeth, G.; Weiss, F.-P.
Lorentz force influence on momentum and mass transfer in natural convection copper electrolysis.
Chemical Engineering Science, accepted

Weier, T.; Gerbeth, G.
Control of separated flows by time periodic Lorentz forces
European Journal of Mechanics B/Fluids, Vol. 23, Nr. 6, 2004, S. 835-849

Willschütz, H.-G.
Simulation of scaled vessel failure experiments and investigation of a possible vessel support against failure
Nuclear Engineering and Design, 228 (2004) 401-414

Willschütz, H.-G.; Altstadt, E.; Weiss, F.-P.; Sehgal, B. R.
Insights from the FOREVER-programme and the accompanying finite element calculations
atw - International Journal for Nuclear Power 49. Jg. 2004 Heft 5, S. 345-349

Xu, M.; Stefani, F.; Gerbeth, G.
Integral equation approach to time-dependent kinematic dynamos in finite domains
Physical Review E 70 (2004)

Xu, M.; Stefani, F.; Gerbeth, G.
The integral equation method for a steady kinematic dynamo problem
Journal of Computational Physics 196 (2004) 102-125

Conference contributions and other oral presentations

Altstadt, E.; Beckert, C.; Freiesleben, H.; Galindo, V.; Grosse, E.; Junghans, A.; Naumann, B.; Weiss, F.-P.
Design of a photoneutron source for time-of-flight experiments at the radiation source ELBE
12th International Conference on Nuclear Engineering ICONE-12, Washington D.C., USA, April 25-29, 2004

Altstadt, E.; Willschuetz, H.-G.; Mueller, G.
FE-simulation of the viscoplastic behaviour of different RPV steels in the frame of in-vessel melt retention scenarios
MPA-Seminar, Stuttgart, October 05-07, 2004

Anikeev, A. V.; Bagryansky, P. A.; Collatz, S.; Noack, K.
Plasma simulations of the SHIP experiment at GDT
5th Int. Conference on Open Magnetic Systems for Plasma Confinement, Budker Institute of Nuclear Physics Novosibirsk, 05.07.2004, Novosibirsk, Russia

Bergner, F.
Scaling of self-similar long fatigue crack growth in aluminium alloys
International Conference on the Fundamentals of Plastic Deformation 'Dislocations 2004', La Colle-sur-Loup, France, September 13-17, 2004

Bergner, F.; Müller, G.; Ulbricht, A.; Ouytsel, K. van; Blank, C.; Bras, W.; Dewhurst, C.
Deformation-induced small-angle scattering contrast in aluminium alloys
4th Conference on Synchrotron Radiation in Materials Science (SRMS4), ESRF Grenoble, 23.08.2004-25.08.2004, Grenoble, France

Bergner, F.; Thieme, M.; Zouhar, G.; Franke, R.
Ermüdungsrissausbreitung in Aluminiumlegierungen – Datenbasis und Anwendungen im Rahmen des Damage-Toleranz-Konzeptes
Deutscher Luft- und Raumfahrtkongress, Dresden, 20.-23. September 2004

Boehmer, B.
Overview of the WWER-440 benchmark results
REDOS Progress Meeting, April 1-2, 2004, Budapest, Hungary

Boehmer, B.
Summary of the WWER-1000 benchmark results
REDOS Progress Meeting, April 1-2, 2004, Budapest, Hungary

Borodkin, G.; Boehmer, B.; Noack, K.; Khrennikov, N.
Creation and evaluation of the VVER-1000 Balakovo-3 ex-vessel dosimetry benchmark for the NEA SINBAD data base
ICRS-10 / RPS 2004 Conferences, Funchal, Madeira, May 9-14, 2004

Buchenau, D.; Eckert, S.; Witke, W.; Gerbeth, G.
Magnetic field control in aluminum investment casting and the problem of electromagnetic flow rate measurements
Int. Workshop on "The History of Magnetohydrodynamics", Coventry (UK), May 26-28, 2004

Cramer, A.; Eckert, S.; Galindo, V.; Gerbeth, G.
Applications of AC and DC magnetic fields in metallurgical or crystal growth processes
International Workshop on Materials Analysis and Processing in Magnetic Fields, National High Magnetic Field Laboratory, 17.-19.03.2004, Tallahassee, FL, USA

Cramer, A.; Eckert, S.; Galindo, V.; Gerbeth, G.
Magnetfeldgesteuerte Formfüllung
VDG-Seminar, Verein Deutscher Giessereifachleute, 12.-13.10.2004, Bad Dürkheim, Germany

Cramer, A.; Stefani, F.; Gundrum, Th.; Varshney, K.
Local velocity measurements in electromagnetically forced confined flows
Seminarreihe der Forschergruppe Magnetofluiddynamik, TU Ilmenau, 20.10.2004, Ilmenau, Germany

Cramer, A.; Varshney, K.; Gerbeth, G.
Investigation of the fluid flow driven by an alternating magnetic field with ultrasonic doppler velocimetry
International Symposium HES-04 Heating by Electromagnetic Sources, Padua (Italy), June 23-25, 2004

Cramer, A.; Varshney, K.; Gerbeth, G.
New possibilities for velocity measurements and model experiments in liquid metal processing
XXI International Congress of Theoretical and Applied Mechanics, 15-21 August 2004, Warsaw, Poland

Dudlik, A.; Schönfeld, S. B. H.; Hagemann, O.; Carl, H.; Prasser, H.-M.
Water hammer and condensation hammer scenarios in power plants using new measurement system
9th International Conference on Pressure Surges, Chester 2004, UK.

Dzugan, J.; Viehrig, H.-W.
Crack initiation determination for Charpy size 3-point bend specimens by ICFPD method
Fatigue and Fracture Mechanics, 20.-22.04.2004, Zinkovy, Tschechien

Eckert, S.; Galindo, V.; Gerbeth, G.; Witke, W.; Buchenau, D.; Gerke-Cantow, R.; Nicolai, H.-P.; Steinrücken, U.
Strömungskontrolle bei Formfüllung mittels Magnetfeldern
Deutscher Giessereitag 2004, Muenchen, 3./4. Juni 2004,

Eckert, S.; Galindo, V.; Gerbeth, G.; Witke, W.; Gerke-Cantow, R.; Nicolai, H.; Steinrücken, U.
Magnetic field control of the mould filling process of aluminium investment casting
Sino-German Workshop on EPM, Shanghai University, 11.10.2004-13.10.2004, Shanghai, China

Eckert, S.; Gerbeth, G.; Stefani, F.
New possibilities for velocity measurements in metallic melts
Sino-German Workshop on EPM, Shanghai University, 11.10.2004-13.10.2004, Shanghai, China

Eckert, S.; Willers, B.; Michel, U.; Zouhar, G.; Nikritjuk, Petr. A.; Eckert, K.
Directional solidification of Pb-Sn alloys affected by a rotating magnetic field
XXI International Congress of Theoretical and Applied Mechanics, 15-21 August 2004, Warsaw, Poland

Galindo, V.; Gerbeth, G.; Eckert, S.; Witke, W.; Gerke-Cantow, H.; Nicolai, H.; Steinrücken, U.
Magnetic field control of the mould filling process of aluminum investment casting
6th World Congress on Computational Mechanics, International Association for Computational Mechanics, 05.09.2004-10.09.2004, Peking, China

Gerbeth, G.
Flow control by tailored magnetic fields
Sino-German Workshop on EPM, Shanghai University, 11.10.2004-13.10.2004, Shanghai, China

Gerbeth, G.
Some metallurgical applications of magnetic fields. The role of model experiments and velocity measuring techniques.
Coventry University (UK), 12.01.2004

Gerbeth, G.; Eckert, S.; Cramer, A.; Stefani, F.
A review on velocity measurements in liquid metals
Workshop: "MHD Couette Flows: Experiments and simulations", Catania (Italy), 29.02.-02.03.2004

Gerbeth, G.; Weier, T.; Shatrov, V.; Mutschke, G.
Electromagnetic seawater flow control - from old ideas to recent results
Int. Workshop on "The History of Magnetohydrodynamics", Coventry (UK), May 26-28, 2004

Grants, I.; Gerbeth, G.
Nonlinear transition of a flow driven by a rotating magnetic field
XXI International Congress of Theoretical and Applied Mechanics, 15 - 21 August 2004,Warsaw (Poland)

Grants, I.; Gerbeth, G.
Non-normal nonlinear transition to turbulence in a magnetically driven swirling flow
10th European Turbulence Conference, Trondheim (Norway), June 29-July 2, 2004

Grundmann, U.; Mittag, S.
DYN3D calculations compared to the measurements in the V-1000 test facility
Annual meeting on nuclear technology 2004, May, 25-27, Düsseldorf, Germany

Grundmann, U.; Mittag, S.
DYN3D calculations for the V-1000 test facility and comparisons with the measurements
PHYSOR-2004 - The Physics of Fuel Cycles and Advanced Nuclear Systems: Global Developments, American Nuclear Society, 25.-29.04.2004, Chicago, USA

Günther, U.; Stefani, F.; Gerbeth, G.
The MHD α^2–dynamo: operator pencil, pseudo-Hermiticity, level crossings, spectral phase transitions
Talk at the 2nd International Workshop "Pseudo-Hermitian Hamiltonians in Quantum Physics II", Prague, Czech Republic, June 14-16, 2004.

Hammer, R.; Kleinwechter, A.; Jurisch, M.; Schaper, M.; Bergner, F.
High-efficient wire sawing of GaAs-wafers by utilization of crack nucleation mechanisms
19th Annual Meeting of the American Society of Precision Engineering (ASPE), Orlando, Florida, October 24-29, 2004

U. Hampel
X-ray computed tomography for experimental investigations of multi-phase flows
Multi-phase Flow: Simulation, Experiment and Applications, ANSYS-CFX / FZR workshop, 28.-30.06.2004, Dresden

Hampel, R.; Kästner, W.; Alt, S.; Seeliger, A.; Krepper, E.; Grahn, A.
Experimental and numerical investigations for fragmentation and insulation particle transport phenomena in water flow
5th International Conference on Multiphase Flow, Yokohama, Japan, May 30–June 4, 2004, Paper No. 555

Hermann, R.; Behr, G.; Gerbeth, G.; Priede, J.; Uhlemann, H.-J.; Fischer, F.; Schultz, L.
Magnetic field controlled FZ single crystal growth of intermetallic compounds
14th "International Conference on Crystal Growth", 9-13 August 2004, Grenoble - France

Hermann, R.; Filip, O.; Gerbeth, G.; Priede, J.; Shatrov, V.
Magnetic field controlled solidification of Nd-Fe-B melts
High performance magnets and their applications, Annecy (France), 29.8.-2.9.2004

Hessel, G.; Hilpert, R.; Kryk, H.; Roth, M.; Schmitt, W.; Weiss, F.-P.
Operational experiences in monitoring of semi-batch hydrogenation using adaptive heat and mass balances
Symposium on knowledge Driven Batch Processes (BATCHPRO), Poros, Greece, June 6-9, 2004

Hiller, W.; Rindelhardt, U.; Voigtländer, I.
Grid connected PV systems in Saxony: a ten years review
EuroSun 2004, Freiburg, 20-23 June 2004

Höhne, T.
Numerical simulation of coolant mixing at the ROCOM test facility with CFX-4 and CFX-5 based on complex meshes
NAFEMS Seminar: „Simulation of Complex Flows (CFD) – Application and Trends“, May 3 - 4, 2004, Niedernhausen/Wiesbaden, Germany

Höhne, T.; Bezrukov, Y.; Kabanova, L.
CFD-simulation of a boron dilution transient during start-up of the coolant pump in the 1:5 scaled VVER-1000 reactor model
14th SYMPOSIUM of AER on VVER Reactor Physics and Reactor Safety, Espoo, Finland, 13-17 September 2004

Höhne, T.; Bieder, U.
Analysis of buoyancy driven coolant mixing by using the code TRIO_U
Annual meeting on nuclear technology 2004, May, 25-27, Düsseldorf, Germany

Höhne, T.; Bieder, U.; Prasser, H.-M.; Kliem, S.
Validation of TRIO_U – numerical simulations of a ROCOM buoyancy driven test case
12th International Conference on Nuclear Engineering, Washington D.C., USA, April 25-29 2004

Höhne, T.; Kliem, S.; Rohde, U.
Numerical simulation of coolant mixing at the ROCOM test facility with CFX-5
22nd CAD-FEM Users' Meeting 2004, International Congress on FEM Technology with ANSYS CFX & ICEM CFD, CAD-FEM, 12.11.2004, Dresden, Deutschland

Hüller, J.; Weier, T.; Gerbeth, G.
Electrochemical activities in the Rossendorf MHD group
COST F2 Symposium "Electrochemical Flow Measurements and Microfluidics", Poitiers, France, 1 – 3 July 2004

Kliem, S.; Höhne, T.; Prasser, H.-M.; Rohde, U.; Weiß, F.-P.
Experimental investigation of coolant mixing in the RPV of a PWR during natural circulation conditions
12th International Conference on Nuclear Engineering ICONE-12, Washington D.C., USA, April 25-29, 2004

Kliem, S.; Mittag, S.; Langenbuch, S.
Uncertainty and sensitivity analysis of a VVER-1000 start-up experiment using the coupled code DYN3D/ATHLET and the statistical code package SUSA
14. AER Symposium, Helsinki, Finnland, 13.-17.09.2004

Koch, R.
Applications of code HELIOS at Research Center Rossendorf and some remarks to formal innovations of the code
Core/Fuel Management Software, European Users Group Meeting 2004, 19.-21.04.2004, Turku, Finland

Koch, R.; Křepel, J.; Grundmann, U.; Rohde, U.
Studies and codes on molten salt reactors
Technical Meeting of the Co-ordinated Research Project on " Incineration of Radioactive Waste", IAEA and Institute of Plasma Physics, Chinese Academy of Sciences, 22.-26.11.04, Hefei, China

Konheiser, J.
Results of TRAMO-calculations of WWER-440 mock-up experiments in the LR-0 reactor
REDOS Progress Meeting, April 1-2 2004 Budapest, Hungary

Krepel, J.; Grundmann, U.; Rohde, U.
Analysis of MSR benchmark by using the code DYN1D-MSR
Annual meeting on nuclear technology 2004, May, 25-27, Düsseldorf, Germany

Krepel, J.; Grundmann, U.; Rohde, U.
Develoment and verification of dynamics code for molten salt reactors
ICONE 12 - 12th International Conference on Nuclear Engineering, ASME, 25.04.2004-29.04.2004, Arlington, Virginia, USA

Krepper, E.
CFD modelling of subcooled boiling
Annual meeting on nuclear technology 2004, May, 25-27, Düsseldorf, Germany

Krepper, E.; Grahn, A.
Numerical investigations of insulation debris transport phenomena in water flow
OECD Workshop on Debris Impact on Emergency Coolant Recirculation, Albuquerque, NM (USA), 25-27 February 2004

Krepper, E.; Lucas, D.; Prasser, H.-M.; Shi, J.-M.; Rohde, U.
Two-phase flow simulations in the FZ Rossendorf using CFX-5
22nd CAD-FEM User's Meeting 2004 and ANSYS CFX & ICEM CFD Conference, Dresden, 10.-12.11.2004

Krepper, E.; Reddy Vanga, B. N.; Prasser, H.-M.; Lopez de Bertodano, M.
Experimental and numerical studies of void fraction distribution in rectangular bubble columns
3rd International Symposium on Two-Phase Flow Modelling and Experimentation Pisa, 22-24 September 2004

Kryk, H.; Schmitt, W.; Hessel, G.; Tefera, N.
Experimentelle Untersuchungen zur reaktionsgetriebenen Druckentlastung
7. Fachtagung "Anlagen-, Arbeits- und Umweltsicherheit" Köthen, 04./05. November 2004

Lantzsch, R.; Galindo, V.; Gerbeth, G.; Cröll, A.
Design of a travelling magnetic field for vertical gradient freeze - crystal growth
Workshop „Angewandte Simulation in der Kristallzüchtung“, Volkach, Febr. 5-6, 2004

Lucas, D.; Krepper, E.; Prasser, H.-M.
Validation of models for bubble forces
42nd European Two-Phase Flow Group Meeting, Genova, 23-25 June 2004

Lucas, D.; Prasser, H.-M.
Scaling effects in vertical bubbly pipe flow
5th International Conference on Multiphase Flow, ICMF’04, Yokohama, Japan, May 30–June 4, 2004

Lucas, D.; Shi, J.-M.; Krepper, E.; Prasser, H.-M.
Models for the forces acting on bubbles in comparison with experimental data for vertical pipe flow
3rd International Symposium on Two-Phase Flow Modelling and Experimentation, Pisa, Italy, September 22-24, 2004

Manera, A.
Stability analysis of natural circulation BWRs at low pressure using the codes FLOCAL and ATHLET
BWR Owners’ Group Global Technical Exchange Conference – BWR Stability-, General Electric Company, 05.05.2004, Valencia, Spain

Manera, A.; Zaruba, A.
Experimental investigations on bubble turbulent diffusion in a vertical large diameter pipe and in a rectangular bubble column by means of different measurement techniques
Multi-phase Flow: Simulation, Experiment and Applications, ANSYS-CFX / FZR workshop, ANSYS-CFX, FZR, 28.06.2004-30.06.2004, Dresden, Germany

Mibus, J.; Lambarki, M.; Küchler, R.
Determination of effective diffusion parameters in compacted kaolinite
Goldschmidt Conference 2004, Copenhagen

Misawa, M.; Suzuki, A.; Morikawa, Y.; Minato, A.; Prasser, H.-M.
Nonlinear charakteristics of gas-liquid two-phase flow and verification of extended two-fluid model
5th International Conference on Multiphase Flow, ICMF'04, Yokohama, Japan, May 30-June 4, 2004

Noack, K.; Pyka, N.; Rogov, A.; Steichele, E.
Shielding design of the panda spectrometer at the munich high-flux reactor frm-ii
International Conferences ICRS-10/RPS 2004,Funchal, Madeira Island (Portugal), May 9-14, 2004

Potapov, S.; Altstadt, E.
Coupled fluid-structure analysis with EUROPLEXUS fast dynamics software of the CWHTF experiment
6th International Conference on Nuclear Thermal Hydraulics, Operations and Safety (NUTHOS-6), Nara, Japan, October 4-8, 2004

Prasser, H.-M.
Influence of the gas injection on the void fraction profiles and bubble size distributions of a air-water flow in vertical pipes
5th International Conference on Multiphase Flow, ICMF'04, Yokohama, Japan, May 30–June 4, 2004

Prasser, H.-M.
Measurement techniques for multiphase flows
Multi-phase Flow: Simulation, Experiment and Applications, ANSYS-CFX / FZR workshop, 28-30 June, 2004, Dresden, Lecture on Short Course on Multiphase Flows

Prasser, H.-M.
NuclearReactor - Reaktorphysik populär im Internet - ein Versuch, den Internetauftritt der KTG attraktiver zu machen
Annual meeting on nuclear technology 2004, May, 25-27, Düsseldorf, Germany

Prasser, H.-M.; Krepper, E.
Air-water flow in a vertical pipe with sudden changes of the superficial water velocity
3rd International Symposium on Two-Phase Flow Modelling and Experimentation, Pisa, 22-24 September 2004

Prasser, H.-M.
Wire-mesh sensors: an experimental tool for two-phase CFD model development and code validation
Advances in the Modeling Methodologies of Two-Phase Flows, Lyons, France, November 24-26, 2004

Prasser, H.-M.
Kernkraft - eine Energiequelle der Zukunft - auch für Deutschland
Vortrag, Industrieclub Sachsen, Schloss Eckberg, Dresden, 5. Oktober 2004

Prasser, H.-M.
Irrtümer über Kernenergie
Vortrag, VDI Bezirksverein Frankfurt-Darmstadt, Darmstadt, 19. November 2004

Prasser, H.-M.
Wire-mesh sensors and tomography methods developed by FZR
Darmstadt University of Technology, Institute of Energy and Poswer Plant Technology, Seminar, Darmstadt, November 29, 2004.

Prasser, H.-M.
Gamma and x-ray tomography for transient two-phase flows and other instrumentation developed by rossendorf
Advances in the Modeling Methodologies of Two-Phase Flows, Lyons, France, November 24-26, 2004

Prasser, H.-M.; Beyer, M.; Böttger, A.; Carl, H.; Lucas, D.; Schaffrath, A.; Schütz, P.; Weiss, F.-P.; Zschau, J.
TOPFLOW tests on the structure of the gas-liquid interface in a large vertical pipe
Annual meeting on nuclear technology 2004, May, 25-27, Düsseldorf, Germany

Priede, J.; Gerbeth, G.
Stabilization effect of a rotating magnetic field on the flow of a conducting liquid in a cylindrical container
Int. Conference on Computational & Experimental Engineering and Sciences, Madeira (Portugal), July 26-29, 2004

Priede, J.; Gerbeth, G.; Shatrov, V.; Gelfgat, Yu.
Electromagnetic levitation: global instabilities and the flow inside a molten sample
Sino-German Workshop on EPM, Shanghai University, 11.10.2004-13.10.2004, Shanghai, China

Rindelhardt, U.
Erneuerbare Energien: Das Beispiel Windenergie
Antrittsvorlesung, TU Chemnitz, 04.05.2004

Rindelhardt, U.; Futterschneider, H.
Performance of differently oriented PV modules - results of a long time measuring program
19th European Photovoltaic Solar Energy Conference and Exhibition, Paris, France 7-11 June 2004

Rindelhardt, U.; Weiss, F.-P.
Recent developments in the field of nuclear safety research
CO-MAT-TECH 2004, Trnava (Slovakia) 14.-15. October 2004: 12th International Scientific Conference, Slovak University of Technology Bratislava

Schäfer, F.; Manera, A.
Investigation of flashing-induced instabilities at the CIRCUS test facility using the code ATHLET
29th International Meeting on Reactor Noise, Budapest, 17-19 May 2004

Sehgal, B. R.; Willschuetz, H.-G.
PWR vessel failure experiments & analysis
PHARE-Seminar Bulgaria BG 01.10.01 13-17/09/2004

Shatrov, V.; Gerbeth, G.
Magnetohydrodynamic drag reduction and efficiency
International Workshop "Flow Control by Tailored Magnetic Fields", 01.-02.04.2004, Dresden, Germany

Shi, J.-M.; Frank, T.; Krepper, E.; Lucas, D.; Rohde, U.; Prasser, H.-M.
Implementation and validation of non-drag interfacial forces in CFX-5.6
5th International Conference on Multiphase Flow, ICMF04, ASME,JSME, 30.05.-04.06.2004, Yokohama, Japan

Shi, J.-M.; Frank, T.; Burns, A.
Turbulent dispersion force - physics, model derivation and evaluation
FZR-ANSYS CFX Workshop on Multiphase Flow, FZR, ANSYS CFX, 29.-30.06.2004, Dresden, Germany

Shi, J.-M.; Frank, T.; Rohde, U.; Prasser, H.-M.
Nx1 MUSIG model -- implementation and application to gas-liquid flows in a vertical pipe
22nd CAD-FEM User Meeting 2004 and CFX & ICEM CFD Conference, Nov. 10-12, 2004, Dresden, Germany, ANSYS, 12.11.04, Dresden, Germany

Speck, M., Wolter, K.-J., Danczak, M., Daniel, D.
Application of computer tomography in microelectronic packaging
9th International Symposium on NDE for Health Monitoring and Diagnostics, San Diego, USA, 15-17 March 2004

Stefani, F.
Hydromagnetic dynamo experiments
Seminarvortrag, TU Delft, 20.Oktober 2004

Stefani, F.
Theorien und Experimente zum hydromagnetischen Dynamoeffekt
Physikalisches Kolloquium, BTU Cottbus, 13. Januar 2004

Stefani, F.; Gerbeth, G.
Magnetorotational instability in Taylor-Dean flows
Workshop: MHD Couette flows: experiments and models, 29 February - 2 March 2004, Acitrezza, Catania, ITALY

Stefani, F.; Gerbeth, G.; Gailitis, A.; Lielausis, O.; Platacis, E.
Dynamo experiments: where we stand and where we go
European Geosciences Union, 1st General Assembly, European Geosciences Union, 25.04.2004-30.04.2004, Nice, France

Stefani, F.; Gerbeth, G.; Gailitis, A.; Lielausis, O.; Platacis, E.
Laboratory astrophysics as examplified by the Riga dynamo experiment
Workshop: MHD Couette flows: experiments and models, 29 February - 2 March 2004, Acitrezza, Catania, ITALY

Stefani, F.; Gerbeth, G.; Gundrum, T.
Contactless inductive flow tomography: theory and experiment
XXI International Congress of Theoretical and Applied Mechanics, 15-21 August 2004, Warsaw, Poland

Stefani, F.; Gerbeth, G.; Gundrum, T.; Xu, M.
Inferring flows from magnetic field constraints
International Workshop on "Flow Control by Tailored Magnetic Fields (FLOWCOMAG)", Dresden, April 1 - 2, 2004

Stefani, F.; Gerbeth, G.; Günther, U.; Gundrum, T.; Xu, M.
Inverse problems in magnetohydrodynamics: theoretical and experimental aspects
Inverse Problems, Design and Optimization Symposium, March 17-19, 2004, Rio de Janeiro, Brazil

Stefani, F.; Xu, M.; Gundrum, T.; Gerbeth, G.
The integral equation approach to kinematic dynamos in finite domains
Joint meeting of COST-P6-Working Group 1 and CNRS-GDR "Dynamo" 22-23 January 2004, Observatoire de Paris

Stiller, J.; Cramer, A.; Frana, K.; Varshney, K.
Stirring with rotating magnetic fields: numerical and experimental results
International Workshop on Flow Control by Tailored Magnetic Fields (FLOWCOMAG), 01.04.2004-02.04.2004, Dresden, Germany

Stiller, J.; Frana, K.; Grundmann, R.; Cramer, A.; Varshney, K.; Gerbeth, G.
Numerical and experimental studies on electomagnetic stirring
Sino-German Workshop on EPM, Shanghai University, 11.10.2004-13.10.2004, Shanghai, China

Thieme, M.; Bergner, F.; Haase, I.; Worch, H.
Comparative investigations to corrosion fatigue of Al-Cu and Al-Mg-Si alloys
4th Kurt Schwabe Corrosion Symposium "Mechanisms of Corrosion and Corrosion Preventio"', Espoo, Helsinki University of Technology, June 13-17, 2004

Ulbricht, A.; Bergner, F.
Detecting irradiation induced damage in RPV steels by SANS
30th MPA-Seminar in conjunction with 9th German-Japanese Seminar, MPA Stuttgart, October 6-7, 2004

Ulbricht, A.; Bergner, F.
SANS-Untersuchungen zur Charakterisierung von Strahlendefekten in RDB-Stählen nach Bestrahlung, Ausheilung und Wiederbestrahlung
Deutsche Neutronenstreutagung, 1.-3. September 2004, Dresden

Ulbricht, A.; Boehmert, J.; Viehrig, H.-W.
Microstructural and mechanical characterization of the radiation effects in model reactor pressure vessel steels
22 ASTM Symposium on Effects of Radiation on Materials, 8-10 June 2004, Boston, Massachusetts, USA

Ulbricht, A.; Böhmert, J.
Characterization of radiation effects in reactor pressure vessel steels by means of small angle neutron scattering
Annual meeting on nuclear technology 2004, May, 25-27, Düsseldorf, Germany

Vallée, C.; Sühnel, T.
Experiments and CFX-5 calculation of the stratified flow in a horizontal channel (Part 2: Measurements)
Joint FZR & ANSYS Multiphase Flow Workshop: Simulation, Experiment and Applications, ANSYS-CFX / FZR, 28.06.2004-30.06.2004, Dresden, Germany

Vanga, B. N. R.; Krepper, E.; Zaruba, A.; Prasser, H.-M.; de Bertodano, L.
On the hydrodynamics of bubble columns: comparison of experimental measurements with computational fluid dynamics calculations
5th International Conference on Multiphase Flow, ICMF 04, Yokohama, Japan, May 30 June 4, 2004. Paper 264

Varshney, K.; Cramer, A.; Gerbeth, G.
New possibilities for velocity measurements in liquid metals by potential probes
Int. Workshop on "The History of Magnetohydrodynamics", Coventry (UK), May 26-28, 2004

Viehrig, H.-W.; Planman, T.; Server, W. L.
Results and conclusions from fracture toughness tests in IAEA CRP-5
IAEA Specialists meeting " Irradiation effects and mitigation in Reactor Pressure Vessel, IAEA, 28.05.2004, Gus Khrustalny, Russia

Weier, T.; Albrecht, T.; Mutschke, G.; Gerbeth, G.
Seawater flow transition and separation control
International Workshop on "Flow Control by Tailored Magnetic Fields (FLOWCOMAG)" Dresden, April 1 - 2, 2004

Weier, T.; Gerbeth, G.; Mutschke, G.
Separation control by stationary and time periodic Lorentz forces
XXI International Congress of Theoretical and Applied Mechanics, 15 - 21 August 2004, Warsaw, Poland

Weier, T.; Mutschke, G.; Gerbeth, G.
Electromagnetic control of flow separation by stationary and time periodic forces
13th European Drag Reduction Meeting, Aussois, France, 14 June 2004

Weiß, F.-P.
Aktuelle Entwicklungen auf dem Gebiet der nuklearen Sicherheitsforschung
Kolloquium: Kompetenz zur Kerntechnik in Lehre und Forschung, Zittau, 25./26.06.2004 eingeladener Vortrag

Weiß, F.-P.
Boron-dilution transients in PWRs
29. Fachsitzung der Internationalen Länderkommision Kerntechnik, 24. Mai 2004, Stuttgart

Weiß, F.-P.
Recents developments in nuclear safety research
Conference on Multi-Phase Flow: Simulation Experiment and Application, Dresden, 28-30 June 2004

Willers, B.; Eckert, S.; Michel, U.; Haase, I.; Zouhar, G.; Nikritjuk, P. A.; Eckert, K.
Application of RMF during solidification and its influence on the microstructure of solidified PbSn Alloys
International Workshop on Flow Control by Tailored Magnetic Fields (FLOWCOMAG), 01.04.2004-02.04.2004, Dresden, Germany

Willschütz, H.-G.; Altstadt, E.
Application of several physics environments for a coupled simulation of pressure vessel creep failure experiments
22nd CAD-FEM Users Meeting 2004, International Congress on FEM Technology with ANSYS CFX & ICEM CFD, CAD-FEM GmbH, ANSYS Germany, 10.11.2004-12.11.2004, Dresden, Deutschland

Willschütz, H.-G.; Altstadt, E.; Mueller, G.; Boehmert, J.; Sehgal, B. R.
Metallographical and numerical investigation of the EC-FOREVER-4 test
International Congress on Advances in Nuclear Power Plants (ICAPP '04), June 13-17, 2004, Pittsburgh, PA, USA

Willschütz, H.-G.; Müller, G.; Altstadt, E.
Discussion of the behaviour of different rpv-steels in vessel creep failure experiments
Annual meeting on nuclear technology 2004, May, 25-27, Düsseldorf, Germany

Xu, M.; Stefani, F.; Gerbeth, G.
Time-Dependent kinematic dynamos in finite cylinders as treated with the integral equation approach
7th MHD-Days, TU Ilmenau, September 20 and 21, 2004

Zaruba, A.; Krepper, E.; Prasser, H.-M.; Schleicher, E.
Measurement of bubble velocity profiles and turbulent diffusion coefficients of the gaseous phase in rectangular bubble column using image processing
3rd International Symposium on Two-Phase Flow Modelling and Experimentation, Pisa, 22-24 September 2004

Zhang, C.; Eckert, S.; Gerbeth, G.
Gas and liquid velocity measurements in bubble chain driven two-phase flow by means of UDV and LDA
5th ICMF, Yokohama, Japan, May 30 - June 4, 2004

Zhang, Ch.; Eckert, S.; Gerbeth, G.
Experiments on the magnetic field influence on liquid metal two-phase flows
Sino-German Workshop on EPM, Shanghai University, 11.10.2004-13.10.2004, Shanghai, China

Zippe, C.; Hoppe, D.; Fietz, J.; Hampel, U.; Hensel, F.; Mäding, P.; Prasser, H.-M.; Zippe, W.
Berührungslose Messung von Phasen- und Konzentrationsverteilungen in Blasensäulen mit positronenemittierenden Radionukliden
2. DECHEMA/GVC VDI-Symposium "Schäume - Grundlagen und Anwendungen", 16.-17.11.2004, Baden-Baden

Contributions to proceedings and other collected editions

Altstadt, E.; Beckert, C.; Freiesleben, H.; Galindo, V.; Grosse, E.; Junghans, A.; Naumann, B.; Weiss, F.-P.
Design of a photoneutron source for time-of-flight experiments at the radiation source ELBE
12th International Conference on Nuclear Engineering ICONE-12, Washington D.C., USA, April 25-29, 2004, Proceedings on CD-ROM paper 49456

Altstadt, E.; Willschuetz, H.-G.; Mueller, G.
FE-simulation of the viscoplastic behaviour of different RPV steels in the frame of in-vessel melt retention scenarios
MPA-Seminar, Stuttgart, October 05-07, 2004, Proceedings pp. 33.1-33.12

Bergner, F.; Thieme, M.; Zouhar, G.; Franke, R.
Ermüdungsrissausbreitung in Aluminiumlegierungen – Datenbasis und Anwendungen im Rahmen des Damage-Toleranz-Konzeptes
Jahrbuch 2004 der Deutschen Gesellschaft für Luft- und Raumfahrt, ISSN 0070-4083, Bonn: DGLR, 2004, S. 81-90.

Burns, A. D.; Frank, T.; Hamill, I.; Shi, J.-M.
The Favre averaged drag model for turbulent dispersion in eulerian multi-phase flows
5th International Conference on Multiphase Flow, ICMF 04, Yokohama, Japan, May 30 June 4, 2004, JSME, ASME, 30.05.-04.06.04, Yokohama, Japan
ICMF2004 Proceedings CD-ROM, paper No. 392, p. 1-17

Cramer, A.; Varshney, K.; Gerbeth, G.
Investigation of the fluid flow driven by an alternating magnetic field with ultrasonic doppler velocimetry
Int. Symposium on Heating by Electromagnetic Sources (ISBN 88-86281-92-7), University of Padua, 23.06.2004-25.06.2004, Padua, Italien, p. 413-420

Dudlik, A.; Schönfeld, S. B. H.; Hagemann, O.; Carl, H.; Prasser, H.-M.
Water hammer and condensation hammer scenarios in power plants using new measurement system
9th International Conference on Pressure Surges, Chester 2004, UK, v. 24. - 26.03.2004, proceedings part I, p. 151 - 165.

Frank, T.; Shi, J.-M.; Burns, A.
Validation of Eulerian Multiphase Flow Models for nuclear safety applications
3rd International Symposium on Two-Phase Flow Modeling and Experimentation, PISA, 22-24 Sept., 2004, ISME,ASME, 22.-24.09.04, Pisa, Italy
Conference Proceedings CD-ROM, p. 1-9

Gailitis, A.; Lielausis, O.; Platacis, E.; Stefani, F.; Gerbeth, G.
Laboratory astrophysics as exemplified by the Riga dynamo experiment
MHD Couette Flows: Experiments and Models, AIP Conference Proceedings Volume 733, 35-44

Galindo, V.; Gerbeth, G.; Eckert, S.; Witke, W.; Gerke-Cantow, H.; Nicolai, H.; Steinrücken, U.
Magnetic field control of the mould filling process of aluminum investment casting
Computational Mechanics, WCCM VI in conjunction with APCOM`04, Sept. 5-10, 2004, Beijing (China), paper No. 677, Tsinghua University Press & Springer-Verlag

Grants, I.; Gerbeth, G.
Non-normal nonlinear transition to turbulence in a magnetically driven swirling flow
10th European Turbulence Conference, Trondheim (Norway), June 29-July 2, 2004; H.I. Andersson, P.-A. Krogstad (Eds.): Advances in Turbulence X, 161-164

Grundmann, U.; Mittag, S.
DYN3D calculations compared to the measurements in the V-1000 test facility
Annual meeting on nuclear technology 2004, May, 25-27, Düsseldorf, Germany, CD-ROM, p. 17-20.

Grundmann, U.; Mittag, S.
DYN3D calculations for the V-1000 test facility and comparisons with the measurements
PHYSOR-2004 - The Physics of Fuel Cycles and Advanced Nuclear Systems: Global Developments, American Nuclear Society, 25.-29.04.2004, Chicago, USA
Proceedings of PHYSOR-2004, La Grange Park, Illinois 60526 (USA): American Nuclear Society, Inc., 0-89448-683-7

Hammer, R.; Kleinwaechter, A.; Jurisch, M.; Schaper, M.; Bergner, F.
High-efficient wire sawing of GaAs-wafers by utilization of crack nucleation mechanisms
Proceedings of the 19th Annual Meeting of the American Society of Precision Engineering (ASPE), Orlando, Florida, October 24-29, ASPE, 2004

Hampel, R.; Kästner, W.; Alt, S.; Seeliger, A.; Krepper, E.; Grahn, A.
Experimental and numerical investigations for fragmentation and insulation particle transport phenomena in water flow
5th International Conference on Multiphase Flow, Yokohama, Japan, May 30–June 4, 2004, Paper No. 555

Hermann, R.; Gerbeth, G.; Filip, O.; Priede, J.; Shatrov, V.
Effect of hydrodynamics on microstructure evolution of Nd-Fe-B alloys
in: *Solidification and Crystallization, edited by Dieter M. Herlach: WILEY-VCH Verlag, 2004, 3-527-31011-8, p. 185-193*

Hessel, G.; Hilpert, R.; Kryk, H.; Roth, M.; Schmitt, W.; Weiss, F.-P.
Operational experiences in monitoring of semi-batch hydrogenation using adaptive heat and mass balances
Symposium on knowledge Driven Batch Processes (BATCHPRO), Poros, Greece, June 6-9, 2004, Proceedings CD-ROM

Hiller, W.; Rindelhardt, U.; Voigtländer, I.
Grid connected PV systems in Saxony: a ten years review
EuroSun 2004, Freiburg, 20-23 June 2004, Proceedings volume 3, p. 401-407

Höhne, T.
Numerical simulation of coolant mixing at the ROCOM test facility with CFX-4 and CFX-5 based on complex meshes
NAFEMS Seminar: „Simulation of Complex Flows (CFD) – Application and Trends“, May 3 - 4, 2004, Niedernhausen/Wiesbaden, Germany, Proceedings p. 24

Höhne, T.; Bezrukov, Y.; Kabanova, L.
CFD-simulation of a boron dilution transient during start-up of the coolant pump in the 1:5 scaled VVER-1000 reactor model
14th SYMPOSIUM of AER on VVER Reactor Physics and Reactor Safety, Espoo, Finland, 13-17 September 2004, Proceedings p.581

Höhne, T.; Bieder, U.
Analysis of buoyancy driven coolant mixing by using the code TRIO_U
Annual meeting on nuclear technology 2004, May, 25-27, Düsseldorf, Germany, CD-ROM

Höhne, T.; Bieder, U.; Prasser, H.-M.; Kliem, S.
Validation of TRIO_U – numerical simulations of a ROCOM buoyancy driven test case
12th International Conference on Nuclear Engineering, Washington D.C., USA, April 25-29 2004, Book of Abstracts, p. 278

Höhne, T.; Kliem, S.; Rohde, U.
Numerical simulation of coolant mixing at the ROCOM test facility with CFX-5
22nd CAD-FEM Users' Meeting 2004, International Congress on FEM Technology with ANSYS CFX & ICEM CFD, November 10-12, 2004, Dresden, Germany, Conference Proceedings 2.6.26

Kliem, S.; Höhne, T.; Prasser, H.-M.; Rohde, U.; Weiß, F.-P.
Experimental investigation of coolant mixing in the RPV of a PWR during natural circulation conditions
12th International Conference on Nuclear Engineering ICONE-12, Washington D.C., USA, April 25-29, 2004, Proc. CD-ROM paper 49424

Kliem, S.; Mittag, S.; Langenbuch, S.
Uncertainty and sensitivity analysis of a VVER-1000 start-up experiment using the coupled code DYN3D/ATHLET and the statistical code package SUSA
14. AER Symposium, Helsinki, Finnland, 13.-17.09.2004, Proceedings pp. 503-516

Končar, B.; Mavko, B.; Krepper, E.; Hassan, Y. A.
Two-phase boundary layer prediction in upward boiling flow
International Conference "Nuclear Energy for New Europe 2004", Portorož · Slovenia · September 6-9

Kozmenkov, Y.
Transient simulations in VVER-1000 – comparison between DYN3D-ATHLET and DYN3D-RELAP5
Annual Meeting on Nuclear Technology 2004, Düsseldorf, 25.-27. May 2004. Proc. CD-ROM paper 104.

Krepel, J.; Grundmann, U.; Rohde, U.
Analysis of MSR benchmark by using the code DYN1D-MSR
Annual Meeting on Nuclear Technology 2004, Düsseldorf, 25. - 27. May 2004, Paper No. 105

Krepel, J.; Grundmann, U.; Rohde, U.
Develoment and verification of dynamics code for molten salt reactors
ICONE 12 - 12th International Conference on Nuclear Engineering, ASME, 25.04.2004-29.04.2004, Arlington, Virginia, USA

Krepper, E.
CFD modelling of subcooled boiling
Annual meeting on nuclear technology 2004, May, 25-27, Düsseldorf, Germany, CD-ROM

Krepper, E.; Grahn, A.
Numerical investigations of insulation debris transport phenomena in water flow
Debris Impact on Emergency Coolant Recirculation, Workshop Proceedings, Albuquerque, NM (USA), 25-27 February 2004OECD 2004/ NEA No 5468, pp. 271-229

Krepper, E.; Lucas, D.; Prasser, H.-M.; Shi, J.-M.; Rohde, U.
Two-phase flow simulations in the FZ Rossendorf using CFX-5
22nd CAD-FEM User's Meeting 2004 and ANSYS CFX & ICEM CFD Conference, Dresden, 10.-12.11.2004

Krepper, E.; Reddy Vanga, B. N.; Prasser, H.-M.; Lopez de Bertodano, M.
Experimental and numerical studies of void fraction distribution in rectangular bubble columns
3rd International Symposium on Two-Phase Flow Modelling and Experimentation Pisa, 22-24 September 2004, Paper MS11

Kryk, H.
Ein Online-Zustandserkennungssystem für Batch-Reaktoren in der chemischen Industrie
P&A Kompendium 2005 / publish-industry Verlag GmbH, 2004

Kryk, H.; Schmitt, W.; Hessel, G.; Tefera, N.
Experimentelle Untersuchungen zur reaktionsgetriebenen Druckentlastung
7. Fachtagung "Anlagen-, Arbeits- und Umweltsicherheit" Köthen, 04./05. November 2004, Proceedings CD-ROM

Kuna, M.; Abendroth, M.
Identification and validation of ductile damage parameters by the small punch test
15th European Conference of Fracture (ECF 15), European Structural Integrity Society (ESIS), 11.-13.08.2004, Stockholm, Sweden

Lucas, D.; Krepper, E.; Prasser, H.-M.
Validation of models for bubble forces
42nd European Two-Phase Flow Group Meeting, Genova, 23-25 June 2004, Paper E1

Lucas, D.; Prasser, H.-M.
Scaling effects in vertical bubbly pipe flow
5th International Conference on Multiphase Flow, ICMF'04, Yokohama, Japan, May 30–June 4, 2004, Paper No. 187

Lucas, D.; Shi, J.-M.; Krepper, E.; Prasser, H.-M.
Models for the forces acting on bubbles in comparison with experimental data for vertical pipe flow
3rd International Symposium on Two-Phase Flow Modelling and Experimentation, Pisa, Italy, September 22-24, 2004, Paper ha04

Manera, A.; Prasser, H.-M.; Lucas, D.; Hagen, T. H. J. J. van der
Bubble size distributions and three dimensional flow pattern visualization in stationary and transient upward flashing flow
3rd International Symposium on Two-phase Flow and Experimentation, Pisa, 22-24, September 2004.

Misawa, M.; Suzuki, A.; Morikawa, Y.; Minato, A.; Prasser, H.-M.
Nonlinear charakteristics of gas-liquid two-phase flow and verification of extended two-fluid model
5th International Conference on Multiphase Flow, ICMF'04, Yokohama, Japan, May 30-June 4, 2004, Paper No. 213.

Ouytsel, K. van; Müller, G.
Development of a SAXS-Method to characterize the damage zone around a crack tip in metals
Austrian Small Angle X-ray Scattering (SAXS) Beamline at ELETTRA, Annual Report 2003, published 2004, 51-52

Potapov, S.; Altstadt, E.
Coupled fluid-structure analysis with EUROPLEXUS fast dynamics software of the CWHTF experiment
6th International Conference on Nuclear Thermal Hydraulics, Operations and Safety (NUTHOS-6), Nara, Japan, October 4-8, 2004

Prasser, H.-M.; Krepper, E.
Air-water flow in a vertical pipe with sudden changes of the superficial water velocity
3rd International Symposium on Two-Phase Flow Modelling and Experimentation, Pisa, 22-24 September 2004, proceedings on CD-ROM, paper ms14.

Prasser, H.-M.
Wire-mesh sensors: an experimental tool for two-phase CFD model development and code validation
Advances in the Modeling Methodologies of Two-Phase Flows, Lyons, France, November 24-26, 2004, proceedings on CD-ROM, paper 001.

Prasser, H.-M., Hampel, U.
Gamma and X-Ray tomography for transient two-phase flows and other instrumentation developed by Rossendorf
Advances in the Modeling Methodologies of Two-Phase Flows, Lyons, France, November 24-26, 2004, proceedings on CD-ROM, paper 002

Prasser, H.-M.
Influence of the gas injection on the void fraction profiles and bubble size distributions of a air-water flow in vertical pipes
5th International Conference on Multiphase Flow, ICMF'04, Yokohama, Japan, May 30–June 4, 2004, Paper No. 187

Prasser, H.-M.
NuclearReactor - Reaktorphysik populär im Internet - ein Versuch, den Internetauftritt der KTG attraktiver zu machen
Annual meeting on nuclear technology 2004, May, 25-27, Düsseldorf, Germany, CD-ROM, paper 1106, proceedings pp. 495-500.

Prasser, H.-M.; Beyer, M.; Böttger, A.; Carl, H.; Lucas, D.; Schaffrath, A.; Schütz, P.; Weiss, F.-P.; Zschau, J.
TOPFLOW tests on the structure of the gas-liquid interface in a large vertical pipe
Annual meeting on nuclear technology 2004, May, 25-27, Düsseldorf, Germany, CD-ROM, proceedings: pp. 69 - 74

Reddy, Vanga B. N.; Zaruba, A.; Prasser, H.-M.; Krepper, E.; Lopez, de Bertodano M. A.
Wire-mesh tomography measurements of void fraction in rectangular bubble columns
2004 International Congress on Advances in Nuclear Power Plants (ICAPP '04), American Nuclear Society (ANS), 13.-17.06.2004, Pittsburgh, USA

Rindelhardt, U.; Futterschneider, H.
Performance of differently orientated PV modules - results of a long time measuring program
Proc. 19th European Photovoltaic Solar Energy Conference and Exhibition, Paris, 7-11 June 2004, p.3149

Schäfer, F.; Manera, A.
Investigation of flashing-induced instabilities at the CIRCUS test facility using the code ATHLET
29th International Meeting on Reactor Noise, Budapest, 17-19 May 2004, published on CD-ROM

Schmitt, W.; Hessel, G.; Kryk, H.
Betriebserfahrungen beim Online-Monitoring exothermer chemischer Prozesse mit adaptiven Stoff- und Wärmebilanzen
Fortschritte in Wissenschaft und industrieller Herstellung von Backhefe, Herausgeber: Versuchsanstalt der Hefeindustrie e.V. (2004) S. 87-96

Shi, J.-M.; Frank, T.; Krepper, E.; Lucas, D.; Rohde, U.; Prasser, H.-M.
Implementation and validation of non-drag interfacial forces in CFX-5.6
5th International Conference on Multiphase Flow, ICMF04, Yokohama, Japan, May 30-June 04, 2004, ASME,JSME, 30.05.-04.06.2004, Yokohama, Japan
ICMF2004 Proceedings CD-ROM, paper No. 400, p. 1-14

Speck, M., Wolter, K.-J., Danczak, M., Daniel, D.
Application of computer tomography in microelectronic packaging
9th International Symposium on NDE for Health Monitoring and Diagnostics, San Diego, USA, 15-17 March 2004, Proc. pp. 194-202.

Stefani, F.; Gerbeth, G.
MRI in Taylor-Dean flows
MHD Couette Flows: Experiments and Models, AIP Conference Proceedings Volume 733 (2004), 100-113

Thieme, M.; Bergner, F.; Haase, I.; Worch, H.
Comparative investigations to corrosion fatigue of Al-Cu and Al-Mg-Si alloys
Proceedings 4th Kurt Schwabe Corrosion Symposium 'Mechanisms of Corrosion and Corrosion Prevention', O. Forsen, J. Aromaa, L. Selin (Eds.), Espoo, Helsinki University of Technology, June 13-17, 2004, pp. 103-111

Ulbricht, A.; Bergner, F.
Detecting irradiation induced damage in RPV steels by SANS
Proceedings of the 30th MPA-Seminar in conjunction with 9th German-Japanese Seminar 'Safety and Reliability in Energy Technology', ISSN 0722-401X, MPA Stuttgart, 2004, Vol. 1, p. 10.1-10.13

Ulbricht, A.; Böhmert, J.
Characterization of radiation effects in reactor pressure vessel steels by means of small angle neutron scattering
Annual meeting on nuclear technology 2004, May, 25-27, Düsseldorf, Germany, CD-ROM, Proceedings, pp. 515-518, Inforum Verlag, Berlin, 2004.

Vanga, B. N. R.; Krepper, E.; Zaruba, A.; Prasser, H.-M.; de Bertodano, L.
On the hydrodynamics of bubble columns: comparison of experimental measurements with computational fluid dynamics calculations
5th International Conference on Multiphase Flow, ICMF 04, Yokohama, Japan, May 30 June 4, 2004. Paper 264

Willers, B.; Eckert, S.; Michel, U.; Zouhar, G.
Effect of the fluid convection driven by a rotating magnetic field on the solidification of a PbSn alloy
in: Dieter M. Herlach: Solidification and Crystallization, Weinheim: WILEY-VCH, 2004, ISBN 3-527-31011-8, p. 194-203

Willschütz, H.-G.; Altstadt, E.
Application of several physics environments for a coupled simulation of pressure vessel creep failure experiments
22nd CAD-FEM Users' Meeting 2004, International Congress on FEM Technology with ANSYS CFX & ICEM CFD, November 10-12, 2004, Dresden, Germany, Paper No. 1.1.13

Willschütz, H.-G.; Altstadt, E.; Mueller, G.; Boehmert, J.; Sehgal, B. R.
Metallographical and numerical investigation of the EC-FOREVER-4 test
International Congress on Advances in Nuclear Power Plants (ICAPP '04), June 13-17, 2004, Pittsburgh, PA, USA, Proceedings on CD-ROM, Paper #4006

Willschütz, H.-G.; Müller, G.; Altstadt, E.
Discussion of the behaviour of different rpv-steels in vessel creep failure experiments
Annual meeting on nuclear technology 2004, May, 25-27, Düsseldorf, Germany, CD-ROM, p. 519-522

Zaruba, A.; Krepper, E.; Prasser, H.-M.; Schleicher, E.
Measurement of bubble velocity profiles and turbulent diffusion coefficients of the gaseous phase in rectangular bubble column using image processing
3rd International Symposium on Two-Phase Flow Modelling and Experimentation Pisa, 22-24 September 2004, proceedings on CD-ROM, paper ms19.

Zhang, C.; Eckert, S.; Gerbeth, G.
Gas and liquid velocity measurements in bubble chain driven two-phase flow by means of UDV and LDA
5th ICMF, Yokohama, Japan, May 30 - June 4, 2004, CD-ROM ICMF2004, Paper-No. 260

FZR reports and other reports

Beyer, M.; Carl, H.; Schütz, P.; Pietruske, H.; Lenk, S.
Betriebshandbuch für die Mehrzweck-Thermohydraulikversuchsanlage TOPFLOW
Wissenschaftlich-Technische Berichte / Forschungszentrum Rossendorf; FZR-405 Juli 2004

Grahn, A.
Strömungsinstabilitäten bei Stoffübergang und chemischer Reaktion an der ebenen Grenzfläche zwischen zwei nicht mischbaren Flüssigkeiten
Wissenschaftlich-Technischer Bericht FZR-417, Dezember 2004

Höhne, T.; Bieder, U.
Validation of Trio_U for transient accident scenarios – numerical studies of the ROCOM buoyancy driven test case simulating ECC Injection during natural convection in PWR
Note technique SMTH/LDTA N° 2003-079, CEA Grenoble, August 2004

Mittag, S.; Grundmann, U.; Kliem, S.; Kozmenkov, Y.; Rindelhardt, U.; et, al
Validation of coupled neutronic/thermal-hydraulic codes for VVER reactors - final report - FIKS-CT-2001-00166
Wissenschaftlich-Technische Berichte / Forschungszentrum Rossendorf; FZR-408 August 2004

Weiß, F.-P.; Rindelhardt, U. (Editors)
Annual Report 2003 - Institute of Safety Research
Wissenschaftlich-Technische Berichte / Forschungszentrum Rossendorf; FZR-407 2004

Werner, M.; Altstadt, E.
Finite-Elemente-Modellierung des Risswachstums an 3-Punktbiegeproben
Wissenschaftlich-Technische Berichte / Forschungszentrum Rossendorf; FZR-397 März 2004

Patents

D. Hoppe
Vorrichtung zur Unterdrückung von Drehmoment-Sprüngen in hydraulischen Turbokupplungen
10 2004 001 047.1, Anmeldung durch Mitinhaber Voith Turbo GmbH & Co KG;

H.-M. Prasser
Vorrichtung zur Vermeidung von Druckstößen in Rohrleitungssystemen
10 2004 025 988.6, Anmeldung durch Mitinhaber Fraunhofer-Gesellschaft

U. Hampel, E. Schleicher
Faseroptischer Sensor zur Bestimmung von Stoff- und Phasenverteilungen
10 2004 037 883.5

S. Eckert
Anlage zur gesteuerten Erstarrung von Schmelzen elektrisch leitender Schmelzen
10 2004 044 637.7, Anmeldung durch Mitinhaber TUD

PhD and diploma theses

PhD theses

Alexander Grahn
Fluid-dynamic instabilities during mass transfer across the interface between to immiscible liquids
TU Dresden, Fakultät Maschinenwesen

Martin Abendroth
Identification of material deformation and damage parameters from the small punch test
TU Bergakademie Freiberg, Fakultät für Maschinenbau, Verfahrens- und Energietechnik

Brahma Nanda Reddy Vanga (external PhD)
Experimental and numerical studies on the hydrodynamics of recirculating turbulent flow in rectangular bubble columns
Purdue University, West Lafayette, IN 47907, USA
B. N. R. Vanga worked out significant parts of his PhD thesis under the supervision of Dr. H.-M. Prasser during several guest stays within ISR

Diploma theses

Thomas Tittel
Thermische und mechanische Auswirkungen einer späten Behälteraußenflutung bei Experimenten zur Rückhaltung von Kernschmelze in einem Reaktordruckbehälter,
TU Dresden, Fakultät Maschinenwesen

Andreas Löwe
Untersuchungen zur Bewertung von Reaktordruckbehälterstählen,
TU Dresden, Fakultät Maschinenwesen

Christian Cierpka
Messung des Geschwindigkeitsfeldes an einer angestellten Platte unter dem Einfluss zeitlich periodischer Lorentzkräfte,
TU Dresden, Fakultät Maschinenwesen

Stephan Boden
Computertomografische Untersuchung von Phasenverteilungen in chemischen Rührkesselreaktoren
TU Dresden, Fakultät Elektrotechnik und Informationssystemtechnik

André Bieberle
Neue Detektorkonzepte für ein computertomografisches Messsystem mit Gamma-Strahlung
TU Dresden, Fakultät Elektrotechnik und Informationssystemtechnik

Martina Speck
Untersuchung iterativer Bildrekonstruktionsalgorithmen für eine Limited-Angle-Röntgentomographie
TU Dresden, Fakultät Elektrotechnik und Informationssystemtechnik

Stefan Bohm
Erarbeitung eines reaktionskinetischen Modells der Veresterung von Essigsäureanhydrid mit Methanol zur Einbindung in Druckentlastungs-Simulationsprogramme und CFD-Codes
Technische Fachhochschule Berlin, Fachbereich Verfahrens- und Umwelttechnik

Michael Rothe
Anwendung von Kreuzkorrelationsverfahren zur Geschwindigkeitsmessung in einer Flüssigkeits-Gas-Strömung mit Hilfe von zwei hintereinander angeordneten Gittersensoren
Fachhochschule Lausitz, Fachbereich Informatik/Elektrotechnik/Maschinenbau

Anja Neubert
Meteorologische Beiträge zur optimierten Betriebsführung von Windparks
Universität Leipzig, Fakultät für Physik und Geowissenschaften

Anette Kantrowitz
Windenergienutzung im Spannungsfeld zwischen Klimaschutz und Umweltschutz
Hochschule Zittau/Görlitz, Fachbereich Mathematik und Naturwissenschaften

Awards

Horst-Michael Prasser, Mathias Beyer, Arnd Böttger, Helmar Carl, Dirk Lucas, Andreas Schaffrath, Peter Schütz, Frank-Peter Weiss, Jochen Zschau

Best Paper Award 2004 of the Thermal Hydraulics Division of the American Nuclear Society for the presentation:
Influence of the pipe diameter on the structure of the gas-liquid interface in a vertical two-phase pipe flow
NURETH-10, Seoul, October 5-9, 2003, paper A00308

Martina Speck

Görges-Preis der Fakultät Elektrotechnik
Award for an excellent diploma thesis in the field of electrical engineering

Analysis of iterative image reconstruction algorithms for a Limited Angle X-Ray tomography

André Bieberle

Best diploma thesis award (Institute of Solid State Electronic, TU Dresden)

Analysis of new detector concepts for a computed tomography measurement system using gamma radiation

Guests

Kabanova, Lyudmilla
09.04.2004 – 26.06.2004
EDO Gidropress Podolsk/Russia

Grants, Ilmars Dr.
16.01.2004 – 31.01.2004
25.09.2004 -09.10.2004
Institute of Physics Riga/Latvia

Bojarevics, Andris Dr.
19.01.2004 – 31.01.2004
Institute of Physics Riga/Latvia

Reddy Vanga, Brahma Nanda
15.03.2004 – 18.07.2004
Purdue University West Lafayette/USA

Forest, Cary
04.02.2004 – 05.02.2004
University Wisconsin/USA

Priede, Janis Dr.
16.02.2004 – 13.03.2004
25.09.2004 – 24.10. 2004
Institute of Physics Riga/Latvia

Kim, John Prof.
29.03.2004 – 02.04.04
UC Los Angeles/USA

Choi, Haecheon Prof.
30.03.2004 – 03.04.2004
Seoul National University/Korea

Gunzberger, Max Prof.
31.03.2004 – 03.04.2004
Florida International University/USA

Bottaro, Alessandro Prof.
31.03.2004 – 03.04.2004
IMFT Toulouse/France

Dulikravich, George Prof.
31.03.2004 – 04.04.2004
Florida International University/USA

Zabras, Nicholas Prof.
31.03.2004 – 04.04.2004
Cornell University/USA

Melnikov, Vladimir Prof.
21.04.2004 – 02.05.2004
Novgorod Technical University/Russia

Dounsev, Andrei Dr.
22.04.2004 – 02.05.2004
Novgorod Technical University/Russia

Kamnev, Mikhail
22.04.2004 – 02.05.2004
02.08.2004 – 30.10.2004
Novgorod Technical University/Russia

Borodin, Vladimir Dr.
02.05.2004
RRC Kurchatov Institute Moscow/Russia

Schlindwein, Dieter
13.05.2004 – 15.05.2004
Forschungszentrum Karlsruhe

Koncar, Bostjan Dr.
01.06.2004 – 31.07.2004
Jozef Stefan Institute Ljubljana/Slovenia

Plevachuk, Yuri Dr.
05.07.2004 – 24.07.2004
11.12.2004 – 18.12.2004
State University Liv/Ukraine

Anikeev, Andrey Dr.
18.07.2004 – 08.08.2004
Budker Institute Novosibirsk/Russia

Gailitis, Agris Prof.
29.08.2004 – 01.09.2004
13.09.2004 – 20.09.2004
Institute of Physics Riga/Latvia

Petkov, Petko Dr.
28.02.2004 – 25.04.2004
15.09.2004 – 13.12.2004
INRNE Sofia/Bulgaria

Gokhmann, Alexander Prof.
01.09.2004 – 31.10.2004
South Ukrainian Pedagogical University K. D. Ushinski Odessa/Ukraine

Kolesnichenko, Ilya
02.10.2004 – 27.11.2004
Institute of Mechanics Perm/Russia

Leorat, Jaques Prof.
13.11.2004 – 16.11.2004
Observatory of Maudon/France

Pivovarov, Valeryi
20.11.2004 – 27.11.2004
Institute of Physics and Power Engineering Obninsk/Russia

Matveev, Yuri Dr.
20.11.2004 – 27.11.2004
Institute of Physics and Power Engineering Obninsk/Russia

Gashenko, Ilya Vladimirovich
07.12.2004 – 24.12.2004
Elektrogorsk Research and Engineering Centre/Russia

Pedcenko, Aleksandrs
15.11.2004 – 20.12.2004
Institute of Physics Riga/Latvia

Khalimonchuk, Volodymyr
28.11.2004 – 05.12.2004
Scientific Technical Centre for Nuclear and Radiation Safety of the Ukraine, Kiev/Ukraine

Kuchyn, Oleksandr
28.11.2004 – 05.12.2004
Scientific Technical Centre for Nuclear and Radiation Safety of the Ukraine, Kiev/Ukraine

Tsidulko, Yuri Dr.
28.11.2004 – 12.12.2004
Budker Institute Novosibirsk/Russia

Magas, Konstyantyn
07.12.2004 – 10.12.2004
Infoatom Kiew/Ukraine

Vallee, Christophe
01.01.2004 – 31.03.2004
France

Chantaraprachoom, Nathavan
01.01.2004 – 31.07.2004
Office of Atoms for Peace Chatuchak/Thailand

Vaibar, Roman
15.03.2004 – 16.07.2004
West Bohemian University Plzen/Czech Republic

Bousbia Salah, Anis
21.04.2004 – 26.04.2004
16.08.2004 – 17.12.2004
University Pisa/Italy

Danitcheva, Irina
06.06.2004 – 11.06.2004
Gosatomnadzor Moscow/Russia

Khrennikov, Nikolay Dr.
06.06.2004 – 11.06.2004
Gosatomnadzor Moscow/Russia

Borodkin, Gennadi
06.06.2004 – 11.06.2004
Gosatomnadzor Moscow/Russia

Gokhman, Alexander Prof.
05.07.2004 – 31.08.2004
SUP University Odessa/Ukraine

Gurevich, Mikail Prof.
06.09.2004 – 18.09.2004
RRC Kurchatov Institute Moscow/Russia

Alexeev, Nikolay Dr.
06.09.2004 – 18.09.2004
RRC Kurchatov Institute Moscow/Russia

Zaritsky Sergei Dr.
06.09.2004 – 18.09.2004
RRC Kurchatov Institute Moscow/Russia

Sydiachenko, Viacheslav Dr.
26.09.2004 – 26.11.2004
Ukrain Akademy of Science Kiev, Ukraine

Myasnikov, Andrey
03.10.2004 – 31.10.2004
RRC Kurchatov Institute Moscow/Russia

Osmera, Bohumil Dr.
25.10.2004 – 30.10.2004
Nuclear Research Institute Rez/Czech Republic

Murasov, Mykhail
25.10.2004 – 24.12.2004
Polytechnical Institute Kiev/Ukraine

Murakawa, Hideki
08.11.2004 – 06.12.2004
Tokyo Institute of Technology/Japan

Strmensky, Ctibor
06.12.2004 – 10.12.2004
VUJE Trnava/Slovakia

Chrapciak, Vladimir
06.12.2004 – 10.12.2004
VUJE Trnava/Slovakia

Meetings and workshops

Flow Control by Tailored Magnetic Fields (FLOWCOMAG)-Workshop
Dresden, 1-2 February 2004
Organizer: Collaborative research center “Electromagnetic flow control in metallurgy, crystal growth and electrochemistry”

Final Meeting of the EU-Project: Validation of Coupled Neutronics/Thermal Hydraulics Codes for VVER Reactors (VALCO)
Rossendorf, 19-21 April 2004

Multi-Phase Flow: Simulation, Experiment and Application-Conference
Dresden, 28-30 June 2004
Organizer: FZR and ANSYS-CFX

Meeting of the EU-Project PERFECT: Prediction of Irradiation Damage Effects on Reactor Components
Rossendorf, 22-23 September 2004

Final Meeting of the EU-Project: Fluid Mixing and Flow Distribution in the Reactor Circuit (FLOMIX)
Rossendorf, 23-24 September 2004

Sino-German Workshop on Electromagnetic Processing of Materials
Shanghai/China, 11-12 October 2004
Organizer: Collaborative research center “Electromagnetic flow control in metallurgy, crystal growth and electrochemistry” and University of Shanghai

Seminars of the Institute

A. Zaruba, Dr. U. Hampel
Videometrische Vermessung von Gasblasen
21. 01. 2004

Dr. T. Höhne
Nachrechnung eines Experiments zur dichtegetriebenen Vermischung mit dem CFD-Code TRIO_U der CEA
29.01.2004

Dr. S. Mittag, Dr. U. Grundmann
Validierung von DYN3D an den V-1000-Experimenten
26.02.2004

Prof. U. Rindelhardt
Wasserstoff als künftiger Energieträger
11.03.2004

Dr. P. Petkov (INRE Sofia)
Two-Dimensional Real Geometry Neutron Transport Calculations by the Method of Characteristics
24.03.2004

Y. Kozmenkov
Transient Simulations in VVER-1000: Comparison between DYN3D-ATHLET and DYN3D-RELAP5
29. 03. 2004

Dr. F. Stefani, Th. Gundrum
Geschwindigkeitstomografie mittels externer Magnetfeldmessungen
22.04.2004

Dr. A. Heinzel (FZ Karlsruhe)
Korrosion von Stählen in LBE bei verschiedenen Temperaturen und Sauerstoffkonzentration - aktueller Stand der Untersuchungen
07.04.2004

Dr. U. Hampel, A. Bieberle
Gammatomografie an Brennelement-Bündeln
06.05.2004

Dr. E. Krepper, A. Grahn
Untersuchung des Verhaltens von freigesetztem Isolationsmaterial in einer Kühlmittel-strömung
19.05.2004

Dr. R. Küchler, Dr. K. Noack
Experimente und Modellierung der Verwitterung in der (Wasser-)ungesättigten Zone
03.06.2004

Dr. H. Kryk, St. Bohm (TFH Berlin)
Untersuchung der Druckentlastung reaktiver Multiphasensysteme
24.06.2004

Dr. H.-W. Viehrig
Anwendung des Master-Curve-Konzeptes zur Integritätsbewertung von Reaktordruckbehältern
02.09.2004

Dr. F. Schäfer, Dr. H.-M. Prasser, D. Walter
EU-Projekt IMPAM: Improved Accident Management for VVER-440 Reactors – Experimente und ATHLET-Rechnungen für ausgewählte Testszenarien
09. 09.2004

Dr. F. Stefani, Dr. G. Gerbeth, Th. Gundrum
Eine Zwischenbilanz zum Rigaer Dynamo-Experiment
07.10.2004

Dr. U. Rohde, Dr. T. Höhne, S. Kliem
EU-Projekt FLOMIX-R: Experimente und CFD-Simulation zur turbulenten Vermischung in DWR
21.10.2004

Prof. Durst (University of Erlangen)
Experiment and numerical methods as basis for new fluid mechanics information
04.11.2004

Dr. Ch. Schuster (TU Dresden)
Experimentelle Untersuchungen zum Stabilitätsverhalten einer zweiphasigen Naturumlaufströmung an der Versuchsanlage DANTON
18.11.2004

B. Böhmer, J. Konheiser
Bestimmung und Verifizierung von Strahlenfeldparametern für das Monitoring von Reaktordruckbehältern (EU-Project REDOS)
03.12.2004

Dr. E. Altstadt, H.-G. Willschütz
Kühlung einer ausgebreiteten Kernschmelze (EU-Project ECOSTAR)
16.12.2004

Lecture courses

Prof. Dr. Frank-Peter Weiss, Dr. Mathias Werner

Zuverlässigkeit und Sicherheit technischer Systeme
TU Dresden, Fakultät Maschinenwesen
SS 2004 und WS 2004

Prof. Dr. Udo Rindelhardt

Erneuerbare Energien II
Universität Leipzig, Fakultät für Physik und Geowissenschaften
SS 2004

Solare Energietechnik I und II
TU Chemnitz, Fakultät für Elektrotechnik/Informationstechnik
SS 2004 und WS 2004

Dr.-Ing. habil. Frank Bergner

Werkstofftechnik
TU Dresden, Fakultät für Maschinenwesen
SS 2004 und WS 2004

Departments of the Institute

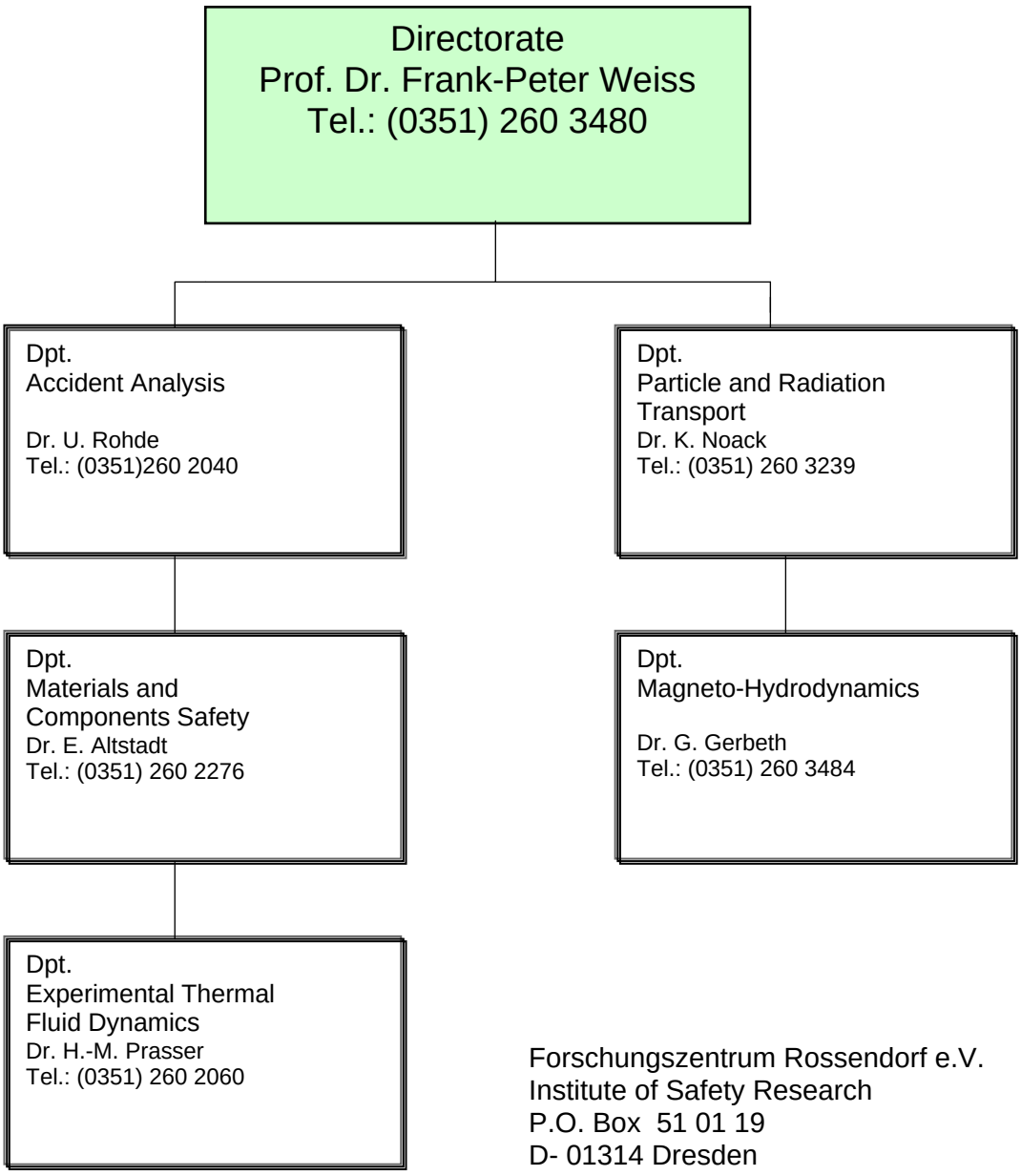

Forschungszentrum Rossendorf e.V.
Institute of Safety Research
P.O. Box 51 01 19
D- 01314 Dresden

Personnel

Director: Prof. Dr. F.-P. Weiss

Scientific Staff

Abendroth, Martin Dr.
Altstadt, Eberhard Dr.
Beckert, Carsten
Bergner, Frank Dr.
Beyer, Matthias
Böhmer, Bertram
Carl, Helmar Dr.
Chatrov, Viktor Dr.
Cramer, Andreas Dr.
Eckert, Sven Dr.
Galindo, Vladimir Dr.
Gerbeth, Gunter Dr.
Grahn, Alexander, Dr.
Grants, Ilmars Dr.
Grundmann, Ulrich Dr.
Gundrum, Thomas
Günther, Uwe Dr.
Hampel, Uwe, Dr.
Heinzelmann, Christian
Hoppe, Dietrich Dr.
Höhne, Thomas Dr.
Hristov, Hristo Vesselin Dr.
Hüller, Jürgen Dr.
Kliem, Sören
Koch, Reinhard Dr.
Konheiser, Jörg
Kozmenkov, Yaroslav
Krepper, Eckhard Dr.
Kryk, Holger Dr.
Küchler, Roland Dr.
Lucas, Dirk Dr.
Manera, Annalisa Dr.
Mittag, Siegfried Dr.
Müller, Gudrun, Dr.
Mutschke, Gerd
Noack, Klaus Dr.
Prasser, Horst-Michael Dr.
Rindelhardt, Udo Prof. Dr.
Rohde, Ulrich Dr.
Schäfer, Frank Dr.
Schleicher, Eckhard
Schmitt, Wilfried Dr.
Schütz, Peter
Shi, Jun-Mei Dr.
Stefani, Frank Dr.
Ulbricht, Andreas
Viehrig, Hans-Werner Dr.
Weier, Tom
Werner, Matthias Dr.
Willers, Bernd
Willschütz, Hans-Georg
Witke, Willy
Xu, Mingtian Dr.
Zurbuchen, Conrad

PhD Students

Bieberle, André
Buchenau, Dominique
Krepel, Jiri
Speck, Martina
Vallee, Christophe
Varshney, Kapil
Zaruba, Aliaksandr
Zhang, Chaojie
da Silva, Marco

Technical Staff

Behrens, Sieglinde
Berger, Torsten
Böttger, Arnd
Bombis, Doris
Borchardt, Steffen
Erlebach, Stephan
Forker, Klaus
Futterschneider, Hein
Gommlich, Andre
Hessel, Günter
Kunadt, Heiko
Leonhardt, Wolf-Dietrich
Lindner, Klaus
Losinski, Claudia
Nowak, Bernd
Pietzsch, Jens
Pietruske, Heiko
Richter, Annett
Richter, Henry
Richter, Joachim
Richter, Petra
Roßner, Michaela
Rott, Sonja
Rußig, Heiko
Schleßiger, Heike
Schneider, Gisela
Skorupa, Ulrich
Spieler, Dagobert
Sühnel, Tobias
Tamme, Marko
Walter, Denis
Webersinke, Wolfgang
Weichelt, Steffen
Weiß, Rainer
Zimmermann, Wilfried
Zippe, Cornelius Dr.

List of acronyms

ACF	auto-correlation function
AD	analogue digital
ADF	assembly discontinuity factors
AEN	L'Agence pour l'énergie nucléaire
ALR	automatic laboratory scale reactor
AMSTER	French molten salt reactor model
ASME	American Society of Mechanical Engineers
ASTM	American Society for Testing and Materials
ATHLET	thermo-hydraulic system code
BEREMIN	cleavage fracture model
BMBF	Federal Ministry of Education and Research
BMWA	Federal Ministry of Economy and Labor
BPG	best practice guidelines
BRICK	simulation software
BWR	boiling water reactor
CAD	computer aided design
CBT	cone-beam X-ray computed tomography
CCD	charge coupled device
CCF	cross-correlation function
CCFL	counter-current flow limitation
CDB	creep data base
CFD	computational fluid dynamics
CFX	CFD program by ANSYS-CFX
CHF	Critical Heat Flux
CIFT	contactless inductive flow tomography
CR	control rod
CT	computer tomography
DBTT	ductile-to-brittle transition temperature
DC	direct current
DFG	Deutsche Forschungsgemeinschaft
DN	delayed neutrons
DYN3D	reactor dynamics code
ECC	emergency core cooling
ECCM	effective conductivity convectivity model
EIT	electrical impedance tomography
ELBE	electron linear accelerator for beams of high brilliance and low emittance
FANP	Framatome Advanced Nuclear Power
FE	finite element
FH	Fachhochschule
FLOMIX-R	Fluid Mixing and Flow Distribution in the Reactor Circuit
FLUENT	CFD code
FOREVER	experiments „Failure Of REactor VEssel Retention”
FORTUM PTS	thermalhydraulic test facility at University of Lappeenranta
FTIR	Fourier transform infrared spectroscopy
FWHM	full width half maximum
FZR	Forschungszentrum Rossendorf e.V.
GPE	general physics environment
GRS	Gesellschaft für Anlagen- und Reaktorsicherheit

HELIOS	2d-transport-code with burnup
HLTF	Hot Leg Test Facility
HPI	high pressure injection
HTO	free tritium
IAEA	International Atomic Energy Agency
IKE Stuttgart	Institut für Kernenergetik und Energiesysteme der Universität Stuttgart
ISR	Institute of Safety Research
LDA	laser doppler anemometry
LINAC	linear accelerator
LOCA	loss of coolant accident
LSC	liquid scintillation counting
LWR	light water reactor
LYRA	LYRA facility of the JRC Petten
MC	master curve
MCNP	Monte-Carlo neutron particle transport code
MCP	main coolant pump
MHD	magneto-hydrodynamics
MOP	mechano-optical probe
MOST	Molten Salt Reactor Technology
MSR	molten salt reactors
MSRE	molten salt reactor experiment
MULTIMAG	test facility “MULTIple MAGnetic fields“
MUSIG	multiple size group model
NEA	Nuclear Energy Agency
NOKO	former test facility of Forschungszentrum Jülich (FZJ)
NPP	nuclear power plant
NURESIM	European software platform for reactor simulation
NURETH	international meeting on nuclear reactor thermal hydraulics
OECD	Organization for Economic Co-operation and Development
ORIGEN	Scientific Graphing and Analysis Software
PET	positron emission tomography
PERFECT	Prediction of Irradiation Damage Effects in Reactor Components
PIC	particle-in-cell method
PIV	particle image velocimetry
PMMA	polymethylmetacrylat
PRZ	pressurizer
PTS	pressurized thermal shock
PWR	pressurized water reactor
PZT	lead-zirconium-titanat
ROCOM	Rossendorf Coolant Mixing Model test facility
RPV	reactor pressure vessel
RT	rate theory
SANS	small-angle neutron scattering
SAPR	semi analytical perturbation reconstruction
SB LOCA	small break loss of coolant accident
SDF	size distribution function
SFB	Sonderforschungsbereich (Collaborative Research Centre)
SIA	self-interstitial atom
SPECT	single photon emission computer tomography
SPHINX	Czech molten salt reactor model

SST	shear stress transport
STC	scientific-technical cooperation
TH	thermal-hydraulic
TOF	time of flight
TOPFLOW	Transient TwO Phase FLOW
TRAMO	transport code system based on the Monte Carlo method by FZR
UDV	ultrasound doppler velocimetry
UPTF	upper plenum test facility
VALCO	Validation of Coupled Neutron Kinetic Thermal Hydraulics Codes
VC	vacancy cluster
VTT	Technical Research Centre of Finland
VVER	WWER - Russian nuclear power plant
wms	wire-mesh sensor